

November 2019

Use of Spectrofluorometry to Detect Petroleum Hydrocarbons in the Marine Environment

Mary Iris Abercrombie
University of South Florida

Follow this and additional works at: <https://digitalcommons.usf.edu/etd>



Part of the [Other Oceanography and Atmospheric Sciences and Meteorology Commons](#)

Scholar Commons Citation

Abercrombie, Mary Iris, "Use of Spectrofluorometry to Detect Petroleum Hydrocarbons in the Marine Environment" (2019). *USF Tampa Graduate Theses and Dissertations*.
<https://digitalcommons.usf.edu/etd/7998>

This Dissertation is brought to you for free and open access by the USF Graduate Theses and Dissertations at Digital Commons @ University of South Florida. It has been accepted for inclusion in USF Tampa Graduate Theses and Dissertations by an authorized administrator of Digital Commons @ University of South Florida. For more information, please contact digitalcommons@usf.edu.

Use of Spectrofluorometry to Detect Petroleum Hydrocarbons in the Marine Environment

by

Mary Iris Abercrombie

A dissertation submitted in partial fulfillment
of the requirements for the degree of
Doctor of Philosophy in Marine Science
with a concentration in Chemical Oceanography
College of Marine Science
University of South Florida

Co-Major Professor: Paula Coble Rhodes, Ph.D.

Co-Major Professor: Kendra L. Daly, Ph.D.

Albert C. Hine, Ph.D.

Robyn N. Conmy, Ph.D.

Ana R. Arellano, Ph.D.

Mark E. Luther, Ph.D.

Date of Approval:

November 8, 2019

Keywords: fluorescence, EEMs, Gulf of Mexico, Deepwater Horizon, wave tank, baffle flask

Copyright © 2019, Mary Iris Abercrombie

ACKNOWLEDGMENTS

I owe a debt of gratitude to many, for the financial, educational, and emotional support provided to me over the long and winding road which resulted in this dissertation. At the outset, I express my thanks to Dr. Richard F. Bopp for supervising my MS in Geology at Rensselaer Polytechnic Institute, which inspired my passion for graduate-level scholarship and research.

I express gratitude to all who provided the financial support which enabled me to do this work: to Dr. Peter R. Betzer and the Mahaffey Family Foundation for graduate fellowships, as well as to NOAA, NASA, NSF, IOOS, and the Alliance for Coastal Technologies for funding support. For *Weatherbird II* ship support, I thank the Florida Institute of Oceanography (FIO)/BP, and for funding support for the baffle flask experimental series, I thank the U.S. EPA and the Department of Fisheries and Oceans, Canada. My thanks, also, to Florida Gulf Coast University for the Grant-in-Aid which provided me a semester away from teaching in order to begin writing.

I would also like to express my appreciation to the crew of R/V *Weatherbird II*, the members of the COOGER group at the Bedford Institute of Oceanography, and all of the scientists who participated in the wave tank series in May/June 2011 and the Seattle workshop in October 2012. In particular, I would like to thank Brian Robinson, Claire McIntyre, and Tom King, who quickly and considerately answered what must have seemed at times to be a never-ending stream of questions from me about their chemical analyses. I also thank the librarians at both the St.

Petersburg and Tampa campuses for their assistance in tracking down obscure research papers and book chapters and delivering them to me at lightning speed.

For assisting with PARAFAC analysis using the PLS toolbox, I thank Rasmus Bro and his colleagues at Eigenvector Research Inc. I also express warm thanks to Kathleen Murphy and Urban Wunsch for welcoming me to Chalmers Technical University in March 2019 to work with them, and for devoting the majority of their time and energy to putting my data through the drEEM toolbox while I was there. I am also very grateful for the warm hospitality extended to me by Dr. Murphy's family during my stay in Gothenburg.

To my committee members – those who have been with me since the outset, and those who have joined along the way – I express deepest appreciation. It has been an honor and a joy to work with all of you. In particular, I thank Ana Arellano for sharing many chilly hours in the Coble Lab showing me how to run the Fluoromax2 and then process data with GRAMS. I am also indebted to Robyn Conmy for her insistence that there must be chemistry to connect with my EEMS results, and for playing a large role in providing the opportunity to make that happen.

I am deeply thankful to my major advisor, Paula Coble Rhodes, for her wisdom, encouragement, and friendship. The week spent with you in Colorado provided the necessary impetus to make this work finally come together, and for that I am eternally grateful. I will think of you every time I wear Madeleine Allbright's shoes. To my co-major advisor, Kendra Daly, I also owe a debt of gratitude. The invitation to join your research cruises on the *Weatherbird* provided the genesis of my research, and your insistence that I conduct appropriate statistical analyses at the

end of this process not only resulted in an enhanced dissertation, it will also enable me to be a better teacher and mentor to my students in the future. Thanks also go to your student, Kate Dubickas, for creating and sharing the map of the sample sites in the Gulf of Mexico.

Finally, I offer deep gratitude to my dear friends and family for their patience, love and support, throughout this long and challenging adventure. To my dad, I offer appreciation for fostering in me an appreciation for education, and to my mom, for teaching me that you can find a way to do anything you set your mind to. I especially want to thank my children, Kelly Jones, Lindsay & Drew Carnevale, and Ian Jones, and my grand-daughter, Mavella Carnevale, for graciously sharing me with this undertaking. I also thank my sweet Frannie for being the best writing buddy ever, content to sleep by my feet as I moved from kitchen table, to dining room table, to chair by the window, as we spent her final summer in our writing retreat by the lake. To my husband, Sim Komisar, words cannot express the depth of my gratitude. I owe you a world of love and appreciation for always encouraging me, being an excellent MATLAB partner, and helping me to finally realize this dream. It is to you that this work is dedicated.

TABLE OF CONTENTS

List of Tables	iv
List of Figures	v
List of Acronyms	xiii
Abstract	xv
General Introduction	1
Fluorescence Spectroscopy	1
Petroleum and Fluorescence Spectroscopy	5
Fluorescence Spectroscopy and the <i>Deepwater Horizon</i> Oil Spill	6
PARAFAC Analysis	8
Summary	10
References	12
Scale Level I – Evaluating Effectiveness of Physical and Chemical Dispersion of Oil in Seawater Using the Baffled Flask Test for Spectrofluorometric Analysis of 25 Types of Petroleum	15
Introduction	15
Chemical Oil Dispersants and the Baffle Flask Test for Dispersion Effectiveness	19
Materials and Methods	24
Artificial Seawater Protocol	25
Dispersed Oil-in-Seawater Experiments	26
Laboratory EPA BFT Protocol	27
Chemical Analysis	33
Dilution Series	34
Results and Discussion	35
Fluorescence as a Function of Chemistry	47
PARAFAC Analysis	56
All 25 Oil Types	59
DOR 0	59
DOR 1:100	59
DOR 1:20	62
Summary of PARAFAC Modelling	64
Conclusions	68
References	70

Scale Level II – Characterizing the Effects of Physical and Chemical Dispersion of Oil in Seawater via Spectrofluorometry in Wave Tank Experiments	75
Introduction	75
Materials and Methods	78
Results and Discussion	85
SAFIre Instrument Response	95
PARAFAC Analysis	97
Conclusions	98
References	101
Scale Level III – Fluorescence EEMS Analysis of Field Samples Collected in the Northern Gulf of Mexico During the Year Following the DWH Spill of National Significance	103
Introduction	103
Materials and Methods	108
December 2010	112
February and May 2011	113
August 2011	116
Results	116
R/V <i>Walton Smith</i> – August 2011	117
R/V <i>Nancy Foster</i> – July 2010	121
R/V <i>Weatherbird II</i> – August 2010	125
R/V <i>Weatherbird II</i> Time Series – December 2010, February 2011, and May 2011	127
Discussion	128
December 2010 – DSH08, DSH10, and PCB06	128
February 2011 – DSH08, DSH10, and PCB06	128
May 2011 – DSH08 and DSH10	130
Sediment Core Pore Water	134
PARAFAC Analysis	137
Conclusions	142
References	144
General Conclusions	149
References	158
Appendix A: Oil Characteristics	162
Appendix B: COOGER Methods for Fluorescence Analysis Using the Baffled Flask Test	166
Appendix C: Coble Lab Protocol for HORIBA Aqualog	169
Appendix D: EEM Contour Plots	187
Appendix E: Field Sample Depth Profiles and EEMs	213

Appendix F: Reprint Permissions234

LIST OF TABLES

Table 2.1:	List of oil used for EEM analyses.....	25
Table 2.2:	Preparation of sample DORs	28
Table 2.3:	Analysis of replicates	32
Table 2.4:	25 oil types fluorescence results and chemical analyses	38
Table 2.5:	Individual hydrocarbon compounds reported as total alkanes, total 2-ring, 3-ring and 4-ring PAHs.....	48
Table 3.1:	Details of wave tank series protocols.....	82
Table 3.2:	Comparison of core experiments – location and concentration (QSE) of maximum fluorescence peak (F_{\max})	90
Table 4.1:	Samples collected in the year following the DWH oil spill which are included in this study	111
Table 4.2:	Samples collected in the year following the DWH oil spill included in PARAFAC analysis	141
Table A:	Oil characteristics.....	163

LIST OF FIGURES

Figure 1.1:	Jablonski diagram illustrating the processes at play in luminescence	2
Figure 2.1:	The wave tank facility at Bedford Institute of Oceanography	21
Figure 2.2:	Twenty-five oil samples received from COOGER DFO – December 2013	25
Figure 2.3:	Trypsinizing (baffle) flasks containing dispersed oil in artificial seawater and corresponding samples removed from each flask, ready for spectrofluorometric analysis	29
Figure 2.4:	Alaska North Slope dispersed oil in artificial seawater at DOR 1:20 with locations of $F_{\max 1}$, $F_{\max 2}$, $F_{\max 3}$ and $F_{\max 4}$ indicated.....	40
Figure 2.5:	Photographs of pre-analysis samples of Type I (left) and II (right) oils for DOR = 1:20.....	42
Figure 2.6:	EEMs of Type I (left) and II (right) oils for DOR = 1:20.....	43
Figure 2.7:	$F_{\max 1}$ fluorescence for Light Oils (API gravity > 31°), in order of increasing density: 1. Scotian Shelf Condensate, 2. Federated, 3. Brent, 4. MC252—Discoverer Enterprise, 5. Hibernia, 6. MC252—generic, 7. Terra Nova, 8. Gullfaks, 9. Arabian Light.....	44
Figure 2.8:	$F_{\max 1}$ fluorescence for Medium Oils (API gravity = 22.3° to 31°), in order of increasing density: 1. MESA, 2. Alaska North Slope (ANS), 3. ANS 10% weathered, 4. Sea Rose, 5. Heidrun, 6. Vasconia, 7. Lago.....	44
Figure 2.9:	$F_{\max 1}$ fluorescence for Heavy Oils (API gravity < 22.3°), in order of increasing density: 1. Santa Clara, 2. IFO 40, 3. Cold Lake Dilbit, 4. Access Western Blend Dilbit, 5. Hondo, 6. IFO 120, 7. IFO 180, 8. Belridge Heavy, 9. IFO 300.....	45
Figure 2.10:	For all oil types at DOR 0, total concentration of 2-ring, 3-ring, and 4-ring PAHs (µg/L) against fluorescence intensity (RU) at $F_{\max 3}$ (top), and against $F_{\max 4}$ (bottom)	50
Figure 2.11:	For all oil types at DOR 0, total concentration of 2-ring, 3-ring, and 4-ring PAHs (µg/L) against fluorescence intensity (RU) at $F_{\max 1}$ (top), and against $F_{\max 2}$ (bottom)	51

Figure 2.12:	For all oil types at DOR 1:20, total concentration of 2-ring, 3-ring, and 4-ring PAHs ($\mu\text{g/L}$) against fluorescence intensity (RU) at $F_{\text{max}3}$ (top), and against $F_{\text{max}4}$ (bottom).....	52
Figure 2.13:	For all oil types at DOR 1:20, total concentration of 2-ring, 3-ring, and 4-ring PAHs ($\mu\text{g/L}$) against fluorescence intensity (RU) at $F_{\text{max}1}$ (top), and against $F_{\text{max}2}$ (bottom).....	53
Figure 2.14:	Fluorescence Dispersibility Ratio (FDR) vs. decreasing oil density shows a moderate relationship between fluorescence and oil density.....	55
Figure 2.15:	Chemical Dispersibility Ratio (CDR), ordered from low to high, with corresponding Fluorescence Dispersibility Ratio (FDR).....	55
Figure 2.16:	Example of split half validation for the 6-component model of 25 oil types at DOR 0 showing individual fit of data splits	60
Figure 2.17:	Mode 3 Loadings (Excitation) and Mode 2 Loadings (Emission) for all 25 oil types—DOR0 using 6-component model.....	60
Figure 2.18:	Variation per component for 6-component model of all 25 oil types at DOR0	60
Figure 2.19:	EEM views of the six components of the PARAFAC model for 25 oil types at DOR 0.....	61
Figure 2.20:	Mode 3 Loadings (Excitation) and Mode 2 Loadings (Emission) for all 25 oil types—DOR 1:100 using 5-component model.....	62
Figure 2.21:	Variation per component for the 5-component model of all 25 oil types at DOR 1:100.....	62
Figure 2.22:	EEM views of the five components of the PARAFAC model for 25 oil types at DOR 1:100.....	63
Figure 2.23:	Mode 3 Loadings (Excitation) and Mode 2 Loadings (Emission) for all 25 oil types — DOR 1:20 using 5-component model.....	64
Figure 2.24:	Variation per component for the 5-component model of all 25 oil types at DOR 1:20	64
Figure 2.25:	EEM views of the five components of the PARAFAC model for 25 oil types at DOR 1:20.....	65

Figure 3.1:	Weathered oil/dispersant mixture is poured onto the water surface on the afternoon of June 3 after wave generation has begun (above). In situ fluorometers attached to a crossbeam in the tank (right)	81
Figure 3.2:	EEM contour of MC252 oil dispersed with Corexit® 9500A (DOR 1:25) in seawater	86
Figure 3.3:	Left: Core experiments with fresh and weathered oil, no chemical dispersant. Right: Core experiments with fresh and weathered oil, with chemical dispersant at DOR 1:25	88
Figure 3.4:	PAH concentrations (ng/L) of 2-, 3-, 4-, and 5-ring benzene compounds in MC252 oil in artificial seawater	92
Figure 3.5:	Fluorescence intensity vs. total 2-ring and 3-ring PAHs (left) and vs. total alkanes and BTEX (right) for the FOW experimental series on the morning of June 5, 2011	93
Figure 3.6:	F_{\max} intensity (QSE), total 2-ring and 3-ring PAHs (left) and F_{\max} intensity (QSE) with total alkanes and BTEX (right) for the FOWO experimental series on the afternoon of June 5, 2011.....	95
Figure 3.7:	Fluorescence intensity at Ex/Em 280 nm/340 nm (left) and at Ex/Em 280 nm/450 nm (right) for the three WOW experiments, two FOW experiments, and two FOWO experiments.....	95
Figure 3.8:	Fluorescence intensity at Ex/Em 280/380 nm and at Ex/Em 280/450 for Experiment #6 with fresh MC252 oil and Corexit® 9500 at DOR 1:25 as recorded by the WETLAB SAFire multi-channel fluorometer	96
Figure 3.9:	Emission and Excitation loadings for the six-component model.....	98
Figure 3.10:	EEM view of each of the six components	98
Figure 4.1:	Map of the northern Gulf of Mexico showing the location of the DWH wellhead and three of the sites where water samples were collected aboard the R/V <i>Weatherbird II</i> oil response cruises in December 2010, February 2011 and May 2011	110
Figure 4.2:	EEMs of typical seawater collected at the surface with a bucket at Perdido Pass on 7 December 2010 (top left), and with the addition of MC252 oil and Corexit® 9500A at DOR 1:25 for a final concentration of 100 ppb (top right)	115

Figure 4.3:	Google Earth image with marked locations of selected water samples collected at the surface aboard the NOAA ship R/V <i>Walton Smith</i> in the Florida Straits in August 2011	118
Figure 4.4:	EEMs of water samples collected at locations identified in Fig. 4.3.....	119
Figure 4.5:	EEMs of water samples collected just to the south of Location 1 in Fig. 4.3.....	120
Figure 4.6:	<i>Chlorophyll a</i> versus the ratio of protein-like to humic-like fluorescence in water samples showing the likely influence of the Mississippi River plume collected aboard the R/V <i>Walton Smith</i> in August 2011	121
Figure 4.7:	Locations of sampling stations NF Sta71, 72 and 73 (top, left), and CTD/LADCP hydrography conducted near the DWH MC252 wellhead on July 1, 2010.....	124
Figure 4.8:	Water samples collected aboard the R/V <i>Nancy Foster</i> from 2.6 m at Station 73 (left) with highest fluorescence signature of oil at or near the surface, and sample from 1150 m at Station 71 (right) showing evidence of the deep water plume in July 2010	125
Figure 4.9:	Plot of fluorescence intensity at five selected excitation/emission pairs (top left) for all water samples collected aboard the R/V <i>Weatherbird II</i> at DSH10 on 10 August 2010 and depth profile of CTD data for dissolved oxygen and salinity (top right).....	126
Figure 4.10:	Fluorescence intensity (ppb QSE) at Ex/Em 275 nm/324 nm, indicative of oil in the water column, at sites DSH08, DSH10, and PCB06 in December 2010.....	129
Figure 4.11:	Fluorescence intensity (ppb QSE) at Ex/Em 275 nm/324 nm, indicative of oil in the water column, at sites DSH08, DSH10, and PCB06 in February 2011 at all depths (upper), and at depths up to 500 m (lower) in order to visually separate shallower samples	131
Figure 4.12:	Fluorescence intensity (ppb QSE) at Ex/Em 275 nm/324 nm, indicative of oil in the water column, at sites DSH08 and DSH10 in May 2011 at all depths (upper), and at depths up to 500 m (lower) in order to visually separate shallower samples	132
Figure 4.13:	EEM of pore water extracted by centrifuge from the top 3 mm (top left), 3-6 mm (top right), 6-10 mm (bottom left), and 10-20 mm (bottom right) of a sediment core collected at DSH10 aboard R/V <i>Weatherbird II</i> in February 2011	135

Figure 4.14:	EEM of pore water extracted by centrifuge from the top 5 mm (top left), 5-8 mm (top right), 8-10 mm (bottom left), and 10-20 mm (bottom right) of a sediment core collected at DSH08 aboard R/V <i>Weatherbird II</i> in February 2011	136
Figure 4.15:	Results of bringing entire Gulf of Mexico water sample dataset (n = 555) into the seven-component model created for the wave tank experiments held at BIO in May/June 2011	142
Figure D.1:	Light Oil Category – IFO-40 oil with dispersant EEMs.....	188
Figure D.2:	Light Oil Category – Arabian Light crude oil with dispersant EEMs	189
Figure D.3:	Light Oil Category – Brent crude oil with dispersant EEMs.....	190
Figure D.4:	Light Oil Category – Federated crude oil with dispersant EEMs.....	191
Figure D.5:	Light Oil Category – Gullfaks crude oil with dispersant EEMs.....	192
Figure D.6:	Light Oil Category – Hibernia crude oil with dispersant EEMs.....	193
Figure D.7:	Light Oil Category – MC252 (Discoverer Enterprise) crude oil with dispersant EEMs	194
Figure D.8:	Light Oil Category – MC252 (Generic) crude oil with dispersant EEMs	195
Figure D.9:	Light Oil Category –Scotian Shelf Condensate crude oil with dispersant EEMs.....	196
Figure D.10:	Light Oil Category – Sea Rose crude oil with dispersant EEMs.....	197
Figure D.11:	Light Oil Category – Terra Nova crude oil with dispersant EEMs	198
Figure D.12:	Medium Oil Category – ANS (Alaskan North Slope) crude oil with dispersant EEMs	199
Figure D.13:	Medium Oil Category – 10% weathered ANS (Alaskan North Slope) crude oil with dispersant EEMs	200
Figure D.14:	Medium Oil Category – Heavy IFO-120 oil with dispersant EEMs	201
Figure D.15:	Medium Oil Category – Heavy IFO-280 oil with dispersant EEMs	202
Figure D.16:	Medium Oil Category – Heidrun crude oil with dispersant EEMs.....	203
Figure D.17:	Medium Oil Category – Lago crude oil with dispersant EEMs.....	204

Figure D.18:	Medium Oil Category – Mesa crude oil with dispersant EEMs	205
Figure D.19:	Medium Oil Category – Santa Clara crude oil with dispersant EEMs	206
Figure D.20:	Medium Oil Category – Vasconia crude oil with dispersant EEMs.....	207
Figure D.21:	Heavy Oil Category – Belridge crude oil with dispersant EEMs	208
Figure D.22:	Heavy Oil Category – Hondo crude oil with dispersant EEMs	209
Figure D.23:	Heavy Oil Category – IFO-300 crude oil with dispersant EEMs	210
Figure D.24:	Heavy Oil Category – Access Western Blend oil with dispersant EEMs.....	211
Figure D.25:	Dilbit Oil Category – Cole Lake oil with dispersant EEMs	212
Figure E.1:	Plot of fluorescence intensity at five selected excitation/emission pairs (top left) for all water samples collected aboard the R/V <i>Weatherbird II</i> at DSH10 on 10 August 2010 and depth profile of CTD data for dissolved oxygen and salinity (top right).....	214
Figure E.2:	Fluorescence intensity at selected Ex/Em wavelength pairs for all water samples at DSH08 in December 2010 (above) and depth profile for oxygen, temperature and salinity from CTD data (below)	215
Figure E.3:	EEMs of water samples with highest oil-type fluorescence signatures at DSH08 in December 2010: at the surface (above) and at 50 m (below)	216
Figure E.4:	Fluorescence intensity at selected wavelength pairs for all water samples at DSH08 in February 2011 (above) and oxygen, temperature and salinity (below) from CTD data.....	217
Figure E.5:	EEMs of water samples at the surface (above) and at 55 m (below) at DSH08 in February 2011, both showing oil fluorescence signatures.....	218
Figure E.6:	Fluorescence intensity at selected wavelength pairs for all water samples at DSH08 in May 2011 (upper) and oxygen, temperature and salinity (lower) from CTD data	219
Figure E.7:	EEMs of water samples at 50 m (top) and 1000 m (bottom) at DSH08 in May 2011 both show reduced oil signatures.....	220
Figure E.8:	Fluorescence intensity at Ex/Em 275 nm/324 nm, indicative of the presence of oil in the water column, at DSH08 in December 2010, February 2011, and May 2011 for all depths (above) and for depths only to	

	400 m (below) in order to visually separate samples collected at shallower depths	221
Figure E.9:	Fluorescence intensity at selected wavelength pairs for all water samples at DSH10 in December 2010 (above) and oxygen, temperature and salinity (below) from CTD data.....	222
Figure E.10:	EEMs of water samples at the surface (top) and 35 m (bottom) at DSH10 in December 2010	223
Figure E.11:	Fluorescence intensity at selected wavelength pairs for all water samples at DSH10 in February 2011 (upper) and oxygen, temperature and salinity (lower) from CTD data	224
Figure E.12:	EEMs of water samples (a) at the surface (b) 75 m (c) 1000 m and (d) 1200 m at DSH10 in February 2011	225
Figure E.13:	Fluorescence intensity at selected wavelength pairs for all water samples at DSH10 in May 2011 (upper) and oxygen, temperature and salinity (lower) from CTD data	226
Figure E.14:	EEMs of water sample at 21 m (top) and 75 m (bottom) at DSH10 in May 2011.....	227
Figure E.15:	Fluorescence intensity at Ex/Em 275 nm/324 nm, indicative of the presence of oil in the water column, in December 2010, February 2011, and May 2011 at DSH10 for all depths (upper) and for depths only to 400 m (lower) in order to visually separate samples collected at shallower depths	228
Figure E.16:	Fluorescence intensity at selected wavelength pairs for all water samples at PCB06 in December 2010 (upper) and oxygen, temperature and salinity (lower) from CTD data	229
Figure E.17:	EEMs of water samples at the surface (top left), 45 m (top right), and 60 m at PCB06 in December 2010.....	230
Figure E.18:	Fluorescence intensity at selected wavelength pairs for all water samples at PCB06 in February 2011 (upper) and oxygen, temperature and salinity (lower) from CTD data	231
Figure E.19:	EEMs of water samples at the surface (top) and 17 m (bottom) at PCB06 in February 2011	232

Figure E.20: Fluorescence intensity at Ex/Em 275 nm/324 nm, indicative of the presence of oil in the water column, in December 2010 and February 2011 at PCB06 for all depths233

LIST OF ACRONYMS

ACT	Alliance for Coastal Technology
ANS	Alaska North Slope
API	American Petroleum Institute
BFT	Baffle Flask Test
BIO	Bedford Institute of Oceanography
BTEX	Benzene, Toluene, Ethylbenzene, and Xylene
CANDECOMP	Canonical Decomposition
CCD	Charge Coupled Device
CDOM	Colored Dissolved Organic Matter
CDR	Chemical Dispersibility Ratio
COOGER	Centre for Offshore Oil, Gas and Energy Research
CPS	Counts per Second (photons)
CTD	Conductivity – Temperature – Density
DE	Dispersant Effectiveness
DFO	Department of Fisheries and Oceans, Canada
DOM	Dissolved Organic Matter
DOR	Dispersant to Oil Ratio
DOSS	Dioctyl Sodium Sulfosuccinate
DWH	Deepwater Horizon
EEM	Excitation Emission Matrix
EEMS	Excitation Emission Matrix Spectroscopy
EPA	Environmental Protection Agency
EXDET	Exxon Dispersant Effectiveness Test
Ex/Em	Excitation/Emission
FDOM	Fluorescent Dissolved Organic Matter
FDR	Fluorescence Dispersibility Ratio
FID	Flame Ionization Detector
FIO	Florida Institute of Oceanography

FIR	Fluorescence Intensity Ratio
F _{max}	Fluorescence maximum
FRET	Fluorescence Resonance Emission Transfer
FWHM	Full Width Half Maximum
GC–FID	Gas Chromatography–Flame Ionization Detector
GC ×GC	Two-Dimensional Gas Chromatography
GC–IRMS	Gas Chromatography – Isotope Ratio Mass Spectrometry
GC–MS	Gas Chromatography–Mass Spectrometry
GC–MS–MS	Gas Chromatography with Metastable Ion Reaction Monitoring
GF/F	Glass Microfiber Filters
HPLC	High Performance Liquid Chromatography
IFE	Inner Filter Effect
IFO	Intermediate Fuel Oil
IOOS	Integrated Ocean Observing System
JAG	Joint Analysis Group for Surface and Sub-Surface Oceanography, Oil and Dispersant Data (NOAA)
MC252	Mississippi Canyon Block 252
MESA	Medium South American (oil type)
MOSSFA	Marine Snow Sedimentation and Flocculent Accumulation
NOAA	National Atmospheric and Oceanic Administration
NCP	National Oil and Hazardous Substances Pollution Contingency Plan
OHMSETT	Oil and Hazardous Materials Simulated Environmental Test Tank
PAH	Polycyclic Aromatic Hydrocarbon
PARAFAC	Parallel Factor Analysis
PTFE	Polytetrafluoroethylene
QSE	Quinine Sulfate Equivalents
RU	Raman Units
SFT	Swirling Flask Test
SMART	Special Monitoring of Applied Response Technologies
SSC	Scotian Shelf Condensate
TPH	Total Petroleum Hydrocarbons
USF	University of South Florida
WSL	Warren Spring Laboratory

ABSTRACT

The genesis of this research was the Deepwater Horizon oil spill, which discharged petroleum and gas into the Gulf of Mexico for 87 days in 2010. High-resolution fluorescence spectroscopy was employed for the detection of petroleum in seawater samples following the oil spill.

Fluorescence arises from the chemical structure of π -bonding in C=C bonds, especially those in aromatic structures. Spectrofluorometry was also used to observe and track the formation of petroleum plumes in seawater undergoing controlled physical dispersion in a wave tank, both with and without the addition of chemical dispersant. Further, the changing fluorescence characteristics of a broad range of 25 types of petroleum, with the addition of chemical dispersant at differing application rates, were investigated in the laboratory.

Following the guidance provided in the U.S. SMART protocol, many researchers employed a variety of in situ fluorometers to inform their water sampling efforts in tracking the oil spill, as well as to gauge the effectiveness of chemical dispersant application to surface slicks. Excitation emission matrix spectroscopy (EEMS) was performed on discrete water samples collected and analyzed, both at sea and in our laboratory in the year following the DWH oil spill, in order to investigate the optimal excitation and emission wavelengths for the detection of petroleum.

In order to further explore the performance of in situ fluorometers used following the DWH oil spill, EEMS analysis was performed on discrete water samples collected in a series of wave tank

experiments conducted at the Bedford Institute of Oceanography (BIO) in Nova Scotia, Canada. In situ fluorometers were mounted within the wave tank, which was then filled with filtered seawater from Halifax Harbor. A randomized series of experiments using oil collected from the DWH oil spill, both fresh and weathered, with and without the addition of chemical dispersant, was conducted over a two-week period. High-resolution EEMs of water samples collected at specific time points were compared with the fluorescence signals collected with in situ instruments, as well as with chemical analysis by GC/MS.

Finally, a series of experiments was conducted to investigate the variation in fluorescence signals exhibited by a broad variety of oil types. EEMS analyses of 25 types of oil, both without the addition of chemical dispersant, and at three different dispersant to oil ratios (DORs) was performed using artificial seawater in baffled trypsinizing flasks on a shaker table. Chemical analysis was also performed by GC/MS on oil-in-water samples, with no chemical dispersant added, and on samples at the highest DOR of 1:20. Parallel Factor Analysis (PARAFAC) was utilized in an attempt to identify components specific to petroleum, dispersant, and/or natural colored dissolved organic matter (CDOM) both within each experimental series and across all samples. Four characteristic oil-type fluorescence peaks were identified in the EEMS analyses. A clear linear relationship was seen between fluorescence intensity and concentration of 2-ring polycyclic aromatic hydrocarbons (PAHs) in oil-water without chemical dispersant; however, the relationship between fluorescence intensity and PAH concentration at highest chemical DOR was not straightforward. Comparison of fluorescence intensity in the four peak regions enabled a division into two overarching oil types related to oil viscosity. As evidenced by EEMS, higher viscosity Type II oils do not respond well to the addition of chemical dispersant. PARAFAC

analysis showed changes in the contribution of intensity from different fluorescence regions with increasing levels of dispersion, likely related to the action of chemical dispersant reducing oil droplet size, which in turn reduces reabsorption of fluorescence.

Results of EEMS analysis of wave tank samples provided good agreement with the signal from all in situ fluorometers tested and showed that all instruments would have been able to detect oil-type fluorescence in the field. Differences were noted in the evolution of fluorescence peak location over the 90-minute course of the experimental series between oil with and without chemical dispersant. Highest intensity oil-type fluorescence was found at the excitation and emission wavelength pair known to be characteristic of naphthalene. Chemical analyses showed a relationship between 2-ring and 3-ring PAHs only with dispersed oil. Good correspondence was also seen between total benzene, toluene, ethylbenzene and xylene (BTEX) concentration and a ratio of fluorescence intensity at two emission wavelengths. PARAFAC analysis showed agreement with components found in the baffle-flask series.

EEMS analyses of field samples collected in the Gulf of Mexico in the year following the DWH oil spill show correspondence between fluorescence intensity in the oil-type regions seen in both the bench-scale and mesoscale experimental series. An interesting evolution of oil-type fluorescence intensity over the course of the three research cruises showed the continued presence of petroleum at or near the surface, as well as a continued deep-water petroleum signature through May 2011. The interplay of fluorescence intensity at oil-type and protein-type fluorescence regions also appeared to show the response of oil-degrading bacteria.

This research has shown the presence of fluorescence peak regions characteristic of petroleum, which can be distinguished from protein-like and CDOM-like fluorescence naturally present in the marine environment. Further, fluorescence measurements can be accomplished with very small quantities of sample (3 mL), are relatively fast to process, do not involve complex pre-processing, and are sensitive down to the ppb range. PAHs are known to be toxic at very low concentrations. Chronic petroleum spills are ubiquitous, and with petroleum exploration in ever more extreme environments, future large-scale spills are unfortunately likely to occur. The ability to track petroleum spills, especially in deep sub-surface plumes, will facilitate rapid response efforts to protect vulnerable marine ecosystems, which are still little-understood or perhaps even remain undiscovered.

GENERAL INTRODUCTION

FLUORESCENCE SPECTROSCOPY

Fluorescence is one of two forms of luminescence, or the emission of light from a substance; the other being phosphorescence. One of the earliest observations of natural fluorescence was made by Sir John Frederick William Herschel in 1845 when he observed the “beautiful celestial blue colour” apparent in a quinine solution exposed to sunlight. We now understand that it is the aromatic ring structure present in the quinine molecule, which is responsible for the phenomenon he observed. Other aromatic molecules that emit fluorescence, including fluorescein and rhodamine b, which give antifreeze a green or red-orange glow, the proteins — tyrosine, tryptophan and phenylalanine, and polycyclic aromatic hydrocarbons (Lakowicz 2006).

Sir G. G. Stokes is responsible for the term “fluorescence” as his initial research involved exposing the mineral fluorspar to UV light and noting the resulting emission of blue light. Following the publication of Herschel’s observation of light emitted by the quinine solution, Stokes did further research with quinine sulfate solutions. In 1852 he noted the fact that emitted fluorescence typically has less energy, or lower wavelength, than the excitation energy absorbed by a material. This is known as Stokes Law or the Stokes Shift (Lakowicz 2006; Abramowitz and Davidson 2012).

The processes that take place between the absorption and emission of light are illustrated by the Jablonski diagram (Figure 1), named for Polish physicist Professor Alexander Jablonski (1898-1980), who is considered to be the father of fluorescence spectroscopy.

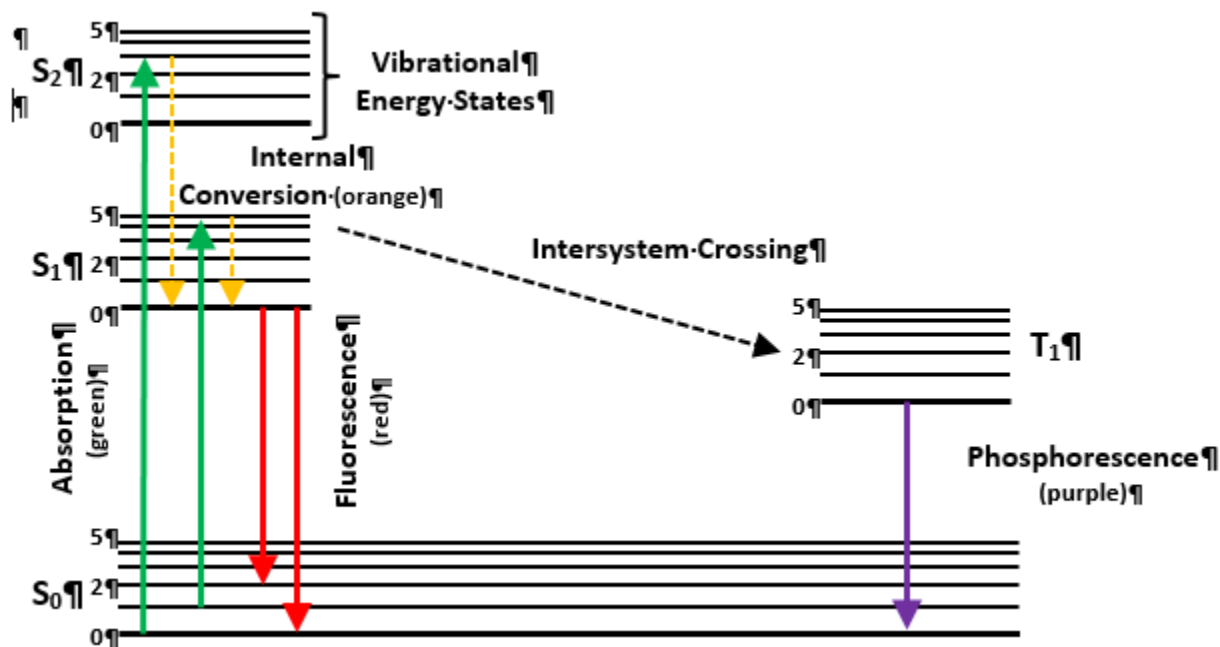


Figure 1.1. Jablonski diagram illustrating the processes at play in luminescence (patterned after Lakowicz 2006).

Upon excitation by incident photons, electrons in fluorophores (molecules capable of fluorescence) are promoted from the ground state to an excited state ($S_0 \rightarrow S_n$). Return of electrons from higher excited states to the S_1 orbital occurs in approximately 10^{-12} s via non-radiative routes—rotational and/or vibrational relaxation. In the excited singlet state, when an electron in the S_1 orbital is paired with an electron having opposite spin in the ground state, return of the excited electron to the S_0 orbital is allowed and takes place rapidly—on the order of 10^{-8} s — occurring with energy released in the emission of a photon. Fluorescence lifetime can thus be defined as the average time between the excitation and the return to ground state of a

fluorophore and is typically on the order of 10 ns, but can be in the sub-nanosecond range (Lakowicz 2006). Formally, the fluorescence lifetime is defined as the time in which the initial fluorescence intensity of a fluorophore decays to $1/e$ (~37 %) of the initial intensity. Quantum yield is the number of emitted photons with respect to the number of absorbed photons; therefore, fluorophores with the highest quantum yields display the brightest emissions (Lakowicz 2006).

When an excited fluorophore collides with another molecule before release of a photon through fluorescence, that energy may be transferred in the collision, resulting in quenching of the fluorophore. Energy may also be transferred between two fluorophores in a non-collisional process known as fluorescence resonance emission transfer (FRET). This process results in quenching of the first fluorophore with enhanced fluorescence of the second.

If, however, an excited electron undergoes spin conversion resulting in a spin, which is parallel to the paired electron in the ground state, intersystem crossing to the T_1 , or triplet state, takes place resulting in phosphorescence rather than fluorescence. The transition from the T_1 state to the ground state is “forbidden,” so transition time is comparatively slow—on the order of 10^{-3} to 10^0 s. Phosphorescent lifetimes are typically in the range of milliseconds to seconds, and may be even longer (Lakowicz 2006; Johnson and Davidson 2012).

Fluorescence spectroscopy has been used for decades to investigate the properties and distribution of the light-reactive constituent of dissolved organic matter (DOM) in the marine environment (Chen and Bada 1992; Coble 1996). Following his earlier work on absorption of

light by seawater, Kurt Kalle discovered in 1949 that seawater fluoresced upon irradiation with ultraviolet light, coining the term “Gelbstoff”—literally “yellow matter” in his native German—to identify the material responsible for this phenomenon (Duursma 1974). Kirk (1976) suggested a change to the term “gilvin” (from the Latin term meaning pale yellow), however we now commonly refer to this material as colored (or chromophoric) dissolved organic matter (CDOM). It is important to note that while all CDOM absorbs light, not all emits fluorescence. Therefore, the portion of dissolved organic matter that emits fluorescence is termed FDOM.

Following on this early work, two overall types of FDOM were identified by researchers: humic-like substances, recognized by excitation at 230-260 nm and 320-350 nm paired with emission at 420-450, and protein-like substances with excitation at 220 nm and 275 nm and with emission at 300-305 nm (characteristic of tyrosine), and emission at 340-350 nm (characteristic of tryptophan). Today, spectrofluorometers are equipped with monochromators, which allow greater wavelength resolution, high-intensity xenon lamps that are capable of excitation energy at the low end of the ultraviolet range, and photomultiplier tubes or CCD detectors. These improvements in fluorescence detection make high resolution characterization of FDOM possible. Coble et al. (1990) introduced the use of excitation-emission matrix (EEM) spectroscopy for the identification of CDOM. To record EEMs, the excitation spectra and emission spectra of a substance are recorded simultaneously. The resulting three-dimensional map of sample fluorescence enables the detection of multiple fluorescence peaks, potentially characterizing multiple components. (HORIBA Instruments Incorporated, 2013) Fluorophores now identifiable in natural waters include proteins, pigments, lignin phenols, humic substances and hydrocarbons (Coble 1996; Coble et al. 2014).

PETROLEUM AND FLUORESCENCE SPECTROSCOPY

Petroleum is an assemblage of naturally-occurring complex mixtures of hundreds, if not thousands, of hydrocarbon compounds. As the chemical composition of crude petroleum varies widely, characterization has historically required the employment of a great deal of time as well as complex instrumentation in gravimetric, solvent extraction, and chromatographic laboratory methods (Ryder 2005). Spectroscopic techniques, however, have been used in the petroleum industry for over half a century in mud logging and in analysis of core samples in the field (Ryder 2005), as well as more recently in the characterization of crude oil for improved optimization in the refining process (Steffens et al. 2011).

Petroleum hydrocarbons fluoresce due to the presence of a wide variety of aromatic structures — from simple benzene ring structures to highly complex asphaltenes. Hydrocarbon fluorescence is strongly influenced by chemical composition, with heavier crude oils having broad, higher-wavelength, and less intense emission bands, as well as shorter fluorescence lifetimes than lighter oils. Fluorescence spectroscopy has great, though as yet unproven, potential for identification of chemical composition. However, the chemical complexity of fluorophores and quenching species present in the composition of petroleum, coupled with inherent physical properties, such as viscosity and optical density, do present unique analytical challenges (Steffens et al. 2011)

With pure substances (e.g., chlorophyll *a*), emission wavelength is independent of excitation wavelength. However, the chemical complexity of petroleum results in differing emission profiles with variation in excitation wavelength, most likely due to the excitation of different

fluorophore populations. Quantum yields and fluorescence lifetimes of petroleum are also highly dependent on excitation wavelength, with UV excitation giving best results (Ryder 2005). This is strong evidence for the need for broad spectrum EEMs analysis in order to determine whether deeper UV excitation would result in improved petroleum detection in the marine environment. The advantages of the high selectivity and sensitivity of fluorescence spectroscopy, coupled with the non-destructive nature and relative ease of sample analysis, and the portability of the latest instruments, combine to make this method a potentially powerful analytical tool for the investigation of petroleum in this arena.

FLUORESCENCE SPECTROSCOPY AND THE *DEEPWATER HORIZON* OIL SPILL

From the initial blowout on April 20, 2010, to the capping of the wellhead on July 15, 2010, an estimated 4.93 million barrels of light sweet crude oil ($\pm 10\%$) were released at a depth of approximately 1500 m (Federal Interagency Solutions Group 2010). Additionally, an estimated 2.1 million gallons of chemical dispersant were applied between May 15 and July 12 in an effort to prevent the oiling of beaches and sensitive wetlands (Mascarelli 2010; National Oceanic and Atmospheric Administration 2010). Approximately 0.77 million gallons of the dispersant Corexit® 9500A were introduced directly via a jet placed into the petroleum flowing from the wellhead and another 1.4 million gallons of Corexit® 9500A and/or Corexit® 9527 were applied at the surface by aircraft or from small vessels (Kujawinski et al. 2011). While dispersant to oil ratios (DORs) varied widely under real-world conditions, the target DOR was 1:20 (Federal Interagency Solutions Group 2010; Incident Specific Preparedness Review Team 2011), based on the successful application of dispersant in a 1966 tanker spill off the coast of Wales (Purnell 2002), as well as work by Khelifa et al. (2009). This was the first time in history that dispersant

was applied at depth, and it appears to have changed not only the physical behavior of the petroleum via enhancing the formation of small droplets, which remained in suspension within a sub-surface plume; but also the solubility of the petroleum compounds, and therefore detectability.

In the month immediately following the blowout, scientists from universities and governmental agencies responded by gathering available instruments and travelling to the vicinity of the *Deepwater Horizon* (DWH) wellhead in order to determine the scope and impact of the spill, including researchers from the University of South Florida (USF) College of Marine Science. The National Atmospheric and Oceanic Administration (NOAA) deployed eight ships on various missions during the summer of 2010, including the R/V *Brooks McCall*. Many research groups conducted water column profiling in the northeastern Gulf of Mexico, and observations recorded often included fluorescence. However, the in situ fluorometers utilized are typically configured to operate within a very narrow range of excitation-emission wavelengths, largely due to the inherent limitations of broad-spectrum light sources. Most of these instruments were configured to wavelengths appropriate either for the detection of CDOM or for detection of chlorophyll *a*. One such instrument was the WET Labs' ECO CDOM fluorometer used on the R/V *Brooks McCall*. Bench-top calibration of the instrument response to various concentrations of dispersed Mississippi Canyon (MC)252 source oil — petroleum from the wellhead — in seawater was conducted at Louisiana State University. While this instrument was designed to be capable of detecting CDOM in the ppb range, results showed that the ECO CDOM fluorometer was capable of detecting petroleum only down to approximately 1 ppm (Joint Analysis Group for the Deepwater Horizon Oil Spill 2011). The testing protocol also found that fluorescence quenching

occurred with increased DOR (Joint Analysis Group (JAG) for the Deepwater Horizon Oil Spill 2011).

Another fluorometer deployed in the Gulf of Mexico in the months following the DWH oil spill was targeted specifically at petroleum detection — the Chelsea AQUAtracka aromatic hydrocarbon fluorometer (λ_{ex} 239 nm/ λ_{em} 360 nm). Camilli et al. (2010) tracked fluorescence to the southwest of the wellhead using this instrument, as well as Seapoint Sensors' SUVF CDOM fluorometer (λ_{ex} 370 nm/ λ_{em} 440 nm). These researchers found the response from the Chelsea instrument was more highly correlated with methane, benzene, and naphthalene levels detected by the TETHYS mass spectrometer than was the response from their SUVF CDOM fluorometer (Camilli et al. 2010), indicating that the deeper UV excitation/emission of the AQUAtracka instrument was better able to identify the complex sub-surface plume. They also found an oxygen anomaly detected at approximately 950 m, which corresponded with the fluorescence response from the Chelsea instrument, but not with the response from the SUVF CDOM fluorometer. This would also appear to indicate that the higher excitation/emission wavelengths of the SUVF instrument configuration might have lied in the region of a fluorescence shoulder rather than targeting the true F_{max} .

PARAFAC ANALYSIS

Originally designed to model complexity in the field of psychometrics (Carroll and Chang 1970; Harshman 1970), parallel factor analysis (PARAFAC), also known as canonical decomposition (CANDECOMP), was first employed in the analysis of fluorescence data within the following decade (Appelhof and Davidson 1981). More recently, PARAFAC has been widely embraced by

chemometricians and used to tease apart the overlapping fluorescence components of complex chemical mixtures containing fluorescent substances ranging from proteins and pigments to pesticides and PAHs (Anderson and Bro 2003). PARAFAC analysis thus enables the decomposition of the complex, three-way data produced in an EEM analysis into some number of component signals (Bro 1997). In their application of PARAFAC analyses to PAH mixtures, Selli et al. (2004) found the ability to separate and identify five different factors correlated with five PAH compounds. More recently, PARAFAC has been used in the analysis of the fate and transport of dispersed oil from the DWH oil spill (Mendoza et al. 2013; Zhou et al. 2013; D'Sa et al. 2016).

Presented with hundreds of complex fluorescence EEM data sets containing [samples x excitation x emission] data, PARAFAC analysis can reduce this complexity to [samples x intensity at a few important wavelength pairs] (Murphy et al. 2014). In the past, this information gathering was often done via time-consuming “peak-picking”, whereby EEMs were visually inspected for apparent F_{\max} location, then fluorescence intensity data at that excitation/emission point was copied and pasted into a spreadsheet for further analysis. While that method is still widely used, PARAFAC provides the capability to turn what is a somewhat qualitative task into a more quantitative exercise. However, careful preparation of the data is critical in order to obtain a meaningful outcome. PARAFAC analysis also allows the consideration of minor fluorescence peaks, which may have been missed due to overwhelm by higher-intensity major peaks, but these may be no less informative in the analysis of EEM results. More importantly, PARAFAC analysis allows for direct comparison to chemical composition upon successful modelling of an EEM data set (Murphy et al. 2014). The steps that must be undertaken for

successful PARAFAC analysis are: (1) importing raw data and assembling the dataset; (2) preprocessing to correct biases, removing scatter and normalizing the data; (3) exploring the dataset to remove possible outliers and developing preliminary models; (4) validating the model by determining the proper number of components and evaluating model fit; (5) interpreting results (Murphy et al. 2013).

SUMMARY

Throughout geologic history, petroleum hydrocarbons have entered the environment through natural seeps and erosion in a fairly limited yet chronic mode (Bartha 1986). As these natural sea floor seepages are not subject to the erosive forces present in the terrestrial environment, they may be vast and sustained over long periods of time (Varney 2000). However, petroleum hydrocarbons in the marine environment occurred at relatively minor levels until human activities radically increased their presence in the 20th century. As input levels become amplified through anthropogenic introduction, either through the chronic, ongoing leaks that constitute the overall largest volume, or through attention-getting catastrophic spill events, petroleum hydrocarbons become marine pollutants, occupying an intermediate position in the range between highly biodegradable and highly recalcitrant substances (Bartha 1986).

While the DWH oil spill was the first time an incident of this proportion and at this extreme depth has occurred, it is undoubtedly not the last. The Gulf Coast is the largest source of offshore U.S. oil and gas resources, and drilling activities have continually increased over the past two decades. Louisiana's outer continental shelf, where the DWH accident occurred, is the most extensively developed petroleum region in the country (Thibodeaux et al. 2011). This was

also the first time that chemical dispersants were utilized in large volume, applied not just at the surface, but injected into the pressurized multiphase jet of gas and petroleum emerging from the wellhead.

At present, many chemodynamic processes involving petroleum and dispersants within the water column and in the benthos are poorly understood, and some are completely unknown (Thibodeaux et al. 2011). As the U.S. moves forward with the extraction of petroleum resources from geologic formations in ever deeper waters, it is imperative that we better understand the potential behavior of hydrocarbons — both petroleum and dispersants — at the extremes of pressure and temperature present in that environment. Our goal was the use of spectrofluorometry coupled with PARAFAC statistical analyses, to quite literally shed new light on these important questions in the hope that this research could also provide first responders with valuable information with respect to instrumentation and approaches suitable for rapid detection of petroleum hydrocarbons in the ocean. This is critical for facilitating quick decision-making during to mitigate the toxicity of petroleum hydrocarbons and dispersants to sensitive marine ecosystems.

Although a catastrophic spill event inspired my interest in this research direction, the widespread use of petroleum hydrocarbons in today's world inevitably results in chronic petroleum discharge to the natural environment, from both accidental and intentional releases during its extraction, transportation, and consumption. It is estimated that approximately 260,000 metric tons of petroleum enter the waters off North America each year; assuming an average specific gravity for petroleum of 0.88, this is equivalent to 1.9 million barrels of oil (U.S. National Resource

Council 2003). Improvements in the use of spectrofluorometry will enable greater sensitivity, as well as faster and easier detection of petroleum in the marine environment. Therefore, this research has the potential to be important for the detection and remediation of chronic petroleum inputs as well for catastrophic events, sparing sensitive marine ecosystems from the known toxicity of components such as PAHs, which are listed in the Clean Water Act as section 307 Toxic Pollutants (JiJi et al. 2000), and can be damaging from the cellular level to lethal for marine organisms as well as humans.

While the chronological order of my investigations ranged from the largest scale to the smallest, the following chapters of my thesis will begin with the smallest scale and progress to the largest scale in order to best inform results found in the field samples.

REFERENCES

- Introduction to fluorescence. 2012. Olympus America Inc.; [accessed 24 September 2012]. <http://www.olympusmicro.com/primer/lightandcolor/fluorointroduction.html>.
- Anderson CM, Bro R. 2003. Practical aspects of parafac modeling of fluorescence excitation-emission data. *Journal of Chemometrics*. 17:200-215.
- Appelhof CJ, Davidson ER. 1981. Strategies for analyzing data from video fluorometric monitoring of liquid chromatographic effluents. *Analytical Chemistry*. 53(13):2053-2056.
- Bartha R. 1986. Biotechnology of petroleum pollutant biodegradation. *Microbial ecology*. 12(1):155-172.
- Bro R. 1997. Parafac. Tutorial and applications. *Chemometrics and Intelligent laboratory Systems*. 38:149-171.
- Camilli R, Reddy CM, Yoerger DR, Van Mooy BAS, Jakuba MV, Kinsey JC, McIntyre CP, Sylva SP, Maloney JV. 2010. Tracking hydrocarbon plume transport and biodegradation at deepwater horizon. *Science*. 330:201-204.
- Carroll JD, Chang J-J. 1970. Analysis of individual differences in multidimensional scaling via an n-way generalization of "eckart-young" decomposition. *Psychometrika*. 35(3):283-319.

- Chen RF, Bada JL. 1992. The fluorescence of dissolved organic matter in seawater. *Marine Chemistry*. 37:191-221.
- Coble PG. 1996. Characterization of marine and terrestrial dom in seawater using excitation-emission matrix spectroscopy. *Marine Chemistry*. 51:325-346.
- Coble PG, Green SA, Blough NV, Gagosian RB. 1990. Characterization of dissolved organic matter in the black sea by fluorescence spectroscopy. *Nature*. 348(6300):432-435.
- Coble PG, Spencer RM, Baker A, Reynolds DM. 2014. Aquatic organic matter fluorescence. In: Coble PG, Lead J, Baker A, Reynolds DM, Spencer RM, editors. *Aquatic organic matter fluorescence*. New York, NY: Cambridge University Press. p. 75-122.
- D'Sa EJ, Overton EB, Lohrenz SE, Maiti K, Turner RE, Freeman A. 2016. Changing dynamics of dissolved organic matter fluorescence in the northern gulf of mexico following the deepwater horizon oil spill. *Environmental science & technology*. 50:4940-4950.
- Duursma EK. 1974. The fluorescence of dissolved organic matter in the sea. In: Jerlov NG, Nielsen ES, editors. *Optical aspects of oceanography*. London: Academic Press. p. 237-256.
- Federal Interagency Solutions Group, Oil Budget Calculator Science and Engineering Team,. 2010. Oil budget calculator--deepwater horizon.
- Harshman RA. 1970. Foundations of the parafac procedure: Models and conditions for an "explanatory" multimodal factor analysis. *UCLA Working Papers in Phonetics*. 16:1-84.
- Incident Specific Preparedness Review Team. 2011. Deepwater horizon oil spill. In: U.S. Department of Homeland Security USCG, editor. Washington, DC.
- JiJi RD, Andersson GG, Booksh KS. 2000. Application of parafac for calibration with excitation-emission matrix fluorescence spectra of three classes of environmental pollutants. *Journal of Chemometrics*. 14:171-185.
- Jablonski energy diagram. 2012. Olympus America Inc.; [accessed 24 September 2012]. <http://www.olympusmicro.com/primer/java/jablonski/jabintro>.
- Joint Analysis Group (JAG) for the Deepwater Horizon Oil Spill, 2011,. 2011. Review of preliminary data to examine subsurface oil in the vicinity of mc252#1, may 19 to june 19, 2010. In: U.S. Department of Commerce, National Oceanic and Atmospheric Administration, editor. Silver Spring, MD.
- Joint Analysis Group for the Deepwater Horizon Oil Spill. 2011. Review of r/v brooks mcall data to examine subsurface oil. In: NOAA, editor. Silver Spring, MD.
- c2009. 2009; Ottawa, Ontario. Environment Canada.
- Kirk JTO. 1976. Yellow substance (gelbstoff) and its contribution to the attenuation of photosynthetically active radiation in some inland and coastal south-eastern australian waters. *Australian Journal of Marine & Freshwater Research*. 27(1):61-71.
- Kujawinski EB, Kido Soule MC, Valentine DL, Boysen AK, Longnecker K, Redmond MC. 2011. Fate of dispersants associated with the deepwater horizon oil spill. *Environmental science & technology*. 45:1298-1306.
- Lakowicz JR. 2006. *Principles of fluorescence spectroscopy*. Springer.

- Mascarelli A. 2010. Debate grows over impact of dispersed oil. *Nature*. [accessed 2 April 2012]<http://www.nature.com/news/2010/100710/full/news.2010.347.html>. doi:doi:10.1038/news.2010.347.
- Mendoza WG, Riemer DD, Zika RG. 2013. Application of fluorescence and parafac to assess vertical distribution of subsurface hydrocarbons and dispersant during the deepwater horizon oil spill. *Environmental Science Processes & Impacts*. 15(1017-1030).
- Murphy KR, Bro R, Stedmon CA. 2014. Chemometric analysis of organic matter fluorescence. In: Coble PG, Lead J, Baker A, Reynolds DM, Spencer RGM, editors. *Aquatic organic matter fluorescence*. Cambridge University Press. p. 339-375.
- Murphy KR, Stedmon CA, Graeber D, Bro R. 2013. Fluorescence spectroscopy and multi-way techniques. *Parafac. Analytical Methods*. 5(23):6557-6566.
- National Oceanic and Atmospheric Administration. 2010. Unh coastal response research center, noaa, epa and coast guard convene science meeting to study dispersant use and ecosystem impacts of dispersed oil in the gulf of mexico. In: Commerce USDo, editor.
- Purnell K. 2002. Oil spill dispersants--myths & mysteries unravelled. *Swedish Club Letter*. [accessed 2 April 2012];1-2002:16-17. http://www.itopf.com/_assets/documents/swedishclub.pdf.
- Ryder AG. 2005. Analysis of crude petroleum oils using fluorescence spectroscopy. In: Geddes CD, Lakowicz JR, editors. *Reviews in fluorescence 2005*. Springer. p. 169-198.
- Selli E, Zaccaria C, Sena F, Tomasi G, Bidoglio G. 2004. Application of multi-way models to the time-resolved fluorescence of polycyclic aromatic hydrocarbons mixtures in water. *Water research*. 38(9):2268-2275.
- Steffens J, Landulfo E, Courrol LC, Guardani R. 2011. Application of fluorescence to the study of crude petroleum. *Journal of fluorescence*. 21:859-864.
- Thibodeaux LJ, Valsaraj KT, John VT, Papadopoulos KD, Pratt LR, Pesika NS. 2011. Marine oil fate: Knowledge gaps, basic research, and development needs; a perspective based on the deepwater horizon spill. *Environmental Engineering Science*. 28(2):87-93.
- U.S. National Resource Council. 2003. Executive summary. *Oil in the sea iii: Inputs, fates and effects*. National Academy of Sciences.
- Varney MS. 2000. *Chemical sensors in oceanography* / edited by mark s. Varney. Amsterdam: Gordon and Breach.
- Zhou Z, Guo L, Shiller AM, Lohrenz SE, Asper VL, Osburn CL. 2013. Characterization of oil components from the deepwater horizon oil spill in the gulf of mexico using fluorescence eem techniques. *Marine Chemistry*. 148:10-21.

**SCALE LEVEL I – EVALUATING EFFECTIVENESS OF PHYSICAL AND
CHEMICAL DISPERSION OF OIL IN SEAWATER USING THE BAFFLED FLASK
TEST FOR SPECTROFLUOROMETRIC ANALYSIS OF 25 TYPES OF PETROLEUM**

INTRODUCTION

Fluorescence spectroscopy has been used for decades to investigate the properties and distribution of the light-reactive constituent of DOM in the marine environment (Chen and Bada 1992; Coble 1996). Coble et al. (1990) first used excitation-emission matrix EEMS for the identification of CDOM and identified a useful new piece of information—the wavelength independent fluorescence maximum (F_{\max}). Fluorophores now identifiable in natural waters include proteins, pigments, lignin phenols, humic substances, as well as hydrocarbons (Coble 1996; Coble et al. 2014).

Petroleum is an assemblage of naturally-occurring complex mixtures of hundreds, if not thousands, of hydrocarbon compounds. As the chemical composition of crude petroleum varies widely, characterization has historically required the employment of time-consuming analyses utilizing complex instrumentation for gravimetric, solvent extraction, and chromatographic laboratory methods (Ryder 2005). Spectroscopic techniques, however, have been used in the petroleum industry for over half a century in mud logging and in analysis of core samples in the field (Ryder 2005), as well as more recently in the characterization of crude oil for improved optimization in the refining process (Steffens et al. 2011).

Petroleum hydrocarbons fluoresce due to the presence of carbon to carbon bonds, especially those within aromatic structures ranging from simple benzene rings to highly complex polynuclear aromatic hydrocarbons (PAHs), such as asphaltenes. However, the greater the molecular weight of the compound, the higher the likelihood of fluorescence suppression (Strausz et al. 2009). Thus fluorescence is strongly influenced by chemical composition, with heavier crude oils having broad, higher-wavelength, less intense emission bands than lighter oils. Therefore, fluorescence spectroscopy has great potential for identification of chemical composition, i.e., fingerprinting. However, instrument to instrument comparisons, as well as relationship with other time and labor intensive petroleum detection methods (i.e., GC-FID, GC-MS, HPLC), have been lacking. Within the past decade, researchers at the Centre for Offshore Oil, Gas and Energy Research, Fisheries and Oceans Canada developed the Fluorescence Intensity Ratio (FIR) in an effort to enable better instrument to instrument comparison for bench-scale fluorometers (Bugden et al. 2008). More recently, other researchers have utilized another ratio of fluorescence intensity at specific wavelength pairs (FI), as well as the changes in spectral shape, in the detection of petroleum in the marine environment (Baszanowska and Otremba 2017). Our project builds on this important research and examines the relationship between fluorescence intensity and chemical analyses.

Petroleum spills in the marine environment, especially those originating from deep-sea drilling operations, result in multi-phase flows leading to plumes of varying inherent densities, as well as slicks of varying thickness on the ocean surface. Dispersion into and within the water column facilitates oil biodegradation by naturally occurring petroleum-degrading microorganisms, which are ubiquitous in the marine environment due to the presence of this rich source of reduced

carbon from natural oil seeps (Hazen et al. 2010; Das and Chandran 2011; Xu et al. 2018).

Naturally occurring physical dispersion by wind and currents can be enhanced by the application of chemical dispersants, which may also serve as an initial food source by oil degrading bacteria (Lee et al. 2013). Dispersants have been employed in response to more than 200 oil spills since first being utilized following the Torrey Canyon grounding off the coast of England and France (Ufford et al. 2014; Molinier et al. 2018). Their use is intended to enhance biodegradation by increasing the ratio of surface area to volume in oil droplets, thus making petroleum hydrocarbons more available to oil-degrading microbes (Lessard and DeMarco 2000; Venosa and Zhu 2003).

Designed for application to a surface slick, chemical dispersants were introduced directly into the petroleum flowing from the wellhead for the first time during the DWH blowout, with approximately 1.4 million gallons of Corexit® 9527 and 9500A applied to the sea surface and an additional 0.77 million gallons of Corexit® 9500A injected into the high-pressure oil flow at a depth of 1.5 km (Kujawinski et al. 2011; Reddy et al. 2011). With the addition of chemical dispersant to the physical forces influencing dispersion and trajectory, the resulting micron-size oil droplets created a neutrally buoyant subsurface plume observed at more than 35 km in length and approximately 1,100 m depth (Camilli et al. 2010). Fluorescence anomalies in surface waters, as well as those correlated with dissolved oxygen depressions at depths below 800 m, provided evidence of two distinct oiled regions (Diercks et al. 2010; Kessler et al. 2011; Smith et al. 2014). In-depth reviews by the Joint Analysis Group (JAG) of data collection following the DWH oil spill found a connection in the subsurface plume between in situ fluorescence intensity and dissolved oxygen (Joint Analysis Group 2010).

The U.S. SMART guidance document recommends fluorometry as the “most technologically advantageous detection method” for monitoring dispersant application. Currently the document refers to in-situ fluorometers, with fixed excitation-emission wavebands (U.S. Coast Guard et al. 2006). Following the DWH blowout, a variety of instruments were used to track spilled oil, including many off-the-shelf in situ fluorometers. Bench top scanning spectrofluorometers capable of producing 3D fluorescence EEMs also proved useful. Upon review of data collected during the spill, uncertainties regarding instrument specifications and capabilities made it clear that performance testing of sensors exposed to simulated, dispersed oil plumes was necessary (Conmy et al. 2014a). Correlating that information with bench-scale experiments would further illuminate best practices for the use of fluorometers in future spill responses. Enhanced detection of dispersed petroleum within the water column will be critical to mounting a timely spill response for effective containment and remediation in the future.

Research was planned by the Canadian Department of Fisheries and Ocean (DFO) Center for Offshore Oil, Gas and Energy Research (COOGER) into the differentiation between physical and chemical dispersion effectiveness (DE) of oil using the wave tank facilities at the Bedford Institute of Oceanography (BIO). In conjunction with that research, a series of bench-scale dispersed oil-in-seawater experiments was conducted in the Coble Lab at the USF College of Marine Science on 25 oils at four dispersant to oil ratios (DORs) using Corexit® 9500A. Analysis of the resulting 3D fluorescence EEMs for oil-specific results, as well as differing effects of dispersant and DORs, were also compared to the chemistry results of oil components, which was carried out at COOGER. Given recent advances with in situ fluorometers, enabling lower UV-wavelength detection, these findings would help to discern wavelength regions

influenced by dispersed oil within seawater, improve interpretation of fluorescence data, and inform decision-making by responders.

Chemical Oil Dispersants and the Baffle Flask Test for Dispersion Effectiveness

Dispersants were first used in the field in 1967, when 10,000 tonnes of a “detergent” manufactured by BP was poured onto the sea and shore following the Torrey Canyon tanker accident in the UK. That first generation of dispersants, which were formulated from industrial degreasers, proved to have relatively high toxicity to oil degrading microbes and, therefore, led to development of second generation dispersants specifically designed to treat oil spills (Ufford et al. 2014; Vaughn 2017). Although less toxic, these were formulated to be applied at a high DOR of 1:1 to 1:3; consequently, the large quantities required for effective oil spill treatment spurred development of third generation dispersants, which are those currently in use. Divided into Type 2, which are intended to be diluted with seawater and applied by surface vessels, and Type 3, which are concentrated and intended for application by aircraft, these are solutions of surfactants (such as dioctyl sodium sulfosuccinate, or DOSS) with minimal solvents, and additives, which may increase biodegradability, improve dissolution into an oil slick, and/or increase long-term stability. Corexit® 9527 incorporates a water matrix, while Corexit® 9500A employs a hydrocarbon solvent (Ufford et al. 2014). The principal action of all dispersants is to reduce the oil-water interfacial tension in order to promote migration of oil droplets into the water column with minimal mixing energy. The application target is to reach a concentration of surfactant molecules, which will form a uniform monolayer at the oil-water interface of oil droplets. Recommended application rates for maximum dispersant effectiveness (DE) range from DOR 1:5 to 1:100 (Ufford et al. 2014).

Studies of DE have been carried out at a wide range of scales: in the laboratory through bench-scale testing, in mid- to large-scale facilities such as wave tanks (among others), and in the field. There are inherent advantages and disadvantages to each. Field testing would understandably have the highest relationship to real-world oil spills, but is expensive, complex, and carries obvious environmental concerns. There is also a lack of control over environmental variables, which is a major drawback of wave-tank testing as well (Ufford et al. 2014). Testing at a facility such as the BIO wave tank (Fig. 2.1) does allow for replication of the same physical dispersion provided in the real world by breaking and plunging waves, but is also not completely representative of open sea conditions due to phenomena such as wall effects (Nedwed and Coolbaugh 2008), and interfacial film formation, which can affect oil spreading (King et al. 2013). The advantages of bench-scale testing, primarily using agitated flasks, are the simplicity, relatively low cost, and short duration of test runs, which make replication possible; however, problems such as wall effects and formation of surfactant films (Nedwed and Coolbaugh 2008), as well as mixing energy not consistent with plunging/breaking waves in the open sea, call into question the connection with real-world results (Ufford et al. 2014).

Before 1994, most laboratories determined DE using the Revised Standard EPA Test (Ufford et al. 2014). Detailed in the Federal Register (40 CFR Part 300; EPA 1984), this method utilized 130 L of seawater in a stainless steel tank to which a measured mass of oil and dispersant was added. A centrifugal pump would then circulate the contents of the tank, and samples would be removed from the bottom of the tank after 10 minutes to 2 hours of mixing. Following extraction into dichloromethane or chloroform, oil concentration was measured by spectrophotometry at 620 nm. Beginning in the mid-1980s, various agitated flask test methods



Figure 2.1. The wave tank facility at Bedford Institute of Oceanography. Dimensions: 32 m long, 0.6 m wide, and 2 m high (1.5 m water depth; 28,800 L volume). Breaking and non-breaking waves generated by a computer-controlled flat-type wave maker situated to provide mixing energies and achieve dispersant effectiveness observed in the field. Reprinted from “Submersible Optical Sensors Exposed to Chemically Dispersed Crude Oil: Wave Tank Simulations for Improved Oil Spill Monitoring,” by R.N. Conmy, et al., 2014, *Environmental Science & Technology*, 48, p. 1803. Copyright 2014 by American Chemical Society. Reprinted with permission.

were developed in order to reduce scale and simplify the determination of DE. These include the Warren Spring Laboratory (WSL), Exxon Dispersant Effectiveness Test (EXDET), and Environment Canada’s Swirling Flask Test (SWT). Performed by the combination of a small amount of water (120-250mL), oil and dispersant in differing types of closed containers, followed by application of various forms of mixing energy, DE was then determined by post-test measurement of oil concentration in the water column by either spectrophotometry or gas chromatography (Clayton et al. 1993). The SFT was adopted by the U.S. Environmental Protection Agency (EPA) in 1994 as the official method for evaluation of DE for the determination of a dispersant’s eligibility for listing on the National Oil and Hazardous Substances Pollution Contingency Plan (NCP) product schedule (Venosa et al. 2002). Inclusion on the list was contingent on a dispersant being at least 45% effective (the fraction of the total mass of oil entrained as droplets within the water) in dispersing South Louisiana crude oil and/or

Prudhoe Bay crude oil, and was required for a dispersant's use in the United States (Sorial et al. 2001).

However, within one year it became clear that large discrepancies existed between DE data submitted by dispersant manufacturers and that obtained by laboratories contracted by the EPA (Venosa et al. 2002). This led to a rigorous examination of all of the variables inherent in the SFT, including consideration of the flask design. Three types of flasks were tested: the modified Erlenmeyer flask with a side spout specified for use in the SFT, a modified Erlenmeyer flask with a glass stopcock added near the bottom for sample withdrawal, and a modified baffled trypsinizing flask with a glass stopcock added near the bottom of the flask for sample withdrawal. Results showed the baffled flask was most effective in DE, with results approaching 100 % (Sorial et al. 2004a; 2004b). Round robin inter-laboratory testing of DE of six dispersants was conducted by nine laboratories on two oils (South Louisiana and Prudhoe Bay crudes), using a slightly modified SFT protocol, and baffled trypsinizing flasks. Results gave better between-lab reproducibility, as well as better within-lab repeatability, using the baffle flask test (BFT) than with the SFT. It was found that, due to the design of the baffle flask, mixing energy was more similar to the over-and-under energy of wave action on the open sea, and sample withdrawal from the stopcock at the bottom of the flask prevented the remixing that occurred with tipping of the flask to decant the sample in the SFT (Venosa et al. 2002).

More recent testing measured the DE of Corexit® 9500 on 23 crude oils, comparing results from bench-scale WSL, EXDET, and BFT protocols, with a pilot test performed at the Oil and Hazardous Materials Simulated Environmental Test Tank (OHMSETT) facility in Leonardo,

New Jersey. Results strengthened the case for using the BFT as the standard test for inclusion of dispersants on the NCP, and it is now pending adoption as the EPA's official testing protocol (Holder et al. 2015).

In summary, studies of bench-scale testing of dispersants differ due to the testing variables in each protocol, including differences in container design, dispersant application method, type of mixing energy, length of settling time, and sampling method. These impact DE results, as well as making inter-method comparisons difficult. In all cases, samples are collected under static conditions following some period of settling, which is one very important difference between bench-scale testing and real world DE. (Ufford et al. 2014). Further, mixing energy differences between breaking/plunging waves and action within a flask have been questioned. Attempts to compare bench-scale testing methods with wave tank testing have been done, with varying results (Trudel et al. 2005; Kaku et al. 2006; Srinivasan et al. 2007; Li et al. 2009; Holder et al. 2015). Of the bench-scale methods included, the BFT protocol results were best correlated with wave-tank testing; however, underestimation of DE, especially for heavier weight oils, was found (S.L. Ross Environmental Research and MAR Inc. 2011; Trudel et al. 2011; Holder et al. 2015). Importantly, in bench-scale testing methods, mixing energy, mixing time, and settling time were purposely adjusted in order to create distinction between high and lower performing dispersants, while wave tank test conditions were designed solely to simulate oil spills at sea (Trudel et al. 2011). Finally, efforts began in the 1980s to correlate bench-scale and/or mid- to large-scale wave tank DE study results with real-world results (Daling and Lichtenthaler 1986/87). Trudel and colleagues found that results of wave-tank testing at OHMSETT reflected at-sea results "reasonably well" (Trudel et al. 2005).

The goal of this project was to provide laboratory analyses for the evaluation of oil fluorescence characteristics, with and without dispersant, of a wide variety of petroleum types from around the world in order to:

- Identify characteristic fluorescence intensity maxima (F_{\max}) for each oil type;
- Characterize changes in fluorescence shape and/or intensity due to the addition of dispersant at set DORs;
- Discover the potential existence of overarching groups into which oil types could be categorized based on their fluorescence characteristics;
- Compare fluorescence EEMS signatures with chemical analysis by GC-MS;
- Create an “EEMS library” containing a wide range of oil types.

MATERIALS AND METHODS

Twenty-five oil samples from the DFO and EPA stockpiles (covering a range of oil types with widely varying viscosity) were received from COOGER DFO in December 2013 (Fig. 2.2). Following an extensive literature search, a table of oil characteristics was created (Appendix A), which includes the oil industry standard, API gravity. A glassware cleaning protocol was followed to ensure highest analytical integrity: 125 mL amber glass bottles with PTFE-lined caps were acid washed followed by rinsing with fresh tap water several times. Bottles were baked overnight in a muffle furnace at 450 °C, then cooled and recapped. All other glassware (beakers, volumetric flasks, Erlenmeyer flasks, graduated cylinders, and Pasteur pipettes) were acid washed and rinsed with deionized water, rinsed with HPLC grade methanol and then placed overnight in a drying oven at 30 °C.

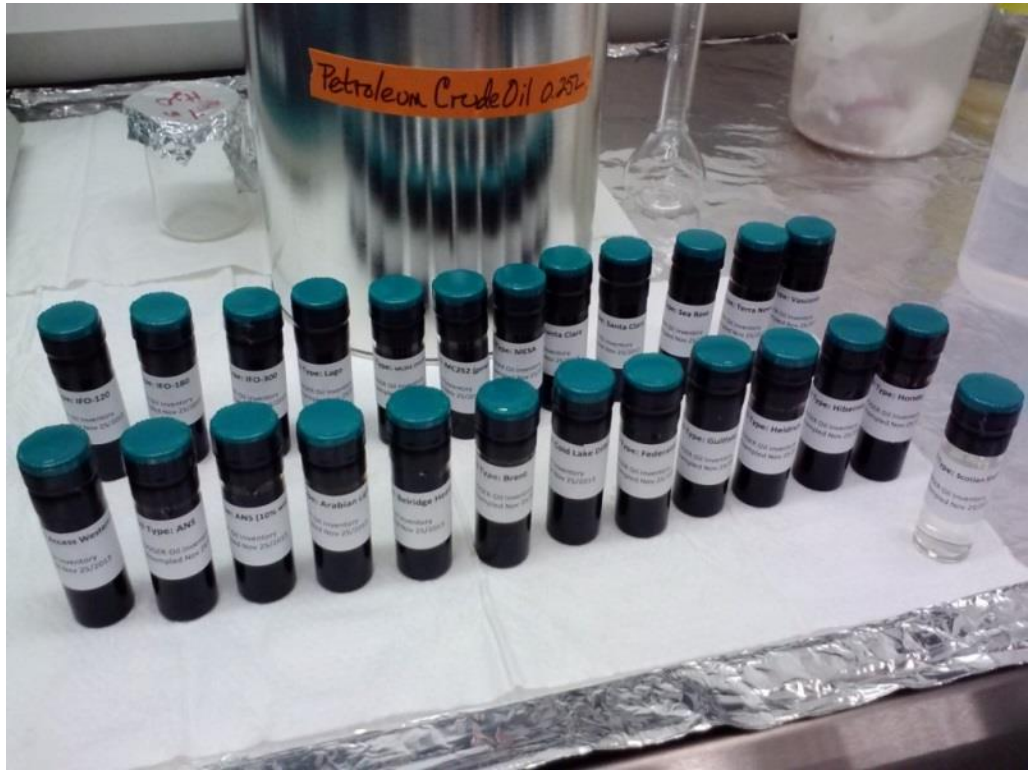


Figure 2.2. Twenty-five oil samples received from COOGER DFO – December 2013.

Table 2.1. List of oil used for EEM analyses

Light (API >31.1°)	Medium (API 22.3 – 31.1°)	Heavy (API <22.3°)
Arabian Light (32.2°)	Alaska North Slope (29.7°)	Access Western Blend Dilbit (21.3°)
Brent (38.2°)	Alaskan North Slope (10% weathered)	Belridge Heavy (13.6°)
Federated (39.4°)	Heidrun (28.6°)	Cold Lake Dilbit (21.5°)
Gulfaks (32.7°)	Lago (25.0°)	Hondo (19.5°)
Hibernia (35.6°)	MESA (30.3°)	IFO 40 (21.9°)
MC252—Discoverer Enterprise (37.2°)	Sea Rose (29.8°)	IFO 120 (18.4°)
MC252—generic (35.2°)	Vasconia (26.3°)	IFO 180 (14.1°)
Scotian Shelf Condensate (53.2°)		IFO 300 (11.9°)
Terra Nova (33.8°)		Santa Clara (22.1°)

Artificial Seawater Protocol

To isolate petroleum/dispersant specific fluorescence, the decision was made to use artificial seawater rather than natural seawater, in order to eliminate complication of the fluorescence

signal from any naturally-occurring CDOM. Fresh artificial seawater was prepared by adding 34.5 g Tropic Marin® salts (Dr. Biener GmbH, Wartenburg, Germany) to 1 L ultrapure water dispensed from Millipore Milli-Q unit (≤ 4 ppb DOM) into a 1.5 L glass beaker. A magnetic stir-bar was added, the beaker was covered with aluminum foil and stirred on an electric stir plate for 20 minutes at room temperature (~ 24 °C). Fresh artificial seawater was prepared in 1 L quantity following this protocol at the beginning of each experiment to be used for creation of dispersed oil in seawater and for blanks to measure fluorescence against.

Dispersed Oil-in-Seawater Experiments

Dispersed-oil-in-seawater experiments were performed by following the COOGER DFO protocol, “Methods for Fluorescence Analysis using the Baffled Flask Test,” (Appendix B), which was based on the BFT method developed by Sorial et al. (2004c) and is currently pending approval as the US EPA’s official DE determination method (Venosa et al. 2002). COOGER DFO provided three 150 mL trypsinizing (baffled) flasks, with stopcocks placed near the bottom of the flasks and an Eppendorf Biomaster 4830 micropipettor with positive displacement Mastertips (1-20 μ L) to ensure accurate pipetting of viscous oils. Artificial seawater, MC252 oil, and Corexit® 9500A were employed to arrive at appropriate concentrations to be used for the entire experimental series on 25 oils with chemical dispersant at multiple DORs. Planned concentrations were 1, 10, 100, and 1,000 ppm (by volume); however, the 1 ppm concentration was dropped due to the limitations of the flask and micropipettor volumes. Based on spectrofluorometric analysis, the 100 ppm dispersed oil in water (10 μ L oil in 100 mL water) concentration was determined to be the target, which would give results within a linear region of fluorescence.

Spectrofluorometric analyses were performed on a HORIBA Scientific Aqualog, while varying the instrument's settings (excitation and emission increments, gain setting, and integration time) in order to determine optimal settings (Appendix C). An artificial seawater blank was analyzed at the beginning of the preliminary experimental procedure, as well as at the beginning of each day for the entire research project, in order to enable subtraction of background fluorescence arising from the artificial seawater in each sample analysis, as well as to collect Raman peak data. This would allow conversion of sample fluorescence intensity into Raman Units (RU) (Lawaetz and Stedmon 2009).

Finally, a quinine sulfate dehydrate dilution series was created consisting of: 0.5N H₂SO₄ solvent; 100 ppm 1° solution; 100 ppb 2° solution; 1, 3, 5, 10, and 20 ppb quinine sulfate solutions. Absorbance was collected on the Aqualog, and results were plotted for the creation of a concentration curve, which would enable cross-calibration of the instrument's built-in quinine sulfate tool, used to convert fluorescence intensity results into Quinine Sulfate Equivalents (QSE) (Velapoldi and Mielenz 1980).

Laboratory EPA BFT Protocol

Fresh artificial seawater was prepared for each step of the series by adding 34.4 g Tropic Marin® salts to 1 L ultrapure water, dispensed from Millipore Milli-Q unit (≤ 4 ppb DOM) into a 1.5 L glass beaker, adding a magnetic stir bar, covering the beaker with aluminum foil, and stirring on electric stir plate for 20 min at room temperature (~ 24 °C).

DORs of 0 (no dispersant added), 1:200, 1:100, and 1:20 were then created from each oil type immediately before analysis as detailed in Table 2.2.

Table 2.2. Preparation of sample DORs

Step	DOR	oil (mL)	dispersant (μ L)	
1	0	0.01	0	No preparation necessary. Pipette 10 μ L oil directly from 20 mL clear glass sample vial with Teflon-lined cap onto surface of 100 mL artificial seawater.
2	1: 200	2.0	10	Pipette oil from 20 mL clear glass sample vial with Teflon-lined cap, followed by dispersant, into an 8.6 mL amber vial, cover with Teflon-lined cap, shake by hand for 30 seconds. Pipette 10 μ L oil/dispersant mixture from amber vial onto surface of 100 mL artificial seawater.
3	1: 100	2.0	20	As above.
4	1: 20	2.0	100	As above.

A slightly modified version of the COOGER DFO protocol, “Methods for Fluorescence Analysis using the Baffled Flask Test,” was employed for sample analysis, as follows. Three replicates of dispersed oil in seawater solution were prepared simultaneously. Erlenmeyer baffle flasks were placed into holders on a New Brunswick Innova 2100 orbital shaker (Eppendorf AG, Germany), with a variable speed (25-500 rpm) and orbital diameter of 0.75" (1.9 cm). 100 mL of freshly prepared artificial seawater was added to each flask, then the flask opening was covered with Parafilm. The film was retracted briefly to dispense 10 μ L oil or dispersed oil onto the water surface in each flask, then replaced. Samples were then mixed on the orbital shaker for 0.2 hr. (12 min.) at 200 rpm.

Immediately upon cessation of mixing, approximately 2 mL solution was drained through the stopcock and discarded, followed by 3.5 mL solution dispensed from each flask directly into each of three 4.0 mL UV-grade quartz cuvettes. These were immediately covered with Teflon stoppers to prevent evasion of volatiles (Fig. 2.3). A fourth cuvette was filled with artificial seawater to serve as a blank for the sample analysis series.

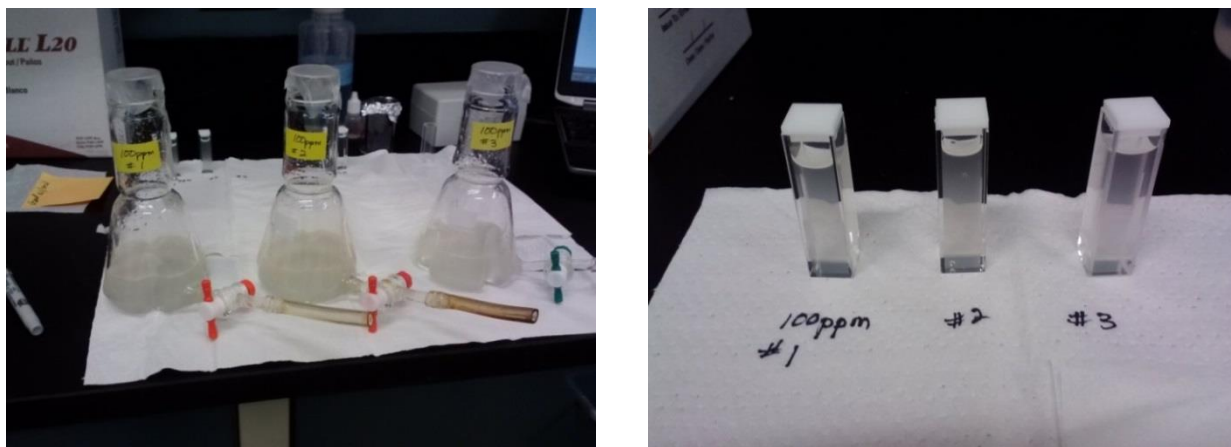


Figure 2.3. Trypsinizing (baffle) flasks containing dispersed oil in artificial seawater (left) and corresponding samples removed from each flask, ready for spectrofluorometric analysis.

Analysis of sample #1 was immediately performed on the HORIBA Scientific Aqualog spectrofluorometer to collect absorbance and fluorescence intensity using the following parameters:

- Excitation from 800 nm to 200 nm at 3 nm increments
- Emission from 249.125 nm to 828.335 nm (CCD detector parked at 534.19) at 8 pixel increments
- Gain set to medium
- Initial integration time of 0.1 sec

If the resulting total photon count was outside the manufacturer's recommended optimal range (15,000 to 65,000), integration time was adjusted and sample #1 was re-analyzed until a total photon count within range was obtained, with a goal of ~30,000 total photons. Samples #2 and #3 were then analyzed using the optimum integration time. Analysis of all three samples usually took less than 10 minutes, and in all cases was accomplished within 20 minutes.

Due to variation from laboratory to laboratory, and even differences in instrument to instrument performance from the same manufacturer, it is necessary to convert fluorescence intensity "raw counts" to a standardized unit for useful reporting purposes. Traditionally, the fluorescence community has utilized a dilution series of quinine sulfate dihydrate in weak acid to convert instrument output to Quinine Sulfate Equivalents (QSE) (Velapoldi and Mielenz 1980; Coble 1996; Conmy et al. 2014b). However, in recent years the alternate method of reporting in Raman Units (RU) has gained favor (Murphy et al. 2010). Due to inherent properties of water molecules, the Raman scatter peak is a reliable feature which can be utilized by collecting a scan of ultra-pure water at the beginning of each day, and then using the ratio of raw counts to the area under the curve of the Raman peak (approximately 381 - 426 nm) to convert fluorescence to RU. As the Quinine Sulfate SRM is no longer available from NIST (National Institute of Standards and Technology), our results are reported in RU and we offer a conversion factor to QSE using the highest quality quinine sulfate dehydrate readily available.

Modifications to the COOGER DFO protocol, "Methods for Fluorescence Analysis using the Baffled Flask Test," based on the BFT procedure (Sorial et al. 2004a) were:

- Mixing of dispersant and oil before dispensing into baffle flasks containing artificial sea water — Limitations of flask and micropipettor volumes would not allow for creation of DOR 1:200 by dispensing oil into the flask followed by dispensing of dispersant onto the oil, so the decision was made to mix dispersant with oil prior to introduction to baffle flasks for all DORs. This is the method employed in the Swirling Flask Test (Fingas et al. 1987).
- Analysis of samples immediately upon cessation of mixing — Settling time was incorporated into the BFT protocol to allow for distinction between DE results for dispersants being considered for inclusion on the NCP (Sorial et al. 2004a). Since we were using only one dispersant already determined to have high DE (Corexit® 9500A), and as our goal was to characterize fluorescence of dispersed petroleum at sea, settling time was eliminated. However, in order to investigate the effect of settling time, at the outset of the project, three additional samples of Arabian Light at DOR 1:20 were collected from the stopcock of flask #2 after approximately 40 min settling time. Spectrofluorometric analysis showed average total photon count from these three samples was only 0.8 % lower than the corresponding sample, which was analyzed after no settling time. For the balance of the project, and for most oils at multiple DORs, two additional replicates were collected from one randomly selected flask after approximately 20 minutes settling time, then analyzed on the Aqualog. In most cases, post-settling results were less than 2 % lower than the corresponding original sample, and in a number of cases post-settling results were actually slightly higher (shown in Table 2.3).
- Oil-in-water samples were analyzed for absorbance as well as fluorescence before as well as following extraction — Due to the small amount of each oil sample (~10 mL), time

Table 2.3. Analysis of replicates

Date	Oil	DOR	Sample Name	Integration time (s)	Settling Time (m)	Total Proton Counts	Mean Total Proton Counts (original samples)	1 StDev (original samples)	Mean Total Proton Counts (replicates)	1 StDev (replicates)	Relative Difference (%)
27-May-14	Arabian Light	1:20	ArLtD1	0.1		56,000					
			D2	0.1		56,400					
			D2b	0.1	~40	55,800					
			D2c	0.1	~40	56,600					
			D2d	0.1	~40	55,000					
			D3	0.1		55,600		56,000	400	55,950	719
24-Jun-14	Heidrun	0	HeidrunA1b	0.05		36,200					
			HeidrunA2	0.05		39,200					
			HeidrunA3	0.05		37,600					
			HeidrunA3r1	0.05	~20	36,800					
			HeidrunA3r2	0.05	~20	37,200		37,667	1501	37,000	283
26-Jun-14	Hibernia	1:100	HiberniaC1b	0.05		39,600					
			HiberniaC2	0.05		40,800					
			HiberniaC3	0.05		39,000					
			HiberniaC1r1	0.05	~10	40,400					
			HiberniaC1r2	0.05	~10	39,400		39,800	917	39,900	707

limitations, and with our goal being the characterization of fluorescence and relationship with chemistry, rather than dispersant efficiency, a post-extraction concentration curve of DE was not created. Instead, post-extraction samples were sent to DFO COOGER for analysis of total petroleum hydrocarbons (TPH).

Statistical analysis of results included linear regression of fluorescence and chemistry data using MS Excel, as well as PARAFAC analysis of fluorescence results using MATLAB (The MathWorks 2018) and the PLS toolbox (Eigenvector Research 2018).

Chemical Analysis

After approximately ten minutes settling time, additional samples were removed from each baffle flask for extraction and analysis of alkanes and PAHs. Approximately 30 mL solution was withdrawn through the stopcock into a 50 mL graduated cylinder (actual volume recorded), then transferred into a 125 mL amber glass bottle with a Teflon-lined cap. The graduated cylinder was rinsed three times with 10 mL methylene chloride. After each rinse, the methylene chloride was transferred into the amber bottle containing the sample (total volume recorded). After capping with a Teflon-lined cap, each bottle was shaken by hand for 30 seconds and then placed inside the laboratory fume hood until the end of the day, at which time all bottles were placed on a New Brunswick Innova 2100 orbital shaker inside a fume hood and gently stirred at 90 rpm for 18 hrs. Samples in amber bottles were then held in the laboratory refrigerator at 4 °C until overnight shipment with blue ice freezer packs to Bedford Institute of Oceanography for chemical analysis of petroleum hydrocarbons at COOGER DFO.

Dilution Series

At the conclusion of the project, three representative oils were selected for creation and analysis of dilution series for analysis on the Aqualog (Alaska North Slope, IFO-120, and MC252 Discoverer Enterprise). Glassware was acid-washed, then rinsed with methanol and placed in a drying oven at 30 °C overnight, then rinsed 3x with artificial seawater before use.

Volumetric flasks were first partially filled with artificial seawater and stoppers inserted.

Following the Experimental BFT Protocol developed for this research project, one flask of 100 ppm dispersed oil in seawater was created to be used as primary stock (1°). At the completion of stirring, approximately 2 mL was drained from the stopcock and discarded, followed by 3.5 mL dispensed into a 4.0 mL quartz cuvette. This cuvette was covered with a Teflon cap, and immediately analyzed for absorbance and fluorescence on the Aqualog using the parameters previously given. While analysis took place, 1 mL 1° solution was removed from the baffle flask using a glass pipette and dispensed into the partially-filled 100 mL volumetric flask to create the 1 ppm secondary (2°) solution. Artificial seawater was added to the fill line using a Pasteur pipette, and the flask was stoppered and inverted 12x to mix thoroughly.

A clean cuvette was then filled with the 2° solution and immediately analyzed in the Aqualog. The remaining 2° solution was then used to create 500, 100, 50, 10, and 1 ppb solutions. Cuvettes were protected from light until analysis in order from highest to lowest concentration on the Aqualog. A maximum integration of time of 10 sec was used on the lowest concentrations in order to avoid questionable results due to photobleaching of fluorophores.

RESULTS AND DISCUSSION

Following spectrofluorometric analysis of all 25 oil types at each of the four DORs, four characteristic excitation/emission (Ex/Em) peak locations were identified: $F_{\max1} - F_{\max4}$ (Fig. 2.4). The highest intensity peak ($F_{\max1}$) occurred, without exception, at Ex 221-239 nm/Em 335-344 nm and was paired with a blue-shifted (towards shorter wavelengths), lower intensity peak ($F_{\max2}$) at Ex 215-221 nm/Em 285-308 nm in all oil samples.

A third broad, low-intensity peak ($F_{\max3}$) was observed at Ex 215-305 nm/Em 418-571 nm, but appeared in only 68% of oil samples. Light crude oils (Table 2.4) exhibited $F_{\max3}$ peaks at all DORs, with the exception of Scotian Shelf Condensate (SSC). Fluorescence in the $F_{\max3}$ region was identified at all DORs in only one medium weight oil (Heidrun), and was not present at any DOR in one medium oil (Vasconia). Two medium-weight oils emitted measurable fluorescence in the $F_{\max3}$ region only with full dispersion (Lago and MESA), while Sea Rose showed fluorescence at DORs 1:100 and 1:20. One medium weight oil, Alaska North Slope (both fresh and 10% weathered), exhibited unusual $F_{\max3}$ behavior, with measureable fluorescence at DOR 0, 1:100, and 1:20, but not at DOR 1:200. Finally, for the heavy weight oils, $F_{\max3}$ was almost completely absent at all DORs, with the exception of fluorescence at DOR 1:20 for Cold Lake Dilbit and IFO-40, and across all DORs for one anomalous member of this group—Access Western Blend Dilbit.

By definition, dilbit is a mixture of bitumen—essentially an extra heavy crude oil with API gravity $< 10.0^\circ$ —and a diluent—either a light condensate or naphtha (Priaro 2014). The chemical composition present in each component may account for the unusual $F_{\max3}$ fluorescence observed

in the dilbits. These results are somewhat similar to the Intermediate Fuel Oils (IFOs), which are not true crude oils, but marine fuels produced from a mixture of heavy post-refinery residuum and the heaviest fraction of distillates, which are added to reach a desired kinematic viscosity (i.e., IFO 300 = 300 mm²/s at 50 °C) (ICF Consulting Group 1999). This may help to explain the appearance of F_{max3} fluorescence in IFO-40. Clearly, the presence of fluorescence in the F_{max3} region, especially at DOR 1:20, appears to be closely tied to API gravity, and thus to density as well as kinematic viscosity, since API gravity = (141.5/Specific Gravity) – 131.5 (Fingas 2011). The absence of F_{max3} region fluorescence in heavy weight oils may be due to retention of energy within the large, complex hydrocarbons, which make up the highest density oils. Additionally, the appearance of fluorescence in the F_{max3} region at highest DORs in the medium weight oils Lago, MESA, and Sea Rose would also seem to suggest that the creation of smaller droplet sizes with effective dispersion leads to a decrease in reabsorption of fluorescence within droplets.

A fourth region of broad, low-intensity fluorescence (F_{max4}) was identified at Ex 269-291 nm/Em 326-353 nm and exhibited in all oils at all DORs. Therefore, F_{max1} and F_{max4} oil-in-water fluorescence regions appear to be analogous to the characteristic CDOM fluorescence regions ‘Ac’ (formerly A) at Ex 260 nm/Em 400-460 nm and ‘C’ at Ex 320-365 nm/Em 420-470 nm (Coble et al. 2014).

In addition to maximum fluorescence intensity (in RU), full width at half maximum (FWHM) was recorded for all peaks. Further, fluorescence intensity at Ex/Em 281/340 nm and Ex/Em 281/450 nm was recorded to enable calculation of the FIR for all samples. Optimum settings for

signal collection on the Aqualog necessitated excitation at 3 nm intervals, which accounts for the 1 nm discrepancy from the published FIR wavelengths (Bugden et al. 2008). Finally, fluorescence intensity of each sample was recorded at wavelength settings as near as possible to the specified Ex/Em wavelength setting of five off-the-shelf in situ fluorometers (Conmy et al. 2014b), which were all employed in the response to the DWH oil spill. Selected results are presented in Table 2.4, along with results of chemical analyses completed by researchers at DFO COOGER, using their Agilent 6890N gas chromatograph with an Agilent 5975B mass spectrometer. Complete fluorescence results are presented in Appendix D.

Finally, EEM contour plots for all oils, which characterize each oil and illustrate the effect of DOR on the fluorescence properties, are presented in Appendix E. The ability to identify oil source would undoubtedly be particularly useful in the prevention and abatement of oil spill pollution. Efforts to determine characteristic fluorescence fingerprints have existed since the 1970s (Frank 1975) and have received renewed attention with the advent of improved fluorescence detection systems (Bugden et al. 2008).

Intensity of $F_{\max 1}$ was consistently strong across all oil samples, with no ambiguity in peak location. The observed Ex/Em range of significant fluorescence intensity was fairly narrow with FWHM of only 37-50 nm, and little to no change in peak location with increasing DOR. However, ten oil samples displayed a slight increase (approximately 4.5 nm) in FWHM with maximum dispersion (DOR 1:20). This was true of six of the nine light oils (Arabian Light, Brent, Federated, Gullfaks, Hibernia and Terra Nova), but only one of the seven medium oils (MESA) and one of the nine heavy oils (IFO-120). One medium weight oil (Lago) and one

Table 2.4. 25 oil types fluorescence results and chemical analyses

Type I Oils	DOR	F _{max} ¹ (RU)	FIR	Alkanes (µg/L)	2-3 rings (µg/L)	4-5 rings (µg/L)	Type II Oils	DOR	F _{max} ¹ (RU)	FIR	Alkanes (µg/L)	2-3 rings (µg/L)	4-5 rings (µg/L)	
Alaska North Slope	0	697.07	21.59	375	160	8	Access Western Blend Dilbit	0	39.58	12.24	93	19	10	
	1:200	715.01	37.73					1:200	46.52	14.20				
	1:100	839.60	6.87					1:100	49.84	8.97				
	1:20	1171.63	0.88	3019	566	65		1:20	60.19	1.15	258	57	38	
Alaska North Slope (10% weathered)	0	812.97	22.75	545	201	14	Belridge Heavy	0	118.69	5.31	42	52	30	
	1:200	831.70	21.86					1:200	161.75	5.65				
	1:100	828.06	8.98					1:100	140.96	4.93				
	1:20	1109.51	0.93	3312	598	74		1:20	147.09	3.51	44	84	52	
Arabian Light	0	400.42	7.90	733	124	12	Cold Lake Dilbit	0	120.61	20.72	155	94	23	
	1:200	357.62	12.06					1:200	120.65	18.01				
	1:100	426.82	2.68					1:100	125.85	13.11				
	1:20	701.75	0.39	6004	642	103		1:20	133.15	1.94	368	210	58	
Brent	0	646.18	7.78	1068	183	12	Heidrun	0	902.69	4.61	382	392	43	
	1:200	660.37	6.88					1:200	909.47	6.32				
	1:100	708.16	2.03					1:100	964.31	3.80				
	1:20	1098.42	0.69	5954	553	59		1:20	1098.90	0.80	684	620	82	
Federated	0	574.35	3.72	1921	238	30	Hondo	0	283.04	21.99	412	84	3	
	1:200	607.97	2.06					1:200	312.27	18.73				
	1:100	645.28	0.97					1:100	274.80	20.66				
	1:20	1223.17	0.37	6501	617	87		1:20	288.01	17.01	319	74	1	
Gullfaks	0	937.00	5.86	762	373	26	IFO-40	0	1173.91	33.15	1324	560	172	
	1:200	934.42	5.64					1:200	1246.63	59.63				
	1:100	933.08	3.30					1:100	1338.56	42.94				
	1:20	1524.21	0.69	1943	749	61		1:20	1458.79	4.40	4354	1508	570	

Table 2.4 (cont'd). 25 oil types fluorescence results and chemical analyses

Type I Oils	DOR	F _{max} ¹ (RU)	FIR	Alkanes (µg/L)	2-3 rings (µg/L)	4-5 rings (µg/L)	Type II Oils	DOR	F _{max} ¹ (RU)	FIR	Alkanes (µg/L)	2-3 rings (µg/L)	4-5 rings (µg/L)
Hibernia	0	938.08	7.46	2289	335	24	IFO-120	0	3030.69	117.26	343	696	51
	1:200	951.49	3.22					1:200	2903.21	334.13			
	1:100	978.62	1.66					1:100	3090.23	88.73			
	1:20	1812.41	0.50	6095	635	59		1:20	2527.73	42.66	840	3097	122
MC252 (Discoverer Enterprise)	0	998.50	4.97	1578	350	30	IFO-180	0	1263.05	38.88	866	645	326
	1:200	1009.18	3.07					1:200	1394.42	42.40			
	1:100	1085.54	1.23					1:100	1703.55	5.76			
	1:20	1998.60	0.39	3992	583	69		1:20	1532.99	12.28	2933	1986	1109
MC252 (generic)	0	857.35	4.81	1468	267	21	IFO-300	0	720.55	65.84	446	295	192
	1:200	877.78	3.11					1:200	443.51	48.50			
	1:100	964.02	0.97					1:100	465.91	75.70			
	1:20	1795.13	0.41	5093	624	68		1:20	661.50	43.02	366	248	162
MESA	0	757.84	20.04	1388	268	24	Lago	0	352.22	12.53	1289	146	18
	1:200	806.76	12.21					1:200	398.40	11.30			
	1:100	745.17	6.33					1:100	367.75	9.10			
	1:20	1107.09	1.09	4088	524	62		1:20	453.10	0.93	4221	346	52
Sea Rose	0	1145.29	10.65	1583	320	19	Santa Clara	0	157.30	23.17	209	28	0
	1:200	1223.98	7.40					1:200	147.55	27.03			
	1:100	1236.63	2.16					1:100	154.98	19.29			
	1:20	1973.55	0.72	5903	721	70		1:20	169.39	7.39	1196	81	3
Terra Nova	0	665.50	6.81	1038	186	11	Scotian Shelf Condensate	0	946.52	43.40	447	127	0
	1:200	719.72	3.96					1:200	1408.59	51.61			
	1:100	821.24	1.47					1:100	1487.16	49.14			
	1:20	1380.34	0.40	5608	540	50		1:20	1337.98	51.42	1057	220	0
							Vasconia	0	844.93	34.44	2550	415	59
								1:200	828.37	53.23			
								1:100	835.62	29.32			
								1:20	935.79	3.64	4402	631	96

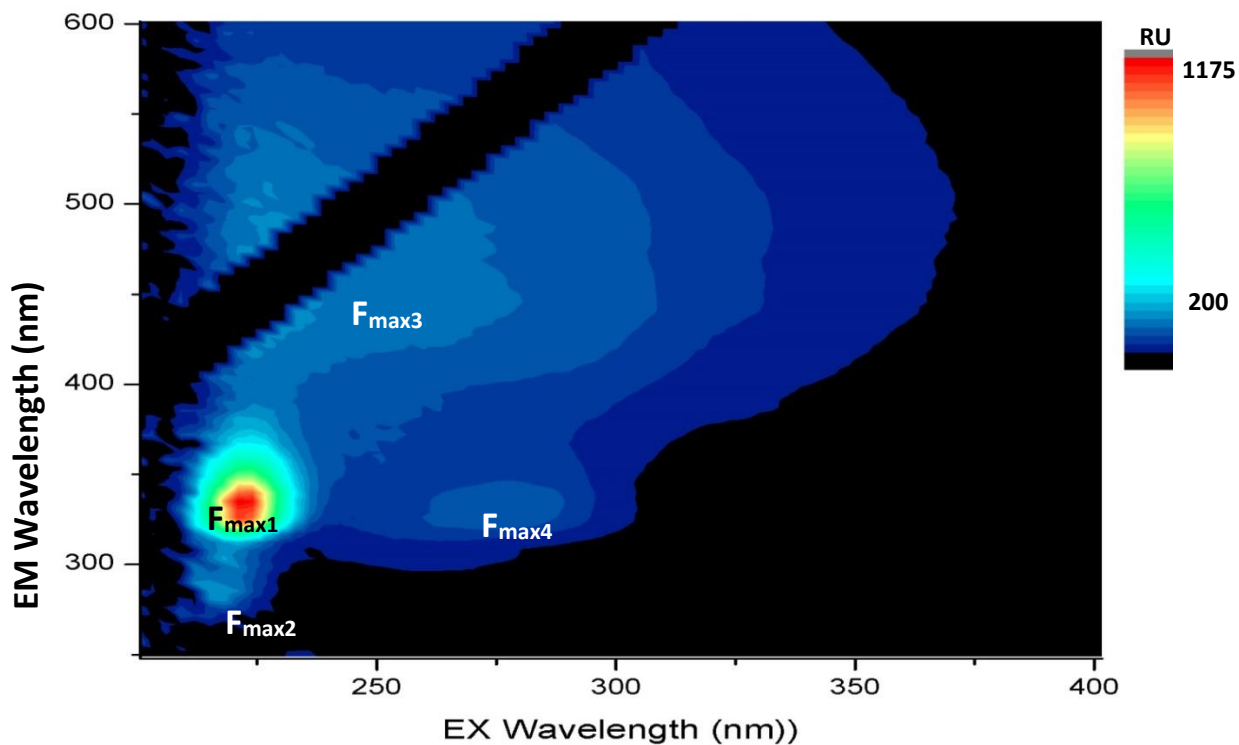


Figure 2.4. Alaska North Slope dispersed oil in artificial seawater at DOR 1:20 with locations of $F_{\max 1}$, $F_{\max 2}$, $F_{\max 3}$ and $F_{\max 4}$ indicated. Note that maximum fluorescence intensity at $F_{\max 3}$ is mostly obscured by masking of second order Rayleigh scattering.

heavy oil (Access Western Blend Dilbit) showed the same slight increase in FWHM at both DORs 1:100 and 1:20.

The impact of applying the Aqualog’s built-in Inner Filter Effect correction tool (IFE) to fluorescence intensity was also calculated for $F_{\max 1}$. This correction utilizes the measured absorbance of the sample to correct for fluorescence emitted by fluorophores within the sample, but then re-absorbed within the sample itself. It is interesting to note that application of the IFE resulted in only a small magnification of the fluorescence signal at DORs 0, 1:200, and 1:100 for all oil samples; however, there was a clear delineation at DOR 1:20 which allowed categorization of oil samples into two overarching categories: Oil Type I, with IFE effect > 2.5 , and Oil Type II, with IFE effect < 2.5 (Table 2.4). This appears to be due to the increase in

optical density, and thus absorbance, caused by interaction between Corexit® 9500A and fully dispersed Type I oils. Photographs of four representative pre-analysis samples, along with the resulting EEMs of oil type are shown in Figs. 2.5 and 2.6 to illustrate the difference in fluorescence between the types regardless of being a light, medium, or heavy crude oil.

The SSC as well as all of the IFOs showed atypical fluorescence profiles, which were quite different from the other oil samples. Condensate is an ultra-light crude oil, defined as having an API gravity of 50 – 120 degrees (Limited 2018). Often associated with natural gas deposits, and sometimes referred to as “natural gasoline,” it is employed in the dilution of heavier crude oils before their use as refinery feedstocks. Comprised largely of relatively short-chain alkanes (also known as paraffins), condensates may contain naphthenes and/or aromatics, which are considered impurities. Characteristically transparent and close to odorless, our SSC sample was completely clear and colorless. Based on the oil analysis by DFO COOGER, SSC had the lowest concentration of 3-ring PAHs (2 µg/L), with the exception of Santa Clara (1 µg/L); these two oils were also alone in containing no 4-5 ring compounds. SSC was unique in that highest fluorescence was seen at DOR 1:100 ($F_{\max 1} = 1487$ RU), decreasing slightly at DOR 1:200 ($F_{\max 1} = 1409$ RU), and even more at DOR 1:20 ($F_{\max 1} = 1338$ RU).

The IFOs, known as “bunker” or marine fuels, also showed confounding fluorescence results. As previously mentioned, these are not crude oils at all, but blends of the heavy residuum remaining after the refining process, which advantageously removes the lighter fractions (kerosene, diesel, and home heating fuels). The process can be managed to result in a specific viscosity by not removing the heaviest fraction of distillate (ICF Consulting Group 1999). The

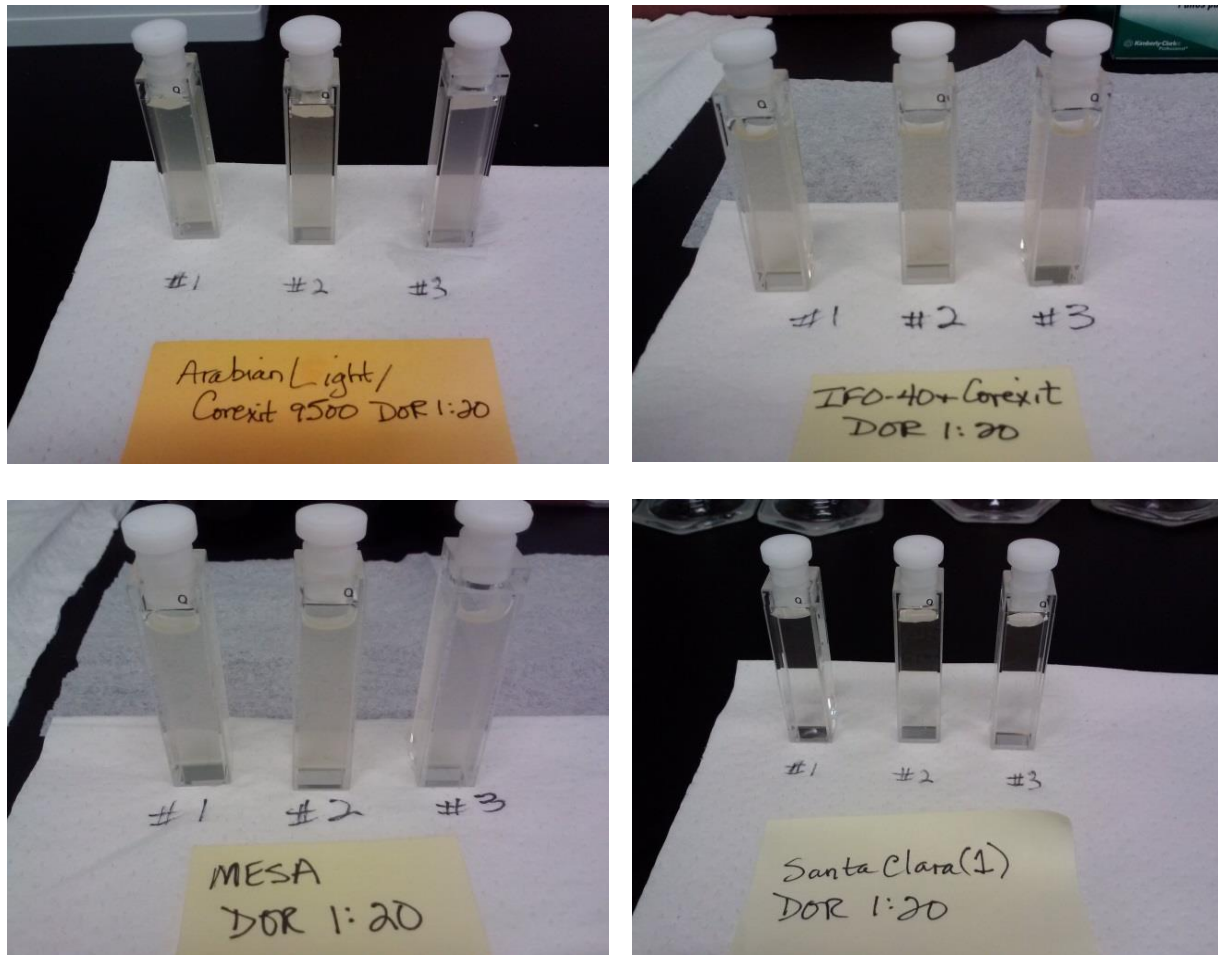


Figure 2.5. Photographs of pre-analysis samples of Type I (left) and II (right) oils for DOR = 1:20. Arabian Light is a light oil (API gravity > 31.1°), MESA is a medium oil (API gravity 22.3 – 31.1°). IFO 40 and Santa Clara are heavy oils (API gravity < 22.3°).

initial production of IFO 380 (kinematic viscosity = 380 mm²/s at 50 °C) is followed by addition of some combination of the light distillate fractions in order to produce lighter IFOs (Vermeire 2012). Therefore, IFOs will retain properties of both the high-molecular-weight residuum and whichever lighter-weight distillate fraction(s) are incorporated. IFOs produced by different refineries will vary in chemical composition due to the source crude oil, as well as the different processing methods employed (Lunel and Davies 2001). As both the SSC and IFOs tended to skew both fluorescence and chemical results, these will be eliminated from the following

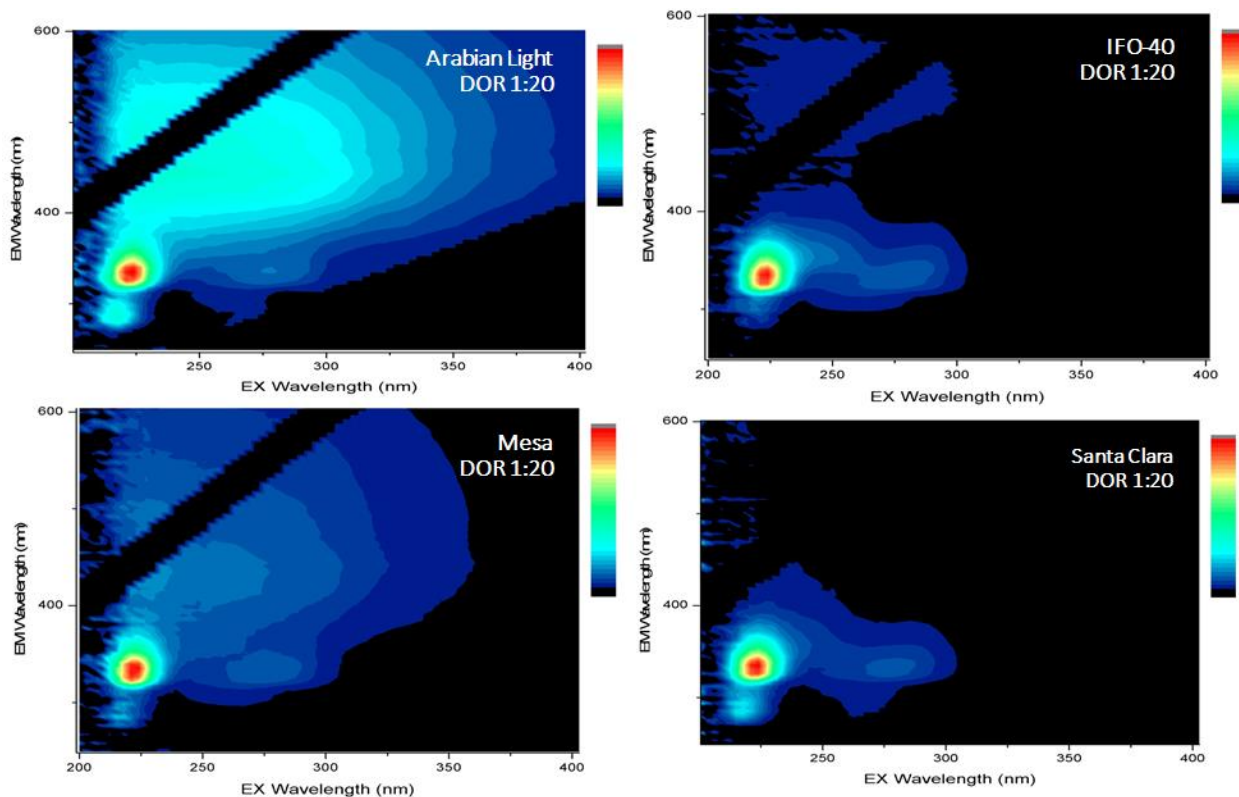


Figure 2.6. EEMs of Type I (left) and II (right) oils for DOR = 1:20. Arabian Light is a light oil (API gravity > 31.1°), MESA is a medium oil (API gravity 22.3 – 31.1°). IFO 40 and Santa Clara are heavy oils (API gravity < 22.3°).

discussion of the ranges observed in fluorescence peaks for the other 21 oils (see Figs. 2.7 and 2.9).

Overall, $F_{\max 1}$ intensity ranged from a minimum of 39.58 RU (Access Western Blend Dilbit DOR 0) to 3090.23 RU (IFO 120 DOR 1:100). $F_{\max 1}$ intensity within Type I oils ranged from 357.62 RU (Arabian Light DOR 1:200) to the overall high 1998.60 RU (MC252 Discoverer Enterprise DOR 1:20), while the range in Type II oils was the overall low of 39.58 RU (Access Western Blend Dilbit DOR 0) to a high of 1098.90 (Heidrun DOR 1:20).

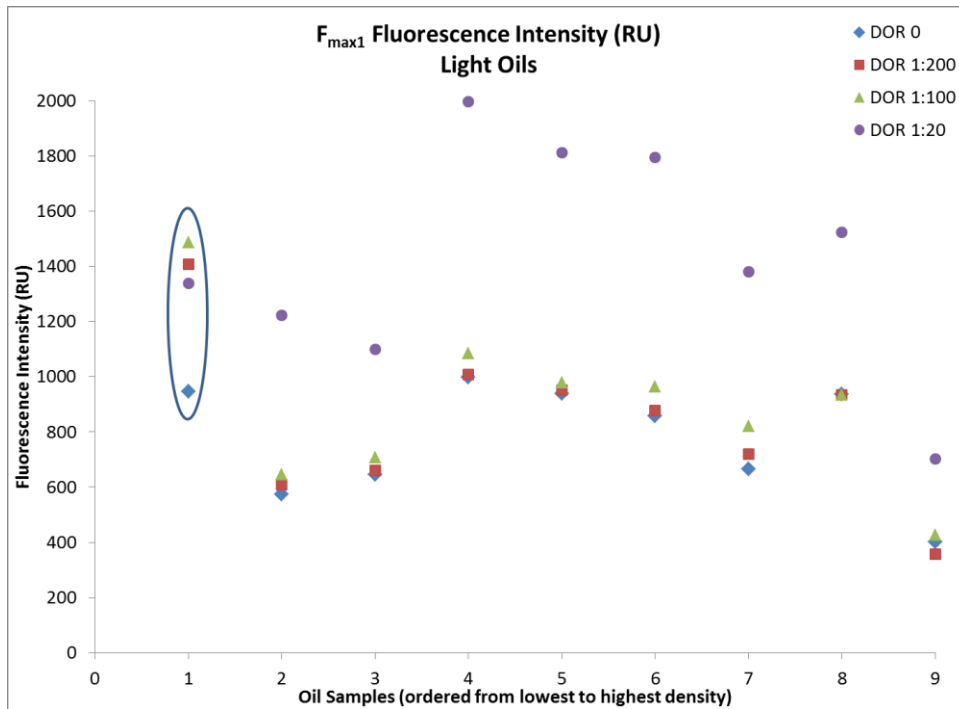


Figure 2.7. $F_{\max 1}$ fluorescence for Light Oils (API gravity $> 31^\circ$), in order of increasing density: 1. Scotian Shelf Condensate, 2. Federated, 3. Brent, 4. MC252—Discoverer Enterprise, 5. Hibernia, 6. MC252—generic, 7. Terra Nova, 8. Gullfaks, 9. Arabian Light. Note discrepancy in Scotian Shelf Condensate fluorescence pattern (circled) from that of all other Light Oils.

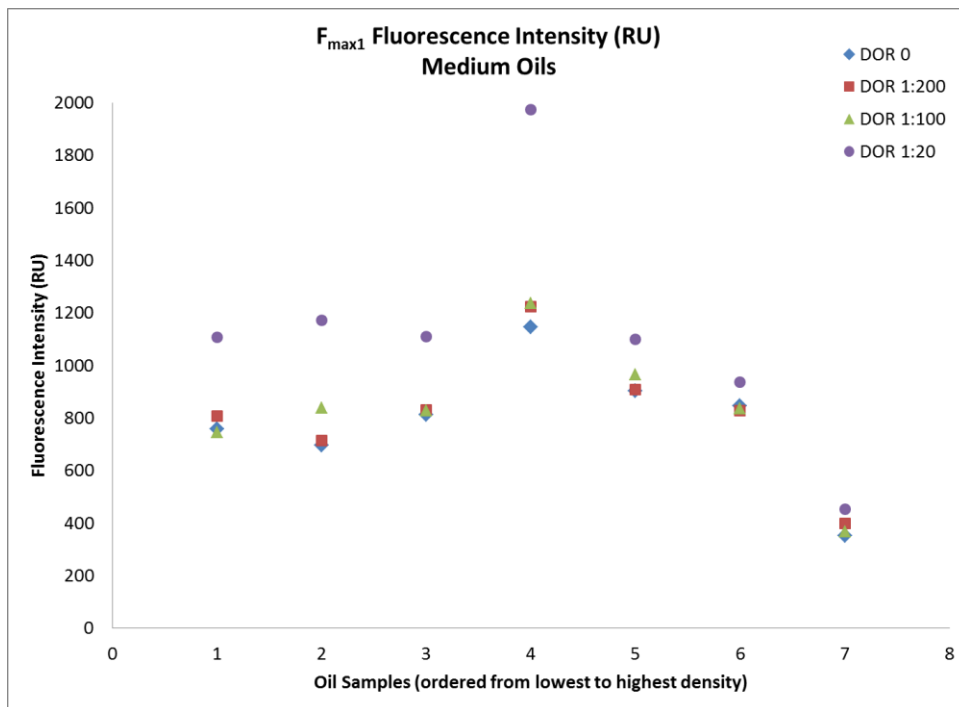


Figure 2.8. $F_{\max 1}$ fluorescence for Medium Oils (API gravity = 22.3° to 31°), in order of increasing density: 1. MESA, 2. Alaska North Slope (ANS), 3. ANS 10% weathered, 4. Sea Rose, 5. Heidrun, 6. Vasconia, 7. Lago.

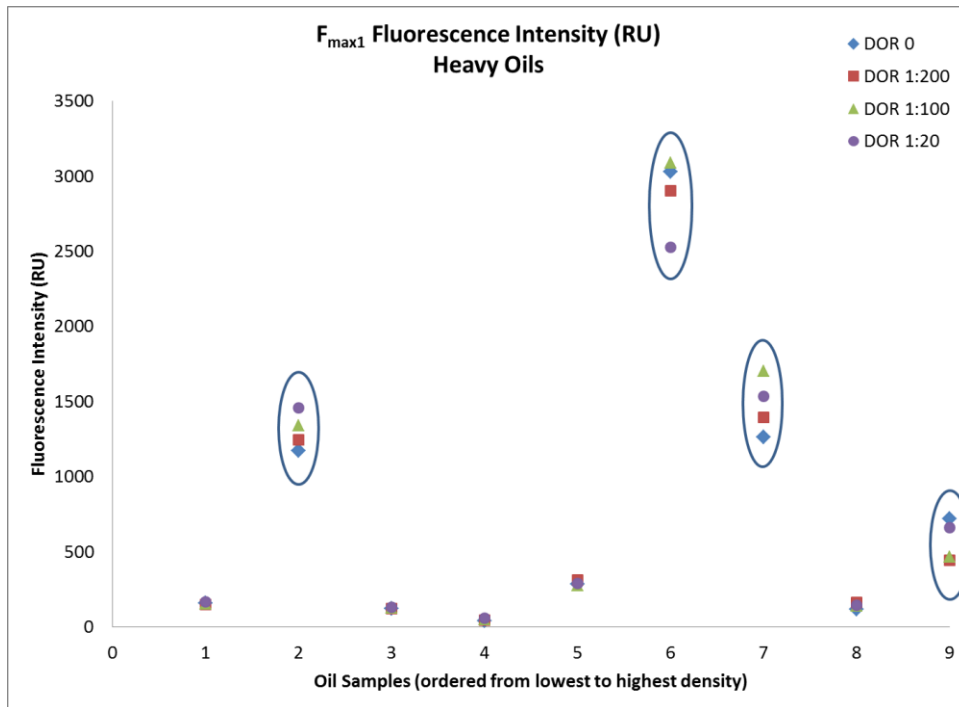


Figure 2.9. $F_{\max 1}$ fluorescence for Heavy Oils (API gravity < 22.3°), in order of increasing density: 1. Santa Clara, 2. IFO 40, 3. Cold Lake Dilbit, 4. Access Western Blend Dilbit, 5. Hondo, 6. IFO 120, 7. IFO 180, 8. Belridge Heavy, 9. IFO 300. Note discrepancy in all Intermediate Fuel Oils (circled) from that of all other Heavy Oils. Shouldn't the title be Intermediate and Heavy Fuel Oils?

While the excitation wavelength of maximum intensity for $F_{\max 2}$ remained relatively consistent, the emission wavelength varied within, as well as among, oil samples. The occurrence of double and triple peaks, as well as minor sub-peaks, within the $F_{\max 2}$ region was fairly common. It was sometimes difficult to distinguish the $F_{\max 2}$ peak from the shoulder of a very strong $F_{\max 1}$ peak, especially at higher DORs. For this reason, determination of the true FWHM was sometimes problematic. For $F_{\max 2}$ intensity, Type I oils ranged from 63.95 RU (Brent DOR 1:200) to 437.32 RU (MC252 Discoverer Enterprise DOR 1:20), and Type II oils ranged from 25.07 RU (Belridge Heavy DOR 0) to 164.07 RU (Heidrun DOR 1:20).

For the oils which did display an $F_{\max 3}$ peak, it was most apparent at the highest DOR (1:20), and some oils exhibited a strong $F_{\max 3}$ peak across all DORs (e.g., Brent, Federated). However, in

those oils the $F_{\max 3}$ peak at DOR 1:20 was significantly blue shifted from the $F_{\max 3}$ location observed at lower DORs. FWHM of the $F_{\max 3}$ peak was much greater than that of any other peak (145-283 nm), with the exception of the three lower DORs of Access Western Blend Dilbit (52-56 nm). Identification of highest $F_{\max 3}$ intensity proved somewhat problematic as it tended to reside in the second order Rayleigh region, a band of high intensity light resulting from scattering by water molecules. The edge of highest intensity might also lie in this region, so determination of the true FWHM was also problematic for many oil types. Traditionally, second order Rayleigh is eliminated by simply masking this region (10-12 nm). Although algorithms have been developed to model the character of fluorescence peaks lying within (Zepp et al. 2004; Bahram et al. 2006), assumptions about the linearity of fluorescence must be made in order to do so, and the true signal behavior cannot be known. For this reason, as our goal was to identify signals which could also be detected by in situ instruments, the decision was made to identify the maximum fluorescence intensity lying outside of the second order Rayleigh region rather than to attempt interpolation of the data.

As previously mentioned, $F_{\max 3}$ intensity was not always present, and it was observed far more often in Type I oils with a range of 2.64 RU (Arabian Light DOR 1:200) to 744.69 (MC252 Discoverer Enterprise DOR 1:20). Only four of the Type II oils exhibited $F_{\max 3}$ peaks and these ranged from 2.45 RU (Access Western Blend Dilbit DOR 0) to 174.93 RU (Heidrun DOR 1:20).

As with $F_{\max 2}$, the $F_{\max 4}$ region sometimes contained double peaks. Interesting spectral shapes for this region were also observed, especially in higher-density oils such as Access Western Blend Dilbit, Belridge Heavy, and Cold Lake Dilbit. FWHM ranged from 27 nm to 73 nm, for

all oils save one. The exception was Access Western Blend Dilbit, with FWHM of 77-110 nm. Intensity at $F_{\max4}$ ranged from 33.53 RU (Arabian Light DOR 1:200) to 231.86 RU (MC252 Discoverer Enterprise DOR 1:20) in Type I oils and from 4.93 RU (Access Western Blend Dilbit DOR 0) to 116.97 RU (Heidrun DOR 1:20) in Type II oils.

Results of the concentration dilution series showed that the Aqualog was consistently capable of detecting dispersed oil in artificial seawater in the three oils tested (Alaska North Slope, IFO-120, and MC252 Discoverer Enterprise) at all four DORs, down to at least 50 ppb. However, detecting dispersed oil below 100 ppb necessitated increasing the integration time to 10 sec/scan in order to collect sufficient total proton counts, which resulted in a total analysis time of approximately 30 minutes for each sample. Since the Aqualog scans from high to low wavelengths, and much of the fluorescence signal from petroleum resides in the low UV wavelength range, photobleaching of the sample as well as temperature effects certainly may have impacted these results.

Fluorescence as a Function of Chemistry

Samples of dispersed oil in artificial seawater (DOR 0 and DOR 1:20 for each oil type), extracted into methylene chloride were analyzed via GC-MS at DFO COOGER. Total alkanes, 2-ring, 3-ring, and 4-ring PAHs (see Table 2.5 for list of hydrocarbons in each class) were each plotted against $F_{\max1}$, $F_{\max2}$, $F_{\max3}$, and $F_{\max4}$. For all samples without chemical dispersion (DOR0), the strongest relationship appeared to be between fluorescence at $F_{\max3}$ and total 2-ring PAHs (Fig.2.10) ($R^2 = 0.87$, $p = 0.04$). However, stronger statistical significance was present in the relationship between fluorescence intensity at $F_{\max4}$ and 2-ring PAHs (Fig. 2.10, bottom) (R^2

Table 2.5. Individual hydrocarbon compounds reported as total alkanes, total 2-ring, 3-ring and 4-ring PAHs

Total Alkanes:	Total 2-ring PAHs:	Total 3-ring PAHs	Total 4-ring PAHs:
n-decane	naphthalene	phenanthrene	pyrene
undecane	methylnaphthalene	anthracene	methylpyrene
dodecane	dimethylnaphthalene	methylphenanthrene	dimethylpyrene
tridecane	trimethylnaphthalene	dimethylphenanthrene	trimethylpyrene
tetradecane	tetramethylnaphthalene	trimethylphenanthrene	tetramethylpyrene
pentadecane	acenaphthene	tetramethylphenanthrene	naphthobenzothiophene
hexadecane	acenaphthylene	fluoranthene	methylnaphthobenzothiophene
heptadecane	fluorene		dimethylNBenzothiophene
2,6,10,14-TMPdecane (pristane)	methylfluorene		trimethylNBenzothiophene
octadecane	dimethylfluorene		tetramethylNBenzothiophene
2,6,10,14-TMHdecane (phytane)	trimethylfluorene		benz[a]anthracene
nonadecane	dibenzothiophene		chrysene
eicosane	methyldibenzothiophene		methylchrysene
heneicosane	dimethyldibenzothiophene		dimethylchrysene
docosane	trimethyldibenzothiophene		trimethylchrysene
tricosane	tetramethyldibenzothiophene		tetramethylchrysene
tetracosane			benzo[b]fluoranthene
pentacosane			benzo[k]fluoranthene
hexacosane			benzo[e]pyrene
heptacosane			perylene
octacosane			
n-nonacosane			
tricontane			
n-heneicontane			
dotriacontane			
tritriacontane			
tetratriacontane			
n-pentatriacontane			
17 α (H), 21 β (H)-hopane			
17 β (H), 21 α (H)-hopane			

= 0.85, $p < 0.001$) and in the relationship between fluorescence intensity at $F_{\max1}$ and 2-ring PAHs (Fig. 2.11, top) ($R^2 = 0.82$, $p < 0.001$). It is important to note; however, that only 12 of the 25 oil types exhibited any fluorescence in the $F_{\max3}$ region at DOR 0 (Access Western Blend Dilbit, Alaska North Slope--both fresh and 10% weathered, Arabian Light, Brent, Federated, Gulfaks, Heidrun, Hibernia, MC252--both Discoverer Enterprise and generic, and Terra Nova). These relationships support the fact that larger, more complex PAHs fluoresce at longer emission wavelengths.

For all oils with chemical dispersion at DOR 1:20, logarithmic rather than linear regressions best modeled all relationships; overall, these were much weaker than those found at DOR 0, though. Linear regression appeared to show the strongest functional relationship between 2-ring PAHs and fluorescence at $F_{\max3}$ (Fig. 2.12, top); however, it was not statistically significant ($R^2 = 0.74$, $p = 0.83$). A moderate relationship was also noted between 4-ring PAHs and fluorescence at $F_{\max3}$ (Fig. 2.12, bottom), although this proved not to be statistically significant as well ($R^2 = 0.73$, $p = 0.93$). Regressions between 2-ring PAHs and fluorescence intensity at $F_{\max1}$ (Fig. 2.13, top) ($R^2 = 0.54$, $p < 0.001$), and between 2-ring PAHs and $F_{\max4}$ fluorescence (Fig. 2.12, bottom) ($R^2 = 0.53$, $p < 0.001$) indicated that oil did not explain as large a percentage of the variability in fluorescence as the previous regressions; however, these two relationships are statistically significant. Interestingly, these are the two relationships that most closely related in the DOR0 water samples, as well. Clearly, the relationship between fluorescence results and chemical analyses is complex and deserves further study. It is likely that the effect of chemical dispersant on petroleum plays a complex role in fluorophore emissions, which might well be specific to each individual oil type.

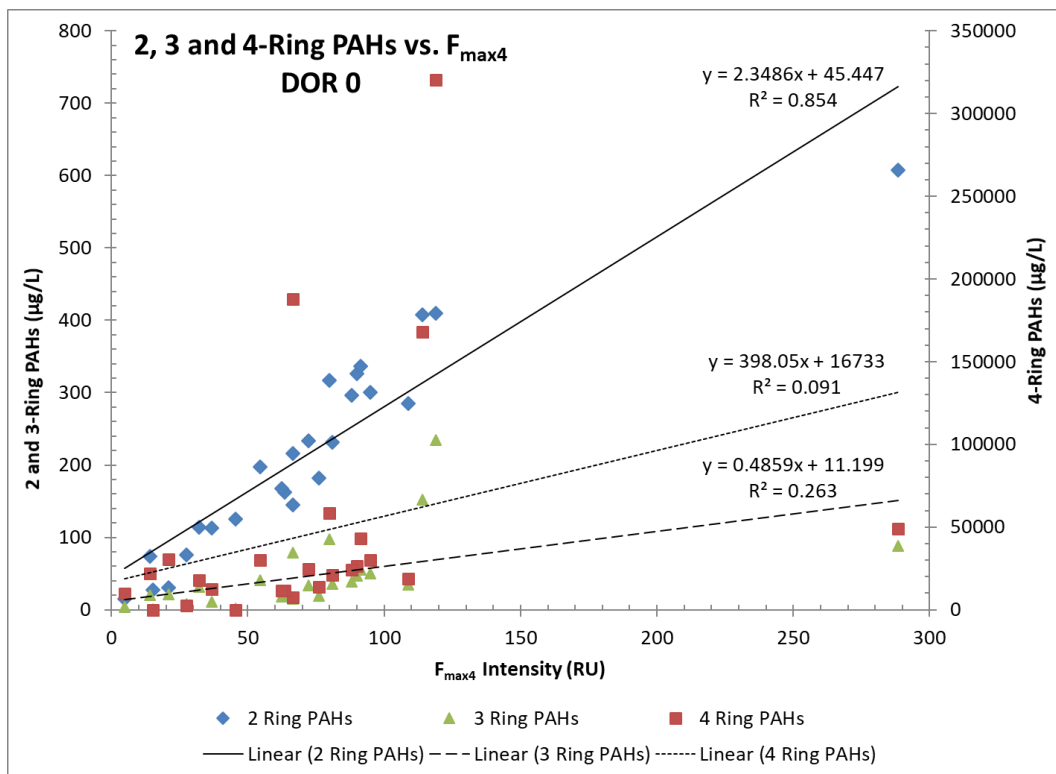
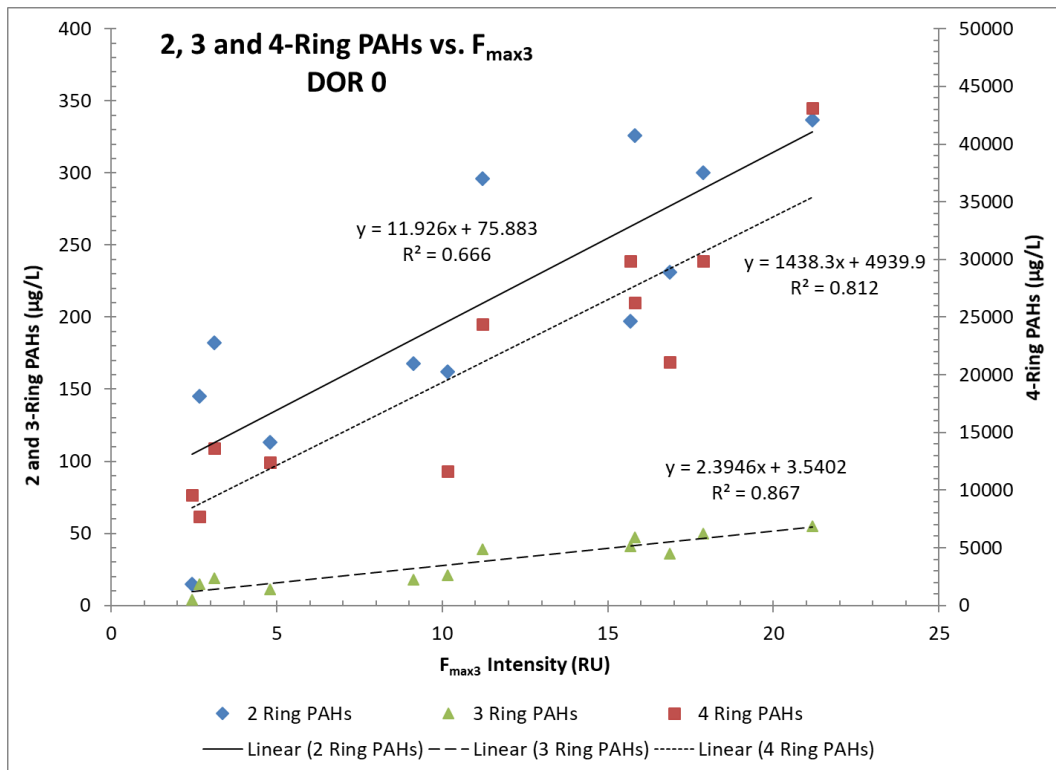


Figure 2.10. For all oil types at DOR 0, total concentration of 2-ring, 3-ring, and 4-ring PAHs ($\mu\text{g/L}$) against fluorescence intensity (RU) at F_{max3} (top), and against F_{max4} (bottom).

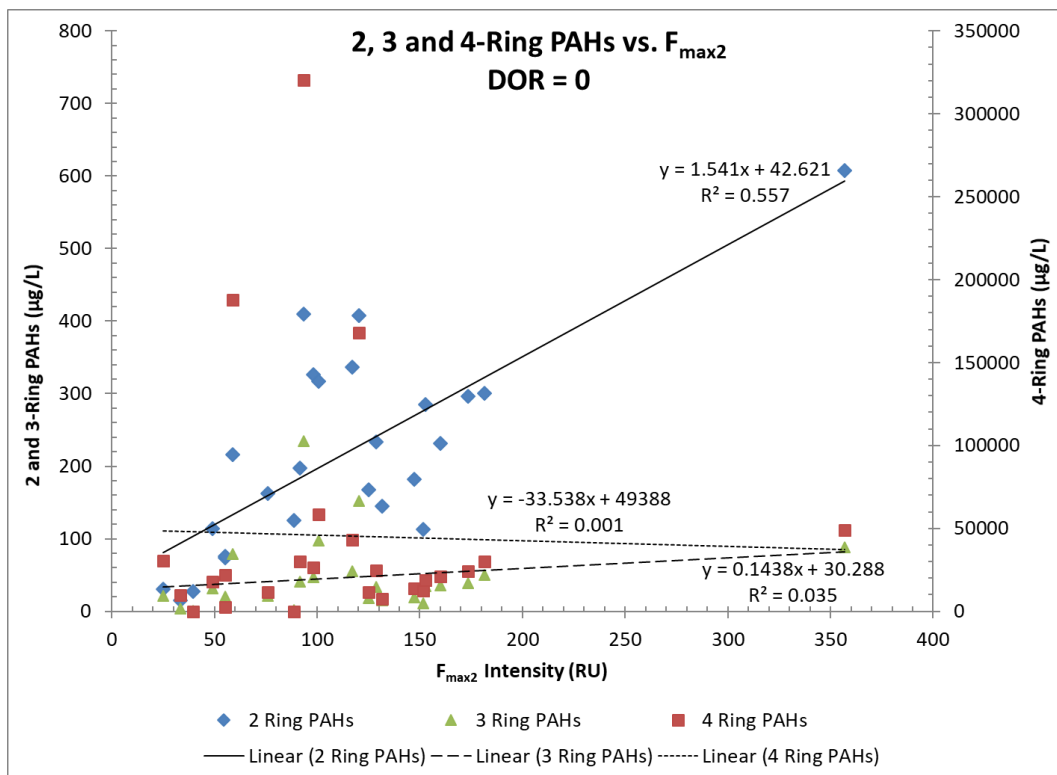
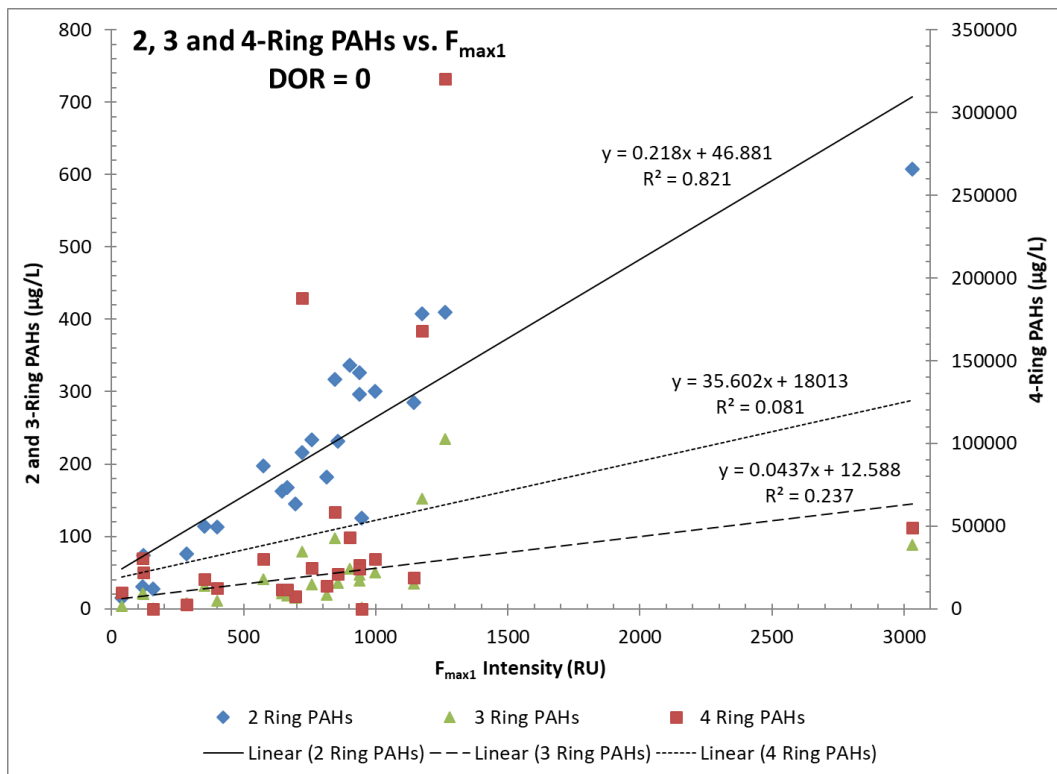


Figure 2.11. For all oil types at DOR 0, total concentration of 2-ring, 3-ring, and 4-ring PAHs ($\mu\text{g/L}$) against fluorescence intensity (RU) at F_{max1} (top), and against F_{max2} (bottom).

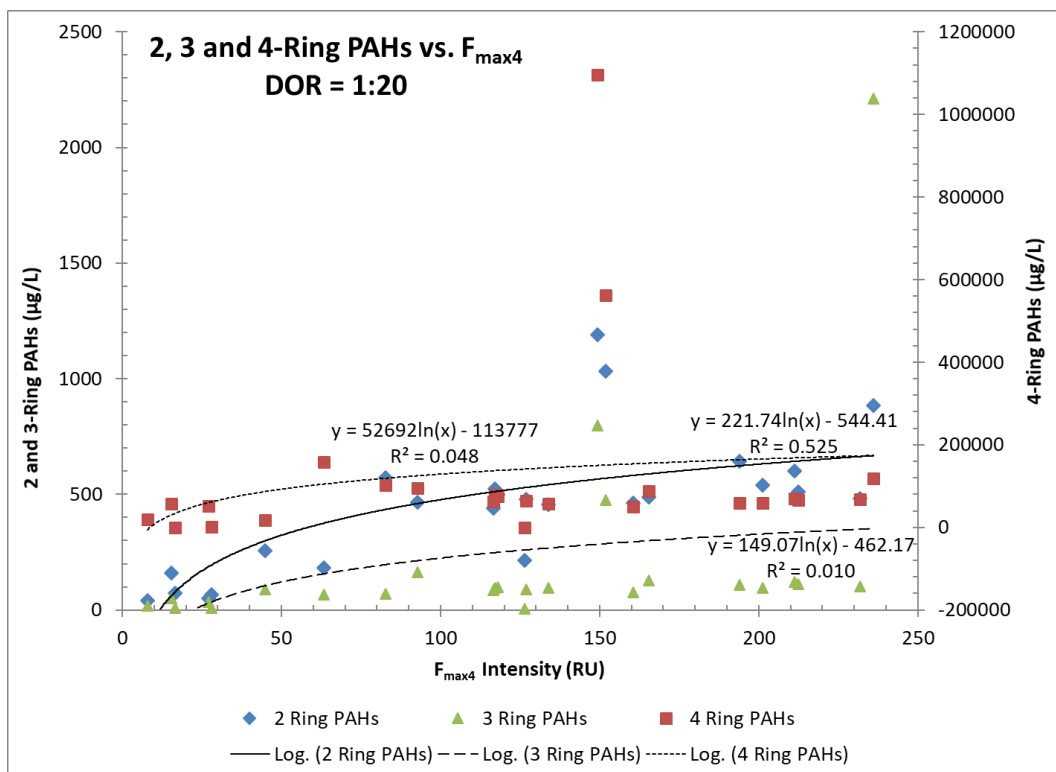
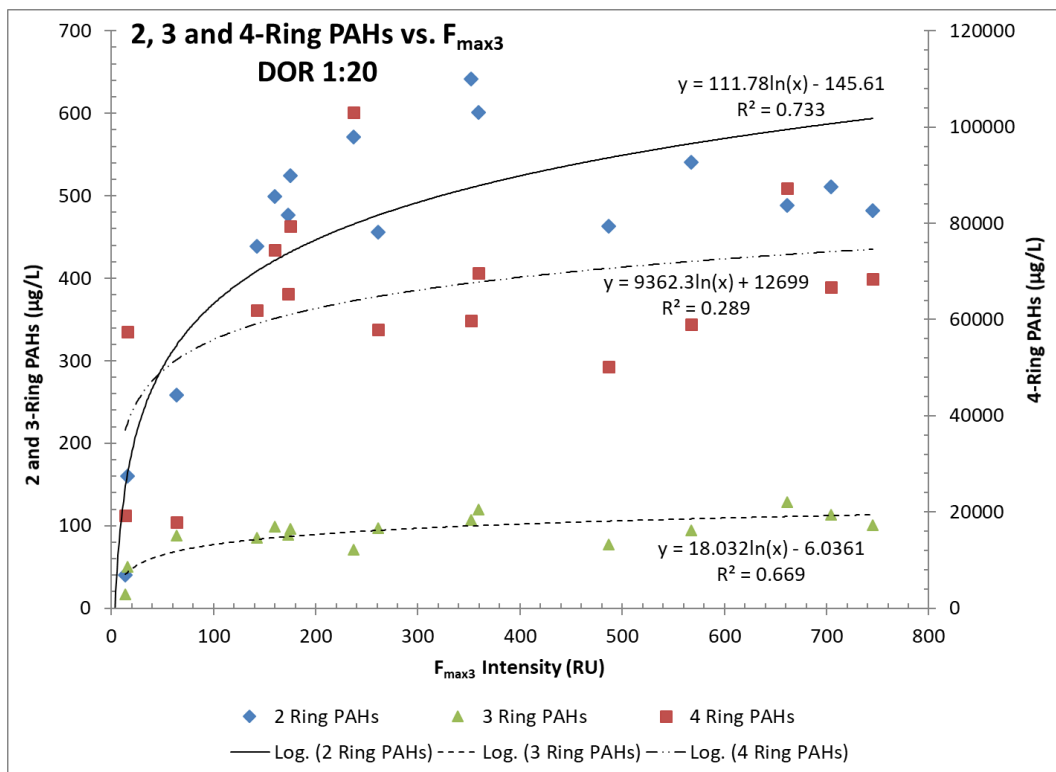


Figure 2.12. For all oil types at DOR 1:20, total concentration of 2-ring, 3-ring, and 4-ring PAHs ($\mu\text{g/L}$) against fluorescence intensity (RU) at F_{max3} (top), and against F_{max4} (bottom).

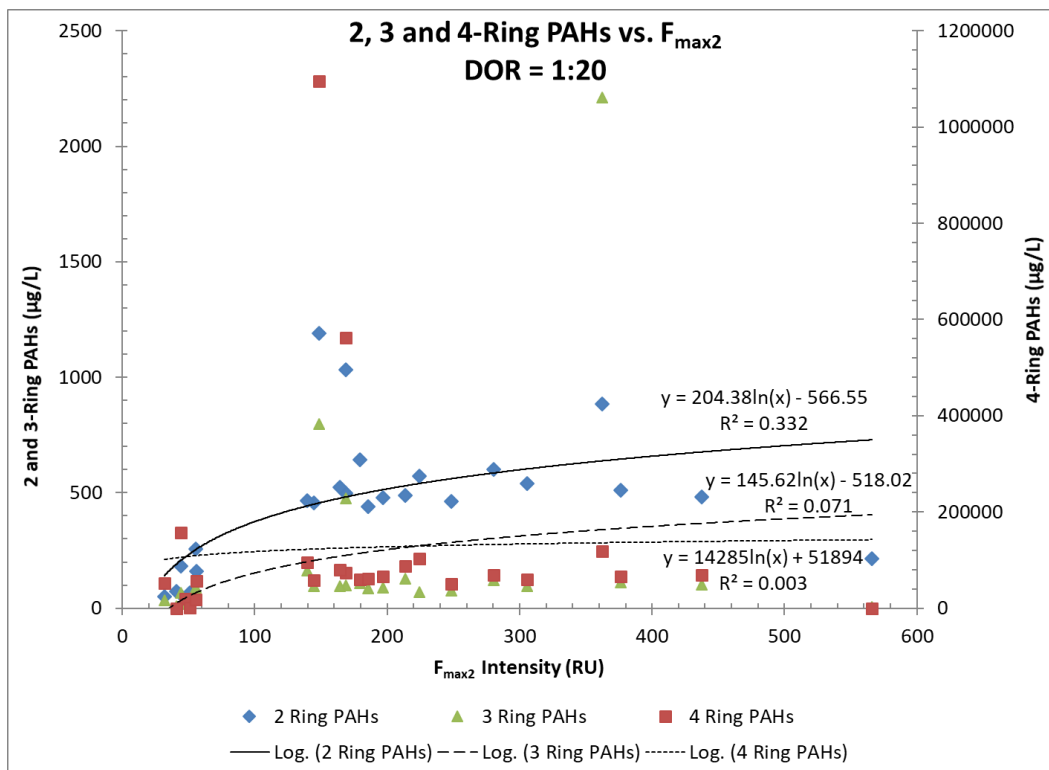
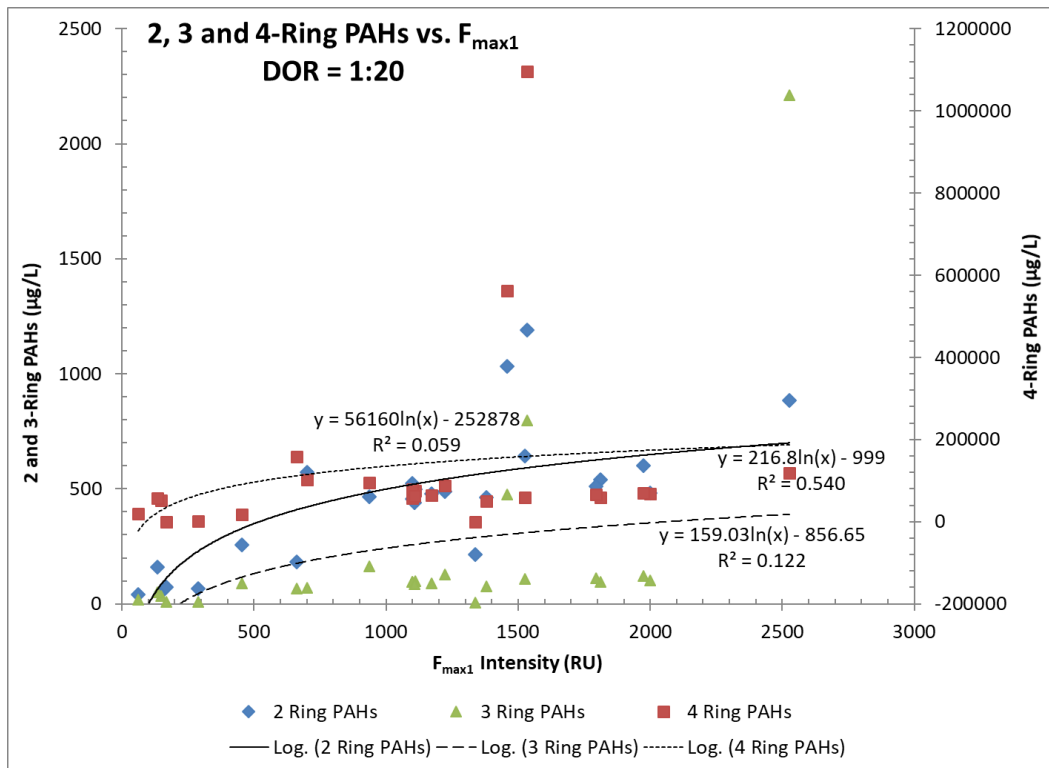


Figure 2.13. For all oil types at DOR 1:20, total concentration of 2-ring, 3-ring, and 4-ring PAHs ($\mu\text{g/L}$) against fluorescence intensity (RU) at F_{max1} (top), and against F_{max2} (bottom).

The effect of full dispersion (DOR 1:20) on dissolved hydrocarbons can also be investigated by taking the ratio of total alkanes + PAHs at DOR 1:20 to total alkanes + PAHs at DOR 0—the Chemical Dispersibility Ratio (CDR). These ranged from a low of 0.8 for two heavy oils—Hondo and IFO 300—up to a maximum of 7.8 for Arabian Light. Although heavy oils tended to have lower CDRs and light oils tended to have higher ratios, oil density was not correlated with chemical dispersion. For example, the heavy oil Santa Clara (API Gravity 22.1°) had the third highest CDR (5.4), while SSC, by far the lightest oil (API Gravity 46.6°), had a CDR of only 2.2. The effect of dispersion on fluorescence intensity can be similarly investigated by taking the ratio of $F_{\max 1}$ fluorescence intensity at DOR 1:20 to that at DOR 0, resulting in the Fluorescence Dispersibility Ratio (FDR). This also shows a general increasing trend with increasing API Gravity, with a statistically significant moderate linear relationship ($R^2 = 0.55$, $p = < 0.001$) (Fig. 2.14).

All four IFOs (IFO-40, IFO-120, IFO-180, and IFO-300), as well as SSC, showed fluorescence and chemistry anomalies that tended to skew overall results. With respect to SSC, all other light oils (API Gravity $< 22.3^\circ$) exhibited increasing fluorescence intensity with increasing DOR, culminating in a marked increase at DOR 1:20; however, SSC actually showed a significant decrease in fluorescence intensity at DOR 1:20, dropping to below the level exhibited at DOR 1:200. It is particularly unusual that fluorescence intensity at the highest DOR is lower than that at DORs 1:200 and 1:100. Additionally, SSC was the only light oil which exhibited no $F_{\max 3}$ fluorescence at any DOR. Chemically, SSC was also unusual, containing a very high proportion of 2-ring to 3-ring PAHs—52.2 for DOR 0 and 58.6 for DOR 1:20. With the exception of Santa Clara, with a 2-ring to 3-ring ratio of 31.9 at DOR 0,

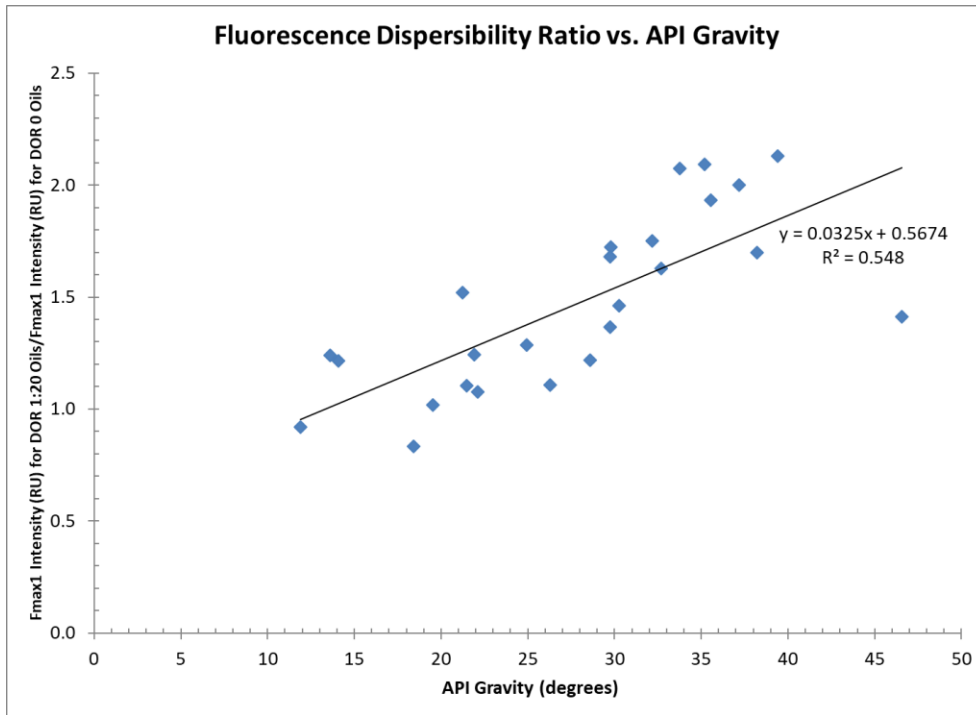


Figure 2.14. Fluorescence Dispersibility Ratio (FDR) vs. decreasing oil density shows a moderate relationship between fluorescence and oil density. With the removal of the data point for SSC, linear regression improves the relationship between fluorescence and oil density ($R^2 = 0.71$).

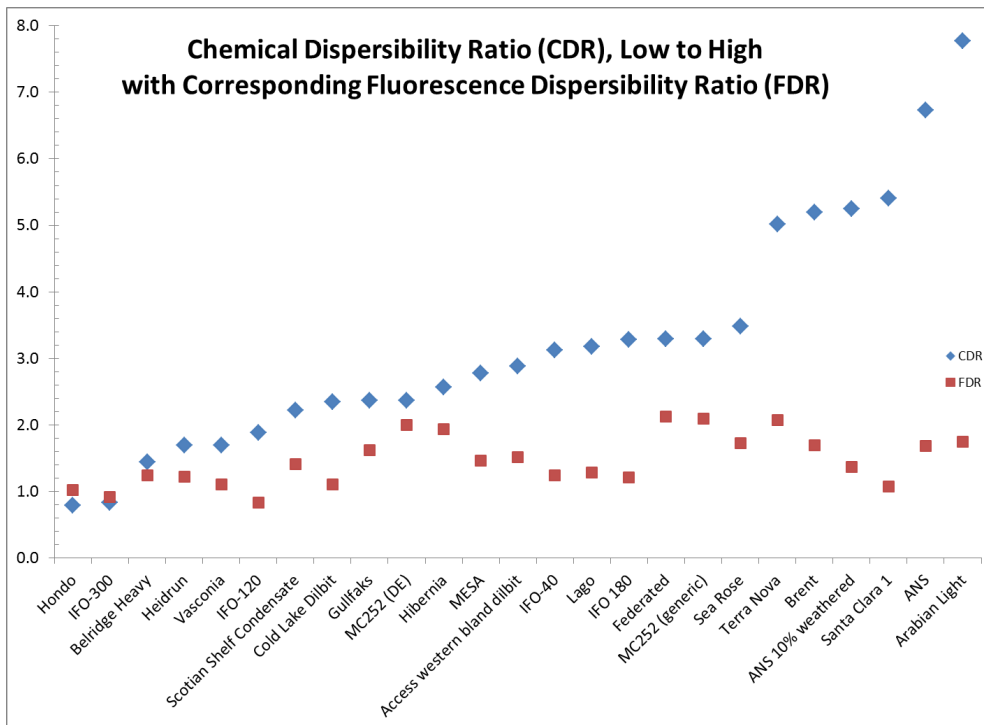


Figure 2.15. Chemical Dispersibility Ratio (CDR), ordered from low to high, with corresponding Fluorescence Dispersibility Ratio (FDR).

all other oil types had a ratio of 10 or less at both DOR 0 and DOR 1:20. SSC also contained no 4-ring or 5-ring PAHs, unlike all other oils with the exception of DOR 0 Santa Clara. All four of the IFOs fell into the heavy oil group (API Gravity $> 31^\circ$), in which all other oils showed little to no increase in fluorescence intensity with increasing DOR, as well as maximum $F_{\max 1}$ intensity of just 60-288 RU. The IFOs, however, showed far greater $F_{\max 1}$ intensity across the board (721-3031 RU) along with clear separation with increasing DOR. Like SSC, IFO-120, IFO-180, and IFO-300 also exhibited a drop in $F_{\max 1}$ intensity at DOR 1:20; in fact, IFO-120 $F_{\max 1}$ at DOR 1:20 was actually 17 % lower than at DOR 0. These same three IFOs also had the highest overall concentration of PAHs, and all four IFOs were the only oils to contain any anthracene. For all oil types, total alkanes as a function of fluorescence intensity was found to be only loosely related, as total concentration increased overall in relation to fluorescence intensity. This is as expected since fluorescence arises from the π -electron cloud present in aromatic compounds rather than from the carbon to carbon bonds present in straight chain compounds.

PARAFAC Analysis

The fluorescence profiles of the 25 oils in the BFT analysis are related to the underlying complexity of the chemical compounds that comprise them. In an attempt to identify those connections, PARAFAC analysis was performed on the fluorescence data. The PLS Toolbox (Eigenvector Research 2018) was used within MATLAB (The MathWorks 2018) to accomplish this task. After importing raw data and assembling datasets, three constraints were applied to all samples: normalization, EEM filtering, and non-negativity. Normalization was done to compensate for the wide variation in fluorescence intensity across oil types (e.g., $F_{\max 1}$

= 39.6 RU for Access Western Blend Dilbit to $F_{\max 1} = 3090.2$ RU for IFO-120) in order to prevent samples with high fluorescence intensity values from skewing the model. Further, normalization of maximum intensity to 1 (inf-Norm) was chosen rather than normalization of the entire area of fluorescence (1-Norm) to preserve differences in spectral shape. EEM filtering was applied in order to remove artifacts of the fluorescence analysis process known as first and second order Rayleigh scatter. This was accomplished by interpolating data across those regions (12 nm for first order Rayleigh and 24 nm for second order Rayleigh); zero values were also assigned to sub-Rayleigh wavelengths since fluorescence emission takes place at wavelengths above excitation due to Stokes shift. Raman scatter, the other light-related artifact which must be removed before PARAFAC analysis can be performed, was accomplished as sample analysis was done by subtracting a sample blank of artificial seawater from each sample. Finally, after running several PARAFAC test models using 4, 5, 6 and 7-components on a dataset containing the DOR 0 sample from flask #1 of all 25 oil types, data between excitation at 200 nm and 212 nm was excluded. The inherent “noise” typically found at excitation < 240 nm, related to the low intensity of xenon lamps in that region, led to this decision. Excluding data at excitation and emission wavelengths above 680 nm was also employed in order to improve processing results since no fluorescence information of value was contained in that region.

The biggest challenge in PARAFAC modelling is in determining the most appropriate number of component factors. While it is important to ensure separation of all individual factors, it is also critical not to select too many components in order to avoid over-fitting the data. Bro (1997) suggests several ways of doing this in his PARAFAC tutorial: comparison of the resulting factor

profiles with background knowledge of expected components, consideration of the residuals, and split half validation of the model. The latter has also been recommended by other researchers (Harshman and Lundy 1994; Murphy et al. 2013). Split half analysis is accomplished by randomly dividing the data into two independent subsets and applying the model to each of the subsets. In theory, if the correct number of components has been selected, the two halves of the data should each fit the model well; however, Murphy cautions that a relatively large data set is necessary in order for this to hold true (2013). Smilde et al. (2004) also caution that some phenomena observed in a data subset which do not match the overall model may just happen to be present in that particular random half of the data. Thus, we might anticipate that split half validation will work better with samples within oil weight subdivisions, than with the dataset containing all 25 oils as a whole.

Bro and Kiers (2003) have also advised using core consistency of the model to validate that the correct number of components has been selected. All of these methods were employed for the following analyses by first noting the percentage of data fit by the model, next checking the core consistency of the model, then inspecting residuals, inspecting the loadings for Mode 3 (excitation) and Mode 2 (emission), and inspecting EEMs of each component. Finally, split half analysis was performed. In all cases, several models were run with different numbers of components to ensure selection of the most appropriate model.

All 25 Oil Types

DOR 0

Initially, a five-component model was fit to the dataset, followed by 4-, 6-, and 7-component models. Best overall fit was obtained with the six-component model, which explained 99.5% of the data. Core consistency was 52%, and split half validation was 56.4% (Fig. 2.16). Review of residuals showed they were minimal with random distribution, and inspection of plots of Mode 2 and Mode 3 loadings (Fig. 2.17), shows that, although components are tightly spaced, all appear as separate and distinct peaks. Variation per component (Fig. 2.18), as well as EEMs of individual components (Fig. 2.19), also supported choice of the 6-factor model for best fit. Fig. 2.18 shows that Component 1 accounted for >20% to 40% (unique fit and fit) of the data, while Component 2 contributed 5-10% (unique fit and fit) and Components 3-6 accounted for 5% or less of the data, respectively. While Component 6 accounted for a very low percentage of the data, the 6-component model was still a better fit to the data than the 5-component model.

DOR 1:100

A six-component model was initially fit to the dataset containing all 25 oil types at DOR 1:00 as that was the best fit for the DOR 0 dataset. However, for the DOR 1:100 dataset, the 5-component model proved to be the best fit, explaining 99.4 % of the data with core consistency of 72 % and split half validation of 75.8 %. Residuals were minimal and randomly distributed, and visual inspection of loadings (Fig. 2.20) again shows that components are tightly spaced, but all appear as separate and distinct peaks. Variation per component (Fig. 2.21) and component EEMs (Fig. 2.22) led to acceptance of the 5-component model. Fig. 2.21 shows Component 1

Similarity measure of splits and overall model 56.4%

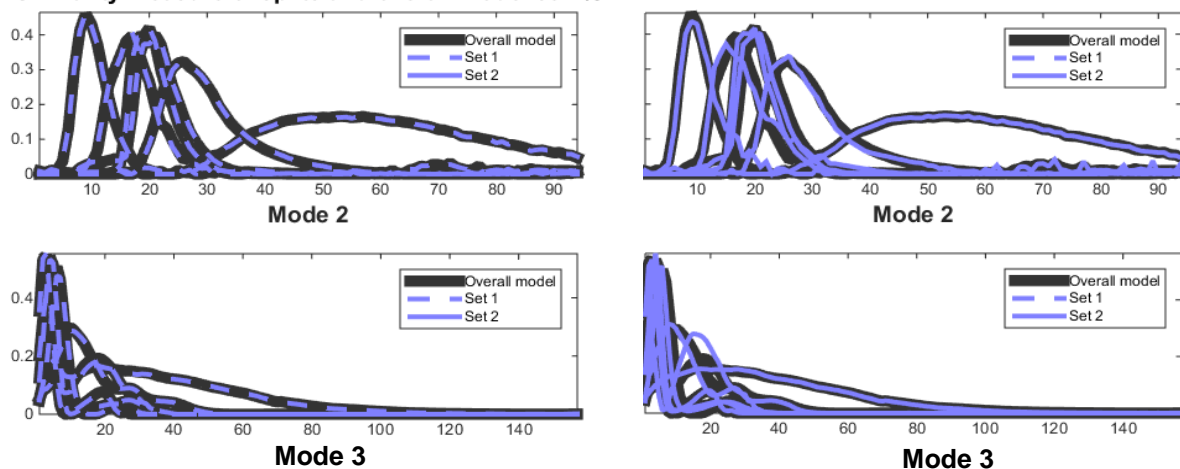


Figure 2.16. Example of split half validation for the 6-component model of 25 oil types at DOR 0 showing individual fit of data splits. Set 1 data vs. the model is shown for Mode 2 and Mode 3 on the left; and Set 2 data vs. the model is presented for Mode 2 and Mode 3 on the right.

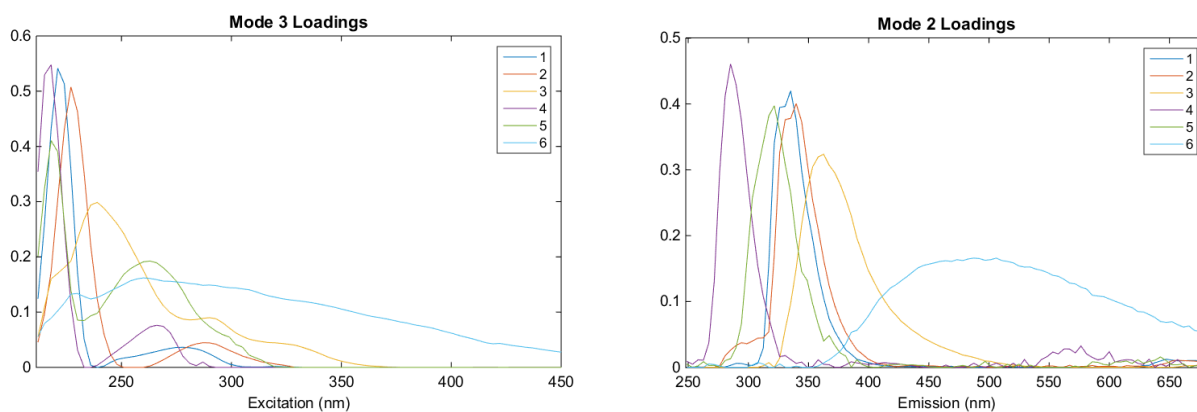


Figure 2.17. Mode 3 Loadings (Excitation) and Mode 2 Loadings (Emission) for all 25 oil types—DOR0 using 6-component model. Note difference in x-axis scales.

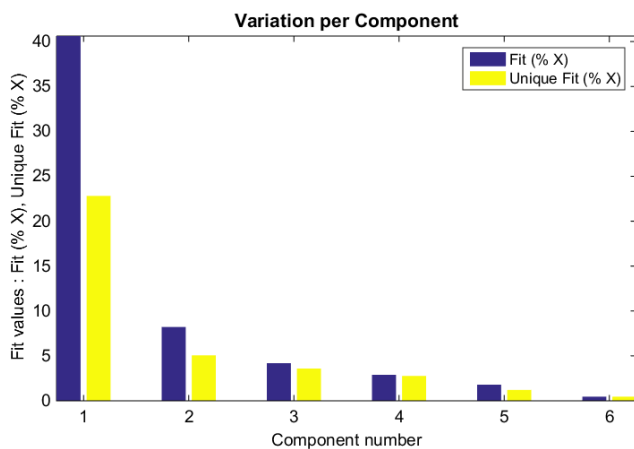


Figure 2.18. Variation per component for 6-component model of all 25 oil types at DOR0.

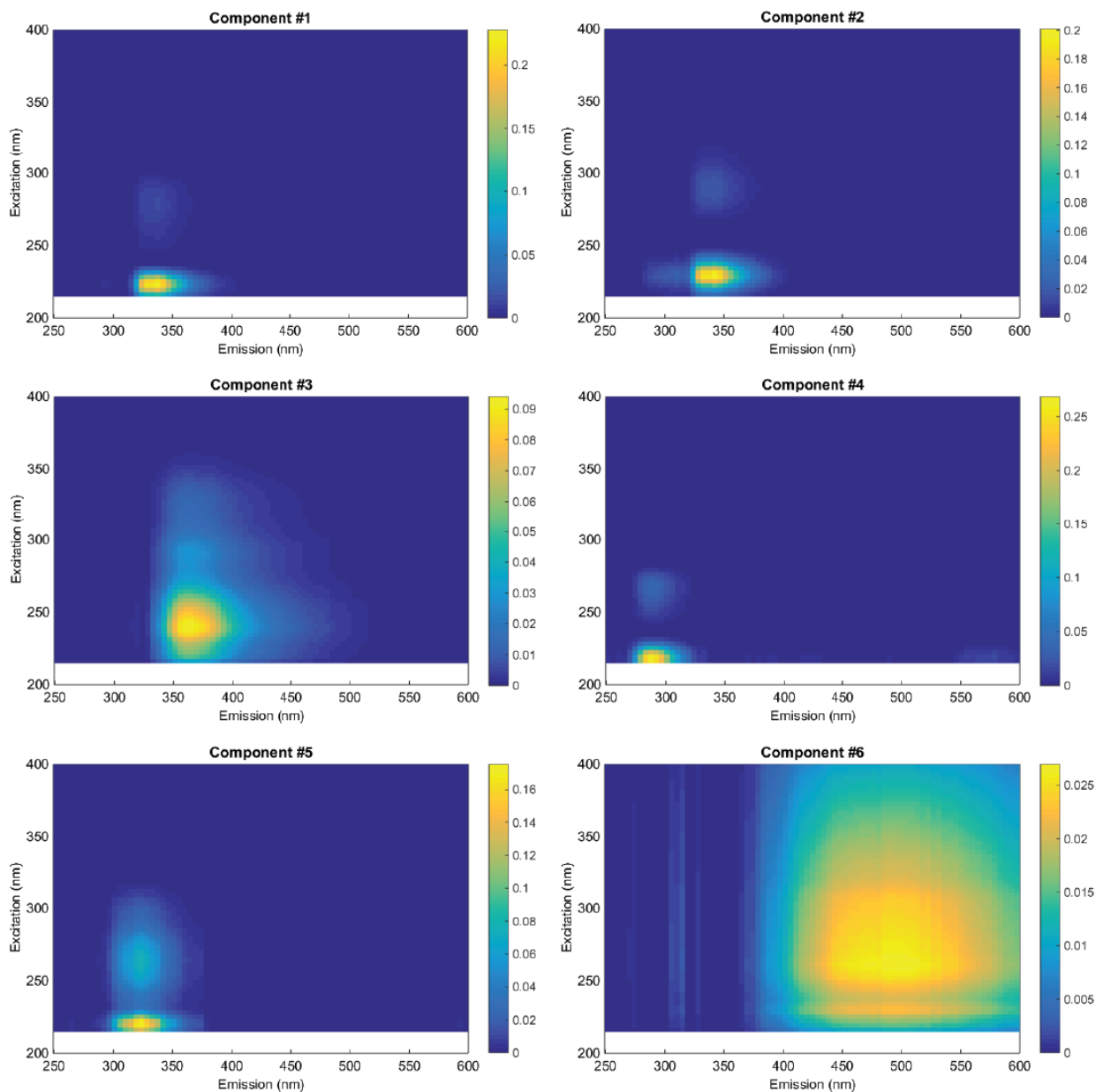


Figure 2.19. EEM views of the six components of the PARAFAC model for 25 oil types at DOR 0. Component #1: $F_{\max} = \text{Ex } 224\text{nm}/\text{Em } 335\text{nm}$; Component #2: $F_{\max} = \text{Ex } 230\text{nm}/\text{Em } 340\text{nm}$; Component #3: $F_{\max} = \text{Ex } 239\text{nm}/\text{Em } 363\text{nm}$; Component #4: $F_{\max} = \text{Ex } 218\text{nm}/\text{Em } 290\text{ nm}$; Component #5: $F_{\max} = \text{Ex } 221\text{nm}/\text{Em } 322\text{nm}$; Component #6: $F_{\max} = \text{Ex } 260\text{nm}/\text{Em } 474\text{-}511\text{nm}$.

accounted for >35% to almost 50% (unique fit and fit) of the data, while Components 2-5 accounted for 5% or less of the data, respectively.

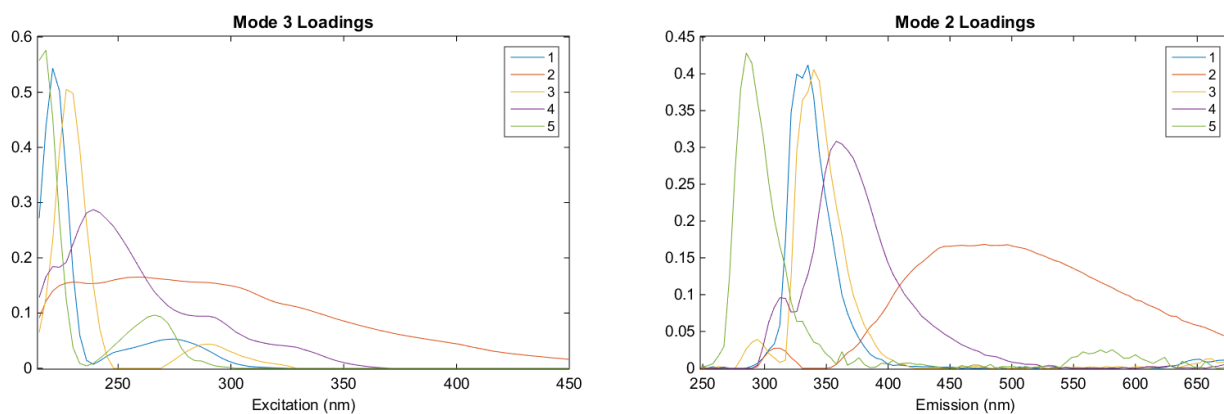


Figure 2.20. Mode 3 Loadings (Excitation) and Mode 2 Loadings (Emission) for all 25 oil types—DOR 1:100 using 5-component model. Note difference in x-axis scales.

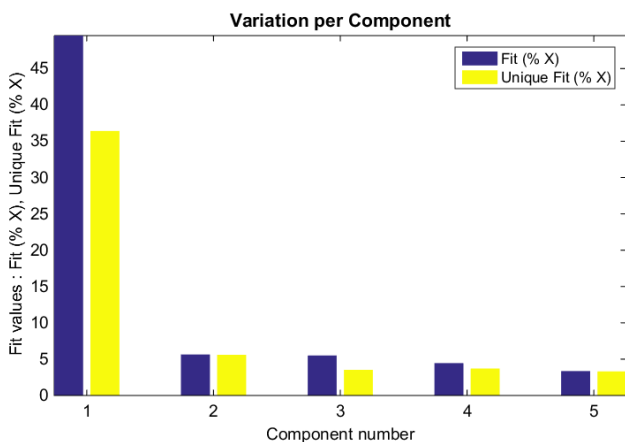


Figure 2.21. Variation per component for the 5-component model of all 25 oil types at DOR 1:100.

DOR 1:20

A six-component was initially fit to the dataset containing all 25 oil types at DOR 1:20; however, an error message warning that two or more components may be fitting the same data was displayed, and the core consistency was <0 %. Fitting a 5-component model to the data, however, resulted in 98.9 % of the data explained by the model as well as core consistency of 84 % and a split half validation of 84 %. Overall, residuals were minimal and randomly distributed; however, residuals appeared to occur at somewhat higher wavelengths than at other DORs.

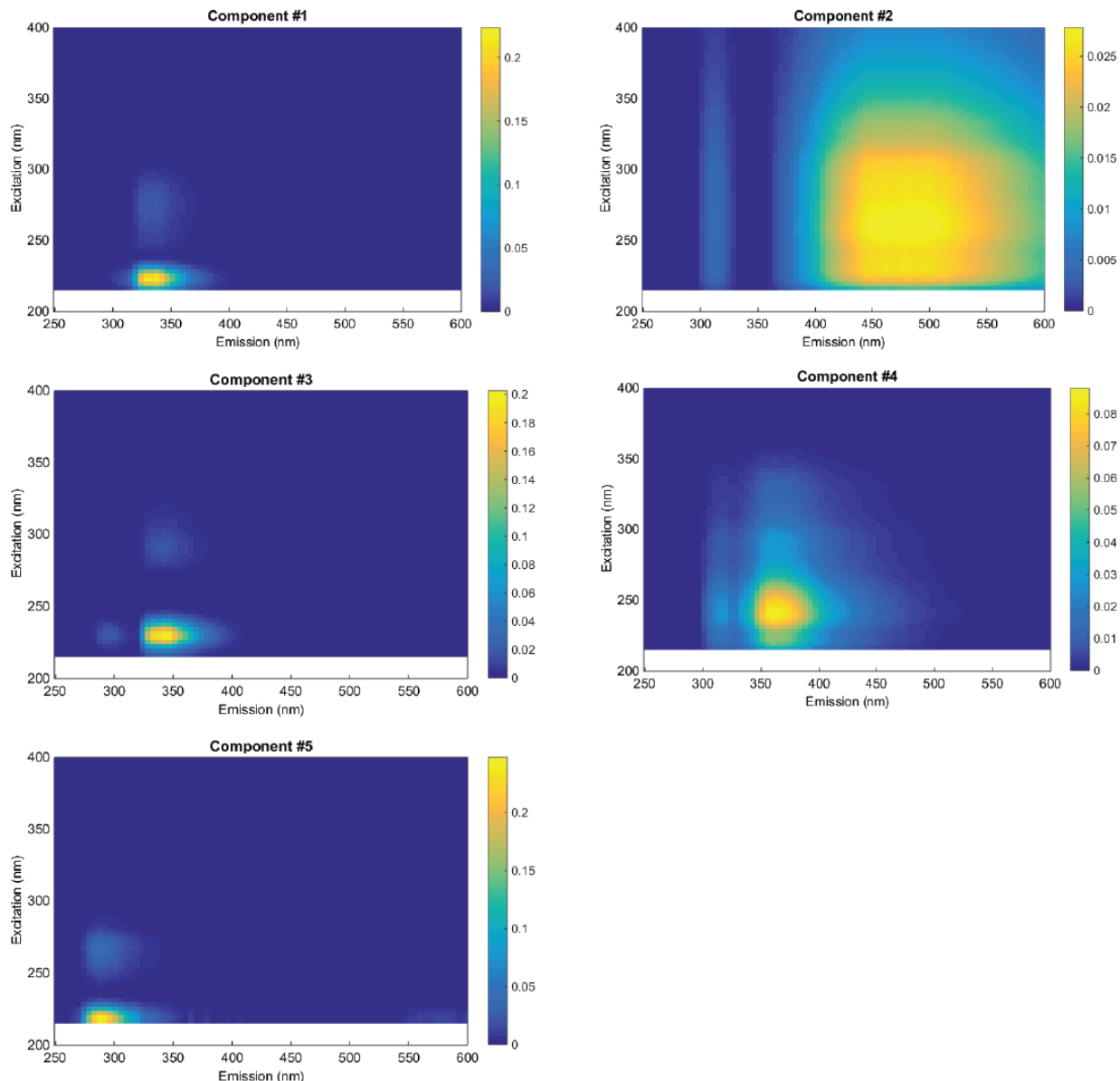


Figure 2.22. EEM views of the five components of the PARAFAC model for 25 oil types at DOR 1:100. Component #1: $F_{\max} = Ex\ 224nm/Em\ 335nm$; Component #2: $F_{\max} = Ex\ 254-266nm/Em\ 455-501nm$; Component #3: $F_{\max} = Ex\ 230nm/Em\ 344nm$; Component #4: $F_{\max} = Ex\ 242nm/Em\ 363\ nm$; Component #5: $F_{\max} = Ex\ 218nm/Em\ 290nm$.

Visual inspection of loadings (Fig. 2.23), and variation per component (Fig. 2.24) led to final acceptance of the 5-component model. Note that the effect of full dispersion appears to broaden and shift emission peaks to longer wavelengths (Fig. 2.25). Analysis of variation per component (Fig. 2.24) shows Component 1 accounted for 25 to 30 % of the data (unique fit and fit) while

Component 2 has increased to >10 % to 25 % (unique fit and fit) of the data. Contribution from Component 3 and 4 have increased, as well.

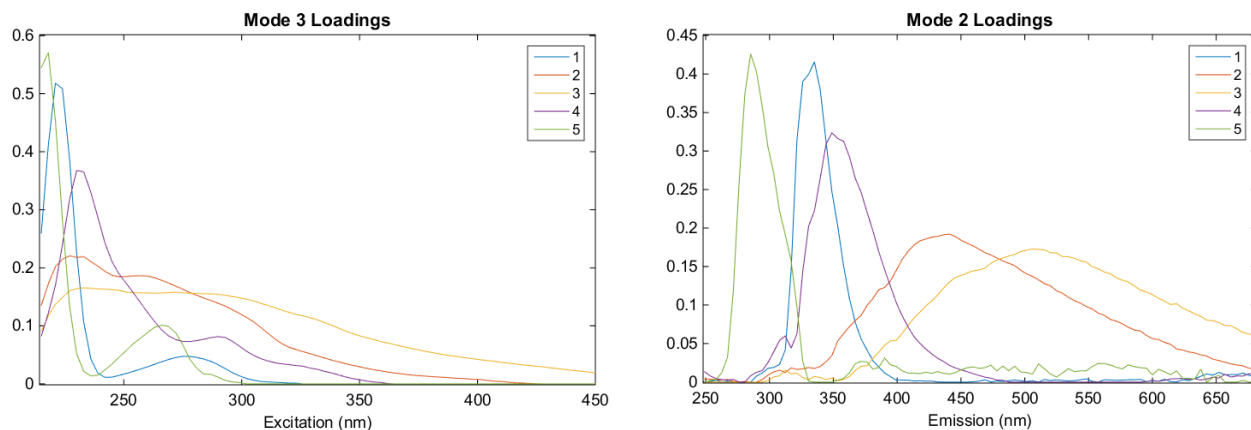


Figure 2.23. Mode 3 Loadings (Excitation) and Mode 2 Loadings (Emission) for all 25 oil types—DOR 1:20 using 5-component model. Note difference in x-axis scales.

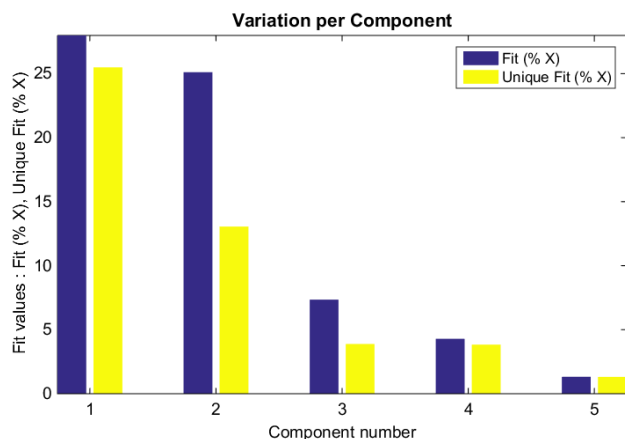


Figure 2.24. Variation per component for the 5-component model of all 25 oil types at DOR 1:20.

Summary of PARAFAC Modelling

PARAFAC analysis of EEM datasets for the 25 oil types at DOR 0, DOR 1:100, and DOR 1:20 show interesting changes in fluorescence intensity with increasing dispersion. However, we see a decrease in distinct components from six at DOR 0 to five at DOR 1:100 and 1:20. Three components at DOR 0 and DOR 1:100 match peak positions identified in previous studies of natural waters (A_T , A_M and A_C) (Coble et al. 2014); however, that is true of only one component

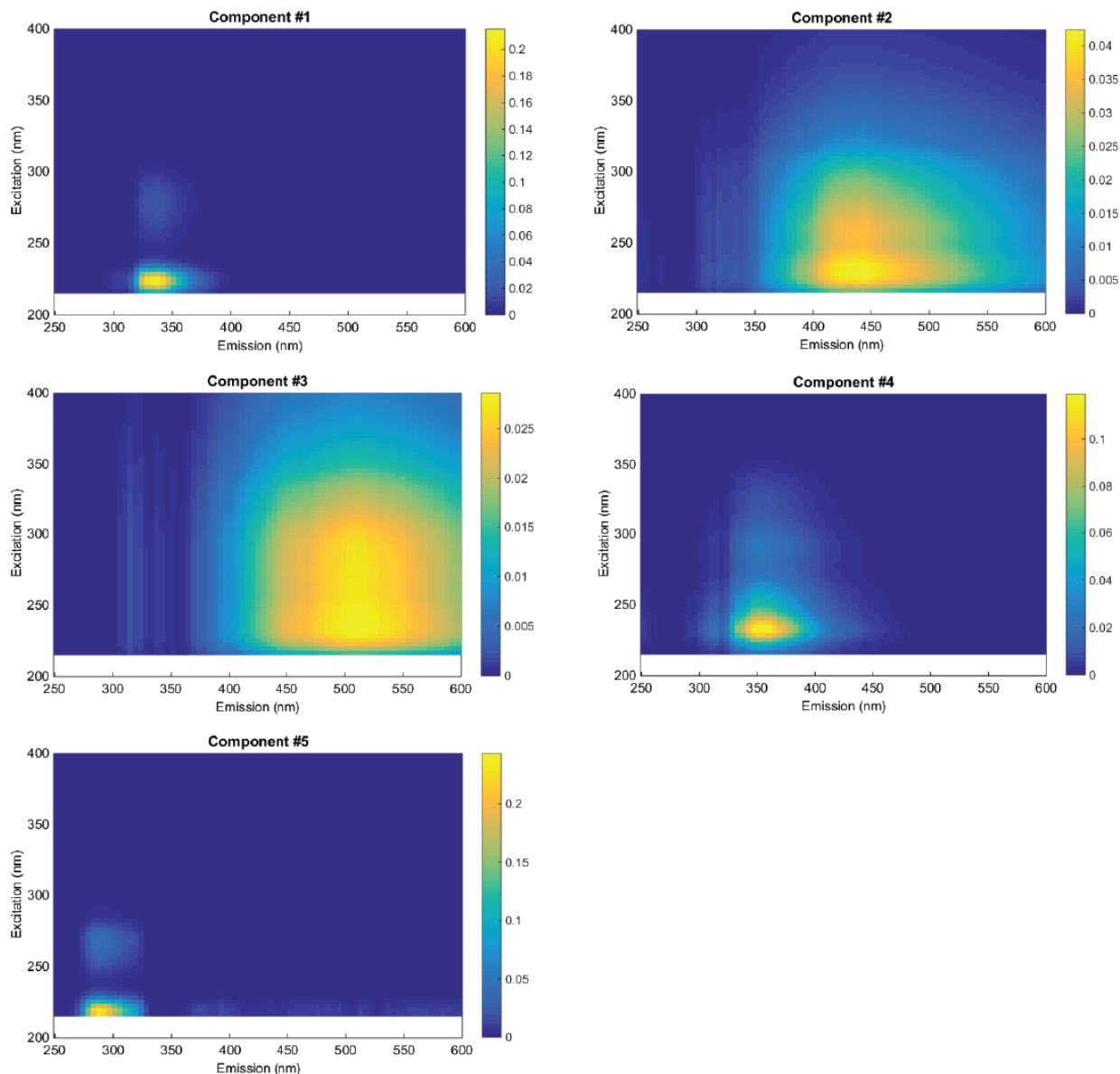


Figure 2.25. EEM views of the five components of the PARAFAC model for 25 oil types at DOR 1:20. Component #1: $F_{\max} = \text{Ex } 224\text{nm}/\text{Em } 335\text{nm}$; Component #2: $F_{\max} = \text{Ex } 233\text{-}266\text{nm}/\text{Em } 432\text{-}450\text{nm}$; Component #3: $F_{\max} = \text{Ex } 230\text{-}242\text{nm}/\text{Em } 501\text{-}520\text{nm}$; Component #4: $F_{\max} = \text{Ex } 233\text{nm}/\text{Em } 349\text{nm}$; Component #5: $F_{\max} = \text{Ex } 218\text{nm}/\text{Em } 290\text{nm}$.

at DOR 1:20 (A_T). The relative contribution from each of these components changes with dispersion as well. The A_C -like component contributes least to the model at DOR 0, and increases in importance to second in the model for DOR 1:100, while the contribution from the A_T -like component drops from second at DOR 0 to third at DOR 1:100 and the contribution from the A_M -like peak drops from third to fourth.

From analysis of plots of Mode 3 (Excitation) and Mode 2 (Emission) Loadings, it appears that increased dispersion results in a broadening and shift to longer emission wavelengths as well as in a larger contribution of fluorescence intensity at longer wavelengths. Upon examination of the EEMs of each component, several other patterns emerge. Even with the minimal dispersion at DOR 1:100, contribution to the overall model from a broad fluorescence peak, which provided the least contribution to the overall model at DOR 0 — Component #6, became second in importance at DOR 1:100, albeit with a contribution to the model of only about 5 %. Upon full dispersion at DOR 1:20, this broad, high-wavelength peak retained importance to the model of approximately 5-7 %; however, another broad, but slightly lower wavelength peak appeared as Component #2 with 12-25 % contribution to the overall model. Throughout the entire analysis, Component #1 at Ex 224 nm/Em 335 nm remained the most important contribution to the model, which confirms this fluorescence region as the best target for detecting oil in the marine environment. However, since the region represented by Component #2 in the DOR 1:20 dataset becomes a major contribution to the model only upon effective dispersion, the FIR ratio (Bugden et al., 2008) can be used to track this important parameter.

The MC252 oil samples used for these analyses, both that either were collected onboard the *Discoverer Enterprise* or the generic version provided by BP, are classified as light, sweet crude based on density and sulfur content. Overall, oil types range from light to heavy due to the proportion of n-alkanes (paraffins) and cyclo-alkanes (naphthenes) vs. aromatic hydrocarbon compounds, while sulfur content determines the rank of sweet (<1 %) vs. sour (>1 %). These characteristics arise from kerogen source and reservoir maturity (Tissot and Welte 1978). The 25 oils analyzed in this project cover a wide range of light to heavy oil types, as well as a range

of sulfur content. Oil fluorescence phenomena arise from the presence of π -bonding in aromatic C=C bonds, leading to highest fluorescence intensity from polycyclic aromatic hydrocarbons (Ryder 2005), with fluorescence intensity tending to increase with increasing molecular weight (Mendoza et al. 2013). However, the presence of fluorescence quenching species, as well as energy transfer between complex molecules, complicates the isolation of compound-specific fluorescence in crude oil analysis. Fluorescence research has shown that heavy oils generally have broad, weak fluorescence while lighter oils have narrower, more intense emission bands (Steffens et al. 2011). Due to the hundreds, if not thousands, of complex hydrocarbons present in crude oils, characterization of fluorescence arising from specific PAH molecules would be time consuming, if not impossible. However, PARAFAC analysis of these 25 oil types has shown that it is possible to use fluorescence characterization in specific wavelength regions for detection of non-dispersed vs. dispersed oil across a wide variety of oil types.

Coming from the well depth of approximately 1,600 m, the MC252 oil source is by far the deepest of all our 25 oil type sources; however, a number of other oil types were sources from offshore well locations. These include the light oils, Brent and Gullfaks from the North Sea (140-230 m water depth), as well as Hibernia, SSC and Terra Nova from offshore eastern Canada (12-100 m water depth). Intermediate weight oils, Heidrun from the Norwegian Sea (350 m water depth) and Sea Rose from off the coast of Newfoundland, Canada (100 m water depth), as well as the heavy oil Hondo from offshore California (260 m water depth) were also included in this study. The intermediate weight Alaskan North Shore, both fresh and 10 % weathered, would be representative of oil, which may be sourced from offshore Alaska in the future. Additionally, with the presence of approximately 3,000 platforms in the U.S. Gulf of

Mexico (BOEM, 2016), understanding the characterization of non-dispersed and dispersed MC252 oil will certainly aid in preparedness for the possibility of future oil spill events in that region.

CONCLUSIONS

Although petroleum is ubiquitous as a low-level, naturally-occurring component of the marine environment due to natural seeps, anthropogenic introduction of much greater concentrations occurs during well-drilling, as well as in transportation of fossil fuels. Just within the Gulf of Mexico, high-volume crude oil flows include the Ixtoc I (> 3 million bbl, from June 1979 to March 1980) (Jernelov and Linden 1981) and the DWH blowout (4.9 million bbl from April to August 2010) (Federal Interagency Solutions Group 2010). Added to this are chronic, lower-level spills such as the that emanating from the Taylor Energy site where Platform 23051 was located before destruction by Hurricane Ivan in 2004 (Harrison 2017). Events such as these combine with intentional as well as accidental releases in the transportation and use of petroleum-based fuels. And of course this is not unique to the Gulf of Mexico, but transpires globally.

Detection of low concentrations of petroleum in the marine environment is critically important in order to enable protection of sensitive ecosystems from the inherent toxicity arising largely from PAHs, which are proven to be toxic, mutagenic and carcinogenic (D'Sa et al. 2016). The use of dispersants must be carefully weighed in order to determine whether the impact of dispersing oil into the water column will be positive due to the enhancement of microbial biodegradation, or overwhelmingly negative due to toxicity to organisms within the water column and in the

benthos. Long-term environmental effects have yet to be fully determined (Ufford et al. 2014). Prevention of slick formation and mitigation of oil on the ocean surface, which will eventually reach shorelines and wetlands, is also an important consideration.

The SMART protocol calls for the use of in situ fluorometers to detect petroleum in the marine environment in this decision-making effort (U.S. Coast Guard et al. 2006). While GC-MS has gained overwhelming acceptance in the scientific community for the quantification of petroleum, due to the sensitivity of the majority of GC-MS instruments, use of this analysis method is not generally practical for use at sea (D'Sa et al. 2016). Off-the-shelf fluorometers have been used to detect petroleum in the marine environment for decades; however, intercomparison between instruments with varying wavelength detection, as well as correlation of the heretofore largely qualitative data with quantitative chemical analyses, such as that presented by Conmy et al. (2014a), is important in order to provide confirmation for first responders. In situ fluorometers capable of delivering two emission wavelengths in order to give FIR data could also prove more useful in future oil response efforts to determine the effectiveness of dispersant delivered in both subsurface and surface applications.

Our results define differences between Type I and Type II oils, which will aid decision-makers in choosing an appropriate course of action in dispersant application. Studies suggest that, while there appears to be an upper limit of dispersant effectiveness with increasing oil viscosity, there is not a direct relationship (Canevari et al. 2001) and chemical composition is more important (Mukherjee et al. 2011). Future work is needed to determine how specific petroleum components play a role. The creation of the database of EEMs for 25 oils at four DORs is a first

step in that direction, and will also allow for advantageous “fingerprinting” characterization in the marine environment of the behavior of oils over a wide range of chemical composition and kinematic viscosity.

REFERENCES

- Bahram M, Bro R, Stedmon C, Afkhami A. 2006. Handling of rayleigh and raman scatter for parafac modeling of fluorescence data using interpolation. *Journal of Chemometrics*. 20(3-4):99-105.
- Baszanowska E, Otremba Z. 2017. Fluorometric index for sensing oil in the sea environment. *Sensors*. 17.
- Bro R. 1997. Parafac. Tutorial and applications. *Chemometrics and Intelligent laboratory Systems*. 38:149-171.
- Bro R, Kiers HAL. 2003. A new efficient method for determining the number of components in parafac models. *Journal of Chemometrics*. 17:274-286.
- Bugden JBC, Yeung CW, Kepkay PE, Lee K. 2008. Application of ultraviolet fluorometry and excitation-emission matrix spectroscopy (eems) to fingerprint oil and chemically dispersed oil in seawater. *Marine pollution bulletin*. 56:677-685.
- Camilli R, Reddy CM, Yoerger DR, Van Mooy BAS, Jakuba MV, Kinsey JC, McIntyre CP, Sylva SP, Maloney JV. 2010. Tracking hydrocarbon plume transport and biodegradation at deepwater horizon. *Science*. 330:201-204.
- Canevari GP, Calcavecchio P, Beckier KW, Lessard RR, Fiocco RJ. 2001. Key parameters affecting the dispersion of viscous oil. *International Oil Spill Conference Proceedings*.479-483.
- Chen RF, Bada JL. 1992. The fluorescence of dissolved organic matter in seawater. *Marine Chemistry*. 37:191-221.
- Clayton JR, Jr., Payne JR, Farlow JS. 1993. *Oil spill dispersants: Mechanisms of action and laboratory tests*. Boca Raton, FL: C.K. Smoley.
- Coble PG. 1996. Characterization of marine and terrestrial dom in seawater using excitation-emission matrix spectroscopy. *Marine Chemistry*. 51:325-346.
- Coble PG, Green SA, Blough NV, Gagosian RB. 1990. Characterization of dissolved organic matter in the black sea by fluorescence spectroscopy. *Nature*. 348(6300):432-435.
- Coble PG, Spencer RM, Baker A, Reynolds DM. 2014. Aquatic organic matter fluorescence. In: Coble PG, Lead J, Baker A, Reynolds DM, Spencer RM, editors. *Aquatic organic matter fluorescence*. New York, NY: Cambridge University Press. p. 75-122.

- Conmy RN, Coble PG, Farr J, Wood AM, Lee K, Pegau WS, Walsh ID, Koch CR, Abercrombie MI, Miles MS et al. 2014a. Submersible optical sensors exposed to chemically dispersed crude oil: Wave tank simulations for improved oil spill monitoring. *Environmental science & technology*. 48(3):1803-1810.
- Conmy RN, Del Castillo CE, Downing BD, Chen RF. 2014b. Experimental design and quality assurance: In situ fluorescence instrumentation. In: Coble PG, Lead J, Baker A, Reynolds DM, Spencer RM, editors. *Aquatic organic matter fluorescence*. New York, NY: Cambridge University Press. p. 190-230.
- D'Sa EJ, Overton EB, Lohrenz SE, Maiti K, Turner RE, Freeman A. 2016. Changing dynamics of dissolved organic matter fluorescence in the northern gulf of Mexico following the deepwater horizon oil spill. *Environmental science & technology*. 50:4940-4950.
- Daling PS, Lichtenhaler RG. 1986/87. Chemical dispersion of oil. Comparison of the effectiveness results obtained in laboratory and small-scale field tests. *Oil & Chemical Pollution*. 3:19-35.
- Das N, Chandran P. 2011. Microbial degradation of petroleum hydrocarbon contaminants: An overview. *Biotechnology Research International*. 2011.
- Diercks A-R, Highsmith RC, Asper VL, Joung D, Zhou Z, Guo L, Shiller AM, Joye SB, Teske AP, Guinasso N et al. 2010. Characterization of subsurface polycyclic aromatic hydrocarbons at the deepwater horizon site. *Geophysical Research Letters*. 37(2).
- Eigenvector Research I. 2018. *Pls_toolbox*. Manson, WA.
- Federal Interagency Solutions Group, Oil Budget Calculator Science and Engineering Team,. 2010. *Oil budget calculator--deepwater horizon*.
- Fingas M. 2011. Introduction to oil chemical analysis. In: Fingas M, editor. *Oil spill science & technology*. Elsevier.
- Fingas MF, Bobra MA, Velicogna RK. 1987. Laboratory studies on the chemical and natural dispersability of oil. *International Oil Spill Conference Proceedings*. 1987(1):241-246.
- Frank U. 1975. Identification of petroleum oils by fluorescence spectroscopy. *International Oil Spill Conference Proceedings*. 1975(1):87-91.
- Harrison SJ. 2017. *Lessons from the Taylor Energy oil spill: History, seasonality, and nutrient limitation*. [Athens, GA]: University of Georgia.
- Harshman RA, Lundy ME. 1994. Parafac: Parallel factor analysis. *Computational Statistics & Data Analysis*. 18:39-72.
- Hazen TC, Dubinsky EA, DeSantis TZ, Andersen GL, Piceno YM, Singh N, Jansson JK, Probst A, Borglin SE, Fortney JL et al. 2010. Deep-sea oil plume enriches indigenous oil-degrading bacteria. *Science*. 330(6001):204-208.
- Holder EL, Conmy RN, Venosa AD. 2015. Comparative laboratory-scale testing of dispersant effectiveness of 23 crude oils using four different testing protocols. *Journal of Environmental Protection*. 6(6):628-639.
- ICF Consulting Group. 1999. In-use marine diesel fuel. In: Agency USEP, editor.

- Jernelov A, Linden O. 1981. Ixtoc i: A case study of the world's largest oil spill. *Ambio*. 10(6):299-306.
- Joint Analysis Group. 2010. Review of preliminary data to examine subsurface oil in the vicinity of mc252#1, may 19 to june 19, 2010. In: National Oceanic and Atmospheric Administration, editor. Silver Spring, MD: U.S. Dept. of Commerce.
- Kaku VJ, Boufadel MC, Venosa AD. 2006. Evaluation of mixing energy in laboratory flasks used for dispersant effectiveness testing. *Journal of Environmental Engineering*. 132(1):93-101.
- Kessler JD, Valentine DL, Redmond MC, Du M, Chan EW, Mendes SD, Quiroz EW, Villanueva CJ, Shusta SS, Werra LM et al. 2011. A persistent oxygen anomaly reveals the fate of spilled methane in the deep gulf of mexico. *Science*. 331(6015):312-315.
- King TL, Clyburne JAC, Lee K, Robinson BJ. 2013. Interfacial film formation: Influence on oil spreading rates in lab basin tests and dispersant effectiveness testing in a wave tank. *Marine pollution bulletin*. 71:83-91.
- Kujawinski EB, Kido Soule MC, Valentine DL, Boysen AK, Longnecker K, Redmond MC. 2011. Fate of dispersants associated with the deepwater horizon oil spill. *Environmental science & technology*. 45:1298-1306.
- Lawaetz AJ, Stedmon CA. 2009. Fluorescence intensity calibration using the raman scatter peak of water. *Applied spectroscopy*. 63(8).
- Lee K, Nedwed T, Prince RC, Palandro D. 2013. Lab tests on the biodegradation of chemically dispersed oil should consider the rapid dilution that occurs at sea. *Marine pollution bulletin*. 73:314-318.
- Lessard RR, DeMarco G. 2000. The significance of oil spill dispersants. *Spill Science & Technology Bulletin*. 6(1):59-68.
- Li Z, Lee K, King T, Boufadel MC, Venosa AD. 2009. Evaluating crude oil chemical dispersion efficacy in a flow-through wave tank under regular non-breaking wave and breaking wave conditions. *Marine pollution bulletin*. 58(5):735-744.
- Condensate. 2018. [accessed]. <https://www.glossary.oilfield.slb.com/Terms/c/condensate.aspx>.
- Lunel T, Davies L. 2001. Response to bunker fuel oil: The options. *Proceedings of the International Oil Spill Conference*. 2001(1):597-603.
- Mendoza WG, Riemer DD, Zika RG. 2013. Application of fluorescence and parafac to assess vertical distribution of subsurface hydrocarbons and dispersant during the deepwater horizon oil spill. *Environmental Science Processes & Impacts*. 15(1017-1030).
- Molinier V, Goue EL, Rondon-Gonzales M, Passade-Boupat N, Bourrel M. 2018. Optimization of chemical dispersants effectiveness in case of subsurface oil spill. *Colloids and Surfaces A*. 541:43-51.
- Mukherjee B, Turner J, Wrenn BA. 2011. Effect of oil composition on chemical dispersion of crude oil. *Environmental Engineering Science*. 28(7):497-506.

- Murphy KR, Butler KD, Spencer RGM, Stedmon CA, Boehme JR, Aiken GR. 2010. Measurement of dissolved organic matter fluorescence in aquatic environments: An interlaboratory comparison. *Environmental science & technology*. 44(24):9405-9412.
- Murphy KR, Stedmon CA, Graeber D, Bro R. 2013. Fluorescence spectroscopy and multi-way techniques. *Parafac. Analytical Methods*. 5(23):6557-6566.
- Nedwed T, Coolbaugh T. 2008. Do basins and beakers negatively bias dispersant-effectiveness tests? *Proceedings of the International Oil Spill Conference*.835-842.
- A bitumen and dilbit primer. 2014. [accessed 2019].
<https://www.behance.net/gallery/16654901/A-BITUMEN-AND-DILBIT-PRIMER>.
- Reddy CM, Arey JS, Seewald JS, Sylvia SP, Lemkau KL, Nelson RK, Carmichael CA, McIntyre CP, Fenwick J, Ventura GT et al. 2011. Composition and fate of gas and oil released to the water column during the deepwater horizon oil spill. *Proceedings of the National Academy of Sciences*. 109(50):20229-20234.
- Ryder AG. 2005. Analysis of crude petroleum oils using fluorescence spectroscopy. In: Geddes CD, Lakowicz JR, editors. *Reviews in fluorescence 2005*. Springer. p. 169-198.
- S.L. Ross Environmental Research, MAR Inc. 2011. Comparison of large-scale (ohmsett) and small-scale dispersant effectiveness test results. In: U.S. Department of the Interior BoSaEE, editor. Ottawa, ON. p. 50.
- Smilde A, Bro R, Geladi P. 2004. Validation and diagnostics. Multi-way analysis with applications in the chemical sciences. John Wiley & Sons, Ltd. p. 145-173.
- Smith RH, Johns EM, Goni GJ, Trinanés J, Lumpkin R, Wood AM, Kelble CR, Cummings SR, Lamkin JT, Privoznik S. 2014. Oceanographic conditions in the gulf of mexico in july 2010, during the deepwater horizon oil spill. *Continental Shelf Research*. 77:118-131.
- Sorial GA, Koran KM, Holder E, Venosa AD, King DW. 2001. Development of a rational oil spill dispersant effectiveness protocol. *Proceedings of the International Oil Spill Conference*. 2001(1):471-478.
- Sorial GA, Venosa AD, Koran KM, Holder E, King DW. 2004a. Oil spill dispersant effectiveness protocol. I: Impact of operational variables. *Journal of Environmental Engineering*. 130(10):1073-1084.
- Sorial GA, Venosa AD, Koran KM, Holder E, King DW. 2004b. Oil spill dispersant effectiveness protocol. II: Performance of revised protocol. *Journal of Environmental Engineering*. 130(10):1085-1093.
- Sorial GA, Venosa AD, Koran KM, Holder E, King DW. 2004c. Oil spill dispersant effectiveness protocol. II: Performance of revised protocol. *Journal of Environmental Engineering-Asce*. 130(10):1085-1093.
- Srinivasan R, Lu Q, Sorial GA, Venosa AD, Mullin J. 2007. Dispersant effectiveness of heavy fuel oils using the baffled flask test. *Environmental Engineering Science*. 24(9):1307-1320.
- Steffens J, Landulfo E, Courrol LC, Guardani R. 2011. Application of fluorescence to the study of crude petroleum. *Journal of fluorescence*. 21:859-864.

- Strausz OP, Safarik I, Lown EM. 2009. Cause of asphaltene fluorescence intensity variation with molecular weight and its ramifications for laser ionization mass spectrometry. *Energy & Fuels*. 23:1555-1562.
- The MathWorks I. 2018. Matlab. Release 2018b ed.
- Tissot BP, Welte DH. 1978. Petroleum formation and occurrence. Germany: Springer-Verlag.
- Trudel BK, Belore RC, Guarino A, Lewis A, Mullin J. 2005. Determining the viscosity limits for effective chemical dispersion: Relating ohmsett results to those from tests at-sea. *Proceedings of the International Oil Spill Conference*. 2005(1):71-76.
- . Review of a decade of dispersant operational research conducted under simulated at-sea conditions at ohmsett. 34th AMOP (Arctic and Marine Oilspill Program) Technical Seminar on Environmental Contamination and Response; 2011; Banff, Alberta, Canada. Environment Canada.
- U.S. Coast Guard, National Oceanic and Atmospheric Administration, U.S. Environmental Protection Agency, Centers for Disease Control and Prevention, Minerals Management Service. 2006. Special monitoring of applied response technologies.
- Ufford A, McKeon CD, Owston RA, Plumlee JG, Supak KR. 2014. Dispersant effectiveness literature synthesis. In: U.S. Department of the Interior BoSaEE, editor. Washington, DC: Southwest Research Institute.
- Vaughn A. 2017 18 March 2017. Torrey canyon disaster--the uk's worst-ever oil spill 50 years on. *The Guardian*.
- Velapoldi RA, Mielenz KD. 1980. A fluorescence standard reference material: Quinine sulfate dihydrate. In: U.S. Department of Commerce NBoS, editor. Washington, DC: U.S. Government Printing Office.
- Venosa AD, King DW, Sorial GA. 2002. The baffled flask test for dispersant effectiveness: A round robin evaluation of reproducibility and repeatability. *Spill Science & Technology Bulletin*. 7(5-6):299-308.
- Venosa AD, Zhu X. 2003. Biodegradation of crude oil contaminating marine shorelines and freshwater wetlands. *Spill Science & Technology Bulletin*. 8(2):163-178.
- Vermeire MB. 2012. Everything you need to know about marine fuels. Ghent, Belgium.
- Xu X, Liu W, Tian S, Wang W, Qi Q, Jiang P, Gao X, Li F, Li H, Yu H. 2018. Petroleum hydrocarbon-degrading bacteria for the remediation of oil pollution under aerobic conditions: A perspective analysis. *Frontiers in Microbiology*. 9(2885).
- Zepp RG, Sheldon WM, Moran MA. 2004. Dissolved organic fluorophores in southeastern us coastal waters: Correction method for eliminating rayleigh and raman scattering peaks in excitation-emission matrices. *Marine Chemistry*. 89(1-4):15-36.

**SCALE LEVEL II – CHARACTERIZING THE EFFECTS OF PHYSICAL AND
CHEMICAL DISPERSION OF OIL IN SEAWATER VIA SPECTROFLUOROMETRY
IN WAVE TANK EXPERIMENTS**

INTRODUCTION

The need for standardized procedures to monitor the effectiveness of response technologies following oil spills has been apparent since the 1980s. To serve as an overarching guide, the Special Monitoring of Applied Response Technologies (SMART) program was initiated by a meeting of Federal oil spill scientists and responders in Mobile, Alabama, in November 1997. Building upon existing protocols and procedures, and created through a joint collaboration between the United States Coast Guard, NOAA, the U.S. EPA, the Centers for Disease Control and Prevention, and a portion of the Minerals Management Service (now under the Bureau of Safety and Environmental Enforcement), the SMART program outlines monitoring protocols to be used in concert with the application of dispersants, as well as the use of in-situ burning. First adopted by the EPA in January 2001, and intended to be a “living document,” the SMART protocol was updated in August 2008 and utilized for the response to the DWH oil spill in 2010 (U.S. Coast Guard et al. 2006).

Inherent in the employment of SMART protocols is the assumption that application of dispersants is an optional method to be used for the remediation of oil spills. Since dispersant application enhances the production of small oil droplets, oil is more easily suspended in the

water column and dispersed by currents (Li and Garrett 1998), and the increased ratio of surface area to volume aids accessibility to oil degrading bacteria (Lessard and DeMarco 2000; Venosa and Zhu 2003). Full dispersant effectiveness (DE) depends upon an optimal dispersant to oil ratio (DOR), along with the presence of mixing energy such as wave action (Chandrasekar et al. 2006). In order to ascertain DE level, three levels of monitoring have been employed:

- Tier I—visual monitoring, coupled with infrared or other remote detection methods;
- Tier II—combination of visual monitoring with real-time in situ monitoring at a single depth, paired with collection of water samples for later laboratory analysis;
- Tier III—an expansion of foregoing methods to include in situ monitoring at multiple depths, the use of a portable water laboratory for further analysis, as well as further water sampling.

The use of fluorometry is specifically suggested as “the most technologically advantageous detection method” in Tier II; however, the type of fluorometer is not specified. The single depth prescribed for data collection is one meter, but it is noted that sea conditions may require monitoring at a depth of up to two meters. Tier III directions call for measurements to be collected at multiple depths in order to observe the dilution of oil to background levels; however, there is no guidance provided on how that determination should be made. (U.S. Coast Guard et al. 2006).

Use of the SMART protocol in response to the DWH oil spill was complicated by the fact that dispersants were not only applied at the sea surface to visible surface slicks, as in past spill response efforts, but also applied to the oil exiting the well-head at 1,500 m. A total of 25,505

bbl (4,054,971 L) of dispersant was applied at the sea surface during the 86-day duration of the spill, and 18,379 bbl (2,922,028 L) were introduced into the sub-sea oil and gas plume over the course of 65 days (Federal Interagency Solutions Group 2010). The high-pressure, high-temperature nature of the flow from the well head resulted in small (<100 μ) droplets that failed to rise, which led to the formation of sub-surface plumes (Camilli et al. 2010; Kessler et al. 2011). Natural dispersion by sub-surface ocean currents took place, as well as additional weathering if and when oil reached the sea surface (Federal Interagency Solutions Group 2010). The presence of a high proportion of gas, in a wide range of bubble sizes, which may have been able to separate from the main oil flow and travel in a separate direction, complicated monitoring (Federal Interagency Solutions Group 2010; Reddy et al. 2011). Therefore, adherence to the SMART protocol required the deployment of monitoring instruments close to the surface, as well as at depths of up to 1,500 meters.

A variety of in situ instruments with various specifications were used by research teams in the response to the DWH oil spill. Variances in fluorometers included differing light sources, different fixed excitation/emission wavelengths, and variation in bandpass settings. In order to provide cross-comparison of data, a series of experiments were planned to evaluate the response of fluorometers to both fresh and weathered oil, with and without the addition of dispersant, using the wave tank facility at BIO in Dartmouth, Nova Scotia in the Spring of 2011. Discrete water samples also were chemically analyzed by the scientists in the BIO laboratory via GC-FID for total petroleum hydrocarbons (TPH) and by GC-MS for PAHs and for benzene, toluene, ethylbenzene and xylene (BTEX).

My research focused on determining the optimal wavelengths for oil detection by analyzing discrete water samples collected from the wave tank using a HORIBA Aqualog—a spectrofluorometer capable of collecting absorbance as well as scanning a broad range of excitation/emission wavelengths. The resulting 3D EEM spectra showed the location of specific excitation/emission fluorescence maxima for fresh oil, with and without dispersant, as well as for weathered oil, both with and without dispersant.

Observation of the evolving changes in fluorescence response over the course of the 90 min experiment resulted in important insights for the analysis of data collected with these specific instruments in the field following the DWH oil spill. Further, the planned experimental series elucidated the effect of dispersant application on petroleum fluorescence, as well as explored the effects of both chemical and physical weathering on the inherent fluorescence of oil with or without dispersant.

MATERIALS AND METHODS

A fourteen-day hydrocarbon fluorescence workshop was held at BIO, in Dartmouth, Nova Scotia, Canada on May 30 to June 10, 2011, hosted by the Centre for Offshore Oil, Gas and Energy Research, with the goal of cross-calibration of fluorometers which were utilized in the response to the DWH oil spill in the Gulf of Mexico. Scientists came from NOAA, the USF College of Marine Science, the U.S. EPA, Moss Landing Marine Labs (representing the Alliance for Coastal Technologies), Louisiana State University, the Oil Spill Recovery Institute at Prince William Sound Science Center, Dalhousie University/Satlantic, WetLabs, and HORIBA, as well as BIO's COOGER group. Payne Environmental Consultants provided a large-volume sampler.

Funding was provided by the U.S. Integrated Ocean Observing System (IOOS) through the Alliance for Coastal Technology (ACT), and NOAA (through supplemental appropriation for DWH), as well as by the visiting scientists' home institutions and Canada's DFO in concert with COOGER.

Through collaboration between the U.S. EPA and DFO Canada, BIO's 16 meter wave tank was originally designed and built in 2004, then extended to 32 m in 2006 (Fig. 2.1). Equipped with a flap-type wave generator capable of creating both rolling and breaking waves, conditions similar to those affecting open ocean DE could be observed within a controlled environment (Fisheries and Oceans Canada 2017). The tank was filled to a depth of 1.5 m with approximately 28,800 L of seawater pumped from the Bedford Basin of Halifax Harbor and filtered through serial 25 μ and 5 μ filters. A crossbeam was affixed to the top of the tank approximately 8 m from the location where oil would be added, and the following instruments were mounted on the cross-beam at a depth of approximately 80 cm:

1. Wetlabs ECO-CDOM fluorometer
2. Wetlabs ECO-Triplet for CDOM fluorometer
3. Turner Cyclops C-7 for Hydrocarbons fluorometer
4. Chelsea UV-AQUAtracka for Crude Oil fluorometer
5. Chelsea UV-AQUAtracka for Refined Oil and CDOM fluorometer
6. Satlantic SUNA – UV Spectrophotometer

COOGER's Sequoia Scientific LISST-1000X optical laser diffraction instrument was mounted in the tank approximately 1 m behind the fluorometers closer to the outflow of the tank. This

instrument, which detects particles (e.g., oil droplets) by measuring beam attenuation and forward scattering, was used in the SMART protocol on the RV *Brooks McCall* following the DWH oil spill. It was included in this experimental series since the goal of maximum DE is a decrease in oil droplet size, and chemical dispersants also have a demonstrated effect on the fluorescence of oil in seawater (Bugden et al. 2008).

A WETLAB SAFire (Spectral Absorption and Fluorescence Instrument) multi-channel flow-through fluorometer was also included in the experimental series as a second potential prototype for future spill responses. Unlike other in situ fluorometers, the SAFire has a wide wavelength range (220 – 700 nm) with six excitation wavelengths and 16 emission wavelengths and is able to acquire data across this wavelength range every 2 sec. It can be deployed to a depth of 500 m. Due to space constraints within the wave tank, the SAFire was positioned in a water bath on the platform adjacent to the tank. This was done in order to maintain temperatures for optimal instrument performance, based on previous research (Conmy et al. 2004). Sample water was introduced into the instrument's flow-through input via Nalgene PVC tubing affixed to the center of the crossbeam to which the other in situ fluorometers were attached.

On May 30, a preliminary planning meeting was held at BIO, resulting in defining plans for four core experiments, each of which would be conducted twice: (1) artificially weathered oil without dispersant, (2) artificially weathered oil with dispersant at a DOR of 1:25, (3) fresh oil without dispersant, and (4) fresh oil with dispersant at a DOR of 1:25. Randomized assignment of protocols was done as shown in Table 3.1. The oil to be used for all experiments was light, sweet Louisiana crude identified as MC252 (for Mississippi Canyon Block 252 of the Macondo

Prospect), which had been collected during the DWH oil spill on board the *Discoverer Enterprise* on July 26, 2010. Artificial weathering for those protocols was accomplished by bubbling ultra-pure nitrogen through a glass pipette into 4 L of oil contained in an amber bottle for approximately 36 hours. The resulting loss of mass equated to weathering of 7.1 % (Robinson 2011). Corexit® 9500A was the dispersant used. Immediately preceding each experimental procedure, 100 mL oil or oil/dispersant mixture was added to 1L of seawater and agitated at standard mixing energy on an orbital shaker for 20 min. The resulting mixture was poured onto the surface of the water in the wave tank 10 m downstream from the wave generating paddles (Fig. 3.1, left). Instruments attached to a rotating crossbeam were located an additional 10 m further downstream (Fig. 3.1, right). The resulting concentration of the oil or oil/dispersant mixture in the tank was ≤ 3 ppb (Conmy et al. 2014).



Figure 3.1. Weathered oil/dispersant mixture is poured onto the water surface on the afternoon of June 3 after wave generation has begun (above). In situ fluorometers attached to a crossbeam in the tank (right).

Table 3.1. Details of wave tank series protocols

Date	Time	Exp#	Temp (°C)	Salinity (ppt)	Oil (ml)	Weathered?	DOR	Start Time	Time Oil Added	End Time	Notes	
May 31	AM	A	14.6	25.8	200	no	1:25		1114	1417	static 45 min, then flow through	Exp A
Jun 2	AM	B	9.9	27.6	200	no	1:25	1045	1108		static 60 min, then flow through	Exp B
Jun 2	AM	1	10	27.3	100	yes	0	915	921	1051	flow through	Exp 1
Jun 2	PM	2	10.3	27.3	100	yes	0	1338	1353	1523	flow through	Exp 2
Jun 3	AM		x	x	x	x	x	x	x		cancelled due to heavy rain	
Jun 3	PM	3	14	26.4	100	yes	1:25	1522	1524	1654	flow through, pollen on tank surface	Exp 3
Jun 4	AM	4	10.4	26.8	100	yes	1:25	912	923	1123	flow through	Exp 4
Jun 4	PM	5	11.2	27.2	100	no	0	1358	1424	1554	flow through	Exp 5
Jun 5	AM	6	10.8	27.6	100	no	1:25	927	940	1110	flow through, sun interference?	Exp 6
Jun 5	PM	7	9.3	28.6	100	no	0	1330	1341	1511	flow through, sunny with tarp	Exp 7
Jun 6	AM	8	11.8	28.0	100	no	1:25	914	921	1051	flow through, rainy with tarp	Exp 8
Jun 6	PM	9	9.8	28.9	100	yes	1:25	1330	1347	1517	flow through, windy	Exp 9
Jun 7	AM	10	10.6		10	no	1:25	839	929	1028	standard additions, static tank	Exp 10
Jun 7	AM	10	11.6		10(20)	no	1:25	1033		1130		
Jun 7	AM	10	12.2		30(50)	no	1:25	1132	1137	1237		
Jun 7	PM	10	12.6		50(100)	no	1:25	1238	1242	1440		
Jun 7	PM	10	13		100(200)	no	1:25	1342	1346	1446		
Jun 7	PM	10	13.4	28.0	200(400)	no	1:25	1450	1450			
Jun 8	AM	11	10.8	28.0 - 29.3	10	no	1:25	815	901	1320	60 min static; then flow through	Exp 11
Jun 8	PM	12			0		4 ml	1525	1543		Corexit® 9500 only, static	Exp 12
Jun 8	PM	12	10.5	29.3	0		40 ml		1625			

On May 31 and June 1, two shakedown experimental runs were conducted (Exp. A and B) in order to test instrument response and finalize specifications for the core experiments. For Exp. A and B, 200 ml of fresh oil was used with dispersant at DOR 1:25. On May 31, the wave tank was operated in static mode for 45 min, then in flow-through mode; on June 1, static mode was increased to 60 minutes, followed by operation in flow-through mode. This was accomplished by continuously pumping filtered seawater into the tank at a rate of 3.8 L/sec (60 gal/min) and allowing the water to exit the opposite end of the tank, resulting in the oil or oil/dispersant mixture traveling as a plume with the flowing water current. Moppers were used to absorb oil or oil/dispersant mixture before discharge back into Halifax Harbor.

For the core experiments (Exp 1 - 9), the amount of oil was decreased to 100 mL, and the tank was operated solely in flow-through mode. Discrete water samples for EEMS analysis as well as chemical analysis were collected from the wave tank via siphon through a Nalgene tube located at the same depth as the instruments. Samples for 3D EEMS analysis were collected in pre-ashed 125 mL amber bottles, first rinsing each bottle three times with sample, then completely filling and immediately closing it with a Teflon-lined cap. Bottles were placed inside a covered cardboard carton and delivered to the laboratory for spectrofluorometric analysis within ten minutes of collection. Samples for TPH and GC-MS analysis were also collected in 125 mL amber bottles, and samples for BTEX analysis were collected in 40 mL P&T vials. Three sample blanks were collected at the start of each experimental run; immediately following the addition of oil or oil/dispersant mixture to the wave tank ($t = 0$), and samples were then collected at $t = 2, 4, 6, 8, 10, 15, 20, 30, 60,$ and 90 min. The tank was then completely drained and cleaned with

Big Orange detergent and seawater between experiments, and sensor optical windows were cleaned as well (Conmy et al. 2014).

Following the completion of the core experiments, several additional experimental protocols were planned and carried out on June 7 and 8, 2011. First, a step-up experiment in which the wave tank was operated in static mode and an additional quantity of oil was added at one hour intervals (Exp. 10) was performed in order to observe instrument performance at or near signal saturation. On the morning of June 8, low end of the instruments' dynamic range was investigated by adding just 10 mL of oil with dispersant at DOR 1:25 (Exp. 11) and operation of the tank in static mode for 60 min, then transitioning to flow-through mode until oil signal was no longer detected. Finally, on the afternoon of June 8, instrument response to dispersant only was tested by the addition of 4 ml of Corexit® 9500A to the wave tank with operation in static mode for approximately 40 min, followed by the addition of another 40 ml of Corexit® 9500A and continued operation of the tank in static mode (Exp. 12).

For full fluorescence analysis, a HORIBA Aqualog spectrofluorometer with charge coupled device (CCD) detector was used to collect absorbance and 3D EEMs in the laboratory at BIO. The detector was set to medium gain with dark current offset. Spectra were generated with excitation from 550 nm to 220 nm in 5 nm increments, using 1 sec integration time, and collection of resulting emission between 213 nm and 610 nm. For each experimental series, three sample blanks were analyzed at the outset, and the mid-range response was then stored and utilized for blank subtraction of Raman scatter for all samples in that series. Following data collection, each sample was individually corrected for inner-filter effect, and both first and

second-order Rayleigh scatter were masked. Finally, the 3D scale was manipulated to normalize output to the maximum intensity present in each sample. A total of 140 discrete samples were analyzed in Canada, and 48 samples from were frozen and transported back to the Coble Laboratory at the USF College of Marine Science for further future fluorescence analyses.

Statistical analysis of results included linear regression of fluorescence and chemistry data using MS Excel, as well as PARAFAC analysis of fluorescence results using MATLAB (The MathWorks 2018) and the PLS toolbox (Eigenvector Research 2018).

RESULTS AND DISCUSSION

Previous work by other researchers examining fluorescence of oil types over a wide range of dynamic viscosities found two broad UV peaks centered at 340 nm (likely associated with PAHs of ≤ 3 rings (Wakeham 1977) and at 445 nm [likely associated with PAHs of ≥ 3 rings (Wakeham 1977; von der Dick and Kaldreuth 1985; Smith and Sinski 1999; Patra and Mishra 2002)] with excitation at 240 – 300 nm (Bugden et al. 2008). Upon mixing with Corexit® 9500A dispersant, an overall increase in emission intensity was observed in all oil types; however, the increase centered at 445 nm was greater. Therefore, Bugden (2008) suggested use of the Fluorescence Intensity Ratio (FIR), i.e., fluorescence intensity at Ex/Em 280 nm/340 nm divided by fluorescence intensity at Ex/Em 280 nm/445 nm, for determination of DE since the ratio decreased with dispersant application. They posited that the use of the FIR would potentially be very useful in future cross-instrument comparisons.

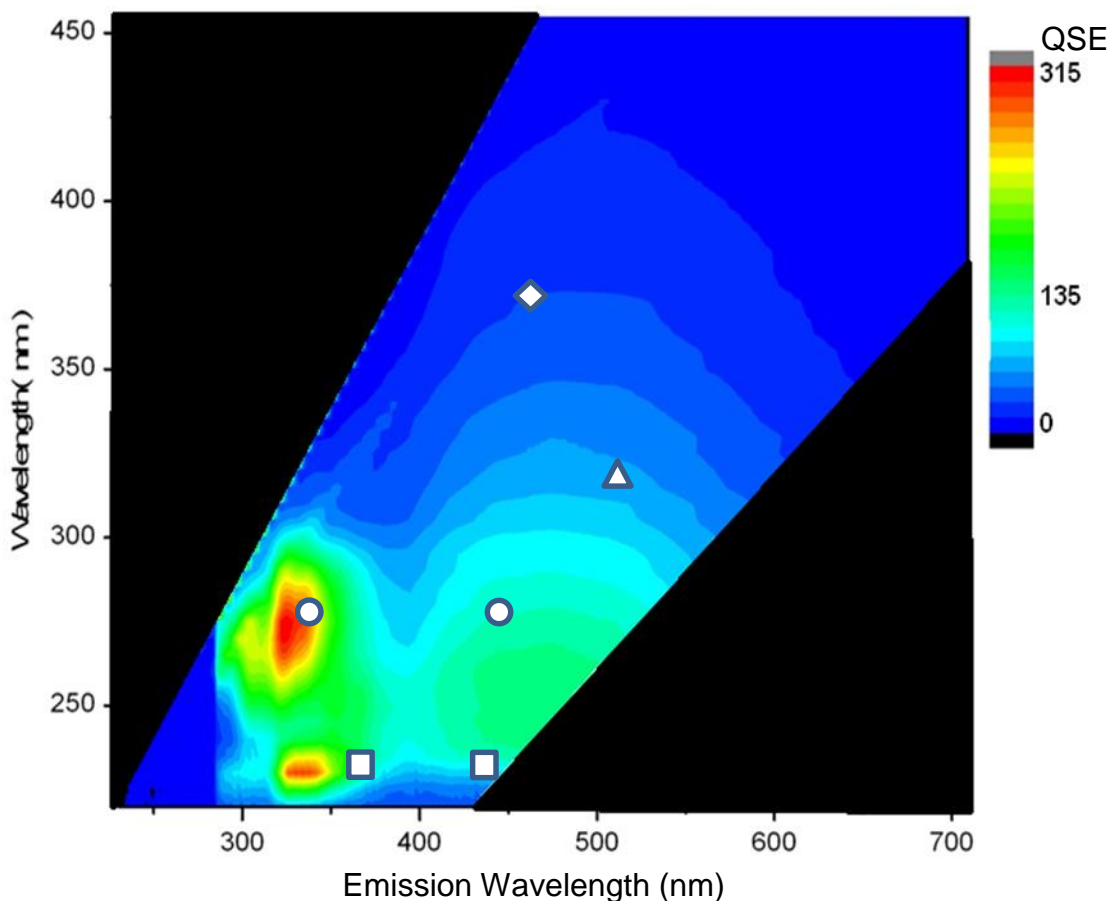


Figure 3.2. EEM contour of MC252 oil dispersed with Corexit® 9500A (DOR 1:25) in seawater. Water was collected at the surface at an uncontaminated location on a December 2010 research cruise aboard the R/V *Weatherbird II*. Final effective concentration of ~100 ppb (4 ul Corexit® 9500A to 1mL MC252 in 100 mL clean seawater) analyzed on Horiba Fluoromax4. Symbols added to represent center wavelengths of in situ fluorimeters: Chelsea Technologies Group AQUAtrackas Ex/Em 239 nm/360 nm and 239 nm/440 nm (□), Turner Designs Cyclops Ex/Em 320 nm/510 nm (△), and WETLabs, Inc. ECO Ex/Em 370 nm/460 nm (◇) along with the FIR of Ex/Em 280 nm/340 nm:280 nm/445 nm (○) after (Conmy et al. 2014).

Early studies of fluorescence in aromatic hydrocarbons (dissolved in cyclohexane) reported fluorescence maximum (F_{\max}) of benzene at Ex/Em 255 nm/278 nm, naphthalene at 275 nm/322 nm, anthracene at 358 nm/418 nm, and pyrene at 338 nm/385 nm (Berlman 1965). Schwarz and Wasik's (1976) work with aromatic hydrocarbons dissolved in water reported almost identical results. They also found F_{\max} of benzene at Ex/Em 255 nm/278 nm, naphthalene at 275 nm/320 nm, and pyrene with major excitation peak at 240 nm, two lower absorbance peaks at 265 nm and 335 nm and a single emission peak at 372 nm. Consulting the new PhotochemCAD online

database, F_{\max} for benzene is reported at Ex/Em 255 nm/285 nm, naphthalene at excitation 276 nm with two emission peaks at 322 and 334, anthracene with two excitation peaks at 356 and 376.5 nm and two emission peaks at 374.5 (almost completely overlapping the latter excitation peak) and 396.5 nm, pyrene with F_{\max} at Ex/Em 241 nm/381 nm and the similar two minor absorbance peaks at 273 and 335 nm (Taniguchi and Lindsey 2018).

In the nine core experiments, behavior of fluorescence intensity observed in 3D EEMs differed markedly between treatments with chemical dispersants and those with only physical dispersion (Fig. 3.3). For fresh oil without chemical dispersant (FOWO), data in Exp. 1 were anomalous. Fluorescence intensity peaked almost immediately ($t = 2$ min.) and exhibited the highest intensity overall in all experiments without chemical dispersant. In fact, the increase in fluorescence to 91.54 QSE at $t = 2$ min. could be treated as an outlier at the 95 % confidence interval according to Dixon's Q Test (Rorabacher 1991); however, at $t = 4$ the fluorescence intensity in FOWO Exp. 7 rose to almost the same level as that present in Exp. 1.

In concert with the change in F_{\max} Ex/Em, the abrupt rise in fluorescence, transitioning from the humic-like range of the traditional A Peak (Coble 1996; del Vecchio and Blough 2004; Cory and McKnight 2005) to Ex/Em 270 nm/325 nm, which is characteristic of naphthalene, clearly marked the beginning of the oil fluorescence signature. The behavior of weathered oil without chemical dispersant (WOWO) Exp. 2 was similar to that seen in FOWO Exp. 7; however, the same shift in F_{\max} Ex/Em and intensity was not observed in the third FOWO experimental series (Exp. 5) until $t = 8$. In every series without chemical dispersant, fluorescence intensity shifted to the naphthalene-like Ex/Em range by $t = 8$ and remained there until $t = 90$ min. Fluorescence

intensity, however, showed a roller-coaster like trend, dropping and rising again to a slightly lower peak three times in all FOWO experiments and twice in the WOWO experimental series (Fig. 3.3, left). At the final time point, the F_{\max} Ex/Em in WOWO Exp. 2 had shifted back to a humic-like signature of Ex/Em 250 nm/354 nm, but all FOWO series remained in the naphthalene-like range to the conclusion of the experiment. In all cases, fluorescence intensity returned to levels slightly elevated from that in the initial samples at $t = 0$.

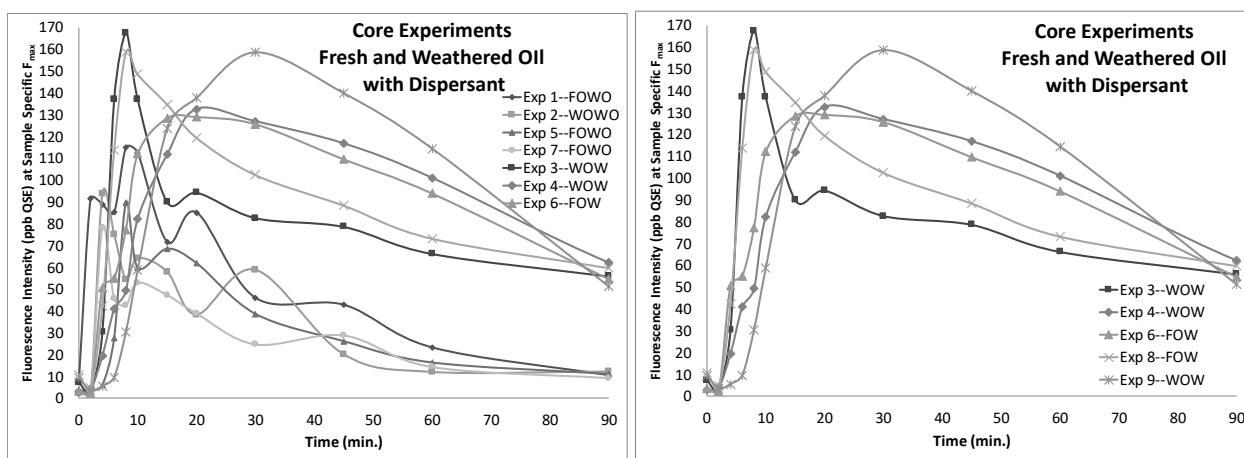


Figure 3.3. Left: Core experiments with fresh and weathered oil, no chemical dispersant. Right: Core experiments with fresh and weathered oil, with chemical dispersant at DOR 1:25.

In the five experimental series for oil plus chemical dispersant, fluorescence trends differed markedly from that observed in the oil dispersed only by wave action (Fig. 3.3, right). Similar changes were observed in F_{\max} Ex/Em location, beginning in the humic-like range and shifting to naphthalene-like at the $t = 4$ time point. With the exception of the anomalous intensity spike in Exp. 1, fluorescence intensities were similar in both treatments at $t = 2$, but then remained much lower in the chemically dispersed series at $t = 4$. At $t = 8$, however, fluorescence intensity in WOWO Exp. 3 and fresh oil with dispersant (FOW) Exp. 8 increased over four times in the former and approximately three times in the latter, greatly surpassing the highest intensity

observed at any time point in the series without chemical dispersant. Fluorescence intensity then dropped by about half at $t = 30$ in weathered oil with dispersant (WOW) Exp. 3, and by about one-third in FOW Exp. 8, but rose dramatically by 2.5 times in WOW Exp. 4, by a multiple of five in Exp. 9 and by slightly less than twice in FOW Exp. 6. All fluorescence intensities decreased steadily from the maximum until the last samples was collected at $t = 90$. The character of sharp initial fluorescence intensity increase followed by continuing decline was greatest in WOWO Exp. 3, but similar in FOW Exp. 8. A more gradual increase in fluorescence intensity as well as a more gradual decline was observed in WOW Exp. 4, as well as in FOW Exp. 6 and WOW Exp. 9. Notably, no evidence of the roller-coaster like fluorescence intensity behavior was observed in any chemically-dispersed oil experiment. The fluorescence intensity also remained significantly elevated from that observed at $t = 0$, and the F_{\max} Ex/Em remained in the naphthalene-like region for all experiments with chemical dispersant. Since oil fluorescence arises largely from PAHs, these results suggest that a greater portion of the water column is exposed to higher concentrations of PAHs and they remain present for a longer period of time following the use of chemical dispersant.

Chemical analysis of MC252 oil at BIO by GC-MS showed less than 0.1 % PAHs with five benzene rings, 13 % with four rings, 8 % with three rings, and 79 % with two rings (Fig. 3.4). The fluorescence signature of oil, both chemically dispersed and physically dispersed only, at naphthalene's characteristic F_{\max} Ex/Em 270 nm/325 nm in the wave tank experimental series, could certainly be related to the high proportion of naphthalene and homologous compounds in MC252 oil.

Table 3.2. Comparison of core experiments — location and concentration (QSE) of maximum fluorescence peak (F_{max})

Treatment	Exp #	t = 0					t = 2					t = 4				
		Ex	Em	QSE	Mean	StDev	Ex	Em	QSE	Mean	StDev	Ex	Em	QSE	Mean	StDev
FOWO	1*	260	299	7.43			270	325	91.54			270	325	88.84		
	5	250	559	3.40			250	374	3.48			250	397	5.85		
	7	255	351	2.46	4.43	2.64	250	293	2.80	32.61	51.04	270	325	78.13	57.61	45.14
WOWO	2	250	446	2.13	2.13	NA	250	492	2.99	2.99	NA	275	325	93.70	93.70	NA
WOW	3	540	553	7.37			250	620	2.98			270	325	30.31		
	4	250	620	2.94			250	364	4.07			270	325	19.50		
	9	255	512	9.49	6.60	3.34	250	338	3.39	3.48	0.55	250	328	5.50	18.44	12.44
FOW	6	250	613	3.47			250	613	2.36			275	325	50.70		
	8	470	610	10.73	6.48	5.13	250	299	4.58	2.87	1.57	270	325	42.35	28.10	5.90

Treatment	Exp #	t = 6					t = 8					t = 10				
		Ex	Em	QSE	Mean	StDev	Ex	Em	QSE	Mean	StDev	Ex	Em	QSE	Mean	StDev
FOWO	1*	270	325	85.20			270	325	115.05			270	325	112.44		
	5	270	325	27.56			275	325	89.54			275	325	59.76		
	7	265	325	45.49	52.75	29.50	275	325	42.47	82.35	36.82	275	325	52.90	75.03	32.58
WOWO	2	270	325	75.11	75.11	NA	270	325	54.43	54.43	NA	270	325	64.14	64.14	NA
WOW	3	270	325	137.20			275	325	167.55			270	325	137.13		
	4	270	325	40.85			275	325	49.28			270	325	82.20		
	9	255	357	9.50	62.52	66.55	270	325	30.30	82.37	74.37	270	325	58.62	92.65	40.28
FOW	6	275	325	54.96			270	325	77.33			270	325	112.02		
	8	270	325	113.69	32.23	41.53	270	325	158.66	53.81	57.51	275	325	148.56	85.32	25.84

Table 3.2 (cont'd). Comparison of core experiments — location and concentration (QSE) of maximum fluorescence peak (F_{max})

Treatment	Exp #	t = 15					t = 20					t = 30				
		Ex	Em	QSE	Mean	StDev	Ex	Em	QSE	Mean	StDev	Ex	Em	QSE	Mean	StDev
FOWO	1*	270	325	71.60			270	325	85.11			270	325	45.91		
	5	270	325	68.47			275	325	61.84			270	325	38.54		
	7	270	325	47.23	62.43	13.26	270	325	38.80	61.92	23.15	265	325	24.65	36.37	10.79
WOWO	2	275	325	57.85	57.85	NA	265	325	38.24			275	325	58.75	58.75	NA
WOW	3	270	325	89.91			275	325	94.27			270	325	82.64		
	4	275	325	111.71			270	325	132.60			270	325	126.92		
	9	270	325	123.58	108.40	17.08	270	325	137.73	121.53	23.75	270	325	158.62	122.73	38.16
FOW	6	270	325	128.50			275	325	129.02			270	325	125.71		
	8	270	325	134.76	126.04	4.43	270	325	119.40	133.38	6.80	270	325	102.38	142.17	16.50

Treatment	Exp #	t = 60					t = 90				
		Ex	Em	QSE	Mean	StDev	Ex	Em	QSE	Mean	StDev
FOWO	1*	275	325	23.17			265	325	10.39		
	5	275	325	16.25			275	325	10.98		
	7	270	322	14.30	17.91	4.66	260	318	9.20	10.19	0.91
WOWO	2	275	325	11.92	11.92	NA	250	354	12.10	12.10	NA
WOW	3	270	325	66.20			270	325	55.86		
	4	275	325	101.04			270	325	62.27		
	9	270	325	114.44	93.89	24.90	270	325	51.13	56.42	5.59
FOW	6	270	325	93.90			265	325	54.58		
	8	270	325	73.16	104.17	14.67	270	325	59.66	52.86	3.59

*Tom King's notes state that this experiment was weathered oil, not fresh.

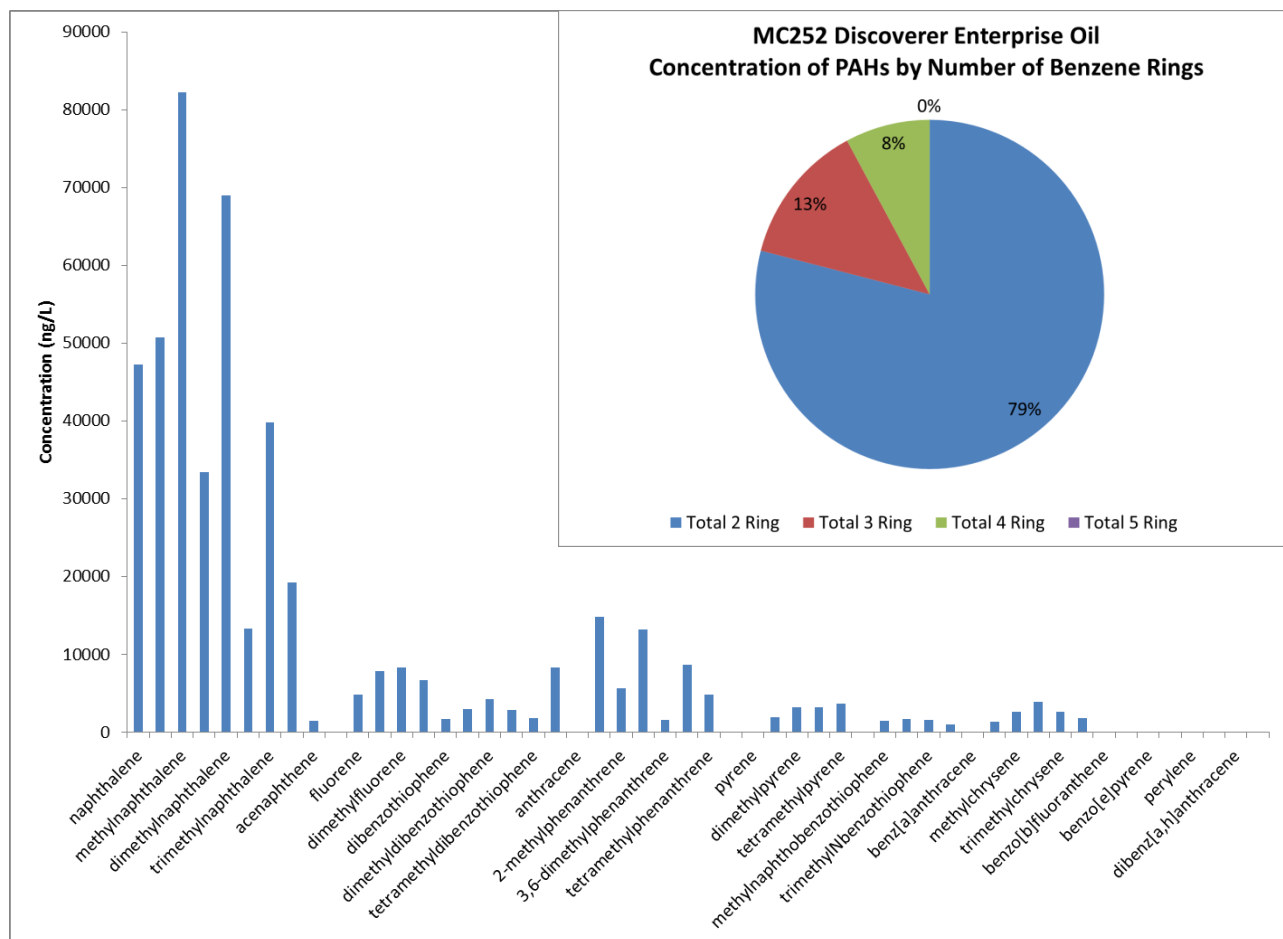


Figure 3.4. PAH concentrations (ng/L) of 2-, 3-, 4-, and 5-ring benzene compounds in MC252 oil in artificial seawater. Oil was collected on board the Discoverer Enterprise on June 26, 2010, mixed with artificial seawater for spectrofluorometric analysis in Coble Lab baffle flask experiments in June 2014, and shipped to Bedford Institute of Oceanography for analysis of PAHs by GC-MS.

Chemical analyses of samples were carried out at all but one experimental time point for FOW Exp. 6 (no BTEX for $t = 4$ min. and no alkanes or PAHs for $t = 45$ min.), but at every experimental time point for FOWO Exp. 7 on June 5, 2011. Comparing F_{\max} intensity to chemistry analyses, the best correspondence is found between fluorescence intensity and BTEX concentration in Exp. 6 (Fig. 3.5, right). A relationship is also noted between fluorescence and both total 2-ring PAHs and total alkanes in the chemically dispersed experimental series; however, there is an early spike at $t = 2$ min. in PAHs and alkanes that is not reflected in the fluorescence results, and there is a slight dip in both PAHs and alkanes at $t = 20$ min, that is also

not observed in fluorescence intensity. As separate water samples were collected in series to be analyzed for BTEX, TPH, and fluorescence, it is possible that individual samples contained slightly differing petroleum components. Overall, F_{\max} fluorescence intensity at Ex/Em 270 nm/325 nm appeared to track BTEX and PAHs in the chemically dispersed oil very well. Maximum fluorescence intensity of 129 QSE (ppb) at $t = 15$ and 20 min time points was approximately 2.5 times the maximum total 2-ring PAH concentration of 52.0 ng/mL (ppb), but was only 40 % of the maximum total alkanes concentration of 314 ng/L (ppb) at $t = 4$ min.

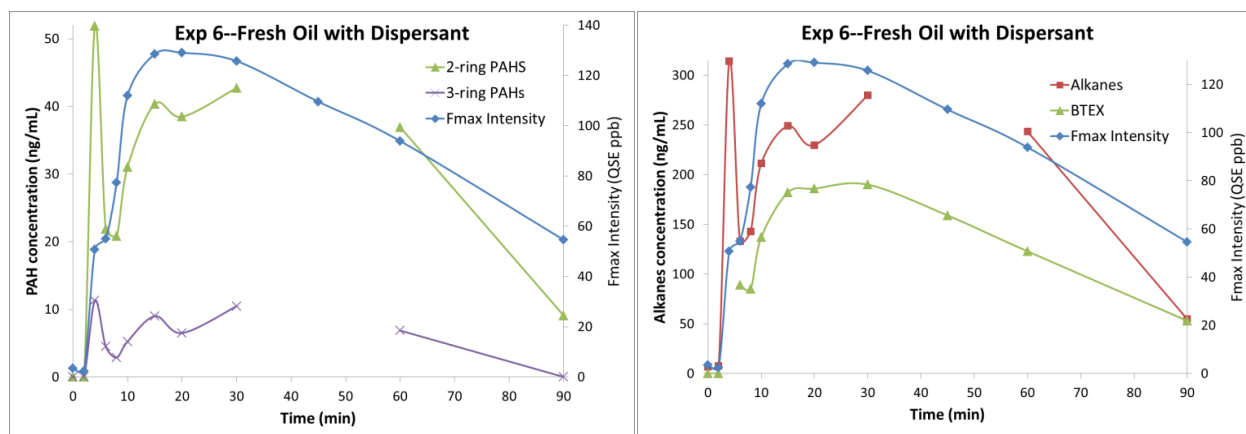


Figure 3.5. Fluorescence intensity vs. total 2-ring and 3-ring PAHs (left) and vs. total alkanes and BTEX (right) for the FOW experimental series on the morning of June 5, 2011.

Chemical analyses of water samples from the afternoon of June 5 in the FOWO Exp. 7 showed that neither 2-ring PAHs nor BTEX corresponded as well with F_{\max} intensity at Ex/Em 270 nm/325 nm as that seen in Exp. 6 (Fig. 3.6). At the outset, BTEX and fluorescence mirrored roller-coaster like behavior until $t = 6$ min, but then went in opposite directions until $t = 45$ min, at which point fluorescence tracked BTEX until the end of the experimental series. Concentration of PAHs also did not follow that overall trend, but alkanes did show some evidence of the roller-coaster like behavior. In this series, fluorescence intensity peaked first at $t = 4$ min, while total 2-ring PAHs did not peak until $t = 6$ min, lending credence to the

possibility that water chemistry differences were present in individual water samples. Maximum fluorescence intensity of 78.1 QSE (ppb) at 4 min was over four times the total 2-ring PAH concentration of 18.4 ng/mL (ppb) at $t = 6$ min. In both experimental series, both 2-ring and 3-ring PAHs dropped before fluorescence intensity fell off, while BTEX and total alkanes did not. This may be partially due to the detection limit of the GC-FID analysis method; however, it is also likely that F_{\max} fluorescence intensity at Ex/Em 270 nm/325 nm is not due solely to the low molecular weight PAHs. Our results confirm previous in-laboratory research, which proposed that the fluorescence signal arising from dispersed oil in seawater as measured by two Turner fluorometers (Ex/Em 254nm /350 nm and 350nm /410-455 nm) was due to a combination of PAHs and was also influenced by the presence of volatile organic compounds including BTEX (Lambert et al. 2003).

In Fig. 3.7, linear regressions show statistically significant functional relationships between BTEX and fluorescence intensity at both Ex/Em 280 nm/340 nm and Ex/Em 280 nm/450 nm, with a slightly lower p value at the lower emission wavelength (left), for each category of experimental protocol. A stronger relationship is seen between BTEX concentration and fluorescence intensity in the FOW and WOW experiments with addition of chemical dispersant, where variability in BTEX explains 92 to 96% of the variation in fluorescence as seen in the linear relationship at the lower emission wavelength. Statistical significance was high, with $p < 0.001$ for each regression, ranging from a low of $p = 7.982 \times 10^{-20}$ for BTEX vs. fluorescence intensity at Ex/Em 280/340 in the WOW series (Fig. 3.7, left) to $p = 5.815 \times 10^{-5}$ for BTEX vs. fluorescence intensity at Ex/Em 280/450 in the FOWO series (Fig. 3.7, right).

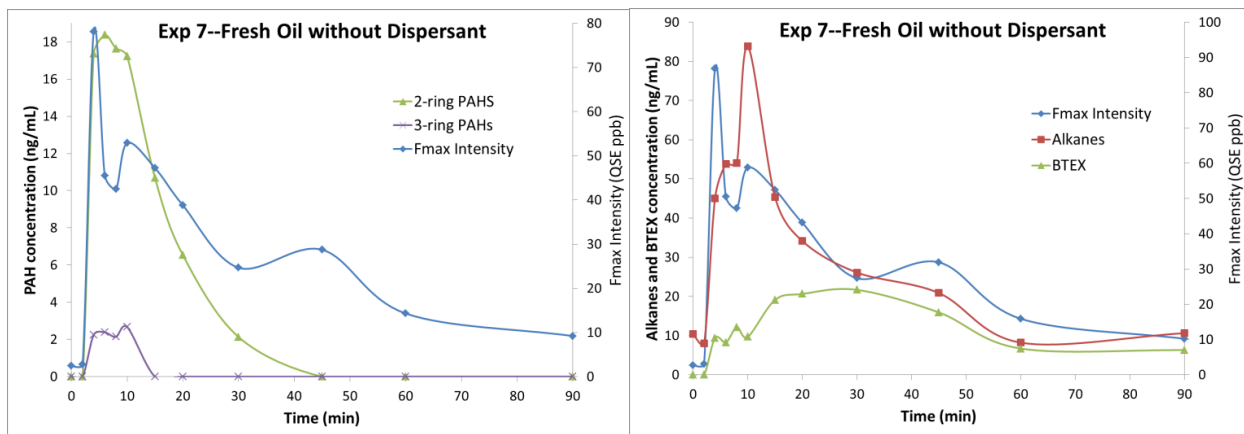


Figure 3.6. F_{max} intensity (QSE), total 2-ring and 3-ring PAHs (left) and F_{max} intensity (QSE) with total alkanes and BTEX (right) for the FOWO experimental series on the afternoon of June 5, 2011.

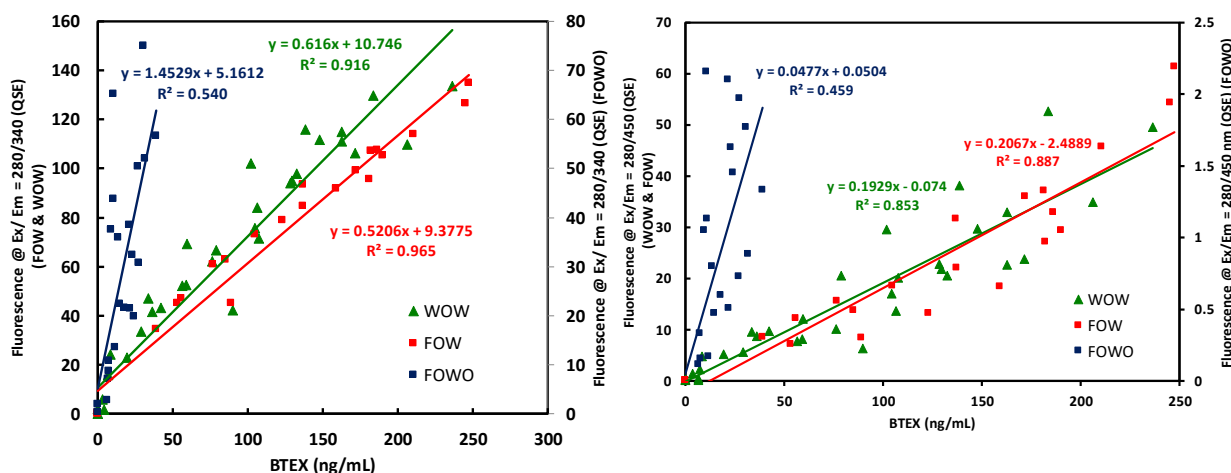


Figure 3.7. Fluorescence intensity at Ex/Em 280 nm/340 nm (left) and at Ex/Em 280 nm/450 nm (right) for the three WOW experiments, two FOW experiments, and two FOWO experiments.

SAFIre Instrument Response

The WETLABs SAFIre fluorometer was positioned in a water bath on the platform adjacent to the tank and water was introduced from a site adjacent to the in situ fluorometers in the wave tank via Nalgene tubing. Fluorescence intensity at six excitation wavelengths and sixteen emission wavelengths was recorded over the course of the wave tank experimental series. Data collected in Exp. #6 using fresh MC252 oil and Corexit® 9500A at DOR 1:25 on the morning of June 5, 2011 are presented in Figure 3.8. Use of the excitation channel at 280 nm and two

emission channels at 380 nm and 450 nm allowed continuous examination of the FIR, which has been found useful in determining DE (Bugden et al. 2008). Fluorescence intensity data at the outset of the experiment displays the same patchy spiking quality as that observed in the Aqualog data, with fluorescence smoothing out at approximately $t = 20$ min. An interesting evolution of fluorescence intensity at these two wavelengths can be seen from $t = 20$ min to the end of the experiment at $t = 90$ min. The evolution of fluorescence intensity from the combination of physical and chemical dispersion resulted in a “horseshoe” appearance in the graph of fluorescence at Ex/Em 280 nm/450 nm vs. Ex/Em 280 nm/380 nm (right). This could be due to the loss of higher molecular weight oil components, but is likely due to loss of larger oil droplets from the water column. The ability to simultaneously observe fluorescence intensity at these two wavelengths could potentially be of great value in tracking the evolution of physical and chemical dispersion of oil in the marine environment. The ability to take the ratio of two fluorescence intensities also results in a unitless measurement, which more easily allows instrument-to-instrument comparisons.

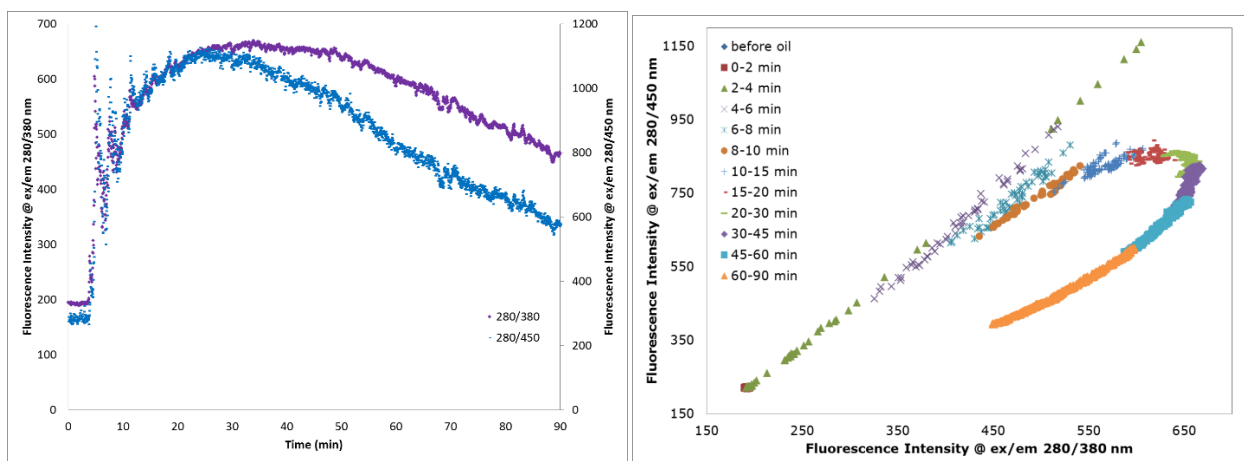


Figure 3.8. Fluorescence intensity at Ex/Em 280/380 nm and at Ex/Em 280/450 for Experiment #6 with fresh MC252 oil and Corexit® 9500 at DOR 1:25 as recorded by the WETLAB SAFire multi-channel fluorometer. Fluorescence intensity is reported in instrument units.

PARAFAC Analysis

Using MATLAB version R2018b with the drEEM and N-way toolboxes (Murphy et al. 2013), and with the assistance of Drs. Kathleen Murphy and Urban Wunsch, PARAFAC analysis was performed on the discrete bottle EEM data from the nine core experiments. The N-way toolbox is a multi-way analysis for PARAFAC analysis, and the drEEM toolbox then makes use of that outcome in the analysis of 3D EEMs. A seven-component model was first used to fit all samples in the nine core experimental series; however, a six-component model was found to give the best overall fit with good core consistency (15.8%) and low residuals. Fig. 3.9 gives Ex/Em loadings for each of the six components. Fig. 3.10 presents the EEM view of each component.

Component 1, with the greatest overall contribution to the model has F_{\max} at Ex/Em 285 nm/328.2 nm, very similar to the naphthalene-like F_{\max} location discovered through peak-picking. Component 2, with F_{\max} Ex/Em at 260 nm/324.9 nm, appears to be modelling more BTEX-like fluorescence. Component 3 has a broad F_{\max} centered at Ex/Em 265 nm/505.8 nm, which appears to be capturing the effect of dispersant on fluorescence. Components 4 and 6 both have double peaks, the former at Ex/Em 255 nm/409.7 nm (A Peak) and 305 nm/409.7 nm (C Peak); the latter at Ex/Em 255 nm/475.8 nm and 370 nm/472.5 nm, which may also be modelling the effects of dispersant on CDOM fluorescence. Component 5 has a petroleum-like F_{\max} at Ex/Em 255 nm/363.9 nm with an intensity nearly equivalent to Components 1 and 2, but contributing far less to the model.

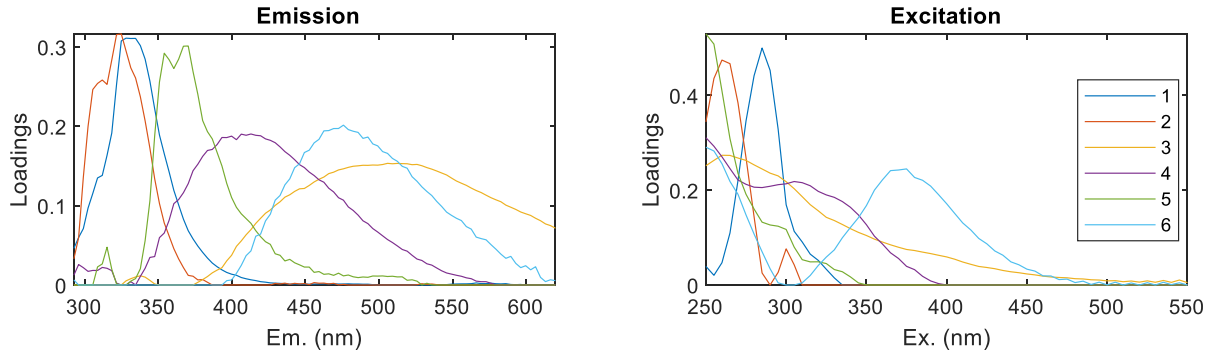


Figure 3.9. Emission and Excitation loadings for the six-component model.

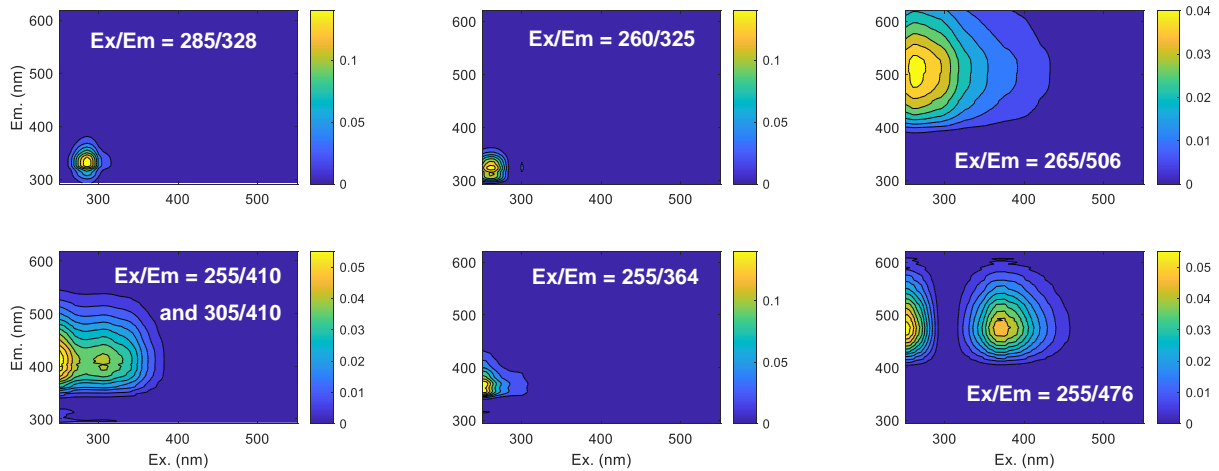


Figure 3.10. EEM view of each of the six components. Components 1-3 (top, left to right) and 4-6 (bottom, left to right), in order of decreasing overall contribution to the model. Fluorescence intensity was normalized before running the model.

CONCLUSIONS

While every attempt was made to hold experimental variables constant, some real-world conditions impacted the wave tank experiments and almost certainly influenced results: high winds, varying air temperature (9.8 to 16.8 °C), water temperature (9.3 to 14.0 °C), and salinity (25.8 to 28.9 ‰), as well as changes in water quality due to heavy precipitation, tide stage, and deposition of wind-blown pollen. In particular, participants’ scientific logs noted visible pollen

on the water surface at the beginning of Exp. 3 on the afternoon of June 3; the tank had been filled at the beginning of the morning and then was not used until afternoon due to heavy precipitation. On June 5, winds were strong and opposite the direction of water flow in the tank, impacting surface oil flow, and participants' notes stated that the surface oil sheen was observed moving upstream during Exp. 7. Although these conditions were likely reflected in the fluorescence data, they also could be typical natural influences to physical and chemical oil dispersion that might be encountered in coastal regions.

The addition of a side tarp to the platform adjacent to the wave tank in order to counteract winds and light rain toward the end of the experimental series also altered experimental conditions, but would not be reflective of real-world conditions. In retrospect, this modification would have been best done prior to the beginning of all experimental series. Additionally, the thorough pre-mixing of dispersant with oil for the chemically-dispersed experiments, as well as the method of adding oil or oil/dispersant mixture to the wave tank by pouring onto the surface of the water, were unlike conditions that would be encountered in real-world spills.

That said, this collaborative effort provided invaluable confirmation of the usefulness of a number of in situ instruments that were used to collect data in the field during the DWH oil spill (Conmy et al. 2014). Through the data collected by the other participating scientists, results of in situ fluorometer and LISST instrument response, and comparison with chemical analyses, results showed that all fluorometers, despite differences in fixed instrument settings, were able to detect chemically dispersed oil down to at least 300 ppb, which is below the limit of detection for the GC-FID method for TPH. The lower limit of GC-MS chemical analysis conducted at BIO was

100 ppb. This demonstrated that all of the tested instruments were capable of providing valuable information during the DWH oil spill (Conmy et al. 2014).

Further, my EEMS analysis of discrete water samples taken at specified time points enabled the determination of the characteristic F_{\max} of MC252 oil, as well as the spectral shape of the full EEM profile of MC252 oil, which confirmed that all in situ instruments tested were “seeing” some portion of the overall EEM oil signature. My work also confirmed the utility of the FIR as a tool to measure DE without the need to convert raw fluorescence units into a standard (e.g., QSE). Since the FIR is a ratio of fluorescence intensity at two wavelength pairs, it is a unitless measurement which could potentially be very useful for instrument cross-comparison. It could also be informative in the development of the next generation of in situ fluorometers capable of detection at multiple emission wavelengths.

The discovery of the same naphthalene-like optimal wavelength of Ex/Em 270 nm/325 nm for F_{\max} intensity in both solely physically dispersed oil as well as in physically and chemically dispersed oil has the potential to inform future instrument specifications. While it is important to consider the possibility of over-saturation of the fluorescence signal with a fixed wavelength setting at the F_{\max} region for oil, such as that observed in the Chelsea AQUAtracka with Ex/Em 239 nm/360 nm, it is also vitally important to be able to detect oil or oil/dispersant plumes at concentrations in the low ppb range. Studies of marine organisms over the years following the DWH oil spill have documented impacts not only from visible surface oiling, but also from chronic, low-level exposure, such as the low reproductive success rate in bottlenose dolphins (Kellar et al. 2017)

REFERENCES

- Berlman IB. 1965. Handbook of fluorescence spectra of aromatic molecules. Academic Press.
- Bugden JBC, Yeung CW, Kepkay PE, Lee K. 2008. Application of ultraviolet fluorometry and excitation-emission matrix spectroscopy (eems) to fingerprint oil and chemically dispersed oil in seawater. *Marine pollution bulletin*. 56:677-685.
- Camilli R, Reddy CM, Yoerger DR, Van Mooy BAS, Jakuba MV, Kinsey JC, McIntyre CP, Sylva SP, Maloney JV. 2010. Tracking hydrocarbon plume transport and biodegradation at deepwater horizon. *Science*. 330:201-204.
- Chandrasekar S, Sorial GA, Weaver JW. 2006. Dispersant effectiveness on oil spills - impact of salinity. *Ices Journal of Marine Science*. 63(8):1418-1430.
- Coble PG. 1996. Characterization of marine and terrestrial dom in seawater using excitation-emission matrix spectroscopy. *Marine Chemistry*. 51:325-346.
- Conmy RN, Coble PG, Castillo CED. 2004. Calibration and performance of a new in situ multi-channel fluorometer for measurement of colored dissolved organic matter in the ocean. *Continental Shelf Research*. 24(3):431-442.
- Conmy RN, Coble PG, Farr J, Wood AM, Lee K, Pegau WS, Walsh ID, Koch CR, Abercrombie MI, Miles MS et al. 2014. Submersible optical sensors exposed to chemically dispersed crude oil: Wave tank simulations for improved oil spill monitoring. *Environmental science & technology*. 48(3):1803-1810.
- Cory RM, McKnight DM. 2005. Fluorescence spectroscopy reveals ubiquitous presence of oxidized and reduced quinoes in dissolved organic matter. *Environmental science & technology*. 39:8142-3149.
- del Vecchio, Rossana, Blough NV. 2004. On the origin of the optical properties of humic substances. *Environmental science & technology*. 38:3885-3891.
- Eigenvector Research I. 2018. *Pls_toolbox*. Manson, WA.
- Federal Interagency Solutions Group, Oil Budget Calculator Science and Engineering Team,. 2010. Oil budget calculator--deepwater horizon.
- Wave tank studies on dispersant effectiveness. 2017. [accessed 5/19/2019]. <http://www.dfo-mpo.gc.ca/science/coe-cde/cooger-crpgee/projects-projets/wavetank-etudescuve-eng.html>.
- Kellar NM, Speakman TR, Smith CR, Lane SM, Balmer BC, Trego ML, Catelani KN, Robbins MN, Allen CD, Wells RS et al. 2017. Low reproductive success rates of common bottlenose dolphins tursiops truncatus in the northern gulf of mexico following the deepwater horizon disaster (2010-2015). *Endangered Species Research*. 33:143-158.
- Kessler JD, Valentine DL, Redmond MC, Du M, Chan EW, Mendes SD, Quiroz EW, Villanueva CJ, Shusta SS, Werra LM et al. 2011. A persistent oxygen anomaly reveals the fate of spilled methane in the deep gulf of mexico. *Science*. 331(6015):312-315.

- Lambert P, Goldthorp M, Fieldhouse B, Wang Z, Fingas M, Pearson L, Collazzi E. 2003. Field fluorimeters as dispersed oil-in-water monitors. *Journal of hazardous materials*. 102:57-79.
- Lessard RR, DeMarco G. 2000. The significance of oil spill dispersants. *Spill Science & Technology Bulletin*. 6(1):59-68.
- Li M, Garrett C. 1998. The relationship between oil droplet size and upper ocean turbulence. *Marine pollution bulletin*. 36(12):961-970.
- Murphy KR, Stedmon CA, Graeber D, Bro R. 2013. Fluorescence spectroscopy and multi-way techniques. *Parafac. Analytical Methods*. 5(23):6557-6566.
- Patra D, Mishra AK. 2002. Total synchronous fluorescence scan spectra of petroleum products. *Analytical and bioanalytical chemistry*. 373:304-309.
- Reddy CM, Arey JS, Seewald JS, Sylvia SP, Lemkau KL, Nelson RK, Carmichael CA, McIntyre CP, Fenwick J, Ventura GT et al. 2011. Composition and fate of gas and oil released to the water column during the deepwater horizon oil spill. *Proceedings of the National Academy of Sciences*. 109(50):20229-20234.
- Robinson B. 2011. Personal communication.
- Rorabacher DB. 1991. Statistical treatment for rejection of deviant values: Critical values of dixon's "q" parameter and related subrange ratios at the 95% confidence level. *Analytical Chemistry*. 63(2):139-146.
- Schwarz FP, Wasik SP. 1976. Fluorescence measurements of benzene, naphthalene, anthracene, pyrene, fluoranthene, and benzo[e]pyrene in water. *Analytical Chemistry*. 48(3):524-528.
- Smith GC, Sinski JF. 1999. The red-shift cascade: Investigations into the concentration-dependent wavelength shifts in three-dimensional fluorescence spectra of petroleum samples. *Applied spectroscopy*. 53(11):1459-1469.
- Taniguchi M, Lindsey JS. 2018. Database of absorption and fluorescence spectra of >30 common compounds for use in photochemcad. *Photochemistry and photobiology*. 94:290-327.
- The MathWorks I. 2018. Matlab. Release 2018b ed.
- U.S. Coast Guard, National Oceanic and Atmospheric Administration, U.S. Environmental Protection Agency, Centers for Disease Control and Prevention, Minerals Management Service. 2006. Special monitoring of applied response technologies.
- Venosa AD, Zhu X. 2003. Biodegradation of crude oil contaminating marine shorelines and freshwater wetlands. *Spill Science & Technology Bulletin*. 8(2):163-178.
- von der Dick, Hans, Kaldreuth W. 1985. Synchronous excitation and three-dimensional fluorescence spectroscopy applied to organic geochemistry. *Advances in Organic Geochemistry*. 10:633-639.
- Wakeham SG. 1977. Synchronous fluorescence spectroscopy and its application to indigenous and petroleum-derived hydrocarbons in lacustrine sediments. *Environmental science & technology*. 11(3):272-276.

**SCALE LEVEL III – FLUORESCENCE EEMS ANALYSIS OF FIELD SAMPLES
COLLECTED IN THE NORTHERN GULF OF MEXICO DURING THE YEAR
FOLLOWING THE DWH SPILL OF NATIONAL SIGNIFICANCE**

INTRODUCTION

Shortly before 10:00 pm on April 20, 2010, an undetected flow of hydrocarbons from the exploratory Macondo well escalated to a blowout, causing two separate explosions and an ensuing fire on the Transocean *Deepwater Horizon* (DWH) submersible drilling platform, located approximately 50 miles southwest of the Mississippi Delta at latitude 28° 44.20' North and longitude 88° 23.23' West (NOAA Office of Response and Restoration 2010; Bureau of Ocean Energy Management 2011). A confluence of events including last-minute changes to well design and construction, misinterpretation of warning indicators, and inadequate response to controlling the well resulted in the death of 11 men on April 20 and a consequent flow of hydrocarbons into the Gulf of Mexico for 87 days (Bureau of Ocean Energy Management 2011). The DWH blowout was identified as a U.S. Spill of National Significance (40 CFR § 300.323 1999), and the challenges to response efforts were characterized by Incident Commander Thad W. Allen as more akin to the first moon landing than to those surrounding the grounding of the *Exxon Valdez*, second in U.S. history to the magnitude of the DWH oil spill (Allen 2010).

Delivery of an estimated 4.9 million barrels (779 million L) of petroleum into the Gulf of Mexico by the time the wellhead was capped on 15 July, 2010, was accompanied by application

of approximately 2.1 million gallons (7.9 million L) of dispersant (Corexit® EC9500A and EC9527A) (Daly et al. 2016). Several factors produced novel transport and fate issues — the extreme 1,522 m depth of the hydrocarbon release, the dispersive force created by large volumes of methane and oil released under high pressure, and the application of dispersant directly into the flow from the wellhead, in addition to application at the surface (Joye et al. 2011; Kessler et al. 2011; Lubchenco et al. 2012; McNutt et al. 2012; Paris et al. 2012; Daly et al. 2016; Rogener et al. 2018).

These factors, acting in concert, supported the development of persistent subsurface oil plumes, which were found associated with O₂ anomalies (Valentine et al. 2010; Joye et al. 2011; Kessler et al. 2011). The depressed O₂ readings were initially questioned as a possible result of instrument fouling (Mascarelli 2010); however the O₂ departures were ultimately found to be correlated with fluorescence spikes by a number of researchers employing in situ fluorometers to track subsurface oil (Diercks et al. 2010; Goni et al. 2010; Joint Analysis Group 2010; Smith et al. 2014).

The SMART protocol developed through a collaborative effort of the U.S. Coast Guard, NOAA, U.S. EPA, Centers for Disease Control and Prevention, and Minerals Management Service calls for three tiers of observation in support of the remediation of oil spills through the application of chemical dispersants. (See Chapter 3 for protocol details.) The guidelines were developed with the use of a flow-through fluorometer as the monitoring instrument of choice, although it is stated that “alternative instruments” may be used (U.S. Coast Guard et al. 2006). In the response to the DWH oil spill over the weeks and months following the blowout, researchers employed a

variety of in situ fluorometers in the effort to track the oil/dispersant. Affixed to CTD rosettes, these instruments were configured to measure fluorescence at instrument-specific fairly narrow excitation and emission wavelengths. These results were reported as simply “fluorescence” in most cases, and some uncertainty surrounded what, exactly, these fluorometers were detecting; analysis was further complicated by the changing spectral qualities of the petroleum due to physical and chemical weathering.

First described by Kalle (1949) and studied since then by many researchers, CDOM has been categorized into two general pools described by the wavelength ranges of their maximum fluorescence intensity — a humic-like component and a protein-like component. The humic-like component was first identified at emission of 420 – 450 nm with excitation at 230 – 260 nm and 320 – 350 nm (C Peak), while the protein-like pool was identified by emission at 300 – 305 nm (B Peak) and 340 – 350 nm (T Peak) upon excitation at 220 and 275 nm (Coble 1996 and references therein). Further research expanded the humic-like pool to identification of the M Peak at emission of 350 – 420 nm with excitation at 240 and 290 – 310 nm; this slightly blue-shifted peak is observed in the marine environment, although less commonly than the previously identified C Peak.

Arising from aromatic structures remaining in the remineralization of terrestrial matter delivered via riverine transport (allochthonous), as well as from sediment and microbial sources in the marine environment (autochthonous), the varied sources and complex chemical composition of the dissolved organic matter gives rise to a multifaceted fluorescence signal, which can be difficult to tease apart (Coble et al. 2014). The addition of the thousands of fluorescent

compounds present in petroleum, whether arising from natural seeps or from anthropogenic input, makes the deconstruction of the fluorescence signature more challenging, but there are important insights that can be brought to bear on this complex puzzle.

Historically, laboratory analysis for TPH in the aqueous environment may be accomplished in a variety of ways; commonly used methods include the gravimetric method, infrared spectroscopy, and gas chromatography with a flame ionization detector (FID) or mass spectrometer (MS) (Adeniji et al. 2017). More recently, gas chromatography has been coupled with metastable ion reaction monitoring (GC-MS-MS) and isotope ratio chromatography (GC-IRMS), and the use of two-dimensional gas chromatography (GC \times GC) has also been employed (Christensen et al. 2004). However, there are multiple drawbacks to using any of these methods at sea. First, all involve collection of a significant quantity of water (usually $\geq 1\text{L}$), followed by the use of toxic and/or flammable organic solvents for pre-analysis extraction — a time-consuming process — followed by analysis with sensitive equipment, which generally does not well tolerate shipboard conditions (Adeniji et al. 2017). Conversely, the use of spectrofluorometry for the identification of petroleum hydrocarbons in the marine environment is an ideal method since it is non-destructive and enables fast analysis with small quantities of sample (3 mL) and gives highly sensitive results (ppb range) (Li et al. 2004).

The intrinsic property of fluorescence in petroleum has likely been recognized since before the dawn of science, and the petroleum industry has long used this property in exploration and drilling operations (DeMent 1947). Scientific researchers have utilized spectrofluorometry in the identification of oil spills, a technique referred to as fingerprinting, since the mid-1970s (Frank 1975; John and Soutar 1976; Mason and Kerley 1988). Earliest studies of the correspondence

between the chemical composition of petroleum and resulting fluorescence dates to the mid-1980s, with the discovery that lower density was related to higher intensity at shorter wavelengths (Henry and Donovan 1984).

Previous researchers in the Coble laboratory analyzed discrete water samples collected with Niskin bottles mounted on a CTD rosette on cruises aboard the R/V *Nancy Foster* in June 2010 and on the R/V *Weatherbird II* in May and August 2010. Samples were collected in the region to the northeast of the DWH wellhead and analyzed using EEMS. Evidence for a deep plume at ~1,100 m was found, along with evidence for another plume at a mid-water depth of 300 – 450 m. The range of EEM fluorescence patterns found in some water samples collected at the surface, as well as at various depths in the water column, compared well with a surface oil mousse sample and with samples of DWH source oil (MC252) with Corexit® 9500A added at a DOR of 1:25 for a final concentration of ~100 ppb. This indicated the presence of oil and oil/dispersant in the water column. Fluorescence intensity at the higher excitation/emission wavelengths typical of naturally occurring CDOM were also observed at some depths, indicating that the oil/dispersant plumes were confined to distinct layers. Highest fluorescence intensities for the sub-surface petroleum plume were observed at the Ex/Em wavelengths of 230 nm/330 nm (Coble et al. 2011; Paul et al. 2013).

Water samples were also collected aboard the NOAA vessel R/V *Walton Smith* in August 2011 and analyzed in the Coble Laboratory with the goal of detection of the Mississippi River plume travelling through the Florida Straits along the southern tip of Florida. Results showed evidence of protein-like and humic-like fluorescence peaks typically present in the marine environment

resulting from new biological production (Coble et al. 2014); these results were contrasted with samples potentially containing the presence of oil and/or dispersants.

The goal of this research was to build on previous results from the Coble Laboratory by continuing to collect water samples from the DeSoto Canyon region, to the northeast of the DWH wellhead, onboard Florida Institute of Oceanography's (FIO) R/V *Weatherbird II* on oil spill response cruises WB1210 in December 2010, WB0211 in February 2011, and WB0511 in May 2011. Through analysis of EEMs of water samples collected over the year following the DWH oil spill, we planned to investigate the continued presence of oil/dispersant in the water column, and, hopefully, to find evidence of recovery. EEMS analysis of pore water extracted from sediment cores collected at several sites on the December 2010 research cruise were also analyzed for the possible presence of an oil signature in sediments. This work will help to better characterize the optimal Ex/Em wavelength target for fluorometer detection of oil/dispersant in the marine environment, and will clarify how the fluorescence signal changes over time following the action of temporal chemical and physical weathering.

MATERIALS AND METHODS

The Coble Laboratory water collection field protocol was used, as follows: 125 mL amber glass bottles with PTFE-lined caps were acid washed, followed by rinsing with fresh tap water several times and then inverting on racks to air dry. Bottles were combusted overnight in a muffle furnace at 450 °C, then cooled, covered with foil and recapped. Before sample collection, bottles were rinsed 3x with 5 – 10 mL sample before filling. The collection protocol for CDOM called for filtration of water samples using a glass syringe and Whatman glass microfiber filters (GF/F)

to remove particles $\geq 0.7 \mu\text{m}$. For acidification of samples, bottles were filled with approximately 80 mL sample water, then acidified to $\text{pH} = 2$ through the addition of 1 mL of 1M HCl, and bottle tops were wrapped with Teflon tape after recapping to prevent leakage.

Water samples were collected aboard the NOAA ship *Nancy Foster* in July 2010 and sent to the Coble Laboratory for fluorescence analysis. A total of eleven water samples were collected at four stations, acidified with HCl to $\text{pH} = 2$, and refrigerated at $4 \text{ }^\circ\text{C}$ until delivery to the Coble Laboratory where they were analyzed on a HORIBA Fluoromax2.

Water samples were collected by members of the Coble Laboratory research group aboard the R/V *Weatherbird II* in August 2010. Sampling sites were selected to the east of the DWH wellhead in order to not only sample visibly oiled surface waters, but also in an attempt to track the subsurface plume. With knowledge of prevailing winds in the Gulf of Mexico and formation of the Loop Current in the summer of 2010, and with the support of modelling based on an existing ocean circulation model (Weisberg et al. 2011), a series of sampling sites were identified (Fig. 4.1). Water samples were collected with Niskin bottles mounted on a CTD rosette at predetermined depths, as well as at the top and bottom of thermocline, chlorophyll maximum, and at indication of oiling (e.g., acoustic scattering layer, high fluorescence or particle density at depth). Three replicates were collected from each Niskin bottle in order to compare results of fluorescence analysis on whole vs. filtered vs. acidified samples. Sample bottles were stored upright and refrigerated at $4 \text{ }^\circ\text{C}$ until analysis on a HORIBA Fluoromax2. Samples were analyzed on a HORIBA Fluoromax2, processed using GRAMS and MATLAB software.

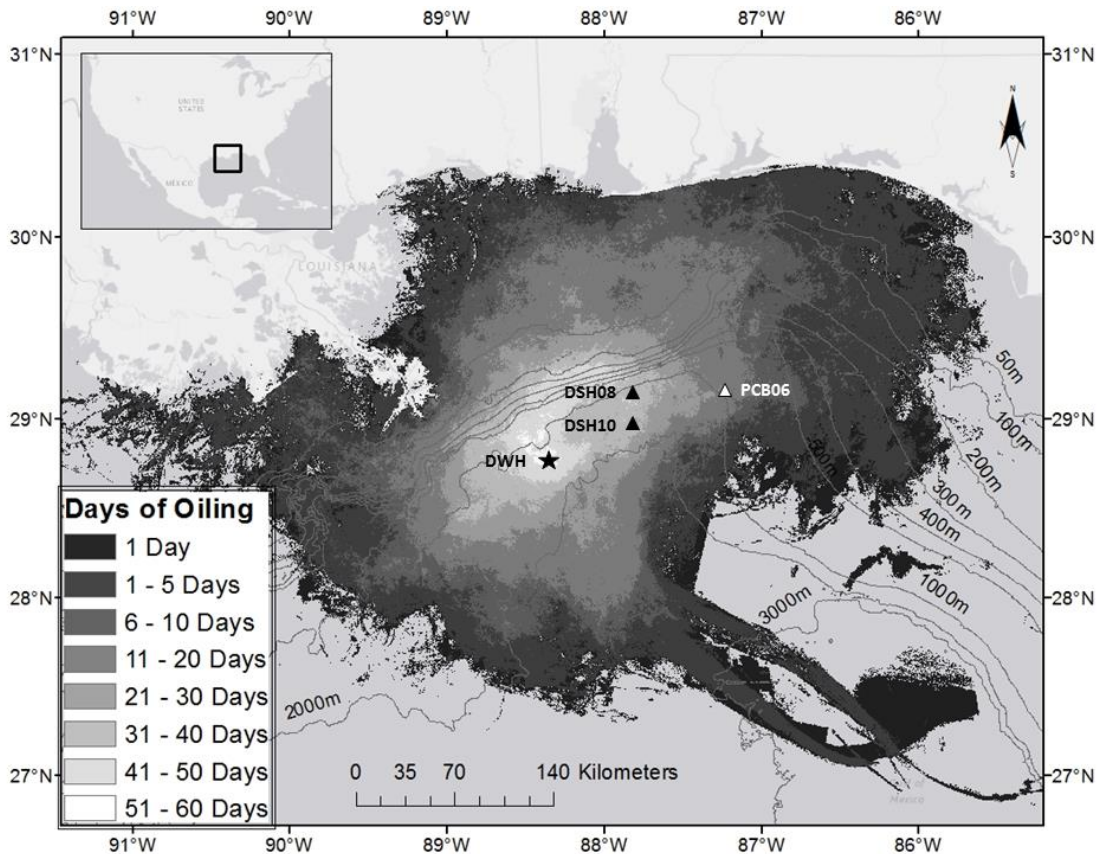


Figure 4.1. Map of the northern Gulf of Mexico showing the location of the DWH wellhead and three of the sites where water samples were collected aboard the R/V *Weatherbird II* oil response cruises in December 2010, February 2011 and May 2011. Days of oiling is superimposed. Map courtesy of Kendra Daly and Kate Dubickas.

Continued water sampling was conducted in the Gulf of Mexico over the year following the DWH blowout in order to detect and monitor presence of oil in the water column. Water samples were collected on three oil response research cruises to the east/northeast of the DWH wellhead aboard the R/V *Weatherbird II* on 1 – 10 December 2010, 17 – 22 February 2011, and 2 – 7 May 2011 (Table 4.1). Twelve 20 L Niskin bottles mounted on a CTD rosette sampler were triggered on the upcast at set depths, as well as at depths where evidence of O₂ minima and/or fluorescence spikes were noted on the downcast. Due to the extreme sensitivity of fluorescence analyses, our samples were the first taken from the Niskin bottles followed by collection of samples for other chemical analyses (gases, nutrients, chlorophyll,

Table 4.1. Samples collected in the year following the DWH oil spill which are included in this study

Station ID	Latitude	Longitude	Date	Sample Collection and (Maximum) Water Depths (m)
July 2010 NOAA NF-10-13-DWHLC (R/V <i>Nancy Foster</i>) to determine potential effects of the Loop Current and associated eddies on the transport of oil to the SSE of the DWH wellhead				
NF Sta70	28.0°N	88.2°W	17 July 2010	4.8, 990.8
NF Sta71	28°37.07'N	88°26.20'W	17 July 2010	3.4, 596, 1150
NF Sta72	28°37.80'N	88°14.79'W'	17 July 2010	2.8, 6, 1340
NF Sta73	28°45.41'N	88°23.95'W	17 July 2010	2.6, 30, 794, 1166
August 2010 FIO/USF (R/V <i>Weatherbird II</i>) to investigate the impact of the BP oil spill on the northern Gulf of Mexico ecosystem, focusing on the lower end of the food web				
DSH10	28 58.542	87 51.992	10 Aug 2010	(1518)
DSH08	29 06.016	87 52.895	10 Aug 2010	(1200)
December 2010 FIO/USF (R/V <i>Weatherbird II</i>) to investigate, in the water column and sediments, the persistence and impact of BP oil to the northern Gulf of Mexico ecosystem				
PCB06	29 6.117	87 17.313	04 Dec 2010	Surface, 45, 60, 250, 300, 965 (1050)
DSH08	29 07.345	87 52.145	08 Dec 2010	Surface, 50, 200, 280, 400, 1100 (1100)
DSH10	28 58.254	87 52.438	08 Dec 2010	Surface, 35, 245, 435, 995, 1500 (1535)
February 2011 FIO/USF (R/V <i>Weatherbird II</i>) to investigate the impact of the BP oil spill on the northern Gulf of Mexico ecosystem, focusing on the lower end of the water column food web and the flux of oil to the seafloor				
DSH10	28 58.57	87 52.10	19 Feb 2011	2, 10, 25, 50, 60, 75, 110, 150, 300, 400, 500, 786, 1000, 1100, 1200, 1400 (1500)
DSH08	29 07.35	87 52.12	20 Feb 2011	Surface, 25, 55, 100, 115, 160, 300, 400, 750, 1000, 1100 (1100)
PCB06	29 07.7	87 16.0	21 Feb 2011	2, 10, 17, 50, 84, 100, 300, 400, 500, 750 (1000)
May 2011 FIO/USF (R/V <i>Weatherbird II</i>) to investigate the impact of the BP oil spill on the northern Gulf of Mexico ecosystem, focusing on the lower end of the water column food web and the flux of oil to the seafloor				
DSH10	28 58.610	87 52.266	07 May 2011	Surface, 10, 21, 50, 75, 90, 215, 300, 400, 500, 1000, 1100, 1200, 1400 (1500)
DSH08	29 7.405	87 52.079	07 May 2011	Surface, 25, 50, 75, 100, 300, 400, 500, 750, 1000 (1100)
August 2011 NOAA (R/V <i>Walton Smith</i>) to acquire shipboard data to corroborate satellite imagery and document the <i>in situ</i> surface characteristics of the Mississippi River plume along the eastern edge of the Loop Current to the Florida Keys				
01	25.64508	80.12412	02 Aug 2011	Surface
15	24.64465	81.01707	03 Aug 2011	Surface
21	24.53642	81.41122	03 Aug 2011	Surface
21.5	24.48428	81.38937	03 Aug 2011	Surface, 19, 70, 133
25	24.39397	82.76852	04 Aug 2011	Surface

pigments/HPLC). After filling, sample bottles were immediately placed upright in the refrigerator and held at 4 °C until analysis on a HORIBA fluorometer.

Samples from the December cruise were analyzed on a HORIBA Fluoromax2 spectrofluorometer at sea as time allowed, and remaining samples were frozen at sea for eventual thaw and analysis on a HORIBA Fluoromax4 spectrofluorometer in the Coble Laboratory.

Unfortunately, the Fluoromax2 was inoperable following the December 2010 cruise, and repair was impossible. Therefore, samples from the February and May 2011 cruises were analyzed solely on the Fluoromax4. Every attempt was made to run samples at sea as soon as practicable following collection; however, if circumstances were not conducive (e.g., rough seas, insufficient travel time between sample sites, problems with shipboard Milli-Q water quality) samples were frozen at sea for future thaw and analysis in the Coble Laboratory. A test of each instrument's xenon lamp was performed at the beginning of each day, and a blank containing Milli-Q water was used to conduct an instrument alignment test, and then used in an EEM analysis before running samples each day. Results were translated into QSE units through dividing proton counts per sec (CPS) by the slope of a quinine sulfate dilution series (conversion factor = 3200) (Coble et al. 1993).

December 2010

Samples were collected aboard the R/V *Weatherbird II* during the 1 – 10 December 2010 cruise; two water samples were collected at each location depth in pre-fired amber bottles. One sample was acidified, and the second was left unaltered. Based on analysis of filtered vs. non-filtered samples on the August 2010 cruise, no filtering was done in order to avoid inadvertent removal

of petroleum hydrocarbons and/or dispersant. The HORIBA Fluoromax2 was used to analyze samples at sea, and a routine for a “short EEM,” with excitation at just four wavelengths, was used to run all samples as soon as possible following collection to look for any signs of oil remaining in the water column. As many full EEMs as possible were also run at sea on both the whole and acidified samples. Samples of pore water centrifuged from upper sections of selected sediment cores collected on the cruise were also analyzed at sea, with dilution as necessary to avoid oversaturation of the fluorescence signal. After returning to the Coble Laboratory at the USF College of Marine Science, the remaining samples were analyzed and processed on the new Fluoromax4 instrument using FluorEscence software. Since excitation and emission corrections were applied automatically with this software, the only post-processing done was translation to QSE units.

February and May 2011

Water samples were collected aboard the R/V *Weatherbird II* on 18 – 22 February 2011 and 5 – 7 May 2011 following the previously noted Coble Laboratory collection protocol; however, due to decay of the fluorescence signal detected in the analysis of acidified vs. frozen samples from the December 2010 cruise, a decision was made to no longer acidify samples. Only a single whole sample was collected at each location depth on these two cruises; they were placed immediately into the onboard laboratory refrigerator and maintained at 4 °C until analysis. The HORIBA Fluoromax4 instrument was taken aboard on both cruises, and as many water column samples as possible were analyzed at sea. Pore water from sections of selected sediment cores was also analyzed at sea, with dilution as necessary to avoid oversaturation of the fluorescence signal. Samples that were not analyzed at sea were analyzed as soon as possible after return to

the Coble Laboratory. Again, the only post-processing to EEMs was translation to QSE units. However, upon deeper inspection of EEMs collected on the Fluoromax4, a problem with the instrument's emission correction file was detected, which required retroactive application of new correction files to all EEMs collected on that instrument. This was accomplished using MATLAB (The MathWorks 2018).

To provide a framework for discussion of water samples collected in the Gulf of Mexico during the response to the DWH oil spill, surface seawater collected during the December 2010 R/V *Weatherbird II* cruise from an unoiled location was analyzed on the Fluoromax4 to provide an EEM of typical seawater. This water was collected in Perdido Pass using a bucket and was stored frozen in the Coble Laboratory until analysis. Another sample of this water was then used to create dispersed oil in seawater using 1 mL MC252 oil (collected from the *Discoverer Enterprise*) and 4 μ L Corexit® 9500A for a DOR of 1:25 (final concentration of ~100 ppb). This enabled conversion of fluorescence in QSE to the equivalent ppb oil with chemical dispersant. Finally, an EEMS analysis of tyrosine was performed on a solution created by dissolving 0.08 g tyrosine (stock on hand in the Coble Laboratory) in 1 L Milli-Q water to show the contrast between the F_{\max} Ex/Em and spectral shape of Peak B and oil-type fluorescence.

In the sample of typical seawater (Fig. 4.2, top left), minor fluorescence intensity is visible at Ex/Em 275 nm/300 nm (B Peak). Note that fluorescence intensity increases in this region in the dispersed oil sample (Fig. 4.2, top right), albeit at a slightly higher emission wavelength. This is joined by high fluorescence intensity at Ex/Em 275 nm/325 nm and a broad, low fluorescence

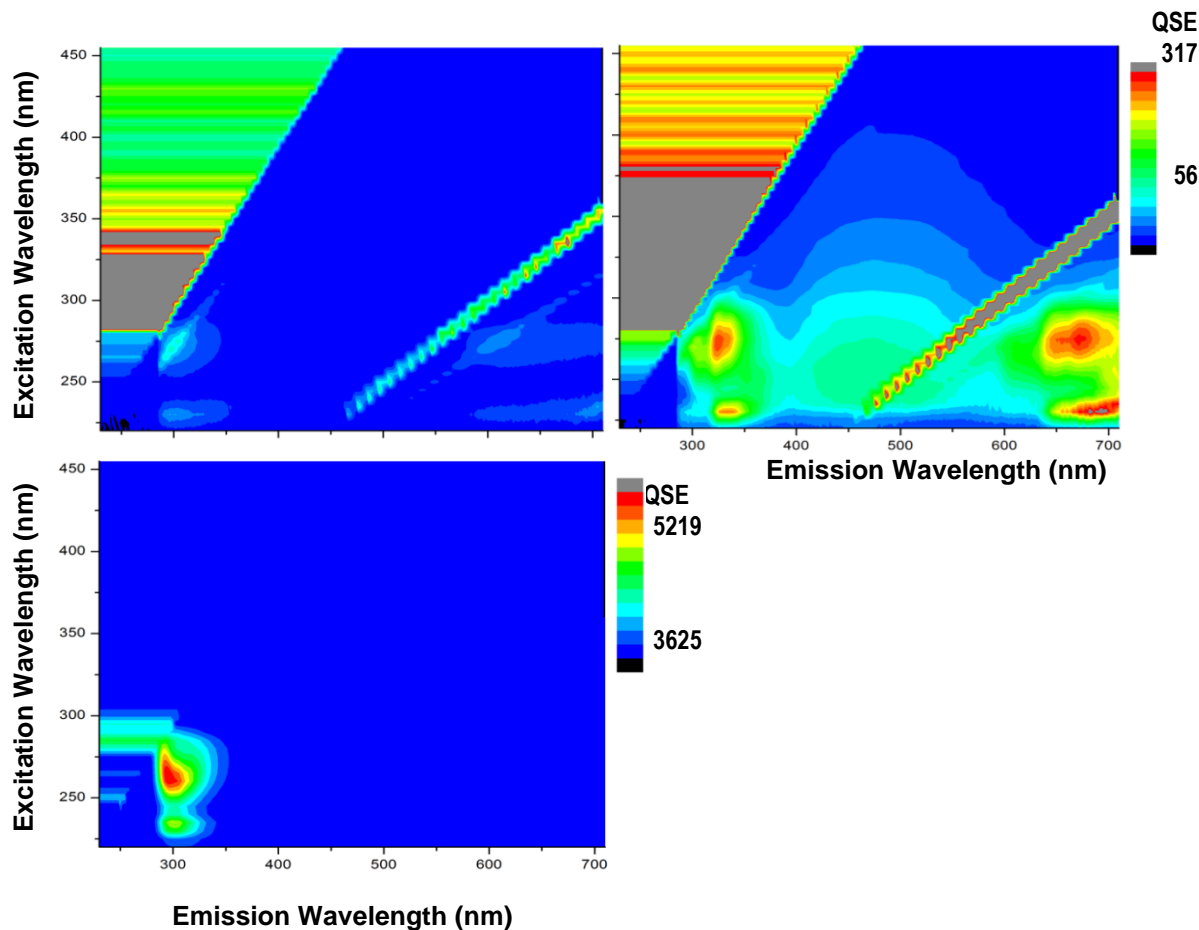


Figure 4.2. EEMs of typical seawater collected at the surface with a bucket at Perdido Pass on 7 December 2010 (top left), and with the addition of MC252 oil and Corexit® 9500A at DOR 1:25 for a final concentration of 100 ppb (top right). The scale is the same for both EEMs. On the bottom right is an EEM of primary stock solution of tyrosine dissolved in Milli-Q water (bottom left). Analysis performed on HORIBA Fluoromax4.

peak centered at Ex/Em 250 nm/450 nm, all of which are typical of dispersed oil in seawater. Of note is the important difference between the fluorescence intensity characteristic of proteins, typified by the EEM of tyrosine dissolved in water (Fig. 4.2, bottom left), and that of dispersed MC252 oil (Fig. 4.2, top right). In addition to the maximum fluorescence intensity shown at Ex/Em 275 nm/300 – 305 nm, tyrosine-like proteins typically display a fluorescence peak of lower intensity at Ex/Em 230 nm/300 – 305 nm. However, the fluorescence intensity of oil in the Ex/Em 230 nm/325 nm range is of equal or even higher intensity than that seen at Ex/Em 275

nm/325 nm. We propose that this difference can be used to facilitate the distinction between proteins and oil in the natural environment.

August 2011

Water samples were collected at the surface only, as well as samples collected at additional depths, at 23 separate stations aboard the NOAA vessel R/V *Walton Smith* in August 2011. The goal of this cruise was to utilize FDOM to look for evidence of the Mississippi River plume along the southwest coast of Florida, through the Florida Straits, and along the southeast Florida coastline. Samples were collected using the Coble Laboratory CDOM protocol, including filtration using a glass syringe and Whatman GF/F; however, samples were not acidified but were frozen at sea. Following thaw in the laboratory refrigerator for two days, samples were analyzed on the HORIBA Fluoromax4 in the Coble Laboratory.

RESULTS

The water samples collected in August 2011 along the Florida coastline aboard the NOAA ship *Walton Smith* are the last samples analyzed in this study; however, we begin with those results in order to provide a fluorescence profile that is very typical of naturally-occurring CDOM and protein fluorescence in the marine environment. This provides an appropriate background against which to compare water samples showing petroleum-related fluorescence profiles. We will then present results from the samples collected in the Gulf of Mexico over the course of the thirteen months following the beginning of the DWH oil spill, first aboard the R/V *Nancy Foster* in July 2010, and then aboard the R/V *Weatherbird II* in August and December, 2010, and in February and May, 2011.

R/V *Walton Smith* – August 2011

Results of EEMs analysis showed elevated fluorescence intensity at Ex/Em 275 nm/350 nm (T Peak) and Ex/Em 320 nm/400 nm (C Peak), evidence of the presence of proteins and FDOM, respectively, potentially arising from the influence of the Mississippi River plume as it traversed the Florida Straits. Samples from locations 15 and 21 (Fig. 4.4, top) show typical “bluewater” fluorescence, while samples from locations 1 and 25 (Fig. 4.4, bottom) show significant protein and CDOM fluorescence. In Fig. 4.5, the surface sample from location 1 shows the strongest protein as well as CDOM fluorescence (top), while the deepest sample (bottom right) shows an insignificant protein peak as well as greatly reduced FDOM fluorescence. This would be a very typical marine depth profile.

An elevated ratio of fluorescence intensity at Peak T to Peak C is indicative of flooding from an urbanized river due to the presence of sewage outflow (Baker 2001; Khamis et al. 2018), and Mississippi River flooding took place at near record levels in April/May 2011. Figure 4.6 presents *chlorophyll a* vs. the ratio of Peak T to Peak C, showing the likely influence of the Mississippi River plume in the R/V *Walton Smith* samples from August 2011.

EEMS analysis of the samples collected on the R/V *Walton Smith* in August 2011 show protein-like fluorescence (Peak T) ranging from 0.22 to 10.8 ppb QSE, with an average of 1.55 and median of 1.11 ppb QSE. The highest values were found in the two samples collected near the outlet of the Shark River at the surface. The Shark River is a major distributary of the Harney River, draining the southwestern Everglades National Park, thus a high level of biological productivity would naturally be reflected in the outflow. These two samples were extremely anomalous, 6.5 and 9.8 times higher than the average found in all other samples. Lowest

protein-like fluorescence was found in the sample from 133 m near the coastline to the south of Big Pine Key. In fact, the lowest six values were all found in deep water samples, and all samples collected below 85 m had levels less than 1.0 ppb QSE. Only two samples collected at the surface had Peak T fluorescence in this range, and these two were located just to the south of the Dry Tortugas and in the middle of the Florida Strait.

CDOM fluorescence ranged from 0.03 to 8.85 ppb QSE, with an average of 1.31 and a median of 0.93 ppb QSE. Remarkably, the levels of CDOM found in the two samples influenced by the Shark River with high protein-like fluorescence had CDOM levels near the mean for all samples collected on this cruise. The highest levels of CDOM fluorescence were found in water samples collected at 70 m and 133 m just off the coast near Big Pine Key; these were both more than five times higher than the mean for samples on this cruise. Interestingly, the second-highest CDOM

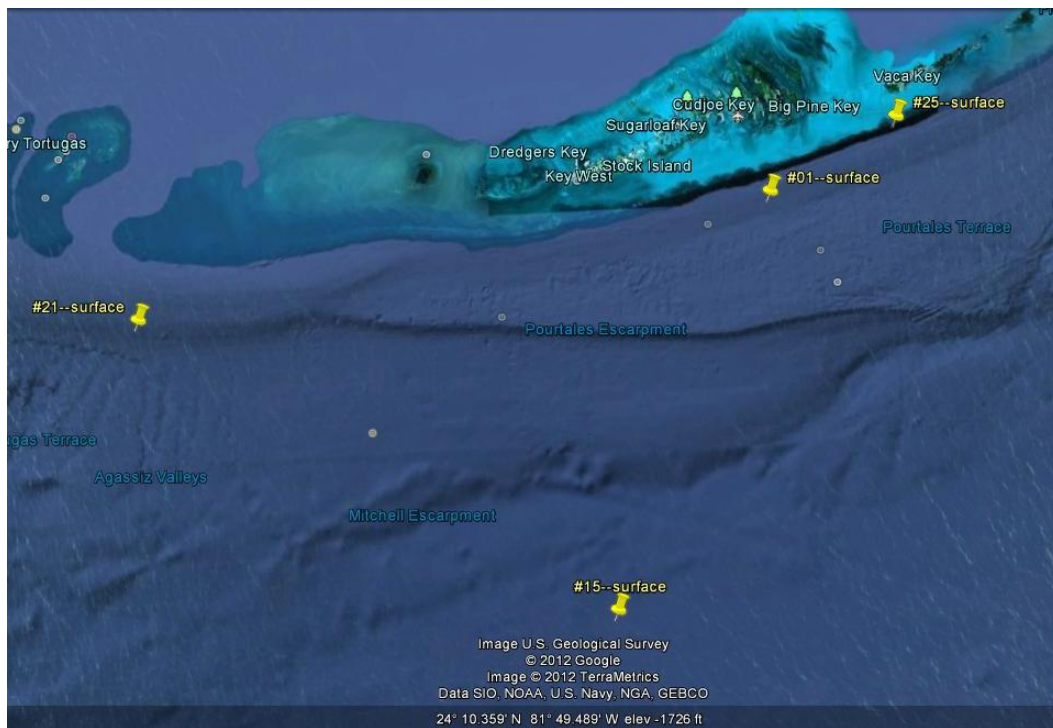


Figure 4.3. Google Earth image with marked locations of selected water samples collected at the surface aboard the NOAA ship R/V *Walton Smith* in the Florida Straits in August 2011.

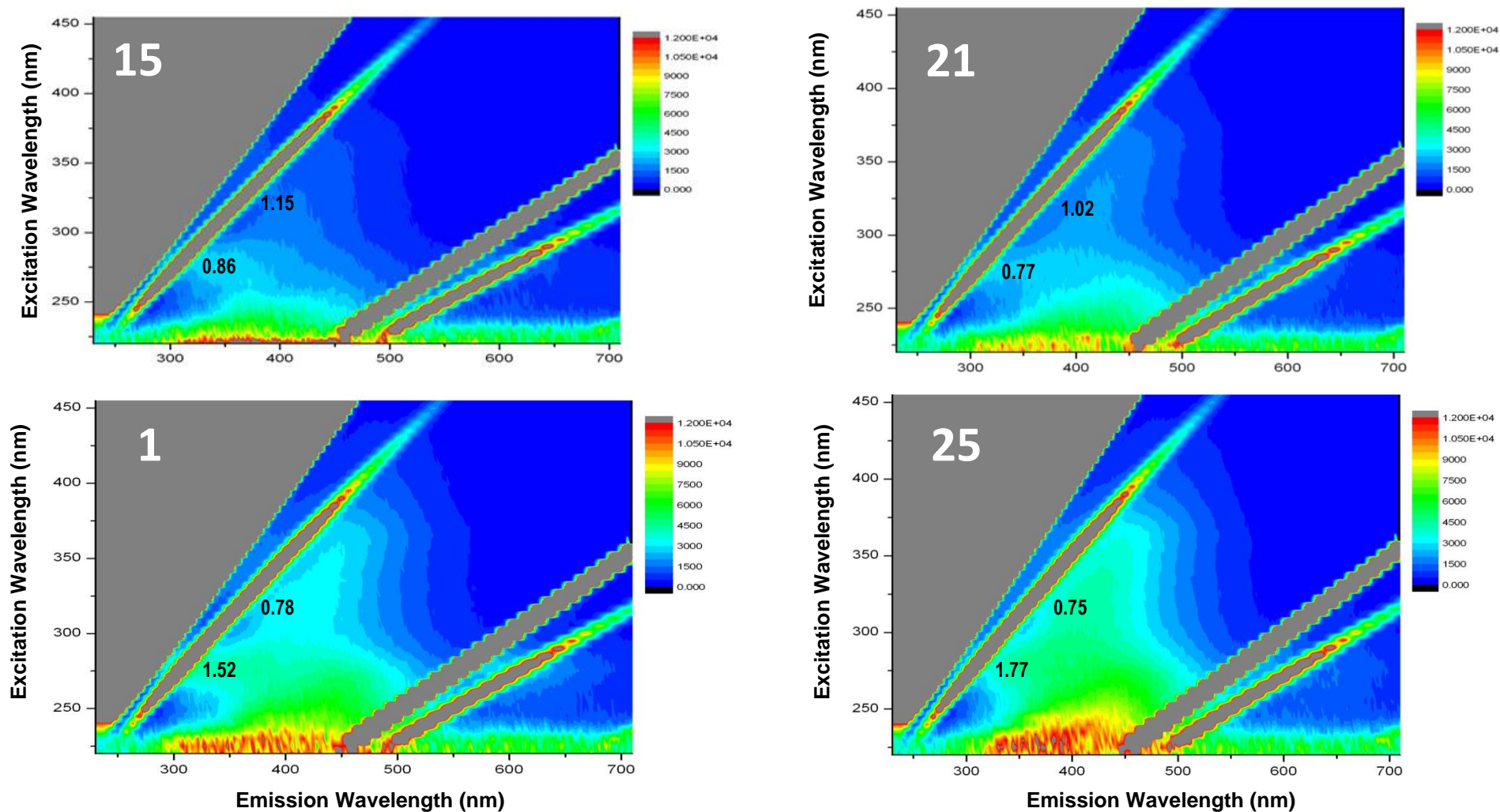


Figure 4.4. EEMs of water samples collected at locations identified in Fig. 4.3. Units on color bar are CPS. Fluorescence intensity in ppb QSE is indicated at Ex/Em 275 nm/350 nm (T Peak) and 320 nm/400 nm (C Peak).

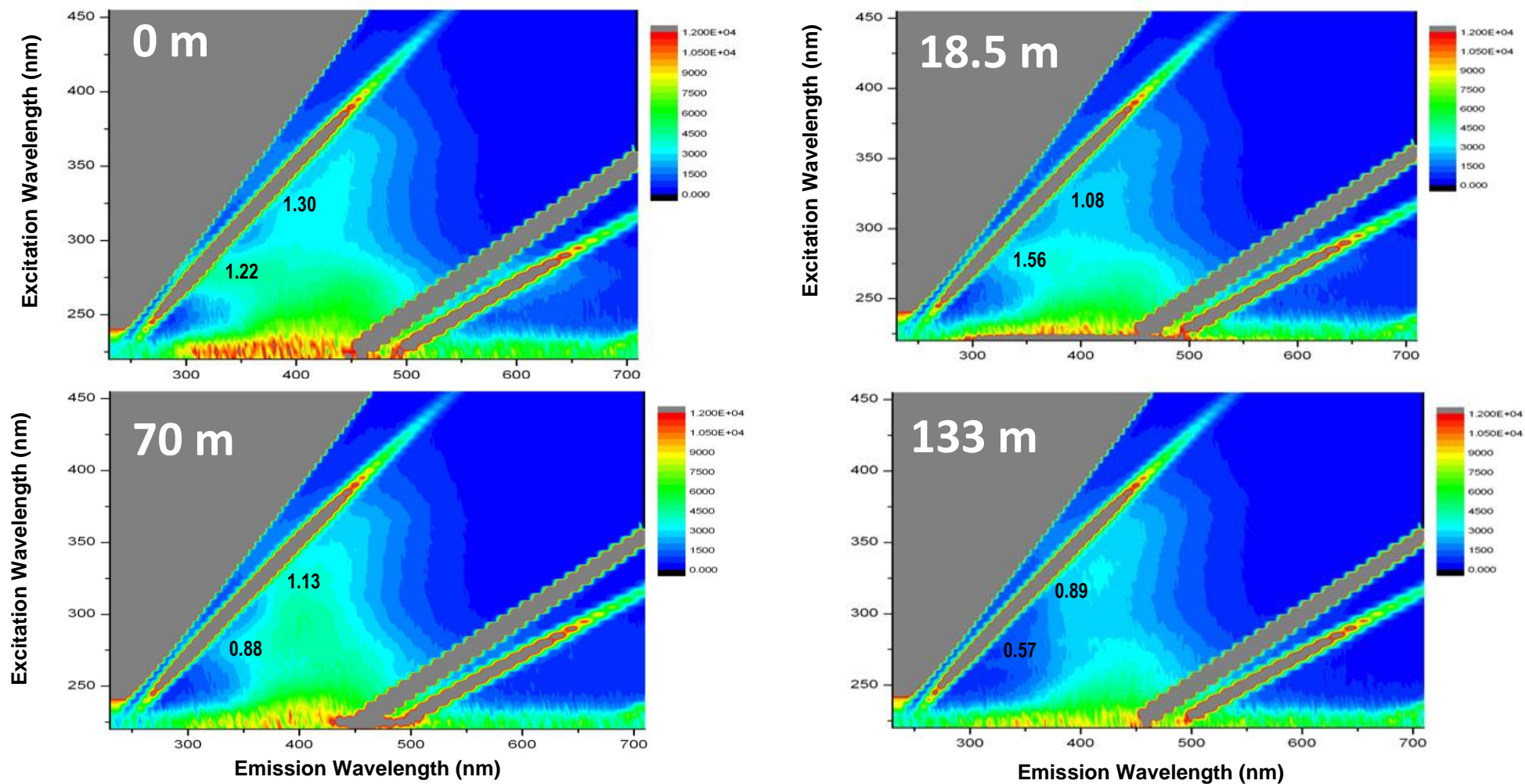


Figure 4.5. EEMs of water samples collected just to the south of Location 1 in Fig. 4.3. Samples collected at the surface (top left), at 18.5 m (top right), at 70 m (bottom left), and at 133 m (bottom right). Units on color bar are CPS. Fluorescence intensity in ppb QSE is indicated at Ex/Em 275 nm/350 nm (T Peak) and 320 nm/400 nm (C Peak).

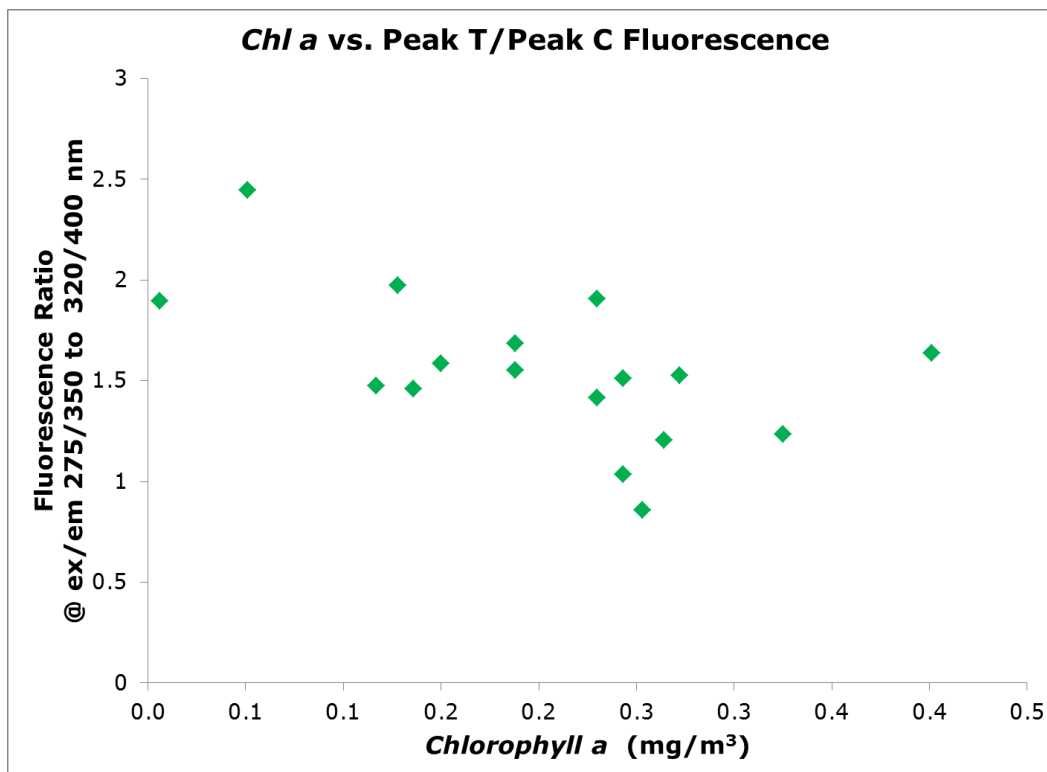


Figure 4.6. *Chlorophyll a* versus the ratio of protein-like to humic-like fluorescence in water samples showing the likely influence of the Mississippi River plume collected aboard the R/V *Walton Smith* in August 2011.

fluorescence was seen in the sample with the lowest protein-like fluorescence. The three lowest values for CDOM fluorescence were found in water samples collected at 137 m, 60 m, and 197 m. The sample from 60 m had higher than average protein-like fluorescence; however, the other two samples had lower than average protein-like fluorescence along with the low CDOM signal. Fluorescence at depths < 100 m typically arises from primary production related DOM, and it rapidly decreases with depth below the photic zone. Any remaining fluorescence signal in the deep ocean is usually a humic-like or protein-like signature (Schifter et al. 2017)

R/V *Nancy Foster* – July 2010

Samples were collected on July 17, 2010, in the vicinity of the DWH wellhead two days after it was successfully capped (Fig. 4.7, top left, and Table 4.1). EEMS analysis of eight samples showed fluorescence peaks at Ex = 230 and 275 nm and Em = 330 nm, indicative of the

presence of petroleum. Of note is the parallel between the fluorescence maxima in this region and the published fluorescence maxima of naphthalene (Mendoza et al. 2013). Naphthalene was found to be the predominant PAH present (65 %) in MC252 crude oil provided to researchers by BP (Liu et al. 2012), which was also confirmed by chemical analyses of water samples collected during the BIO wave tank experiments reported in Chapter 2.

Further evidence for the correspondence between fluorescence in this region and petroleum hydrocarbons arises from the reported fluorescence maxima of BTEX compounds at $E_m = 285 - 291$ nm with excitation at $252 - 275$ nm (Taniguchi and Lindsey 2018). Mendoza et al. (2013) reported three fluorescence peaks for benzene at Ex/Em 225 nm/335 nm, 250 nm/275 nm, and 250 nm/550 nm (in order of decreasing intensity), as well as three for toluene at Ex/Em 260 nm/280 nm, 260 nm/560 nm, and 225 nm/415 nm (2013). Naphthalene has a reported double peak at $E_m = 320 - 322$ nm and 324 nm upon excitation at 275 nm (Giamarchi et al. 2000; Taniguchi and Lindsey 2018). Mendoza et al. (2013) also noted three peaks for naphthalene at Ex/Em 275 nm/330 nm, 225 nm/330 nm, and 230 nm/495 nm, again in order of decreasing intensity. These results are well-correlated with the appearance of oil-related fluorescence maxima at Ex/Em 225 nm/330 nm and 275 nm/330 nm in our EEMS analysis at all three scales — baffle flask experiments, wave tank experiments and field samples.

The highest level of oil-type fluorescence was observed in the sample from Station 71 collected at 1,150 m (23.8 ppb QSE), providing evidence of a sub-surface oil plume; however, as expected at this depth, CDOM fluorescence was very low in this sample (0.77 ppb QSE) (Fig. 4.8, right). Based on the standard created in the Coble Laboratory, the oil-

type fluorescence in this sample was equivalent to 7.51 ppb MC252 oil with Corexit® 9500A at DOR 1:20. This signal was associated with the fluorescence detected by a CTD-mounted WET Labs ECO FLCDRTD in situ fluorometer, as well as with a slight O₂ depression (Fig. 4.7) (Goni et al. 2010; Smith et al. 2014).

The second-highest oil-fluorescence signal was in the sample from Station 73 at 2.6 m (16.7 ppb QSE); however, CDOM fluorescence was also elevated in this sample (5.04 ppb QSE), as would be expected in a typical surface water sample. Moderate levels of oil-type fluorescence were seen in two samples, from Station 71 at 3.4 m (7.19 ppb QSE) and from Station 72 at 2.8 m (7.07 ppb QSE). The shallower sample also displayed typical surface CDOM fluorescence of 2.39 ppb QSE. Minor levels of oil-type fluorescence were seen at Station 70 in both samples collected at that site, with 3.63 ppb QSE in the sample at 4.8 m and 3.14 ppb QSE in the sample at 991 m. The latter provided further evidence of a deepwater plume, along with the oil-type fluorescence seen in the sample at Station 73 from 1,166 m (3.32 ppb QSE). Finally, the sample from 30 m at Station 74 displayed oil-type fluorescence of 2.13 ppb QSE.

The sample from Station 71 at 1,150 m (23.8 ppb QSE) was the highest oil-type fluorescence signal seen overall in any of our field samples from the Gulf of Mexico for the entire experimental series. Based on the standard created in the Coble Laboratory, this was equivalent to 7.51 ppb MC252 oil with Corexit® 9500A at DOR 1:20.

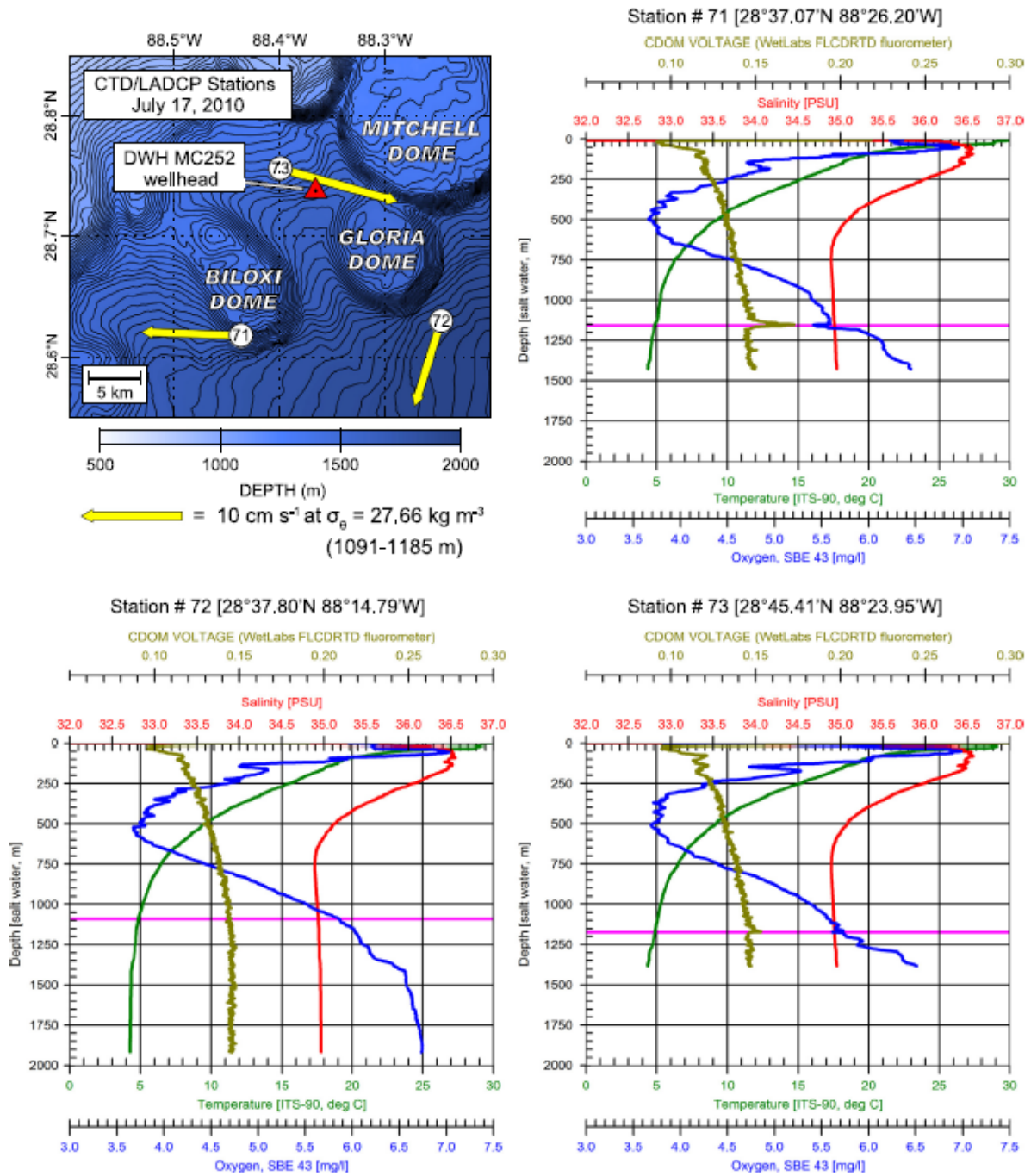


Figure 4.7. Locations of sampling stations NF Sta71, 72 and 73 (top, left), and CTD/LADCP hydrography conducted near the DWH MC252 wellhead on July 1, 2010. From “Oceanographic conditions in the Gulf of Mexico in July 2010, during the Deepwater Horizon oil spill,” by R.H. Smith, et al., *Continental Shelf Research*, 77, p. 118. Copyright 2014 by Elsevier Ltd. Reprinted with permission.

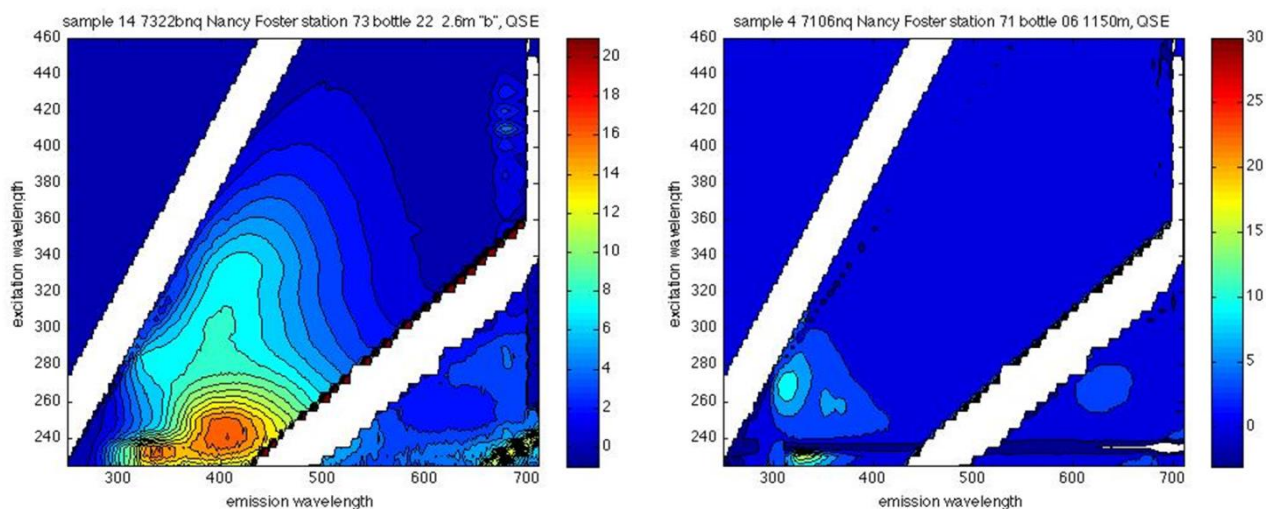


Figure 4.8. Water samples collected aboard the R/V *Nancy Foster* from 2.6 m at Station 73 (left) with highest fluorescence signature of oil at or near the surface, and sample from 1150 m at Station 71 (right) showing evidence of the deep water plume in July 2010.

R/V *Weatherbird II* – August 2010

Water samples collected aboard the R/V *Weatherbird II* on 10 August 2010 at DSH10 were analyzed on a HORIBA Fluoromax2, and EEMs were created with MATLAB (The MathWorks 2018). Figure 4.9 depicts fluorescence intensity at selected Ex/Em wavelength pairs in all water samples collected at DSH10 (top left). Elevated fluorescence intensity at Ex/Em 225 nm/330 nm and 275 nm/330 nm, is again noted.

These fluorescence results appear to characterize a subsurface plume at 400 m, which is corroborated by the dissolved oxygen depression at 452 m shown in the depth profile of CTD data for dissolved O₂ and salinity (Fig. 4.9, top right). Mendoza et al. (2013) also found evidence of a sub-surface plume at 400 m to the north of the DWH wellhead in May/June 2010 aboard the NOAA ship *Gordon Gunter*. EEMs of water samples at the surface (Fig. 4.9, bottom left) and at 400 m (Fig. 4.9, bottom center) show the presence of oil at 9.2 ppb QSE and 8.7 ppb QSE, respectively. However, the sample collected at 1,000 m (Fig. 4.9, bottom right) shows only normal marine CDOM fluorescence peaks C and A_C (1.2 ppb QSE).

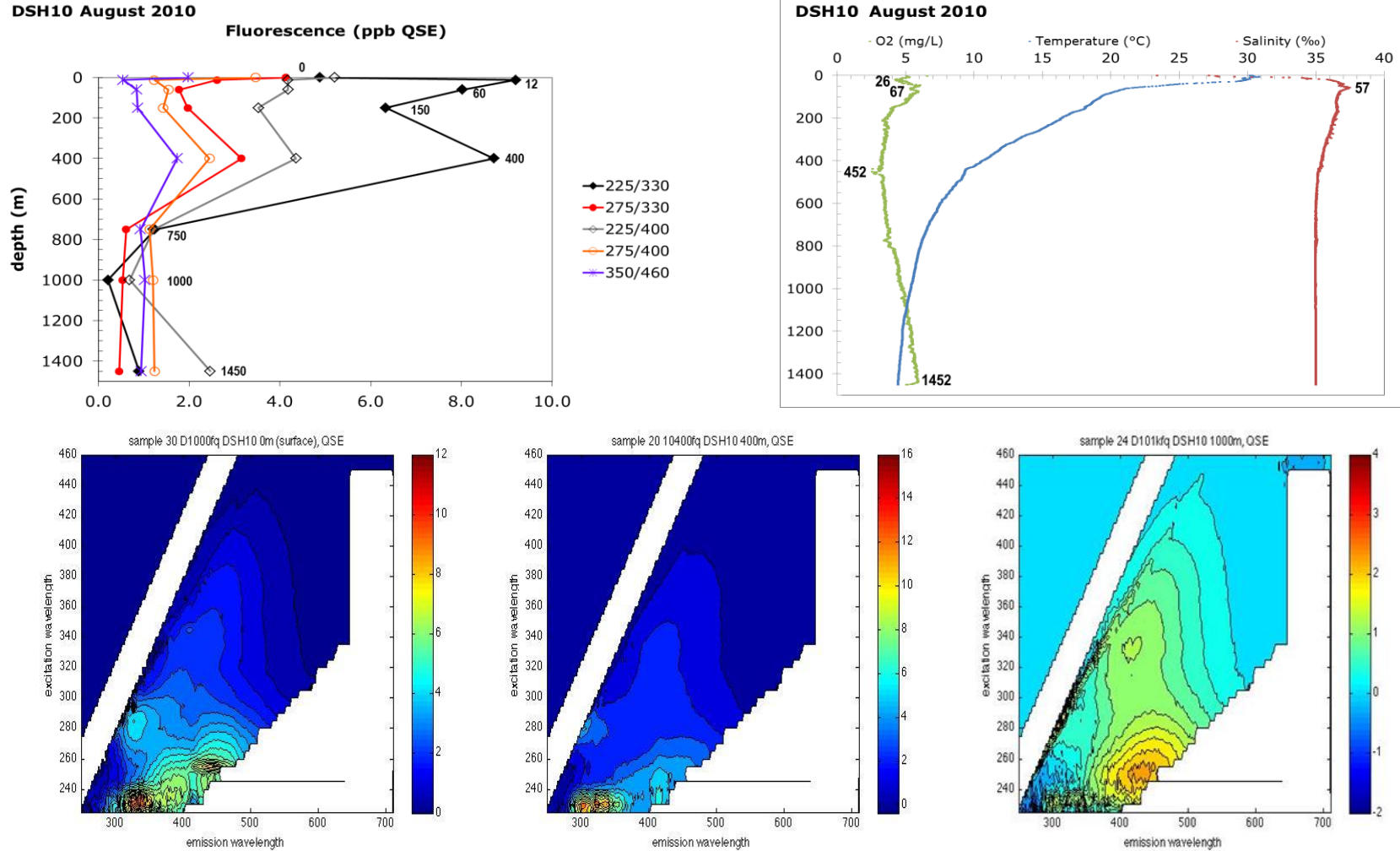


Figure 4.9. Plot of fluorescence intensity at five selected excitation/emission pairs (top left) for all water samples collected aboard the R/V *Weatherbird II* at DSH10 on 10 August 2010 and depth profile of CTD data for dissolved oxygen and salinity (top right). EEMs of water samples collected at the surface, 400 m and 1,000 m (bottom, left to right).

R/V *Weatherbird II* Time Series – December 2010, February 2011, and May 2011

Due to storms and resulting rough seas on both the December 2010 and February 2011 cruises, it was not possible to visit all sites on the cruise plan for every cruise; however, samples were collected from sites DSH08 and DSH10 on all three cruises. Although site PCB06 was not on the plan for the May 2011 cruise, samples were collected at that site in both December 2010 and February 2011. Therefore, fluorescence analyses of water samples from these three sites are presented as they best represent the evolving presence of oil to the northeast of the DWH wellhead over the year following the initial blowout. The site with maximum water depth was DSH10 at ~1,500 m, followed by DSH08 at ~1,100 m, and PCB06 at ~1,000 m. Fig. 4.1 shows the spatial relationship of these sites to the DWH wellhead, and specific latitudes and longitudes are given in Table 4.1.

Although previous analyses of water samples by the Coble Laboratory research group showed maximum fluorescence associated with the presence of oil with excitation at 225 nm, output of the 150-W xenon lamp source in the Fluoromax4 is very low below 250 nm, which requires the application of a very high correction factor. The resulting signal is extremely variable, and it is difficult to distinguish true fluorescence from noise at excitation = 225 nm. Since fluorescence maxima of small molecular weight aromatic hydrocarbons at excitation wavelengths of 252 – 275 nm is supported by the scientific literature, Ex/Em 275 nm/324 nm and 275nm /330 nm are presented in the following figures as indicative of the presence of oil.

Appendix E presents the results EEMS analysis of all water samples collected aboard the R/V *Weatherbird II* oil response cruises at sites DSH08 and DSH10 in December 2010, February 2011, and May 2011, as well as of all water samples collected at PCB06 in December 2010

and February 2011. Also presented are depth profiles for selected fluorescence intensity peaks in those analyses as well as depth profiles of CTD data.

DISCUSSION

Among other findings, fluorescence intensity characteristic of oil was detected at all sites in surface samples (< 21 m) to at least some degree over the entire series; however, oil concentration (in ppb QSE) behaved somewhat differently over time at each site.

December 2010 — DSH08, DSH10, and PCB06

Results at all three sites showed a consistent pattern of the highest oil concentrations being present in the surface samples on this research cruise, with the single highest overall concentration measured (2.52 ppb QSE, 0.79 ppb dispersed oil) at DSH08 on this research cruise (Fig. 4.10). Evidence of the presence of a deep sub-surface plume was also seen in December 2010 in slightly elevated fluorescence intensity at Ex/Em 275/324 nm in the sample from 955 m at DSH10 and from 1,000 m at DSH08; however, this phenomenon was not observed at PCB06.

February 2011 — DSH08, DSH10, and PCB06

In February 2011, a marked increase in fluorescence intensity indicating the presence of oil was observed both at or near the surface as well as at the maximum water sample depths at all sites (Fig. 4.11). Oil-like fluorescence intensity at Ex/Em 275 nm/324 nm at DSH10, closest in proximity to the DWH wellhead, was highest at the surface (4.65 ppb QSE, or 1.47 ppb dispersed oil), while at DSH08 it was highest at 55 m (4.98 ppb QSE, or 1.57 ppb dispersed oil). In fact, oil-like fluorescence intensity at Ex/Em 275 nm/324 nm in the surface sample at DSH10 was 2.3 times that observed at the surface in December 2010, and that seen in the

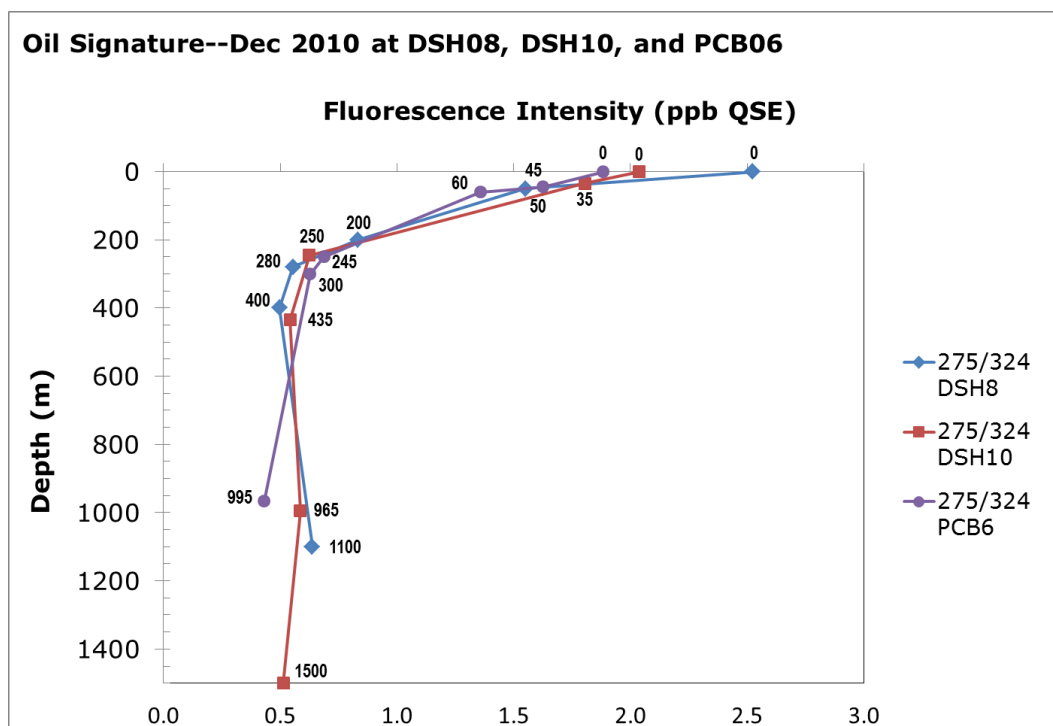


Figure 4.10. Fluorescence intensity (ppb QSE) at Ex/Em 275 nm/324 nm, indicative of oil in the water column, at sites DSH08, DSH10, and PCB06 in December 2010.

sample from 55 m at DSH08 was 3.2 times higher in February 2011 than in December 2010.

In the sample from the surface at DSH10, secondary fluorescence intensity at Ex/Em 250 nm/450 nm (Peak A_C) and at 360 nm/450 nm (Peak C) are also of note, due to the presence of naturally occurring FDOM. Note that in the sample from 75 m, the fluorescence signal is blue-shifted to Ex/Em 250 nm/400 nm (Peak A_M) and 300 nm/400 nm (Peak M). It is believed that FDOM in the marine environment fluoresces at this slightly lower wavelength range due to the fact that marine humics are less aromatic than those of terrestrial origin (Coble 2007). The sample collected at 17 m at PCB06 in February 2011 was the highest oil-type fluorescence observed at that site as well (3.35 ppb QSE, or 1.06 ppb dispersed oil), which was 1.78 times that seen in the surface sample in December 2010.

Deep water samples collected at both DSH08 and DSH10 increased in oil-type fluorescence intensity in February 2010 as well. Closest to the DWH wellhead, the greatest increase was

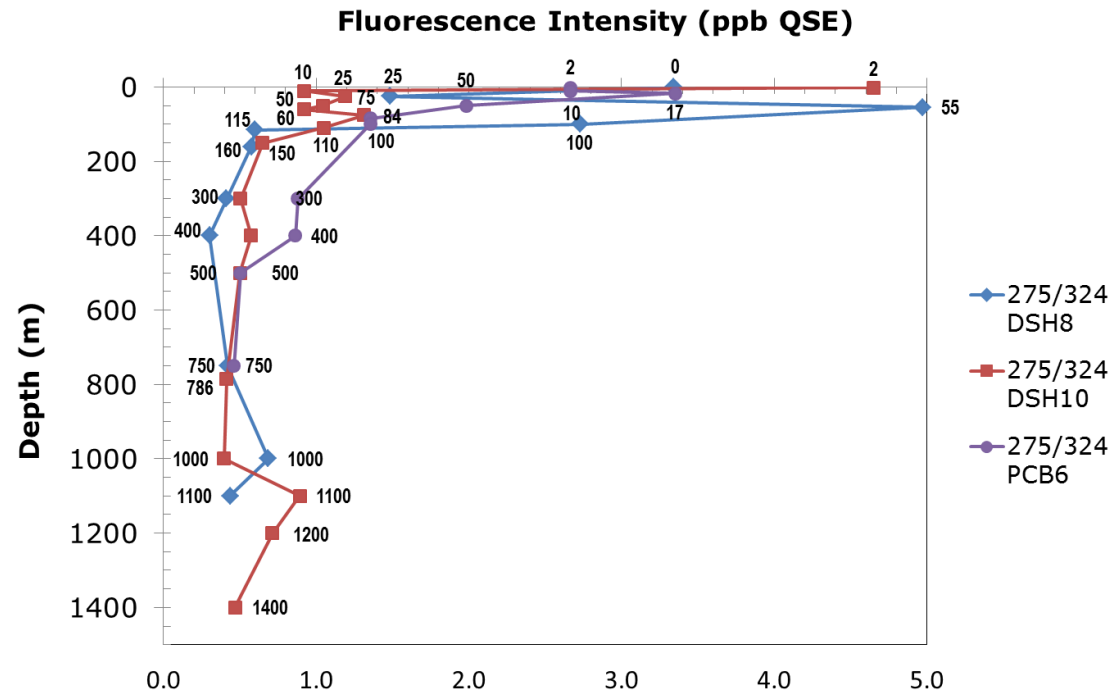
seen at 1,100 m (0.89 ppb QSE, or 0.28 ppb dispersed oil) at DSH10 on this cruise. Concentration increased only slightly at DSH08 in the sample from 1,000 m from that found at 1,100 m in December 2010 (0.64 to 0.69 ppb QSE, or 0.20 to 0.22 ppb dispersed oil). However, the samples from DSH08 at 750 m and 1,100 m in February 2011 had lower oil-type fluorescence intensity than that at 1,000 m, indicating the continuing presence of a defined deepwater plume. These results suggest that oil in the water column was still making its way to the surface a full seven months after the DWH wellhead was capped. Only at PCB06 was a continuing decrease in oil fluorescence observed at maximum sample depth on this cruise, from 0.43 ppb QSE (0.14 ppb dispersed oil) at 965 m to 0.45 ppb QSE (0.14 ppb dispersed oil) at 750 m.

May 2011 — DSH08 and DSH10

In May 2011, significant oil-type fluorescence (3.96 ppb QSE, or 1.25 ppb dispersed oil) was still apparent in the water sample from 21 m collected at DSH10, and a slight increase was noted in the deep water samples collected from 1,000 m to 1,400 m as well (Fig. 4.12). Results at DSH08 were somewhat surprising, with the highest overall fluorescence intensity for that cruise seen in the sample from 1,000 m (1.77 ppb QSE, or 0.45 ppb dispersed oil); however elevated oil fluorescence was also seen at 50 m (1.64 ppb QSE, or 0.52 ppb dispersed oil). Concentrations at all depths below 55 m were greater in May 2011 than in February 2011 at DSH08. It is important to note that PCB06 was not visited in May 2011 so no observations of continuing oil fluorescence at that site are available.

The highest overall oil-type fluorescence in the field samples collected in the Gulf of Mexico was found in the water sample collected aboard the R/V *Nancy Foster* in July 2010 at Station

Oil Signature--Feb 2011 at DSH08, DSH10, and PCB06



Oil Signature--Feb 2011 at DSH08, DSH10, and PCB06

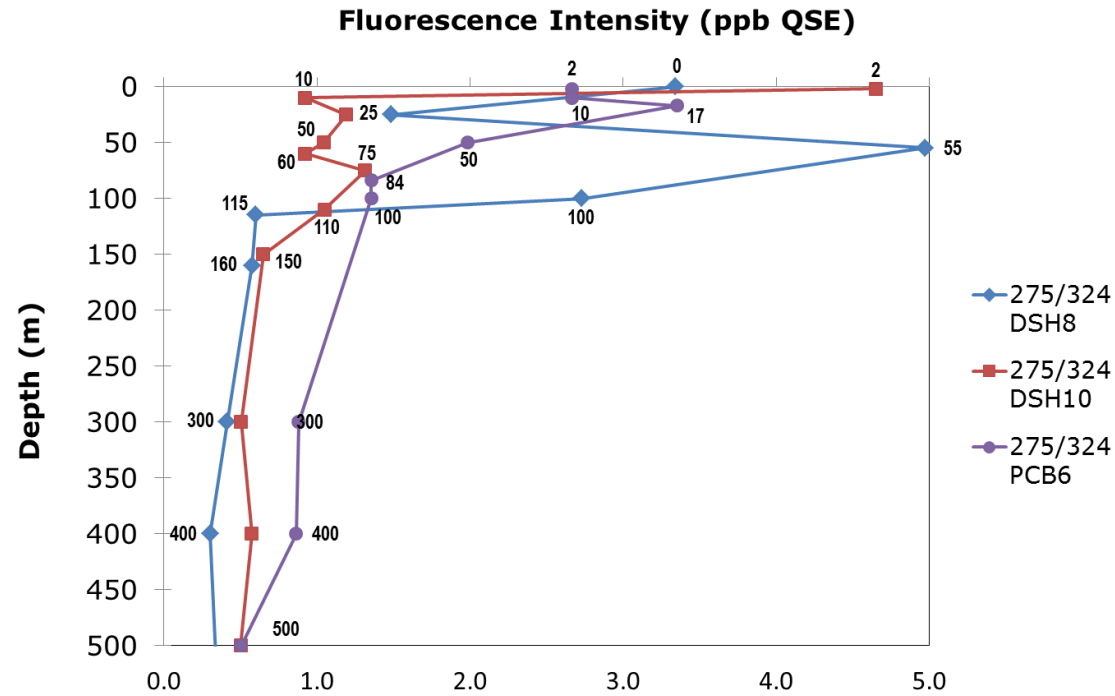
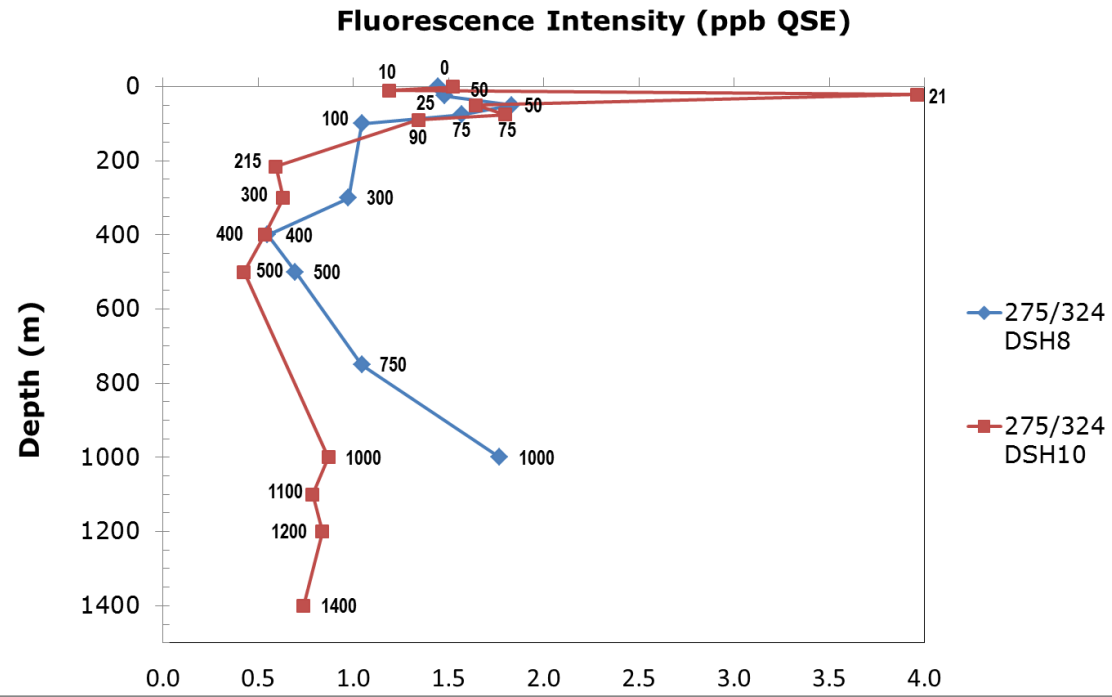


Figure 4.11. Fluorescence intensity (ppb QSE) at Ex/Em 275 nm/324 nm, indicative of oil in the water column, at sites DSH08, DSH10, and PCB06 in February 2011 at all depths (upper), and at depths up to 500 m (lower) in order to visually separate shallower samples.

Oil Signature--May 2011 at DSH08 and DSH10



Oil Signature--May 2011 at DSH08 and DSH10

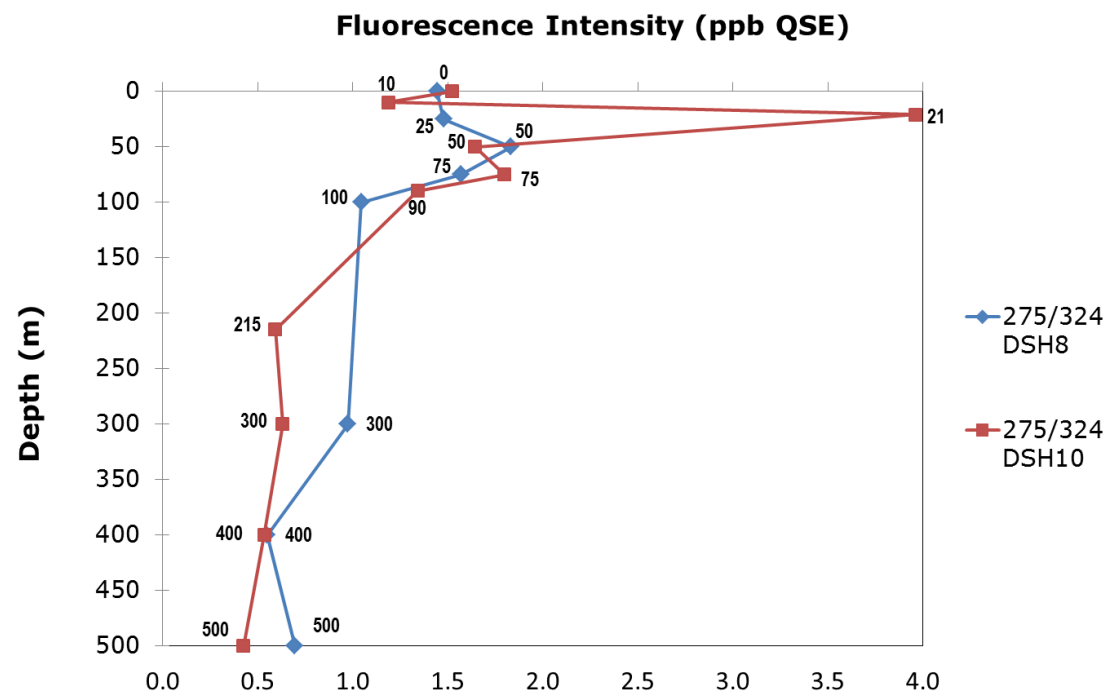


Figure 4.12. Fluorescence intensity (ppb QSE) at Ex/Em 275 nm/324 nm, indicative of oil in the water column, at sites DSH08 and DSH10 in May 2011 at all depths (upper), and at depths up to 500 m (lower) in order to visually separate shallower samples.

71 from 1,150 m (23.8 ppb QSE), equivalent to 7.51 ppb dispersed oil. Highest oil-related fluorescence in water samples collected on the R/V *Weatherbird II* in August 2010 were at DSH10 in the samples collected at 60 m (8.02 ppb QSE) and 400 m (8.71 ppb QSE), equivalent to 2.53 ppb and 2.75 ppb dispersed oil, respectively. The highest concentration found in the three-cruise series aboard the *Weatherbird II* which encompassed December 2010 to May 2011 was 4.98 ppb QSE in the water sample collected at 55 m at DSH08 in February 2011, equivalent to 1.57 ppb dispersed oil.

For comparison with the wave tank experimental series, the concentration of oil-type fluorescence in Experiment #6 (weathered oil with dispersant) at $t = 90$ min. was 54.58 ppb QSE. Using the standard created in the Coble Laboratory, this would be equivalent to 17.22 ppb dispersed oil. Chemical analysis by scientists at BIO of a separate water sample collected at that time point was 53 ng mL^{-1} (ppb) BTEX and 9.07 ng mL^{-1} (ppb) naphthalene and homologs. The overall concentration of oil/dispersant in the wave tank was calculated to be ≤ 3 ppb (Conmy et al. 2014); however, the actual oil/dispersant concentration at the port from which the water samples was collected would certainly have varied.

Schifter et al. (2017) found unexpected levels of fluorescence at depths of 1,100 m or greater at 19 of the 40 stations sampled throughout the southern Gulf of Mexico in October 2013 and proposed that this could potentially be due to the deepwater plume that traveled from the DWH to the southwest. Hydrocarbonoclastic bacteria were present in the water samples collected at these locations, suggesting that the fluorescence may be at least partially due to their biological activity. As these authors point out, the lack of research into deepwater FDOM in the Gulf of Mexico makes a more conclusive determination impossible.

Sediment Core Pore Water

Pore water samples centrifuged from sediment cores collected on the *Weatherbird II* oil spill response cruise in February 2011 showed evidence of oil fluorescence as well. At DSH10, the highest oil-like fluorescence intensity (12.8 ppb QSE) was found in the top three millimeters of the core (Fig. 4.13), which would be equivalent to 4.04 ppb dispersed oil.

Although fluorescence intensity was higher (16.7 ppb QSE) in the top section of the sediment core at DSH08, it was more typical of proteins (Fig. 4.14) in that fluorescence at the deep UV Ex/Em 230 nm/325 nm was of lower intensity than at the higher Ex/Em of 275 nm/325 nm. Progressing down core, the intense fluorescence in the deep UV Ex/Em increased while the fluorescence at the higher Ex/Em pair lessened, characteristic of oil rather than proteins, indicating the highest concentration of oil was present in the top 5 mm of the sediment.

Studies have shown that potentially up to 47% of the oil not recovered following the DWH oil spill was delivered to the sea floor in an approximate 110,000 km² region surrounding the wellhead (Romero et al. 2017). This likely took place both through impingement of the deepwater plume on the sediment surface and the large scale MOSSFA event (Romero et al. 2015). The resulting oil-enriched sediment layer which accumulated in the summer and fall of 2010 was ~1cm thick (Brooks et al. 2015). Schifter et al. (2017) found PAH concentrations of 0.45 to 11.72 ng g⁻¹, dominated by fluoranthrene, pyrene and acenaphthylene, in surficial sediment samples collected by box corer in the southern Gulf of Mexico in October 2013. Another study of PAHs in sediments in the Gulf of Mexico following the DWH oil spill found significant levels of naphthalenes, phenanthrenes and chrysenes in surface sediments, as well (Snyder et al. 2014).

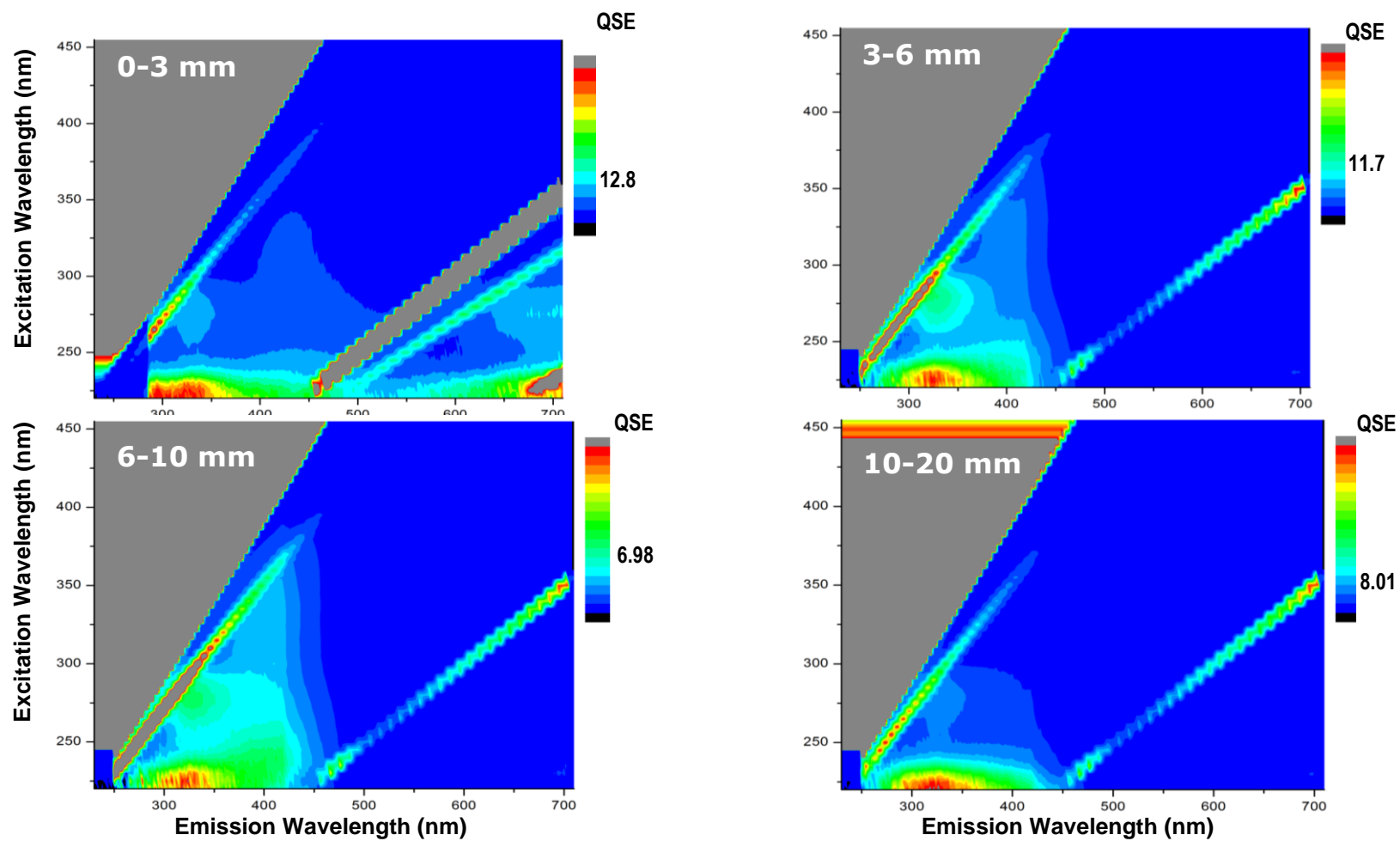


Figure 4.13. EEM of pore water extracted by centrifuge from the top 3 mm (top left), 3-6 mm (top right), 6-10 mm (bottom left), and 10-20 mm (bottom right) of a sediment core collected at DSH10 aboard R/V *Weatherbird II* in February 2011. Sample was diluted 4:1 with Milli-Q water to avoid over-saturation of the fluorescence signal and analyzed on Fluoromax4. Each EEM is normalized to peak fluorescence, and concentration in the oil-type fluorescence region at Ex/Em 275 nm/325 nm is noted on color bar.

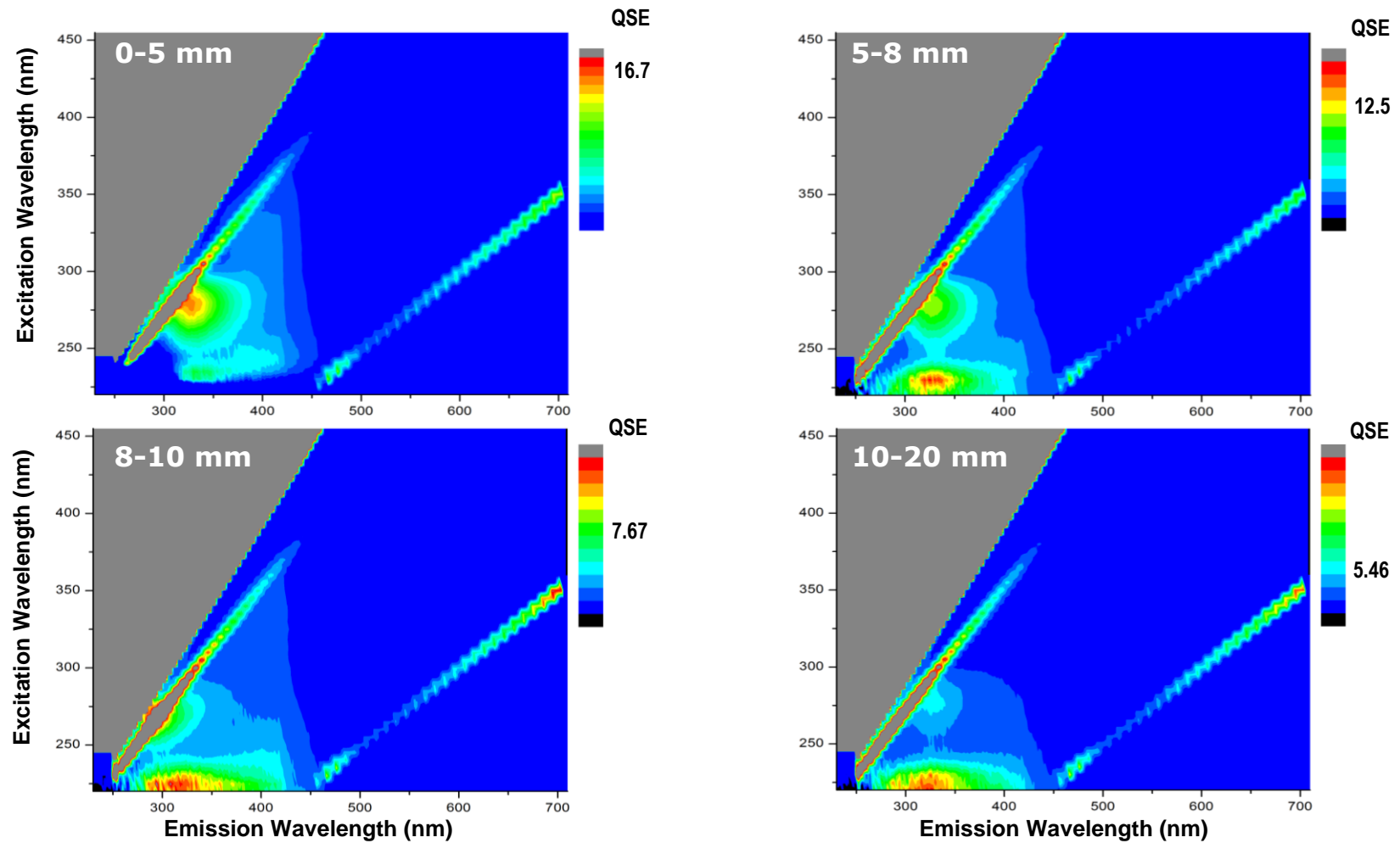


Figure 4.14. EEM of pore water extracted by centrifuge from the top 5 mm (top left), 5-8 mm (top right), 8-10 mm (bottom left), and 10-20 mm (bottom right) of a sediment core collected at DSH08 aboard R/V *Weatherbird II* in February 2011. First three samples were diluted 4:1 with Milli-Q water, and the sample from 10-20 mm was diluted 10:1, to avoid over-saturation of the fluorescence signal. Each EEM is normalized to peak fluorescence, and concentration in the oil-type fluorescence region at Ex/Em 275 nm/325 nm is noted on color bar.

PARAFAC Analysis

A number of studies have employed EEMS analysis of water samples to track petroleum in the Gulf of Mexico following the DWH oil spill, and have additionally employed the use of parallel factor analysis (PARAFAC) in an attempt to resolve the complex fluorescence signals into varying numbers of individual contributing factors (Zhou and Guo 2012; Mendoza et al. 2013; Zhou et al. 2013; Bianchi et al. 2014; Zhou et al. 2015; D'Sa et al. 2016). Described as complementary to GC-FID analysis and useful for field identification of oil spills, Christensen et al. (2005) first used the combination of EEMS analysis and PARAFAC to fingerprint oiled water samples following a tanker spill off the coast of Denmark.

The first study published after the DWH oil spill that utilized EEMs with PARAFAC identified four components in a dataset of 91 samples collected in October 2010 and October 2011 (Zhou and Guo 2012). Their Components 1 through 3 identified oil-related fluorescence and the fourth was humic-like, based on excitation and emission peak locations. These authors found only weak oil signatures in the samples collected in October 2011; however, it is possible that this was due to the use of Whatman GF/F filters on all of their water samples. As found in our study, these authors also found strong presence of oil-related fluorescence in their deepwater samples in May 2010, October 2010, and October 2011 (Zhou and Guo 2012). In collaboration with other researchers, these authors then examined 94 different samples collected in May and June 2010. In this study they found six components, three oil-related, one that combined terrestrial humics and dispersed oil signals, one protein-like, and one degradation product of terrestrial humics (Zhou et al. 2013). It was pointed out that the protein-like component might be explained by the presence of oil-degrading bacteria, as we also hypothesize based on our results.

In their analysis of samples collected at ten stations within 8.67 to 49.74 km from the DWH wellhead, Mendoza et al. (2013) also utilized GC-MS analysis in an attempt to correlate total PAH with a single fluorescence Ex/Em maximum. Unfortunately, they found this method significantly underestimated concentration. In their PARAFAC analysis, seven components were identified and related to specific PAHs by Ex/Em maxima. In addition to the oil-related Component 1, three components were identified as benzene/naphthalene-like, one was related to Corexit®, and one was humic-like. Component 1 was found to be related to the Ex/Em maximum of MC252 source oil; however, only three of their seven components were well-correlated with the Zhou et al. (2013) six-component model. These authors noted a relationship between their Corexit®-related component, the humic-like component and a benzene-enriched component in their deepwater samples and called for future work to better understand the co-variation of these components (Mendoza et al. 2013).

D'Sa et al. (2016) collected and analyzed water samples from both 2009, before the DWH oil spill, during the spill in May 2010, and post-spill in April 2012 and April 2013. PARAFAC analysis of the pre-spill samples resulted in three components: one humic-like, one marine humic-like, and one protein-like. Analysis of the post-spill samples collected within 16 km of the wellhead resulted in four components: the aforementioned humic-like and marine humic-like, with the addition of two in the UV range. Due to the excitation/emission peaks, these authors hypothesize that component 3 is Corexit®-like and component 4 is naphthalene-like; however, they note that the latter could be a blue-shifted form of tryptophan and point to oil plume-related bacterial activity as a complicating factor. This study also employed the use of GC-MS in a diagnostic ratio analysis to correlate water samples with MC252 oil, but results were

inconclusive for all but one sample collected at the surface approximately 1 km from the wellhead (D'Sa et al. 2016).

Bianchi et al. (2014) collected and analyzed water samples to the south of the DWH wellhead in July 2012 in order to assess the fate of the spilled petroleum. These samples were combined with EEMs from Zhou et al. (2013) and remodeled, and it was determined that a four-component model best fit the combined dataset. Component 1 was terrestrial humic-like, and Component 4 was amino acid-like. Components 2 and 3 were oil-related, the former similar to the Zhou et al. (2013) degraded oil component, and the latter matching crude oil components in the OpenFluor database (Murphy et al. 2014). Table 4.2 presents the Ex/Em peak locations of components identified in each of these studies.

It is important to note that both the D'Sa and Bianchi research groups used filtered water samples in their analyses, employing 0.2 μm nucleopore polycarbonate membrane filters and pre-combusted 0.7 μm Whatman GF/F filters, respectively. In our experience, filtering reduced the oil fluorescence signature in water samples, probably by adsorption of the more hydrophobic oil constituents. Even so, D'Sa et al. (2016) as well as Bianchi et al. (2014) note the long-term change in the characteristics of the deepwater DOM pool in the Gulf of Mexico resulting in elevated protein-like and/or oil-like fluorescence were still present two to three years after the event which warrant further study and monitoring.

With the assistance of Dr. Kathleen Murphy, our entire dataset of water samples collected in the Gulf of Mexico during the December 2010, February 2011 and May 2011 oil response cruises (n

= 555) were brought into the seven component PARAFAC model, which was developed for the BIO wave tank sample dataset presented in Chapter 2. The result was the presence of only two distinct components, well-modeled with low residuals: Component 1 with peak at Ex/Em 280 nm/336 nm, and Component 2 with peak at Ex/Em 265 nm/312 nm (Fig. 4.15). Based on the Ex/Em peak locations, these two components appear to be naphthalene-like and BTEX-like, respectively, as were Component 1 and Component 2 in the wave tank experiments (Chapter 3).

No correspondence was found between these two datasets for Components 3 – 6 in the wave tank experiments; however, that is not surprising since the source of the seawater in both sample sets was quite different. The water used for the BIO wave tank experiments was sourced from Halifax Harbor, which is heavily influenced by terrestrial runoff, especially given the heavy precipitation event which occurred during the course of the wave tank experiments in May/June 2011. While the waters in the Gulf of Mexico to the east/northeast of the DWH wellhead could be influenced by outflow from the Mississippi River, impact would have likely been negligible, especially during the December 2010 and February 2011 cruises. It is also possible that Corexit®-related components may only be present for a limited time following the application of chemical dispersants. Perhaps this component could have been identified in samples collected in summer 2010, but the majority of our samples from the Gulf of Mexico were collected beginning five months after the cessation of all chemical dispersant applications.

Table 4.2. Samples collected in the year following the DWH oil spill included in PARAFAC analysis

PARAFAC Component	Excitation Wavelength (nm)	Emission Wavelength (nm)	Description	Reference
Component 1	224	328	Oil	(Zhou and Guo 2012)
Component 2	264	324	Oil	
Component 3	232	346	Oil	
Component 4	248	446	Humic-like	
C1	226	340	Oil-related, dominant component	(Zhou et al. 2013)
C2	236	350	Oil-related, degradation component	
C3	256, 340	460	Terrestrial humic substance and chemically dispersed oil	
C4	232, 275	324	Amino acids	
C5	224	290, 477	Photchemically degraded terrestrial organic matter	
C6	252	311	Oil-related, degradation product	
Comp 1	220	380	Oil mixture	(Mendoza et al. 2013)
Comp 2	220, 255, 270	330	Benzene/Arene-like enriched and Naphthalene-like	
Comp 3	250	440	Humic-like	
Comp 4	225, 270, 280	340	Naphthalene-like enriched	
Comp 5	235, 310	304, 415	Corexit®-related	
Comp6	225, 280	340	Naphthalene-like and Arene-like	
Comp 7	240	365	Phenanthrene-like	
C1	250, 365	480	Humic-like	(D'Sa et al. 2016)
C2	250, 305	405	Marine humic-like	
C3	265	310	Corexit®-containing	
C4	270	320	Oil-related, degraded and enriched naphthalene-like	
C1	240	400-436	Terrestrial humic-like	(Bianchi et al. 2014)
C2	220, 255	290	Degraded oil-like; PAH	
C3	225	338	Crude oil-like	
C4	230, 280	314	Amino acid-like	

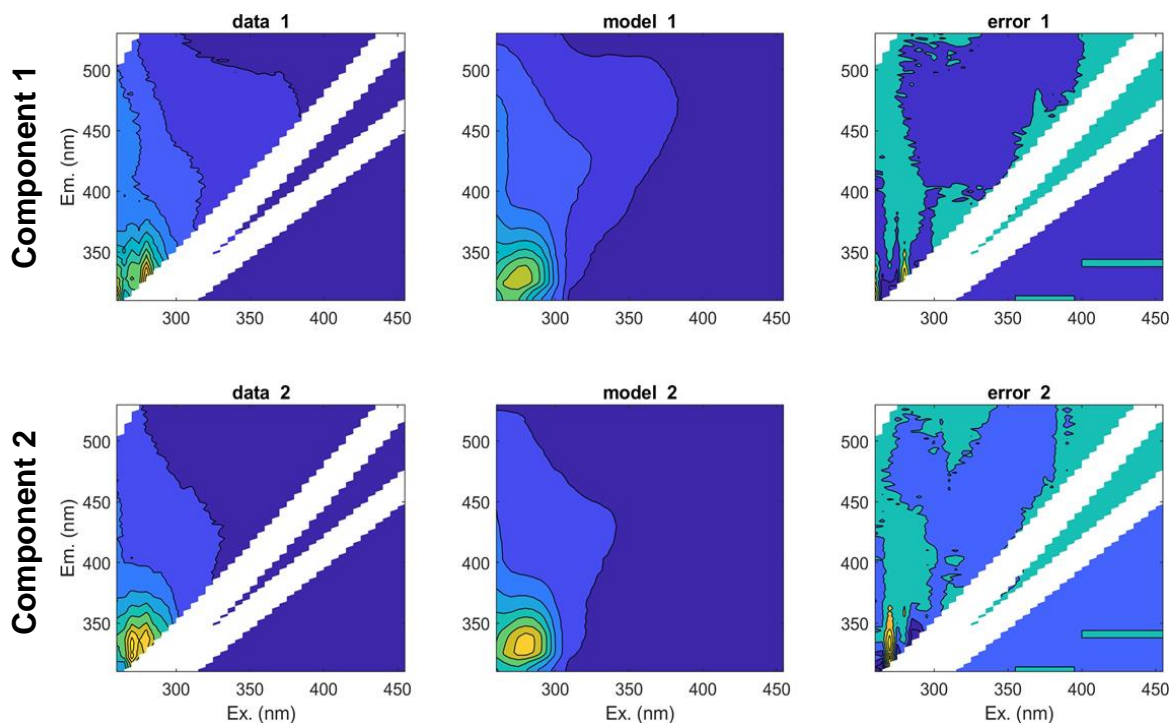


Figure 4.15. Results of bringing entire Gulf of Mexico water sample dataset ($n = 555$) into the seven-component model created for the wave tank experiments held at BIO in May/June 2011.

CONCLUSIONS

Although naphthalene (along with its alkylated homologs) was the predominant PAH found in the analysis of MC252 reference oil provided to researchers by BP, it had decreased to 3 – 9 % in the weathered mousse collected from the sea surface and salt marshes and in sediments collected near the wellhead during the same time period as this research study (Liu et al. 2012). It is quite possible that small PAH compounds were lost to biodegradation in the water column and/or to or evasion upon reaching the surface. Therefore, it is reasonable to assume that naphthalene, and other small molecular weight PAHs would have been detected through spectrofluorometry, borne out by fluorescence intensity in these water samples at Ex/Em 275 nm/324 nm and 275 nm/330 nm.

It is worth noting that fluorescence peaks for proteins, which are commonly found in the marine environment, have wavelengths in close proximity to the Ex/Em 275 nm/324 – 330 nm oil peak. Fluorescence characteristic of tyrosine at Ex/Em 275 nm/300 – 355 nm, also known as the B Peak, and that of tryptophan at Ex/Em 275 nm/340 – 350 nm, also known as the T Peak (Coble et al. 2014) is commonly found associated with FDOM in the marine environment. Clearly, the fluorescence intensity that we have found to be characteristic of oil lies directly between these two peaks. It might be possible to distinguish the oil peak from the B and T Peaks through the application of PARAFAC to enhance the separation of overlapping fluorescence intensity; however, the fluorescence intensity from fresh oil, with or without the addition of chemical dispersant, would likely overwhelm any protein signal. As hydrocarbons travel through the water column, these protein peaks would likely increase due to the presence of natural oil-degrading microorganisms, which have evolved to take advantage of the hydrocarbons present in the environment emanating from natural seeps in the Gulf of Mexico (Kleindienst et al. 2015). This may result in the transformation of the original focused, high intensity fluorescence peak due to oil to a broader peak spanning wider emission wavelengths due to the additional presence of proteins exuded in the process of biodegradation. However, this phenomenon could certainly be complicated by a moving plume of oil and/or resuspension of oiled sediments.

It is clear that spectrofluorometric analysis of water samples was successful in detecting the continued presence of oil in the water column through May 2011. The evolving water column fluorescence detected during the year following the DWH blowout helps to illuminate a very small piece of the puzzle of how the oil traveled both horizontally and vertically as it moved to the east/northeast of the wellhead. Evidence of the continuing presence of the deep sub-surface

plume first discovered by other scientists in the summer of 2010 was shown by elevated fluorescence at Ex/Em 275 nm/324 – 330 nm in samples from 1,100 m at DSH08 in December 2010, where it was surprisingly renewed in May 2011. However, evidence of the deep plume was greatest at DSH10 in February 2011. This phenomenon could be due to resuspension of oiled sediments known to be present to the northeast of the wellhead (Brooks et al. 2015; Romero et al. 2017) or it may be due to continued leakage from the wellhead, as reported by Kolian et al. (2015). Other researchers have also detected an altered deep-water DOM pool with elevated protein-like and/or oil-like fluorescence present for up to three years following the DWH oil spill (Bianchi et al. 2014; D'Sa et al. 2016)

REFERENCES

- 40 CFR § 300.323. 1999. Spills of national significance. In: Government USF, editor. 40 Protection of Environment.
- Adeniji AO, Okoh OO, Okoh AI. 2017. Analytical methods for the determination of the distribution of total petroleum hydrocarbons in the water and sediment of aquatic systems: A review. *Hindawi Journal of Chemistry*.
- Allen TW. 2010. National incident commander's report: Mc252 deepwater horizon. In: Guard USC, editor.
- Baker A. 2001. Fluorescence excitation-emission matrix characterization of some sewage-impacted rivers. *Environmental science & technology*. 35:948-953.
- Bianchi TS, Osburn C, Shields MR, Yvon-Lewis S, Young J, Guo L, Zhou Z. 2014. Deepwater horizon oil in gulf of mexico waters after 2 years: Transformation into the dissolved organic matter pool. *Environmental science & technology*. 48:9288-9297.
- Brooks GR, Larson RA, Schwing PT, Romero I, Moore C, Reichart G-J, Jilbert T, Chanton JP, Hastings DW, Overholt WA et al. 2015. Sedimentation pulse in the ne gulf of mexico following the 2010 dwh blowout. *PloS one*. 10(7).
- Bureau of Ocean Energy Management RaE. 2011. Report regarding the causes of the april 20, 2010, macondo well blowout. In: Interior USDot, editor.
- Christensen JH, Hansen AB, Mortensen J, Andersen O. 2005. Characterization and matching of oil samples using fluorescence spectroscopy and parallel factor analysis. *Analytical Chemistry*. 77(7):2210-2217.

- Christensen JH, Hansen AB, Tomasi G, Mortensen J, Andersen O. 2004. Integrated methodology for forensic oil spill identification. *Environmental science & technology*. 38:2912-2918.
- . Fluorescence detection and characteristics of oil during the deepwater horizon oil spill. European Geosciences Union General Assembly 2011; 2011; Vienna, Austria.
- Coble PG. 1996. Characterization of marine and terrestrial dom in seawater using excitation-emission matrix spectroscopy. *Marine Chemistry*. 51:325-346.
- Coble PG. 2007. Marine optical biogeochemistry: The chemistry of ocean color. *Chemical Reviews*. 107:402-418.
- Coble PG, Schultz CA, Mopper K. 1993. Fluorescence contouring analysis of doc intercalibration experiment samples: A comparison of techniques. *Marine Chemistry*. 41(1):173-178.
- Coble PG, Spencer RM, Baker A, Reynolds DM. 2014. Aquatic organic matter fluorescence. In: Coble PG, Lead J, Baker A, Reynolds DM, Spencer RM, editors. *Aquatic organic matter fluorescence*. New York, NY: Cambridge University Press. p. 75-122.
- Conmy RN, Coble PG, Farr J, Wood AM, Lee K, Pegau WS, Walsh ID, Koch CR, Abercrombie MI, Miles MS et al. 2014. Submersible optical sensors exposed to chemically dispersed crude oil: Wave tank simulations for improved oil spill monitoring. *Environmental science & technology*. 48(3):1803-1810.
- D'Sa EJ, Overton EB, Lohrenz SE, Maiti K, Turner RE, Freeman A. 2016. Changing dynamics of dissolved organic matter fluorescence in the northern gulf of mexico following the deepwater horizon oil spill. *Environmental science & technology*. 50:4940-4950.
- Daly KL, Passow U, Chanton J, Hollander D. 2016. Assessing the impacts of oil-associated marine snow formation and sedimentation during and after the deepwater horizon oil spill. *Anthropocene*. 13:18-33.
- DeMent J. 1947. Fluorescent techniques in petroleum exploration. *Geophysics*. 12(1):1-98.
- Diercks A-R, Highsmith RC, Asper VL, Joung D, Zhou Z, Guo L, Shiller AM, Joye SB, Teske AP, Guinasso N et al. 2010. Characterization of subsurface polycyclic aromatic hydrocarbons at the deepwater horizon site. *Geophysical Research Letters*. 37(2).
- Frank U. 1975. Identification of petroleum oils by fluorescence spectroscopy. *International Oil Spill Conference Proceedings*. 1975(1):87-91.
- Giamarchi P, Stephan L, Salomon S, Bihan AL. 2000. Multicomponent determination of a polyaromatic hydrocarbon mixture by direct fluorescence measurements. *Journal of fluorescence*. 10(4):393-402.
- Goni G, Wood AM, Smith R, Cummings S, Baringer M, Kelble C, Lumpkin R, Johns L, Lamkin J. 2010. Monitoring and assessing implications of the deepwater horizon oil spill: Potential impacts of the loop current on downstream marine ecosystems in the gulf of mexico and florida straits. In: U.S. Department of Commerce NOaAA, editor. Miami.
- Henry ME, Donovan TJ. 1984. Luminescence properties and chemical composition of crude oils. In: U.S. Department of the Interior GS, editor. Flagstaff, Arisona. p. 34.

- John P, Soutar I. 1976. Identification of crude oils by synchronous excitation spectrofluorometry. *Analytical Chemistry*. 48(3):520-524.
- Joint Analysis Group. 2010. Review of preliminary data to examine subsurface oil in the vicinity of mc252#1, may 19 to june 19, 2010. In: National Oceanic and Atmospheric Administration, editor. Silver Spring, MD: U.S. Dept. of Commerce.
- Joye SB, MacDonald IR, Leifer I, Asper V. 2011. Magnitude and oxidation potential of hydrocarbon gases released from the bp oil well blowout. *Nature Geoscience*. 4:160-164.
- Kalle K. 1949. Fluoreszenz und gelbstoff im bottnischen und finnischen meerbusen. *Deutsch Hydrogr Z*. 2:117-124.
- Kessler JD, Valentine DL, Redmond MC, Du M, Chan EW, Mendes SD, Quiroz EW, Villanueva CJ, Shusta SS, Werra LM et al. 2011. A persistent oxygen anomaly reveals the fate of spilled methane in the deep gulf of mexico. *Science*. 331(6015):312-315.
- Khamis K, Bradley C, Hannah DM. 2018. Understanding dissolved organic matter dynamics in urban catchments: Insights from in situ fluorescence sensor technology. *Wiley Interdisciplinary Reviews: Water*. 5(1):e1259.
- Kleindienst S, Seidel M, Ziervogel K, Grim S, Loftis K, Harrison S, Malkin SY, Perkins MJ, Field J, Sogin ML et al. 2015. Chemical dispersants can suppress the activity of natural oil-degrading microorganisms. *Proceedings of the National Academy of Sciences of the United States of America*. 112(48):14900-14905.
- Kolian SR, Porter SA, Sammarco PW, Birkholz D, Jr. EWC, Subra Wa. 2015. Oil in the gulf of mexico after the capping of the bp/deepwater horizon mississippi canyon (mc-252) well. *Environ Sci Pollut Res*. 22:12073-12082.
- Li JF, Fuller S, Cattle J, Way CP, Hibbert DB. 2004. Matching fluorescence spectra of oil spills with spectra from suspect sources. *Analytica chimica acta*. 514(1):51-56.
- Liu Z, Liu J, Zhu Q, Wu W. 2012. The weathering of oil after the deepwater horizon oil spill: Insights from the chemical composition of the oil from the sea surface, salt marshes and sediments. *Environmental Research Letters*. 7.
- Lubchenco J, McNutt MK, Dreyfus G, Murawski SA, Kennedy DM, Anastas PT, Chu S, Hunter T. 2012. Science in support of the deepwater horizon response. *Proceedings of the National Academy of Sciences*.
- Mascarelli A. 2010. Muddying the waters on gulf oxygen data. *Nature*.
- Mason RP, Kerley GIH. 1988. Identification of spilled oils by fluorescence spectroscopy. *Oil & Chemical Pollution*. 4:57-70.
- McNutt MK, Chu S, Lubchenco J, Hunter T, Dreyfus G, Murawski SA, Kennedy DM. 2012. Applications of science and engineering to quantify and control the deepwater horizon oil spill. *Proceedings of the National Academy of Sciences*.
- Mendoza WG, Riemer DD, Zika RG. 2013. Application of fluorescence and parafac to assess vertical distribution of subsurface hydrocarbons and dispersant during the deepwater horizon oil spill. *Environmental Science Processes & Impacts*. 15(1017-1030).

- Murphy KR, Stedmon CA, Wenig P, Bro R. 2014. Openfluor— an online spectral library of auto-fluorescence by organic compounds in the environment. *Analytical Methods*. 6(3):658-661.
- Deepwater horizon. 2010. [accessed June 13, 2019].
<https://incidentnews.noaa.gov/incident/8220>.
- Paris CB, Henaff ML, Aman ZM, Subramaniam A, Helgers J, Want D-P, Kourafalou VH, Srinivasan A. 2012. Evolution of the macondo well blowout: Simulating the effects of the circulation and synthetic dispersants on the subsea oil transport. *Environmental science & technology*. 46:13293-13302.
- Paul JH, Hollander D, Coble P, Daly KL, Murasko S, English D, Basso J, Delaney J, McDaniel L, Kovach CW. 2013. Toxicity and mutagenicity of gulf of mexico waters during and after the deepwater horizon oil spill. *Environmental science & technology*. 47:9651-9659.
- Rogener MK, Bracco A, Hunter KS, Saxton MA, Joye SB. 2018. Long-term impact of the deepwater horizon oil well blowout on methane oxidation dynamics in the northern gulf of mexico. *Elementa Science of the Anthropocene*. 6.
- Romero IC, Schwing PT, Brooks GR, Larson RA, Hastings DW, Ellis G, Goddard EA, Hollander DJ. 2015. Hydrocarbons in deep-sea sediments following the 2010 deepwater horizon blowout in the northeast gulf of mexico. *PloS one*. 10.
- Romero IC, Toro-Farmer G, Diercks A-R, Schwing P, Muller-Karger F, Murawski S, Hollander DJ. 2017. Large-scale deposition of weathered oil in the gulf of mexico following a deep-water oil spill. *Environmental pollution*. 228:179-189.
- Schifter I, Sánchez-Reyna G, González-Macías C, Salazar-Coria L, González-Lozano C. 2017. Fluorescence characteristics in the deep waters of south gulf of méxico. *Marine pollution bulletin*. 123(1):165-174.
- Smith RH, Johns EM, Goni GJ, Trinanes J, Lumpkin R, Wood AM, Kelble CR, Cummings SR, Lamkin JT, Privoznik S. 2014. Oceanographic conditions in the gulf of mexico in july 2010, during the deepwater horizon oil spill. *Continental Shelf Research*. 77:118-131.
- Snyder RA, Ederington-Hagy M, Hileman F, Moss JA, Amick L, Carruth R, Head M, Marks J, Tominack S, Jeffrey WH. 2014. Polycyclic aromatic hydrocarbon concentrations across the florida panhandle continental shelf and slope after the bp mc 252 well failure. *Marine pollution bulletin*. 89(1):201-208.
- Taniguchi M, Lindsey JS. 2018. Database of absorption and fluorescence spectra of >30 common compounds for use in photochemcad. *Photochemistry and photobiology*. 94:290-327.
- The MathWorks I. 2018. Matlab. Release 2018b ed.
- U.S. Coast Guard, National Oceanic and Atmospheric Administration, U.S. Environmental Protection Agency, Centers for Disease Control and Prevention, Minerals Management Service. 2006. Special monitoring of applied response technologies.
- Valentine DL, Kessler JD, Redmond MC, Mendes SD, Heintz MB, Farwell C, Hu L, Kinnaman FS, Yvon-Lewis S, Du M et al. 2010. Propane respiration jump-starts microbial response to a deep oil spill. *Science of The Total Environment*. 330:208-211.

- Weisberg RH, Zheng L, Liu Y. 2011. Tracking subsurface oil in the aftermath of the deepwater horizon well blowout. In: Liu Y, MacFadyen A, Ji Z-G, Weisberg RH, editors. Monitoring and modeling the deepwater horizon oil spill: A record-breaking enterprise. Washington, DC: American Geophysical Union. p. 205-215.
- Zhou Z, Guo L. 2012. Evolution of the optical properties of seawater influenced by the deepwater horizon oil spill in the gulf of mexico. Environmental Research Letters. 7.
- Zhou Z, Guo L, Osburn C. 2015. Fluorescence eems and parafac techniques in the analysis of petroleum components in the water column.
- Zhou Z, Guo L, Shiller AM, Lohrenz SE, Asper VL, Osburn CL. 2013. Characterization of oil components from the deepwater horizon oil spill in the gulf of mexico using fluorescence eem techniques. Marine Chemistry. 148:10-21.

GENERAL CONCLUSIONS

Although the foregoing chapters progress from the smallest scale to largest, starting with experiments in baffled flasks in the Coble Laboratory, through the mid-level range in the wave tank series at BIO, to collection of water samples in the Gulf of Mexico, this research took place in reverse order in real time. My introduction to the spectrofluorometric detection of petroleum in the marine environment after the DWH oil spill began as I was just getting acquainted with the nuances of aqueous CDOM fluorescence. I came to understand that evidence of the petroleum spill in those water samples was truly just a special case of FDOM in the marine environment. Revisiting sample data from that first year of research and then performing a well-informed reanalysis of those fluorescence signals has resulted in a richer interpretation of my early research, which in turn informed the analyses of research performed in the interim in the baffle flask and wave tank experimental series.

The first and most important question to be addressed is what led to this investigation into the presence of petroleum in the marine environment? As I began my doctoral research in the months following the DWH Spill of National Significance, the entire scientific community's attention was focused on understanding the continuing aftermath of this catastrophic event. Not only the largest oil spill in United States history, it was the first to take place at an extreme depth (~1,500 m), and was complicated by the continuing flow of oil for 87 days despite multiple attempts to cap the well. Further, the application of chemical dispersants both at the surface and,

for the first time, into the stream of oil and gas emitted at the wellhead added incredible complexity to the task of tracking the petroleum's eventual fate (Bureau of Ocean Energy Management 2011; Kessler et al. 2011; Lubchenco et al. 2012; McNutt et al. 2012; Daly et al. 2016). Understanding the effects of physical weathering as well as the impact of Corexit® 9500A on the fate and transport of the oil is critical to those seeking to understand all of the impacts to the natural ecosystem.

Developed in the Triassic, the Gulf of Mexico is a small ocean basin, yet is a hydrocarbon megaprovince with many active hydrocarbon seeps (Galloway 2009; Joye 2016). It is the largest U.S. source of offshore petroleum, as well as host to the country's most extensively developed petroleum region off the coast of Louisiana (Thibodeaux et al. 2011). An associated diverse and unique marine ecosystem has evolved in concert with this natural carbon source, especially in the area of the DWH wellhead; however, the sudden major spill event had the potential to quickly upset that delicate balance (Bergquist et al. 2003). The impact from any oil spill can range from minimal to decimating, with effects ranging from physical smothering, to alteration of habitats, toxic effects at sub-lethal to fatal levels, shifts in the food web, and impacts to fisheries, tourism, and other industries (Baker 2001).

Although intended to enhance biodegradation of the petroleum, the unprecedented use of dispersants was an added unknown in this spill event. Some scientists have argued that the synergistic combination of oil and dispersants may pose an even greater risk than that based solely on either compound (National Research Council 1989). Mesocosm studies on Sargassum found that the addition of Corexit® 9500A to MC252 oil compromised its natural buoyancy and

caused sinking within 48 hours of oiling (Stout et al. 2018). Almeda et al. (2013) also found Corexit® to be more toxic to zooplankton than oil alone. Just a few of the other casualties of the effects of the combination of MC252 oil and dispersants in the aftermath of the DWH oil spill include oysters (Vignier et al. 2016), deep-sea corals (Girard and Fisher 2018) and other benthic organisms (Prouty et al. 2016), bottlenose dolphins (Venn-Watson et al. 2015; Kellar et al. 2017), and sea turtles (Putman et al. 2015). Many studies note apparent ongoing effects almost a decade after the spill and voice the need for further long-term monitoring and assessment (Paul et al. 2013; Beyer et al. 2016).

Certainly, more research into the pros and cons of using dispersants, especially at depth, is called for (Bejerano 2018). Studies have shown that the oil flowing from the wellhead at high temperature and pressure would have resulted in small, neutrally buoyant droplets that formed a sub-surface plume without their use (Paris et al. 2012). Others have found that chemical dispersants can suppress the ability of naturally-occurring microorganisms to decompose the oil (Kleindienst et al. 2015), and that DOSS became sequestered in subsurface oil plumes and resisted biodegradation for an extended period of time (Kujawinski et al. 2011).

Along with alkanes and cycloalkanes, the most prevalent components of petroleum include the single benzene ring compounds in BTEX and multiple-ring PAHs (Tissot and Welty 1978). Moderately to highly toxic to aquatic life (Abdel-Shafy and Mansour 2016), and with significant potential for bioaccumulation, the lower molecular weight aromatic compounds are generally more soluble, more volatile, and often have greater toxicity than higher molecular weight PAHs (Cole et al. 1999). Arising from the absorbance and re-emission of photons within the π orbitals

of C=C bonds in the molecular structure, the intrinsic property of petroleum fluorescence is due to the presence of these aromatic ring structures (Pradier et al. 1989). Further, lower molecular weight results in fluorescence at shorter wavelengths, as well as of higher intensity, due to self-quenching and/or intramolecular charge transfer resulting in the reabsorption of fluorescence within larger, more complex structures (Smith and Sinski 1999; del Vecchio and Blough 2004). Therefore, petroleum fluorescence is directly related to the chemical composition of petroleum, and spectrofluorometry can be used to identify and quantify PAHs (Sinski and Exner 2007). Laboratory studies provided evidence for identification of individual PAHs by their unique absorption spectra in the 1950s (Jones and Taylor 1955), and fluorescence of individual PAHs was related to chemical concentration in laboratory studies in the 1970s (Schwarz and Wasik 1976).

Combined with the ease of use and capability for rapid analysis that the latest instrumentation possesses, spectrofluorometry holds great promise in the detection of the most toxic fraction of petroleum. Using GC-MS, Diercks et al. (2010) found PAH concentrations of 189 mg L^{-1} (ppb), levels toxic to marine organisms, correlated with fluorescence at depths of $> 800 \text{ m}$ to the southwest of the DWH wellhead in May 2010 ($R^2 = 0.980$, $N = 8$, $p < 0.001$). The challenge lies in identifying the unique contribution of petroleum to the complex fluorescence spectra arising from natural proteins and dissolved organic matter in the marine environment. Our broad spectrum EEMS analysis, coupled with statistical decomposition of the fluorescence spectra, advances the progress toward this goal.

Our bench-scale research into the fluorescence spectra of 25 types of oil, with and without the addition of chemical dispersant at three different DORs, gave evidence of common fluorescence maxima (F_{\max}) across all oil types. The strongest fluorescence was located in the deep UV at Ex/Em 221-239 nm/335-344 nm, which was paired with a broader, lower intensity peak at Ex/Em 269-291 nm/326-353 nm. This is in itself somewhat surprising since the array of oil types examined ranged from the low density oils Arabian Light and MC252 (API 32.2° and 35.2°, respectively) to high density Access Western Blend Dilbit and Belridge Heavy (API 21.3° and 13.6°, respectively) as well as Intermediate Fuel Oils (API 21.9° to 11.9°). We also found these paired F_{\max} peaks, with higher intensity at the lower wavelength pair, in our water samples from the Gulf of Mexico in the year following the DWH oil spill. These results point to the existence of characteristic fluorescence arising from low molecular weight PAHs in all oil types.

The second important finding from the baffle flask experimental series was the effect of chemical dispersant on petroleum-related fluorescence, which was observed in a broad region ($F_{\max3}$) centered at Ex/Em 250 nm/450 nm. This resulted in a distinction between two overarching types of oil; Type I exhibiting increasing fluorescence with increasing DOR, and Type II which did not. These findings will inform future decisions on the application of dispersant to an oil spill. As an example, based on the fluorescence profile discovered in this research, the use of dispersant on IFOs or dilbit is likely to be ineffective and therefore should be avoided.

The third finding from this research is the relationship discovered through linear regression between fluorescence intensity in the $F_{\max1}$ region and 2-ring PAHs, as well as between

fluorescence intensity and 3-4 ring PAHs in the $F_{\max4}$ region for oil types without chemical dispersion. While chemical analyses corresponding to our water samples from the Gulf of Mexico are not available, the correspondence between fluorescence and chemical concentration in the baffle flask series results point to the real possibility of using fluorescence to determine petroleum concentration in future spills. We did find, however, that the addition of dispersants at highest DOR (1:20), resulted in a reduced relationship between fluorescence intensity and chemical concentration. The effects of chemical dispersant on petroleum clearly need additional study with respect to the determination of chemical concentration.

The research done in the wave tank experiments enabled both application of results from the bench-scale research and correspondence with data from our samples from the Gulf of Mexico. This research not only confirmed that a variety of in situ fluorometers used during the response to the DWH oil spill were in fact able to detect oil down to 300 ppb (Conmy et al. 2014), the results of my EEMS analyses showed that the transition from fluorescence typical of CDOM to the oil-like fluorescence of the $F_{\max4}$ region in the baffle flask experiments. An interesting distinction was seen in the fluorescence behavior of oil with and without chemical dispersants over the course of each 90 minute experiment, with a blue shift beginning later in the time sequence and showing more variability until the end of the experiments with non-dispersed oil. This research confirmed the optimal Ex/Em of 270 nm/325 nm for the detection of MC252, both with and without dispersant, as noted in our samples from the Gulf of Mexico. A relationship was also seen between chemical concentration of BTEX and fluorescence intensity at Ex/Em 270 nm/325 nm, as well as a connection between PAHs and fluorescence intensity. However, chemical analyses were only carried out for two experimental series, so further work is clearly

needed in order to determine whether a strong functional response between oil and fluorescence may be present. The utility of taking the ratio between emission at two fluorescence wavelengths (Bugden et al. 2008) to determine DE was shown to be useful as well. Taking the ratio of fluorescence emission collected at two wavelengths would also solve the perennial problem of intercalibration between fluorometers.

In our analysis of the samples collected in the Gulf of Mexico, the effectiveness of taking a ratio of fluorescence collected at two emission wavelengths also was proven; however, the two wavelengths of interest were those typical of protein at Ex/Em 275 nm/305 nm (Peak B) and the oil-like fluorescence at Ex/Em 275 nm/324 nm. This allowed the differentiation of samples showing oil from those with a more protein-like signature. In the samples collected during the summer of 2010, the oil-like signature dominated, while the protein signature became stronger over time. Differences are also seen in this transition from site to site, pointing to the complex recirculation and surfacing of petroleum in the Gulf of Mexico through at least May 2011.

In the wave tank experiments, we were able to note the transition from humic-like fluorescence to oil-like fluorescence over the 90-minute duration of the experimental series; however, the evolution of fluorescence due to the interaction of oil-degrading microbes with petroleum and dispersants certainly could not be observed on such a short time scale. The ratio of humic-like fluorescence and protein-like fluorescence to oil-like fluorescence seen in the depth profiles of water samples collected over the course of the year following the DWH oil spill clearly delineate that interaction. EEMS analysis of pore water from sediment cores also points to the deposition of a significant portion of the sub-surface petroleum plumes to the ocean floor. Future work to

investigate the direct correlation of those fluorescence signatures with chemical concentrations of oil would be useful.

Our research into the fluorescence signature of petroleum and dispersant at a range of scales will enable better tracking potential future petroleum spills in the marine environment. It also sheds light on the recovery of the Gulf of Mexico ecosystem through the evolution of the fluorescence signatures observed over the year following the DWH oil spill. Also, as Coble (2007) noted, the study of CDOM in the marine environment is essential because of its critical role in carbon cycling. In our EEMS analyses of water samples from the surface to extreme depths in the Gulf of Mexico following the DWH oil spill, we have seen, through the evolution of fluorescence at various wavelengths, that CDOM is clearly tied to the degradation and remineralization of petroleum.

Clearly, spectrofluorometry can be a useful tool in the detection and monitoring of future spills, and the ability to collect fluorescence emission at multiple wavelengths has been shown. The next generation of in situ instruments would ideally be designed to accomplish this, as evidenced by the data collected by the WETLABS SAFire in the wave tank experimental series. The scientific community as well as governmental agencies tasked with oil-response would benefit from this fast and nimble way to track subsurface oil plumes since they do not necessarily follow the same track as surface slicks.

Confirmation of EEMS fluorescence associated with the presence of petroleum hydrocarbons has been reported by other researchers (Wade et al. 2011; Schifter et al. 2017). Others have noted

that the signal from dissolved organic matter in the deep water of the Gulf of Mexico was still anomalous up to three years after the DWH oil spill (Bianchi et al. 2014). Many scientists have noted that there was a lack of pre-spill data to help with a determination of when the system returned to background levels, as well (Adhikari et al. 2015; D'Sa et al. 2016; Wade et al. 2016). There is also a dearth of information from the years following the Ixtoc I oil spill (Sun et al. 2015). Continuing to collect and analyze water samples in the Gulf of Mexico is critical in order to develop robust datasets (Daly et al. 2016). Hydrocarbons have been detected in the Gulf of Mexico for decades, largely due to the widespread presence of natural hydrocarbon seeps and coastal industrial discharges (Schifter et al. 2017). Continuing water sampling and analysis will enable us to better understand the true background level of naturally present hydrocarbons. This in turn will help us to better understand how the marine ecosystem responds to and recovers from a major spill event, and to aid in the detection of chronic spills, such as the ongoing Taylor Energy spill. It will also aid in the necessary regulation of exploration and drilling in the Gulf of Mexico, as well as inform response efforts to future spills.

Anthropogenic input of hydrocarbons to the marine environment contributes an estimated 668,000 tonnes per year worldwide, with the largest contribution related to consumption of petroleum products, especially from land-based runoff and riverine inputs (National Research Council 2003). Future oil spills will undoubtedly occur resulting from transportation, deepwater drilling in the Gulf of Mexico and elsewhere, and potential exploration in the Arctic. As climate change and a warming ocean also negatively impact marine ecosystems, care must be taken to safeguard marine organisms from the additional insult of oil spills; monitoring the state of the marine ecosystem through spectrofluorometry can enable this essential work.

REFERENCES

- Abdel-Shafy HI, Mansour MSM. 2016. A review on polycyclic aromatic hydrocarbons: Source, environmental impact, effect on human health and remediation. *Egyptian Journal of Petroleum*. 25:107-123.
- Adhikari PL, Maiti K, Overton EB. 2015. Vertical fluxes of polycyclic aromatic hydrocarbons in the northern gulf of Mexico. *Marine Chemistry*. 168:60-68.
- Almeda R, Wambaugh Z, Wang Z, Hyatt C, Liu Z, Buskey EJ. 2013. Interactions between zooplankton and crude oil: Toxic effects and bioaccumulation of polycyclic aromatic hydrocarbons. *PloS one*. 8(6):e67212 67211-67221.
- Baker JM. 2001. Oil pollution. *Encyclopedia of ocean sciences*. p. 191-199.
- Bejerano AC. 2018. Critical review and analysis of aquatic toxicity data on oil spill dispersants. *Environmental Toxicology and Chemistry*. 37(12):2989-3001.
- Bergquist DC, Andras JP, McNelis T, Howlett S, Horn MJv, Fisher CR. 2003. Succession in gulf of Mexico cold seep vestimentiferan aggregations: The importance of spatial variability. *Marine Ecology*. 24(1):31-44.
- Beyer J, Trannum HC, Bakke T, Hodson PV, Collier TK. 2016. Environmental effects of the deepwater horizon oil spill: A review. *Marine pollution bulletin*. 110:28-51.
- Bianchi TS, Osburn C, Shields MR, Yvon-Lewis S, Young J, Guo L, Zhou Z. 2014. Deepwater horizon oil in gulf of Mexico waters after 2 years: Transformation into the dissolved organic matter pool. *Environmental science & technology*. 48:9288-9297.
- Bugden JBC, Yeung CW, Kepkay PE, Lee K. 2008. Application of ultraviolet fluorometry and excitation-emission matrix spectroscopy (eems) to fingerprint oil and chemically dispersed oil in seawater. *Marine pollution bulletin*. 56:677-685.
- Bureau of Ocean Energy Management RaE. 2011. Report regarding the causes of the April 20, 2010, Macondo well blowout. In: Interior USDot, editor.
- Coble PG. 2007. Marine optical biogeochemistry: The chemistry of ocean color. *Chemical Reviews*. 107:402-418.
- Cole S, Codling ID, Parr W, Zabel T. 1999. Guidelines for managing water quality impacts within UK European marine sites. In: Project UMS, editor. Wiltshire UK.
- Conmy RN, Coble PG, Farr J, Wood AM, Lee K, Pegau WS, Walsh ID, Koch CR, Abercrombie MI, Miles MS et al. 2014. Submersible optical sensors exposed to chemically dispersed crude oil: Wave tank simulations for improved oil spill monitoring. *Environmental science & technology*. 48(3):1803-1810.
- D'Sa EJ, Overton EB, Lohrenz SE, Maiti K, Turner RE, Freeman A. 2016. Changing dynamics of dissolved organic matter fluorescence in the northern gulf of Mexico following the deepwater horizon oil spill. *Environmental science & technology*. 50:4940-4950.
- Daly KL, Passow U, Chanton J, Hollander D. 2016. Assessing the impacts of oil-associated marine snow formation and sedimentation during and after the deepwater horizon oil spill. *Anthropocene*. 13:18-33.

- del Vecchio, Rossana, Blough NV. 2004. On the origin of the optical properties of humic substances. *Environmental science & technology*. 38:3885-3891.
- Diercks A-R, Highsmith RC, Asper VL, Joung D, Zhou Z, Guo L, Shiller AM, Joye SB, Teske AP, Guinasso N et al. 2010. Characterization of subsurface polycyclic aromatic hydrocarbons at the deepwater horizon site. *Geophysical Research Letters*. 37(2).
- Galloway WE. 2009. Gulf of Mexico. *GEOExPro*. 6(3).
- Girard F, Fisher CR. 2018. Long-term impact of the deepwater horizon oil spill on deep-sea corals detected after seven years of monitoring. *Biological Conservation*. 225:117-127.
- Jones LC, Taylor LW. 1955. Far ultraviolet absorption spectra of unsaturated and aromatic hydrocarbons. *Analytical Chemistry*. 27(2):228-237.
- Joye SB. 2016. The Gulf of Mexico ecosystem - before, during and after the deepwater horizon oil well blowout. *Deep-Sea Research II*. 129:1.
- Kellar NM, Speakman TR, Smith CR, Lane SM, Balmer BC, Trego ML, Catelani KN, Robbins MN, Allen CD, Wells RS et al. 2017. Low reproductive success rates of common bottlenose dolphins *Tursiops truncatus* in the northern Gulf of Mexico following the deepwater horizon disaster (2010-2015). *Endangered Species Research*. 33:143-158.
- Kessler JD, Valentine DL, Redmond MC, Du M, Chan EW, Mendes SD, Quiroz EW, Villanueva CJ, Shusta SS, Werra LM et al. 2011. A persistent oxygen anomaly reveals the fate of spilled methane in the deep Gulf of Mexico. *Science*. 331(6015):312-315.
- Kleindienst S, Seidel M, Ziervogel K, Grim S, Loftis K, Harrison S, Malkin SY, Perkins MJ, Field J, Sogin ML et al. 2015. Chemical dispersants can suppress the activity of natural oil-degrading microorganisms. *Proceedings of the National Academy of Sciences of the United States of America*. 112(48):14900-14905.
- Kujawinski EB, Kido Soule MC, Valentine DL, Boysen AK, Longnecker K, Redmond MC. 2011. Fate of dispersants associated with the deepwater horizon oil spill. *Environmental science & technology*. 45:1298-1306.
- Lubchenco J, McNutt MK, Dreyfus G, Murawski SA, Kennedy DM, Anastas PT, Chu S, Hunter T. 2012. Science in support of the deepwater horizon response. *Proceedings of the National Academy of Sciences*.
- McNutt MK, Chu S, Lubchenco J, Hunter T, Dreyfus G, Murawski SA, Kennedy DM. 2012. Applications of science and engineering to quantify and control the deepwater horizon oil spill. *Proceedings of the National Academy of Sciences*.
- National Research Council. 1989. *Using oil spill dispersants on the sea*. Washington, D.C.: The National Academies Press.
- National Research Council. 2003. *Oil in the sea iii: Inputs, fates, and effects*. Washington, DC: The National Academies Press.
- Paris CB, Henaff ML, Aman ZM, Subramaniam A, Helgers J, Wang D-P, Kourafalou VH, Srinivasan A. 2012. Evolution of the Macondo well blowout: Simulating the effects of the circulation and synthetic dispersants on the subsea oil transport. *Environmental science & technology*. 46:13293-13302.

- Paul JH, Hollander D, Coble P, Daly KL, Murasko S, English D, Basso J, Delaney J, McDaniel L, Kovach CW. 2013. Toxicity and mutagenicity of gulf of mexico waters during and after the deepwater horizon oil spill. *Environmental science & technology*. 47:9651-9659.
- Pradier B, Largeau C, Derenne S, Martinez L, Bertrand P. 1989. Chemical basis of fluorescence alteration of crude oils and kerogens--i. Microfluorimetry of an oil and its isolated fractions; relationships with chemical structure. *Organic Geochemistry*. 16(1-3):451-460.
- Prouty NG, Campbell PL, Mienis F, Duineveld G, Demopoulos AWJ, Ross SW, Brooke S. 2016. Impact of deepwater horizon spill on food supply to deep-sea benthos communities. *Estuarine, Coastal and Shelf Science*. 169:248-264.
- Putman NF, Abreu-Grobois FA, Iturbe-Darkistade I, Putman EM, Richards PM, Verley P. 2015. Deepwater horizon oil spill impacts on sea turtles could span the atlantic. *Biology Letters*. 11(12):20150596.
- Schifter I, Sánchez-Reyna G, González-Macías C, Salazar-Coria L, González-Lozano C. 2017. Fluorescence characteristics in the deep waters of south gulf of méxico. *Marine pollution bulletin*. 123(1):165-174.
- Schwarz FP, Wasik SP. 1976. Fluorescence measurements of benzene, naphthalene, anthracene, pyrene, fluoranthene, and benzo[e]pyrene in water. *Analytical Chemistry*. 48(3):524-528.
- Sinski JF, Exner J. 2007. Concentration dependence in the spectra of polycyclic aromatic hydrocarbon mixtures by front-surface fluorescence analysis. *Applied spectroscopy*. 61(9):970-977.
- Smith GC, Sinski JF. 1999. The red-shift cascade: Investigations into the concentration-dependent wavelength shifts in three-dimensional fluorescence spectra of petroleum samples. *Applied spectroscopy*. 53(11):1459-1469.
- Stout SA, Litman E, Baker G, Franks JS. 2018. Novel biological exposures following the deepwater horizon oil spill revealed by chemical fingerprinting. *Oil spill environmental case studies*. Elsevier. p. 757-784.
- Sun S, Hu C, Tunnell JW. 2015. Surface oil footprint and trajectory of the ixtoc-i oil spill determined from landsat/mss and czcs observations. *Marine pollution bulletin*. 101(2):632-641.
- Thibodeaux LJ, Valsaraj KT, John VT, Papadopoulos KD, Pratt LR, Pesika NS. 2011. Marine oil fate: Knowledge gaps, basic research, and development needs; a perspective based on the deepwater horizon spill. *Environmental Engineering Science*. 28(2):87-93.
- Tissot BP, Welty DH. 1978. Classification of crude oils. *Petroleum formation and occurrence*. Springer-Verlag. p. 369-377.
- Venn-Watson S, Colegrove KM, Litz J, Kinsel M, Terio K, Saliki J, Fire S, Carmichael R, Chevis C, Hatchett W et al. 2015. Adrenal gland and lung lesions in gulf of mexico common bottlenose dolphins (*tursiops truncatus*) found dead following the deepwater horizon oil spill. *PloS one*. 10(5):e0126538.
- Vignier J, Soudant P, Chu FLE, Morris JM, Carney MW, Lay CR, Krasnec MO, Robert R, Volety AK. 2016. Lethal and sub-lethal effects of deepwater horizon slick oil and

dispersant on oyster (*crassostrea virginica*) larvae. *Marine environmental research*. 120:20-31.

Wade TL, Sericano JL, Sweet ST, Knap AH, Guinasso NL. 2016. Spatial and temporal distribution of water column total polycyclic aromatic hydrocarbons (pah) and total petroleum hydrocarbons (tph) from the deepwater horizon (macondo) incident. *Marine pollution bulletin*. 103(1):286-293.

Wade TL, Sweet ST, Sericano JL, Guinasso NL, Jr., Diercks A-R, Highsmith RC, Asper VL, Joung D, Shiller AM, Lohrenz SE et al. 2011. Analyses of water samples from the deepwater horizon oil spill: Documentation of the subsurface plume. In: Liu Y, MacFadyen A, Ji Z-G, Weisberg RH, editors. *Monitoring and modeling the deepwater horizon oil spill: A record-breaking enterprise*. American Geophysical Union. p. 77-82.

APPENDIX A
OIL CHARACTERISTICS

Table A. Oil characteristics

Oil Types	Origin	Sulfur (wt %)	Ref.	Avg Sulfur	API Gravity (with ref.)	Avg API Gravity	density* (g/cm3 or g/mL) (with ref.)	Avg density	Pour Point (°C) (with ref.)	Dynamic viscosity* (mPa.s or cP) (with ref.)
Access Western Blend Dilbit	Athabasca region, Alberta, Canada	3.91 e (5 yr avg)		3.91	21.6 ±0.9 e	21.25	0.9233 ±.0053 e	0.9243		
					20.9 i		0.9253 i		<-25 i	347 i
ANS	Prudhoe Bay, Alaska	0.96 c		1.09	31.4 c	30.25	0.8686 c		-19 c	
(1989)	North Slope, US	1.04 d-API81			26.8 d-EETD89		0.8936 d-EETD89	0.8799	-8 d-EETD89	23 d-EETD89
(2002)		1.11 d-ESTD02			30.89 d-ESTD02		0.8663 d-ESTD02		-32 d-ESTD02	11.5 d-ESTD02
					31.9 t					
(Middle Pipeline)		1.16 d-ESD97			29.9 d-ESD96		0.8761 d-ESD96		-54 d-ESD96	16 d-ESD96
(Northern Pipeline)		1.14 d-ESD97			30.6 d-ESD96		0.8719 d-ESD96		-55 d-ESD96	14 d-ESD96
(SOCSEX)		1.11 d-OGJ99			25 d-ESD96		0.8814 d-ESD95		-18 d-OGJ99	
					27.5 d-OGJ99		0.8899 d-EGJ99			
ANS - 10% Weathered (data for "2002")	DFO	1.20 d			26.8 d-ESTD02 & calc		0.8940 d-ESTD02		-20 d-ESTD02	31.8 d-ESTD02
Arabian Light	Saudi Arabia	1.77 d-OGJ99		1.85	33.4 d-OGJ99	32.30	0.8658 d-ESD92	0.8633	-28 d-ESD92	14 d-ESD92
					31.8 d-ESD92		0.8581 d-OGJ99		-53 d-OGJ99	
(2000)		1.93 d-ESTD02			31.3 d-ESTD02		0.8660 d-ESTD02		-21 d-ESTD02	13 d-ESTD02
					32.7 t					
Belridge Heavy	San Joaquin Valley, Calif	1.03 d-ESD93		1.03	13.6 d-ESD92	13.6	0.9746 d-ESD92		2 d-ESD92	12610 ESD92
Brent	East Shetland Basin, North Sea, UK (water depth 140 m)	0.4 c		0.40		38.20	0.8351 a	0.8340		6 a
		0.4 d-OGJ99			38.5 c		0.8324 c		0 c	
					38.3 d-OGJ99		0.8334 d-OGJ99		-42 d-OGJ99	6 d-ESD94
					37.8 d-ESD94		0.8351 d-ESD94		-6 d-ESD95	
					37.9 t					
Cold Lake Dilbit	NE Alberta, Canada	3.77 c		4.03	19.71 c	21.42	0.9358 c	0.9199	-38 c	
		4.72 d-EETD88			22.6 d-EETD88		0.9172 d-EETD88		-45 d-EETD88	150 d-EETD88
		3.6 d-OGJ92			22.6 d-OGJ92		0.9177 d-OGJ92		-46 d-OGJ92	
					21.0 i		0.9249 i		<-25 i	285 i
					21.2 t					
Federated	NW Alberta, Canada (Federated Co-op is located in Regina,	0.29 d-ESD97		0.32		39.40	0.8293 a	0.8280		4 a
		0.34 d-ESD99			39.9 ±0.9 e		0.8250 ±4.1 e			
(1998)					38.9 d-ESD99		0.8298 d-ESD99		-22 d-ESD99	5 d-ESD99
Gulfaks	North Sea, Norway (water depth 230 m)	0.18 c		0.31	37.8 c	33.63	0.8358 c	0.8530	-36 c	
		0.3 d-ESD97			29.3 d-OGJ99		0.8701 a, d-ESD93		-32 d-ESD93	13 a, d-ESD93
		0.44 d-OGJ99			31 d-ESD93				<-30 d-Daling91	
					36.4 t				-57 d-OGJ99	
Heidrun	Norwegian Sea (water depth 350 m)	0.46 d-Statoil97		0.46	28.6 d-ESD97	28.60	0.8835 d-ESD97	0.8834	-45 d-ESD97	18 d-ESD97
					28.6 d-Statoil97		0.8833 d-Statoil97		-48 d-Statoil97	
					25 t					

Table A (cont'd). Oil characteristics

Oil Types	Origin	Sulfur (wt %)	Ref.	Avg Sulfur	API Gravity (with ref.)	Avg API Gravity	density* (g/cm3 or g/mL) (with ref.)	Avg density	Pour Point (°C) (with ref.)	Dynamic viscosity* (mPa.s or cP) (with ref.)	
Hibernia	Newfoundland, Canada (water depth 80 m)	0.44 c		0.41	34.6 c	35.63	0.8519 c	0.8552	0 c		
		0.37 d-OGJ99			37.1 d-Mackay82a		0.8390 d-Mackay82a		6 d-Mackay82a	49 b	
					35 d-OGJ99		0.8500 d-SLRoss99a		2 d-OGJ99	49 d-Mackay82a	
					35.8 t				-6 d-SLRoss99a	30 d-SLRoss99a	
(1999) (EPA 86)						28.3 d-EETD86		0.8504 d-ESD00 0.8849 d-EETD86		10 d-ESD00 15 d-EETD86	13 d-ESD00 44 d-EETD86
Hondo	Santa Barbara Channel,	4.3 d-ESD98		4.41	19.6 d-ESD91	19.53	0.9356 d-ESD91	0.9364	-15 d-ESD91	735 d-ESD91	
Blend	California, US (water depth 260 m)	4.29 d-OGJ99			20.8 d-OGJ99		0.9288 d-OGJ99		-21 d-OGJ99		
Monterey		4.7 d-OGJ99			18.3 d-ESD98		0.9377 d-OGJ99		-23 d-OGJ99	1599 d-ESD98	
		4.34 d-ESD99			19.4 d-OGJ99		0.9435 d-ESD98		-9 d-ESD98		
IFO-40	unknown	2.51 g		2.51	21.9 g	21.9	0.9286 g				
IFO-120	unknown	2.89 g		2.89	18.4 g	18.4	0.9530 h				
IFO-180	unknown	1.54 d-ESD97		1.54	14.7 d-ESD95	14.10	0.9778 d-ESD94		-10 d-ESD95	2324 d-ESD94	
					12.9 i		0.9664 i		15 i	1920 i	
(SOCSEX)					14.7 d-ESD94		0.9670 d-ESD94			2324 d-ESD94	
IFO-300	unknown	1.72 d-ESD97		1.72	<16 s	11.90	0.9859 a	0.9859	-6 d	14,470 a	
					11.90 d		0.9859 d			14,470 d	
(SOCSEX)											
Lago	Maracaibo Basin, Venez	0.3 d-ESD99		0.3	27.3 d-ESD93	27.3	0.8907 d-ESD93	0.8907	21 d-ESD93	153 d-ESD93	
MC252--Discoverer Enterprise	Louisiana, US (< 1500 m)	<0.1 MSDS		<0.1	37.2	37.2	0.8500				
MC252--generic (MC194)	Louisiana, US (< 1500 m)	0.21 d-ESD94		0.21	35.2 d-ESD94	35.2	0.8483 d-ESD94		-40 d-ESD94	7 d-ESD94	
MESA (Medium South American)	Orinoco Basin, Venezuela	0.85 j		0.87	30.5 j	30.25			-46 j		
		0.88 t			30 k, t						
					29.7 v						
Santa Clara	Ventura County, Califor	2.85 d-ESD93		2.85	22.1 d-ESD91	22.1	0.9202 d-ESD91		-3 d-ESD91	304 d-ESD91	
Scotian Shelf Condensate (Scotian Light)	Nova Scotia, Canada	0.03 d-EETD86		0.016	53.2 d-ESD99	51.4	0.7655 d-ESD99	0.7943	-22 d-ESD99	1 d-ESD99	
Scotian Shelf (Sable Island) Condensate	(water depth 12-20 m)	0.002 c			39.9 d-SLRoss82		0.8230 d-SLRoss82		-22 d-SLRoss82	2 d-SLRoss82	
					61.1 c				3 d-Mackay82a	3 d-McKay82a	
									-51 d-EETD86		
Sea Rose (White Rose)	Newfoundland, Canada (water depth 100 m)	0.53 c		0.53	29.8 t	29.8	0.8738 d-ESD00	0.8649	13 d-ESD00	30 d-ESD00	
						>31 m		0.8560 (20°C) m			16.3 (20°C) m
Terra Nova	Newfoundland, Canada (water depth 90-100 m)			0.43	33.2 c, t	33.78	0.8591 c	0.8558	12 c		
						33.7 d-EETD89		0.8560 d-EETD89		27 d-Buist89	22 b, d-EETD89
(1994)			0.43 d-ESD97			35.7 d-ESD94		0.8457 d-ESD94		5 d-ESD95	11 d-ESD94
(Petawawa)			0.43 d-ESD97			32.5 d-ESD93		0.8624 d-ESD93		15 d-ESD93	30 d-ESD93
(SOCSEX)											11 d-ESD94
Vasconia	Colombia	0.56 d-ESD99		0.56	26.3 d-ESD98	25.3	0.8958 d-ESD98		6 d-ESD98	72 d-ESD98	
						24.3 u					

*at 15°C (~60°F), unless otherwise noted. Note: 1 centi-Stoke (cSt) = 1 mm ² /s
**SOCSEX: The oil was used in the 1994/95 Subsurface Oil in Coarse Sediments Experiment (SOCSEX) (in reference d).
^a Stoffyn-Egli & Lee, Spill Science & Technology Bulletin, 2002
^b Bugden et al., Marine Pollution Bulletin, 2008
^c http://www.exxonmobil.com/crudeoil/about_crudes_api.aspx
^d Environment Canada ETC database, 2001 (http://www.etc-cte.ec.gc.ca/databases/OilProperties/)
^e Crude Quality Inc., 2014 (http://www.crudemonitor.ca/home.php)
^f POLARIS Applied Science Inc., 2013 (http://www.crrc.unh.edu/sites/crrc.unh.edu/files/comparison_bitumen_other_oils_polaris_2014.pdf)
^g http://www.bunkering.co.kr/bunker_spec/30CST.htm
^h SLRoss Environmental Research Ltd., 2006. Dispersant Effectiveness Testing on Water-in-Oil Emulsions at OHMSETT for US Dept of the Interior Minerals Management Canadian Federal Government Technical Report, Properties, Composition and Marine Spill Behaviour, Fate and Transport of 2 Dilbit Products from the Canadian Oil Sands--November 2013. http://www.genesisny.net/Commodity/Oil/OSpecs.html#Mesa ; also Caplinepipeline.com report accessed 15Feb2015
^k http://www.pdvsa.com/index.php?tpl=interface.en/design/salaprensa/readnew.tpl.html&newsid_obj_id=2214&newsid_temas=1
^l http://www.uncw.edu/cms/documents/HazenPublic11152011.pdf
^m B.Robinson & T.King. 8 July 2014. personal communication
ⁿ Rhodes, Anne K. "Four California OCS crudes assayed." The Oil and Gas Journal 30 Mar. 1992: 67+. General OneFile. Web. 19 Oct. 2014.
^o Corbett, Richard A. "Import Norwegian crude assays updated." The Oil and Gas Journal 12 Mar. 1990: 37+. General OneFile. Web. 19 Oct. 2014.
^q Environment Canada, Emergencies Science Division Information Sheet--Marine Fuel Oils, December 1999 (www.env.gov.bc.ca/eemp/resources/pdf/info_sheet_on_marine_fuels.pdf)
^r Pipeline Planning and Construction Field Manual by E. Shashi Menon (2011) Note: Viscosity, cSt = (Viscosity, cP)/Sg where cSt = centistokes, cP = centipoise and Sg = specific gravity
^s Bunker Specification on the Bunker Delivery Receipt from www.bunkering.co.kr/bunker_spec/30CST.htm (used solely as a way to estimate API for IFO 300)
^t The Crude Oils and their Key Characteristics (http://www.energyintel.com/pages/eig_article.aspx?DocId=200017)
^u http://www.ecopetrol.com.co/documentos/upload/Especificaciones_Crudo_Vasconia.pdf

APPENDIX B
COOGER METHODS FOR FLUORESCENCE ANALYSIS
USING THE BAFFLED FLASK TEST

Approximately 100- μ L of oil was added to a 250-mL baffled flask containing 120-mL of 0.45- μ m filtered seawater from Bedford Basin, Nova Scotia (salinity 30-32 ppt), and placed, prior to the addition of the oil/dispersant, on an OS-500 orbital shaker with an orbital diameter of 2cm (0.75 in., manufactured for VWR International by Henry Troemner LLC, Thorofare, NJ) set to 200 rpm.. Approximately 300- μ L of oil was aspirated into a 1-mL turberculin syringe (Benton Dickinson, Franklin Lakes, NJ), and then pushing the plunger to the 100- μ L mark to give about 100 μ L of oil. The oil and syringe were then weighed, and then the contents of the syringe (approximately 100 μ L of oil) carefully dispensed on to the surface of the seawater in the baffled flask. The syringe was then re-weighed. By using the density of the oil being tested, the exact volume of oil added was calculated, allowing for the proper amount of dispersant (Corexit 9500) to be dispensed to provide the required dispersant to oil ratio (DOR - 1:10, 1:20, or 1:40). The Corexit was added with a 20- μ L Pipet-Plus Pipetman (Gilson) as a drop to the surface of the oil, in much the same way as Soriel, *et al.* (2004). The oil/dispersant/seawater was allowed to mix for ten minutes, after which approximately 3-mL of the dispersed oil/seawater mixture was dispensed into a 4.5-mL UV-grade quartz cuvette (10 mm light path – Hellma (Canada) Limited, Concord, Ontario) out through a spigot located near the bottom of the flask for ultra-violet

fluorescence spectroscopy (UVFS). The cuvette was then placed in a Shimadzu 5301-PC UV-fluorometer, and scans run as outlined in Bugden *et al*, 2008.

About 30-mL (the exact volume was recorded) was then drawn into a 50-mL graduated cylinder fitted with a stopper, for Total Petroleum Hydrocarbon (TPH) analysis (Li et al, 2008a). Care was taken to prevent the transfer of non-dispersed oil which was present in the spigot, though this was not always possible. The sample was then transferred into a 100 mL amber bottle with a tin foil coated screw cap. The graduated cylinder was rinsed three times with di-chloro-methane (DCM); two times with 10 mL and once with 20 mL. The graduated cylinder was stoppered after each rinse, the contents shaken (with the stopper removed after every few shakes to release pressure which would build up in the cylinder), the contents transferred to an amber bottle which was then placed into a refrigerator at 4°C, allowing the DCM to settle for a minimum of 24 hours. After extraction, the oil/DCM extract was transferred to a 40 mL glass vial using a lime glass pipette and a glass syringe, and adjusted to a final volume of 10 mL with DCM. The samples were scanned on a Genesys 20 spectrophotometer at 340, 370 and 400nm (Thermo Fisher Scientific Inc., Waltham, MA, U.S.A), using the same quartz cuvette as for the UVFS measurement. Calibration curves were generated from stock solutions by putting 1 mL of oil by mass in a 10 mL volumetric flask with DCM. Dispersant was added to achieve the appropriate DOR using a 20 µL Rainin pipet-plus with a 20 µL tip. For each DOR and oil, 5 standards were made up in a 10 mL volumetric flask with DCM with the following stock volumes; 10, 20, 40, 100, 200, 400, and 500 µL (standard concentrations varied between oils). The standards and samples were run on the same day, under the same conditions, to eliminate variation due to changes in bulb intensity over time. Absorbance and percent transmission were recorded and

the data was entered into an excel spreadsheet to calculate sample concentration. Some sample had to be diluted up to 100 mL because they were too concentrated to obtain a reading on the spectrophotometer. The dispersant effectiveness was calculated by dividing the concentration of the oil extracted from the water column (dispersed fraction) by the total amount of oil that had been added to the flask. The result was recorded as a percentage.

APPENDIX C

COBLE LAB PROTOCOL FOR HORIBA AQUALOG

Coble Lab Protocol for HORIBA Aqualog

Daily Start-up Routine

First, power up Aqualog (power switch is on left side near the back of the instrument)

Second, start Aqualog 3.6 software

- Must be done in this order
- Turn off computer WiFi and do not open any other software while Aqualog is running

Instrument must be allowed to warm up for at least 20 minutes to ensure lamp is at full intensity.

While it's warming up, cover workspace with a paper towel and gather equipment:

- Quartz cuvettes (1x1x4 cm)
- Nitrile gloves—do NOT ever touch cuvettes with bare hands!
- Kimwipes
- Ultrapure water (Milli-Q or similar) at room temperature

Remove samples from refrigerator and shield from light while they come to room temperature

Rinse cuvettes 20-30x with ultrapure water; rinse caps (if using).


Note: If samples are volatile, Teflon plug-type caps should be used; otherwise, use of caps is personal preference. Try running with and without and compare results.

Daily Tests

Before running samples, three tests should be performed each day:

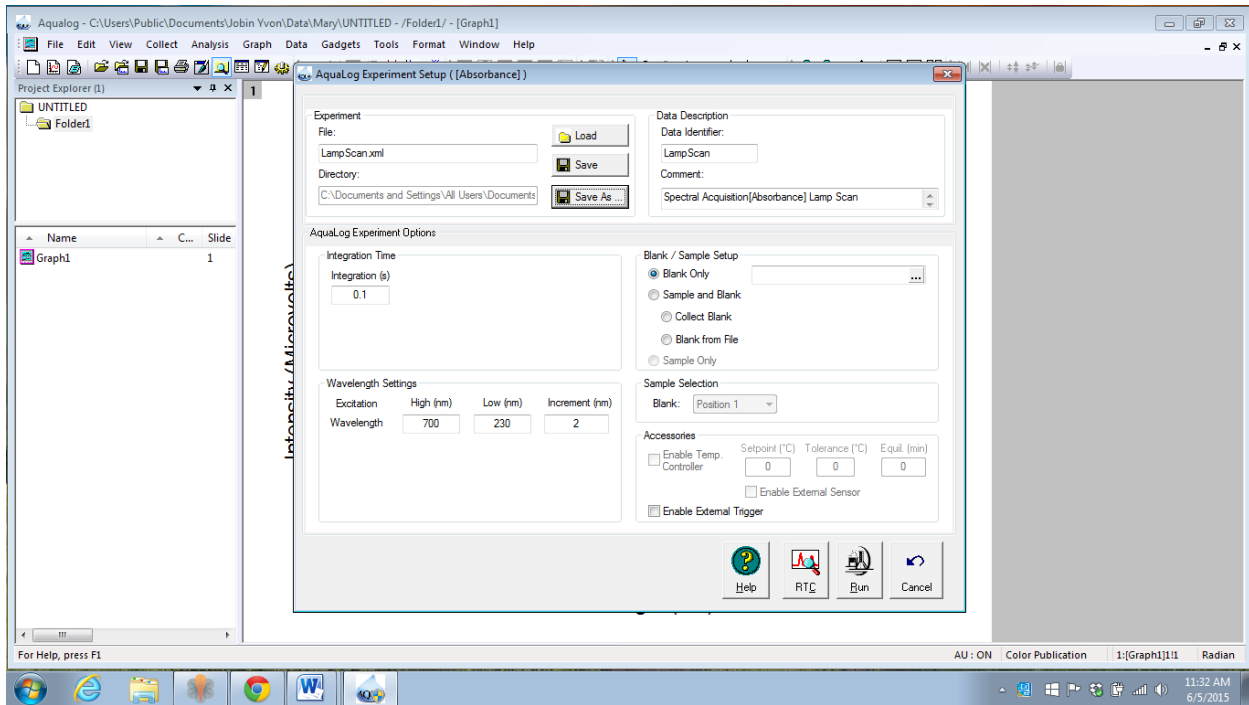
1. Lamp Scan
2. Water Raman SNR & Emission Calibration
3. Raman Scattering Area Unit

1. Lamp scan (to track lamp performance):

Click  icon; instrument will initialize. Select Spectra → Absorbance, click 'Next'.

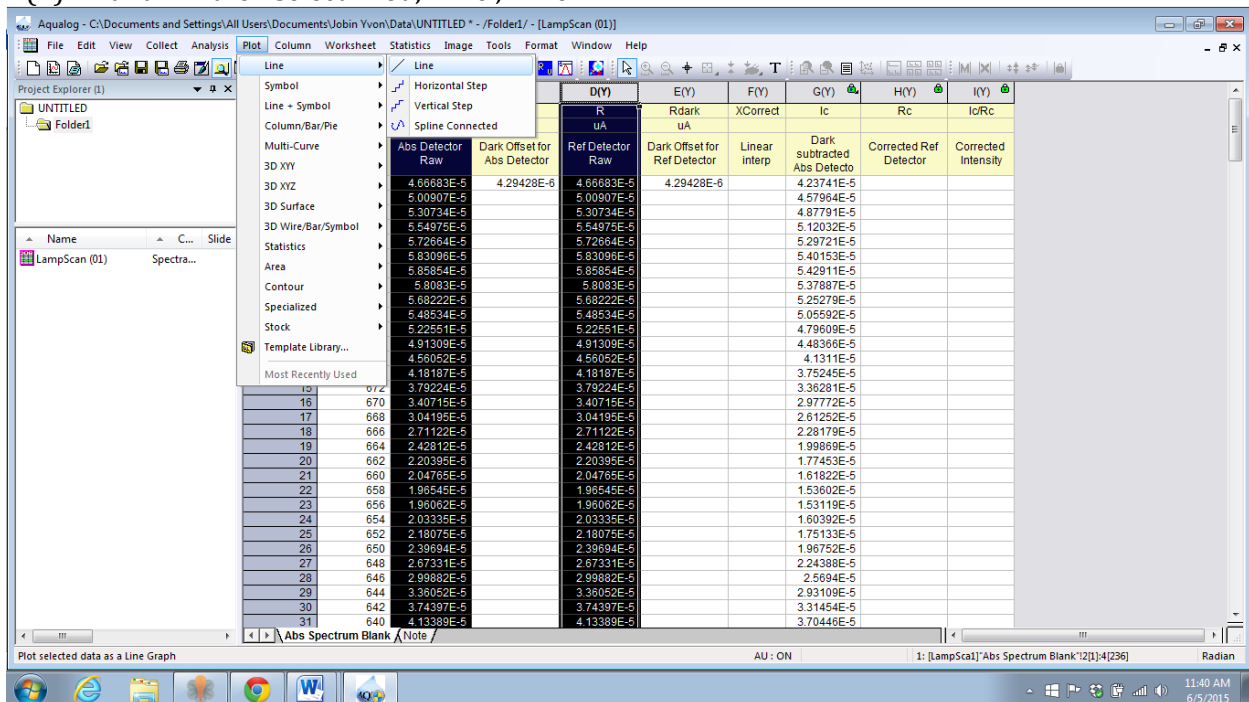
Change 'Aqualog Experiment Setup (Absorbance)' default settings to those shown below.


First time, select 'Save As' → Lamp Scan; thereafter, select 'Load' and select Lamp Scan file.



With no cuvette in the sample chamber, click 'Run'.

When resulting table appears, while holding down 'Ctrl' key click on column headings B(Y) and D(Y)—I and R—then select 'Plot', 'Line', 'Line'.

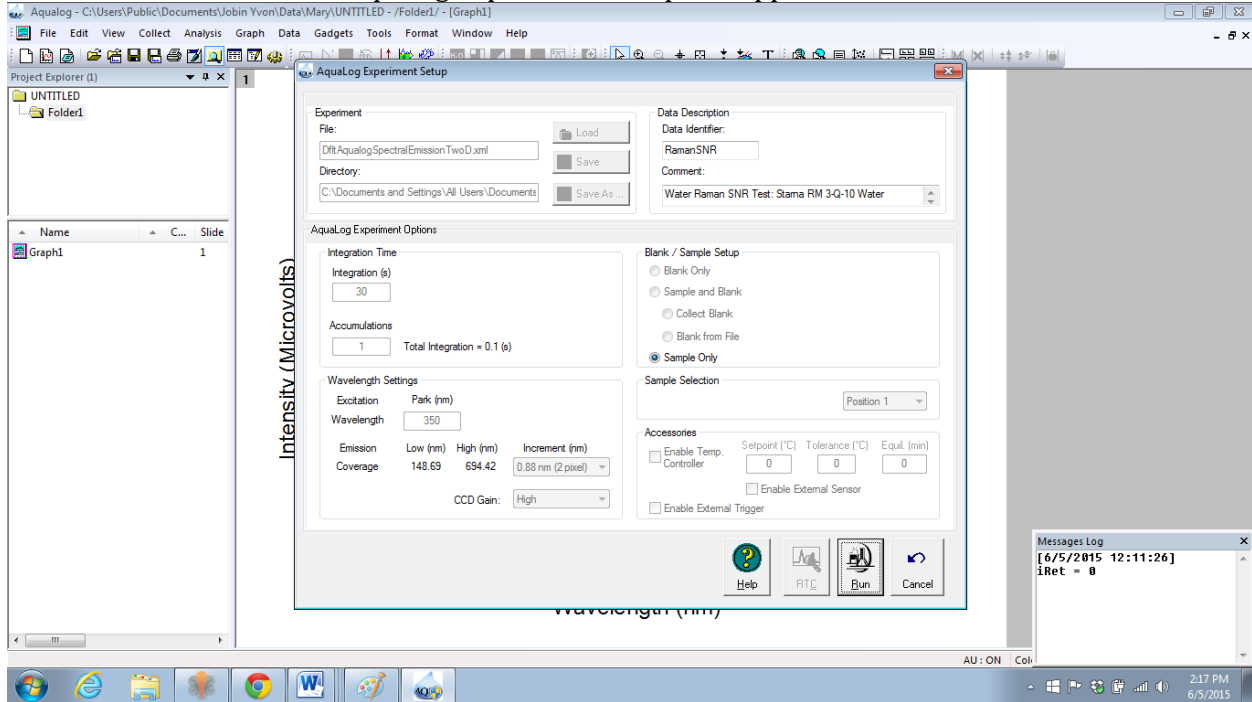


After the plot appears, click on  (Screen Reader) icon, then click to place screen reader on peak on black line (Abs Detector Raw). X should be 467 (±1nm), Y should be ≥ 7. If X value is more than 1nm below or above 467nm, call HORIBA for service. When intensity (Y value) falls below 7, lamp must be replaced. Make a note of Y value in your daily log.

2. Water Raman SNR & Emission Calibration Test

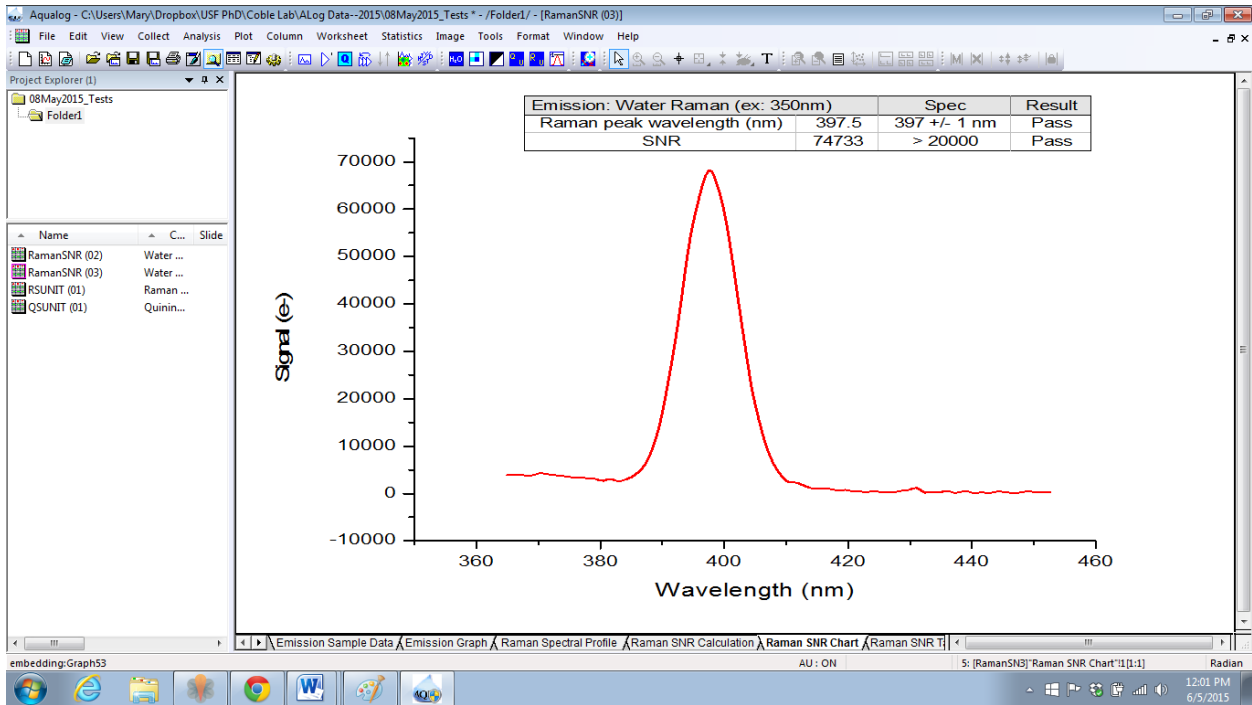
With gloves on, fill a cuvette about $\frac{3}{4}$ full with Milli-Q water. Holding it near the top, wipe all sides with Kimwipe. Check to be sure there are no bubbles in the cuvette. Insert cuvette into sample holder. Be sure that water level is above the optical window in the sides of the sample holder.

From Aqualog dropdown menu, select 'Collect' → 'Aqualog Validation Tests' → 'Water Raman SNR and Emission Calibration'. Aqualog Experiment Setup box appears:



Under 'Comment:' at top right change "Starna RM 3-Q 10 Water" to "Lab Milli-Q" and add TOC reading from the Milli-Q system. Leave all other settings as is. Click 'Run'.

This test returns two results—location of water Raman peak and signal-to-noise ratio (SNR). You should get a nice, smooth curve with peak at 397 nm (± 1 nm) and $\text{SNR} \geq 20,000$ similar to:

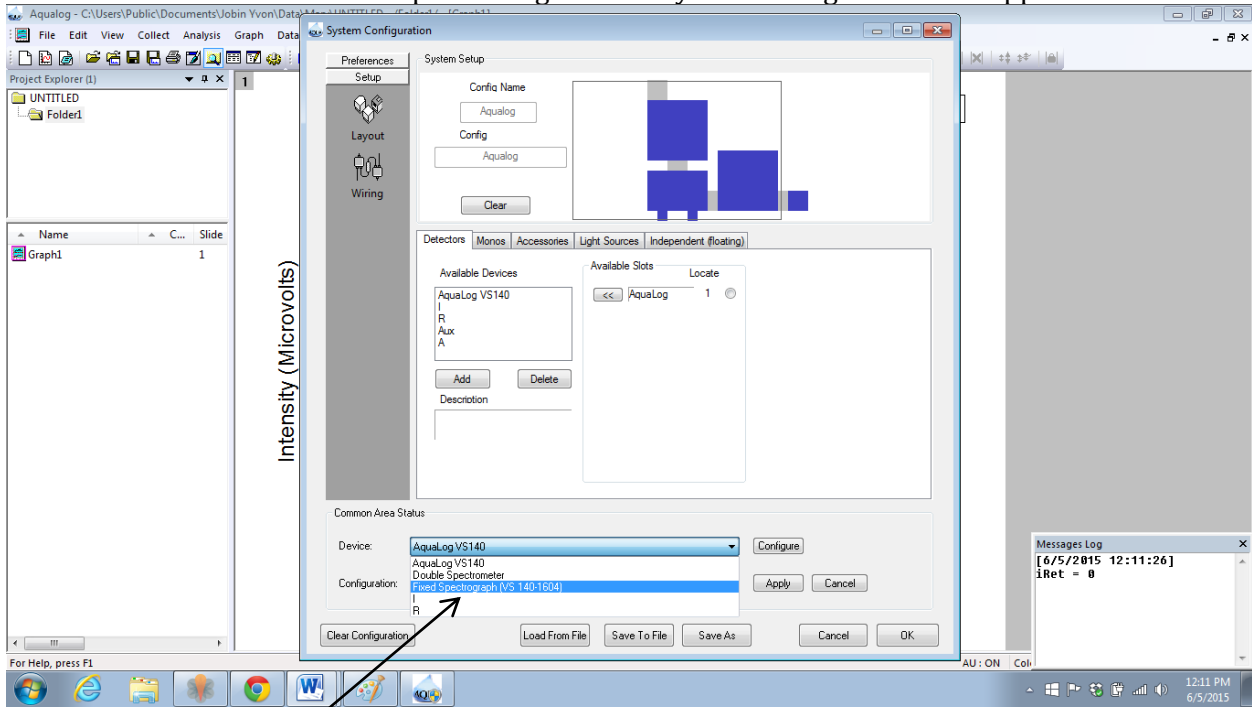


Enter Raman Peak wavelength and SNR in your daily log.

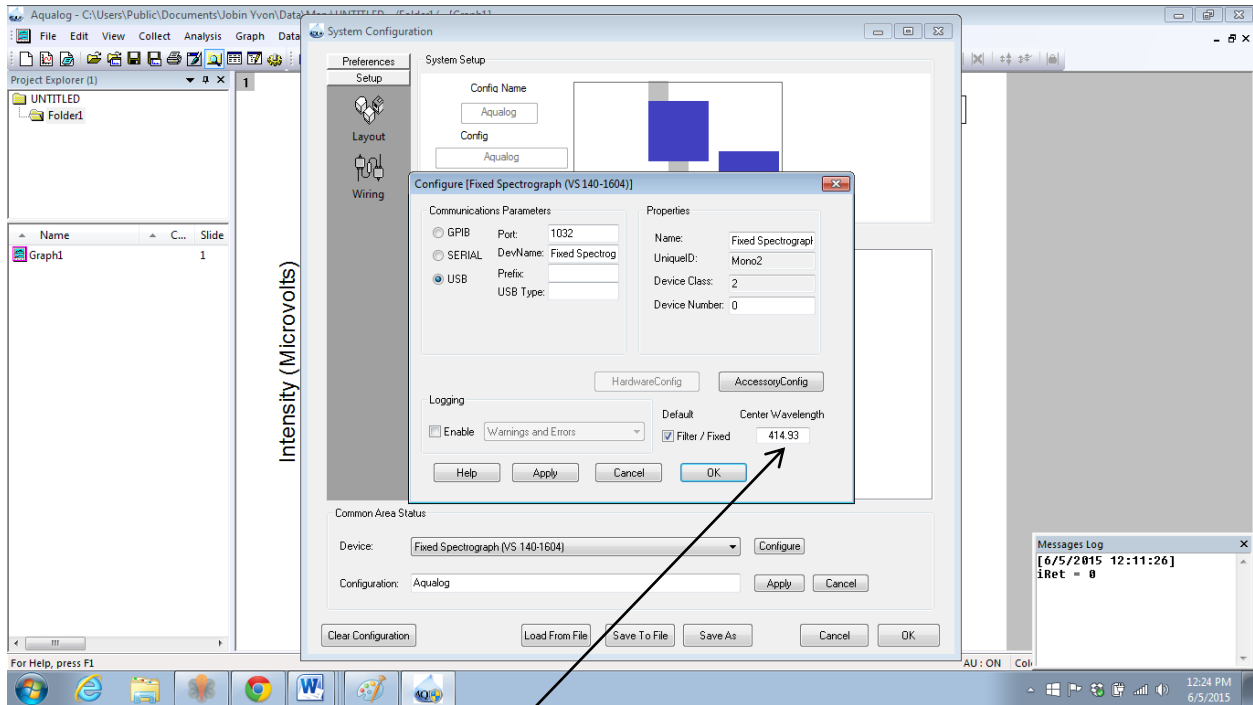
Note: for SNR <20000, call HORIBA for service; for Raman Peak >1nm below or above 397nm, peak must be recentered.

To Recenter Raman Peak:

Select 'Collect' → Advanced Setup → Configuration. System Configuration box appears:



From 'Device' dropdown, choose 'Fixed Spectrograph...' Click 'Configure'



Adjust figure in 'Center Wavelength' box by entering a slightly larger number if Raman Peak needs to be raised, or a slightly smaller number if it must be lowered. Click 'OK', 'OK'.

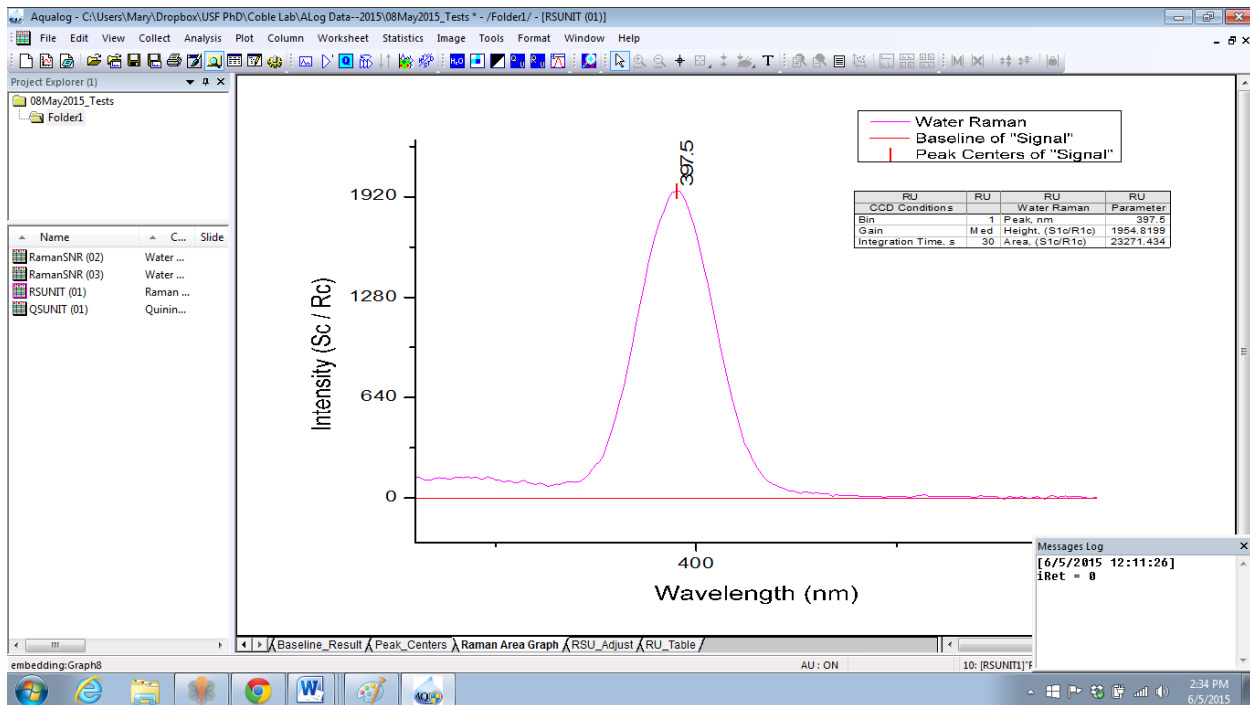
Next re-run Water Raman SNR and Emission Calibration test.

Repeat these instructions until test results show Raman Peak wavelength = 397nm.

3. Raman Scattering Area Unit

Leave cuvette filled with Milli-Q in the sample holder.


From Aqualog dropdown menu, select 'Collect' → 'Aqualog Validation Tests' → 'Raman Scattering Area Unit'. Leave all settings as is. Click 'Run'.



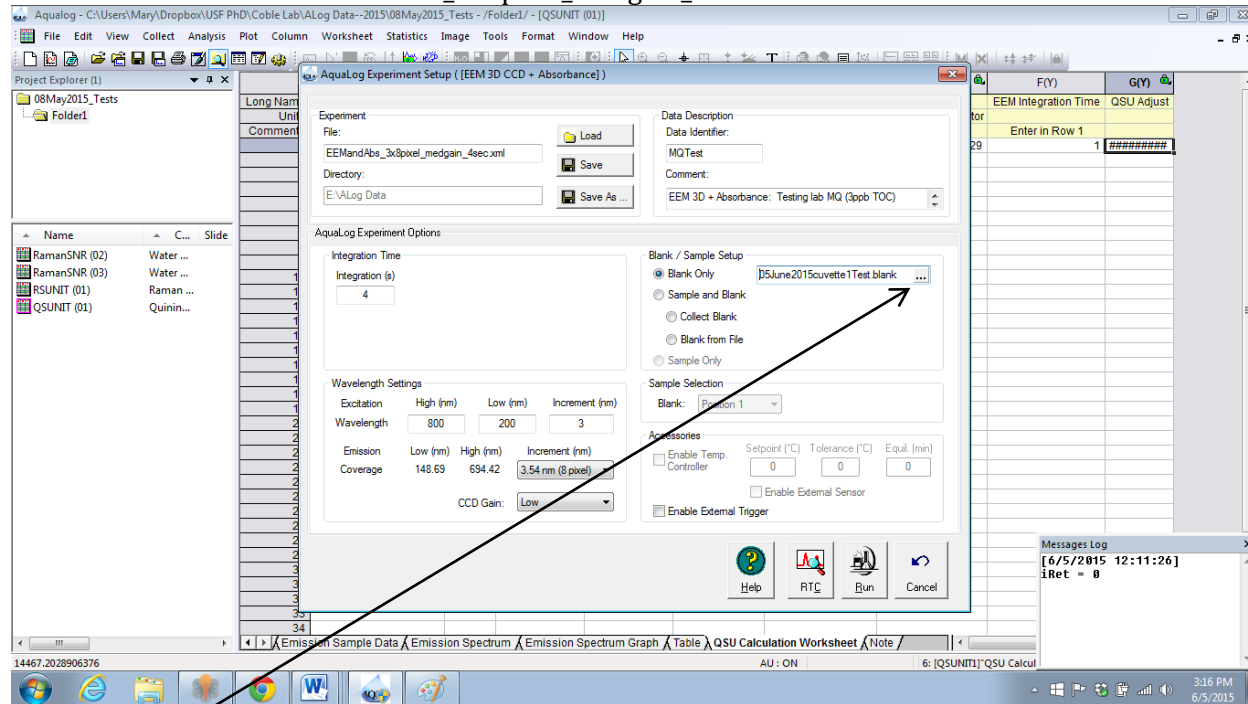
This test returns three results—location, height, and area of water Raman peak. Peak location should agree with Water Raman SNR and Emission Calibration Test ($\pm 0.5\text{nm}$). Record the position, height and area of peak in your daily log. Area will also be used to translate raw fluorescence intensity counts into Raman Scattering Units for each day's samples.

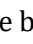




Note: This test may be re-run at the beginning of each new batch of samples so there is an RSUNIT file in each project.

Analyzing Blanks

Next, analyze Milli-Q water in each of the cuvettes you'll be using to ensure they are completely clean and there is no contamination in the Milli-Q water. To do so click on  icon, then select 3D → EEM 3D CCD + Absorbance, click 'Next'.

Click 'Load' and select EEMandAbs_3x8pixel_medgain_4sec.xml file. It should look like this:




Click on  and rename blank (e.g., 05June2015cuvette1Test.blank), click 'Open'. With Milli-Q filled cuvette in the sample chamber, click 'Run'. When sample analysis is complete, click on  (Inner Filter Effect correction) icon. When processing is complete, click on  (Rayleigh Masking Tool). Select check boxes for both First and Second Order Rayleigh Masking, and change 'SUM of slit widths' from 10 to 12, click 'OK'. To analyze additional blanks, click on  (Previous Experiment Setup) icon to recall the settings, click on  to give the new blank a different name, click 'Run', and repeat the post-processing steps when each analysis is complete.

Save Project

At this point, select File → Save Project As... and name the project with the day's date and 'Tests' (e.g., 05June2015_Tests.opj).

Running Samples


Select File → New → Project to start running samples. First, you'll need to determine the optimal integration time for the samples, assuming they all have similar fluorophore concentration.

Click on  Aqualog Main Experiment Window. Select 3D → EEM 3D CCD + Absorbance, click 'Next'.

Load template file "EEMandAbs_3x8pixel_medgain_onetenthsec".

Leave all settings on the left side of the Aqualog Experiment Setup box as is. At the top right in the 'Data Description' box enter an appropriate sample name. **Note:** this field is limited to 10 characters so you'll need to devise some kind of shorthand naming scheme such as ddmmyya, b, c, etc., and keep track of the full sample details in your daily log.

In the 'Comment' box you can enter as much information about your sample as you'd like.



In the 'Blank/Sample Setup' box, select 'Sample and Blank' and 'Collect Blank from File', then click on  and give your blank a name. I'd suggest ddmmyyMQ.blank (or ddmmyySW.blank for seawater, etc.)

Fill a cuvette with the appropriate solvent blank which you wish to subtract from the sample (MQ, artificial seawater, DCM, etc.). This will help to eliminate Raman Scatter interference.




Rinse the second cuvette 3x with sample (filling at least halfway), then fill approximately ¾ full.

Holding each cuvette near the top, wipe all sides with a Kimwipe.

Place cuvette containing the blank in the sample chamber and click 'Run'. (Software will prompt for blank insertion, click 'OK'.) When blank analysis is complete, software will prompt for sample insertion. Remove blank and insert sample, click 'Run'.

When sample analysis is complete, the 'Sample - Blank Waterfall Plot' tab will be active. Click on  (Inner Filter Effect correction) icon. When IFE processing is complete, click on  (Rayleigh Masking Tool). Select check boxes for both First and Second Order Rayleigh Masking, and change 'SUM of slit widths' from 10 to 12, click 'OK'.

To determine whether 0.1 sec is an appropriate integration time to run the rest of your samples (assuming similar fluorophore concentration), refer to the table below. The goal is f_{\max} signal intensity between 30,000 and 65,000 counts. After following post-processing directions (below) to determine true f_{\max} intensity, re-run the blank and sample at a longer integration time, if necessary.

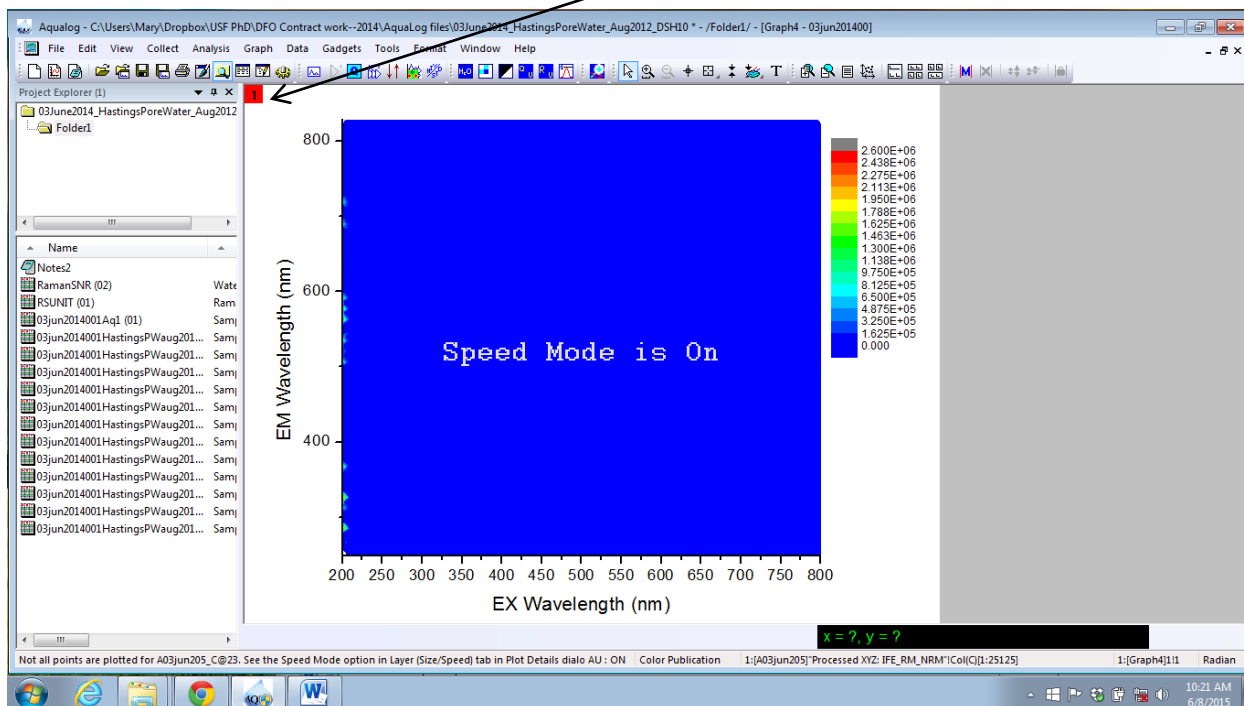
Click  (Previous Experiment Setup) icon and change integration time, sample name, and blank name. If 0.1 sec. is a good integration time, click  to recall the previous experiment and click 'Blank from File'. Click  to navigate to reuse the information from the blank already collected. This speeds processing time and eliminates possible blank-to-blank variation.

Signal intensity (counts)	Estimated integration time (seconds)
100 to 1000	4.0
1001 to 5000	2.0
5001 to 50 000	1.0
50 001 to 65 535	0.1

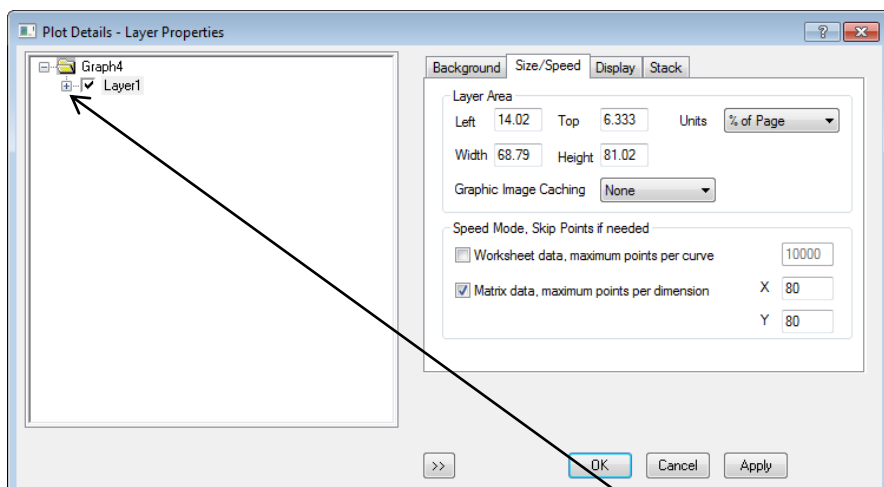
Note: If 0.1 sec integration time results in intensity >65,535, check the absorbance of your sample to be sure it is not too concentrated. See "An Important Caveat" below. Also, I have run samples at integration times >4 sec, although I do not run samples at integration time >10 sec since water chemistry changes and temperature effects are a potential issue. Since the Aqualog analyzes from high to low wavelengths, fluorescence of proteins and PAHs could be considerably altered at extended integration times.

Post-Processing of EEMs

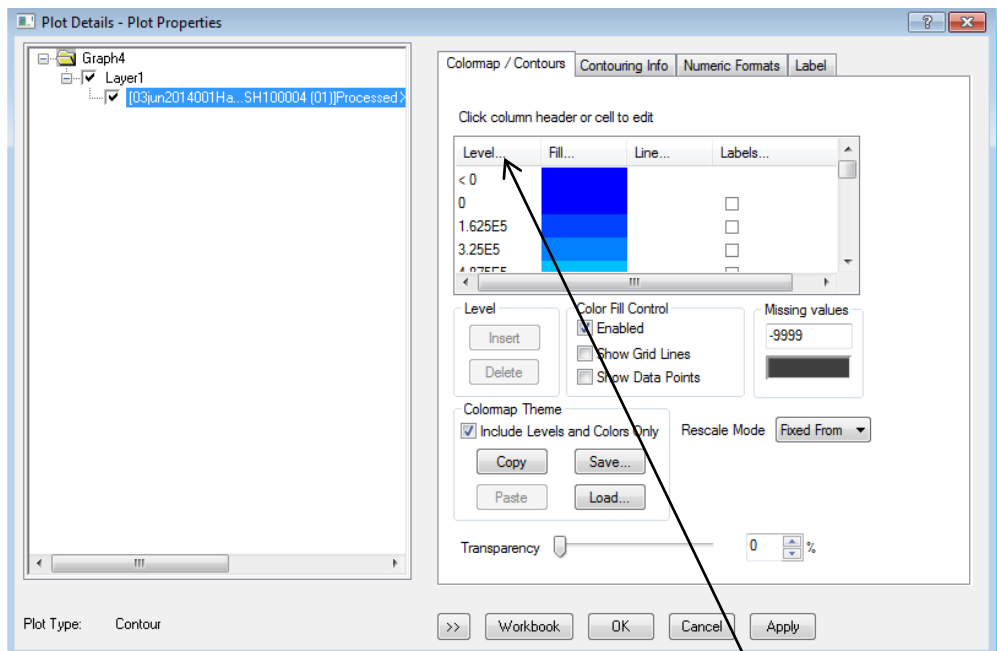
After IFE and Rayleigh Masking is complete, click on 'Processed Contour: IFE_RM' tab to make the full-color EEM contour plot active. You may see something like the screen below, leading you to believe there's no fluorescence in your sample. Keep processing! Double-click anywhere on the EEM contour plot to enable the image processing window. Right click on the small, red square that has appeared at the upper left corner of EEM window then select 'Layer Properties'.



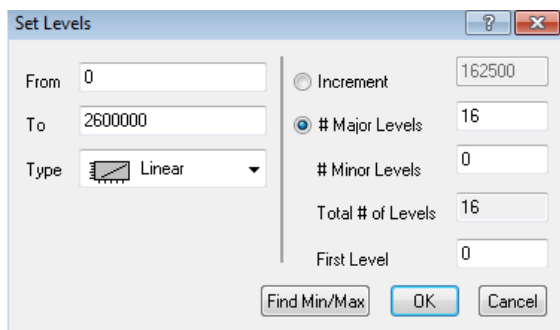
The 'Plot Details' window appears:



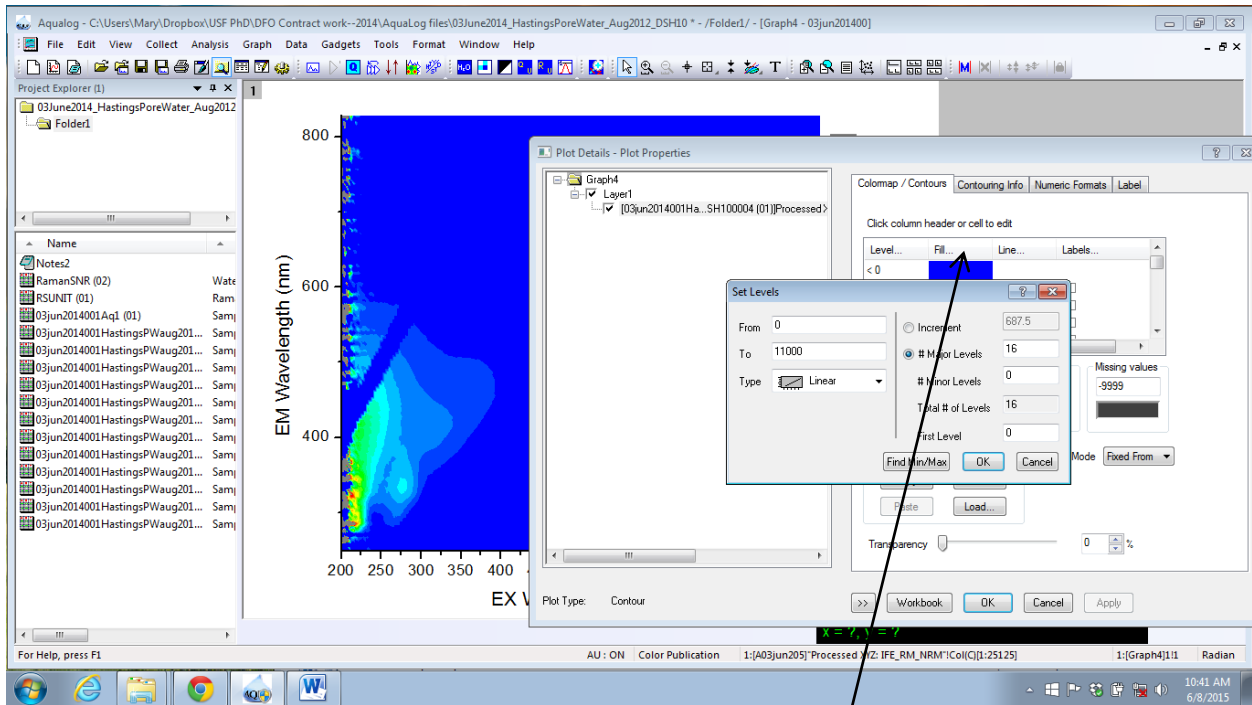
In 'Plot Details' box, first click on Size/Speed tab at right (above) then uncheck 'Worksheet data, maximum points per curve'. Then, at the far left, click on '+' to expand Layer1, then click on file name to bring up new tab selections at right (below).



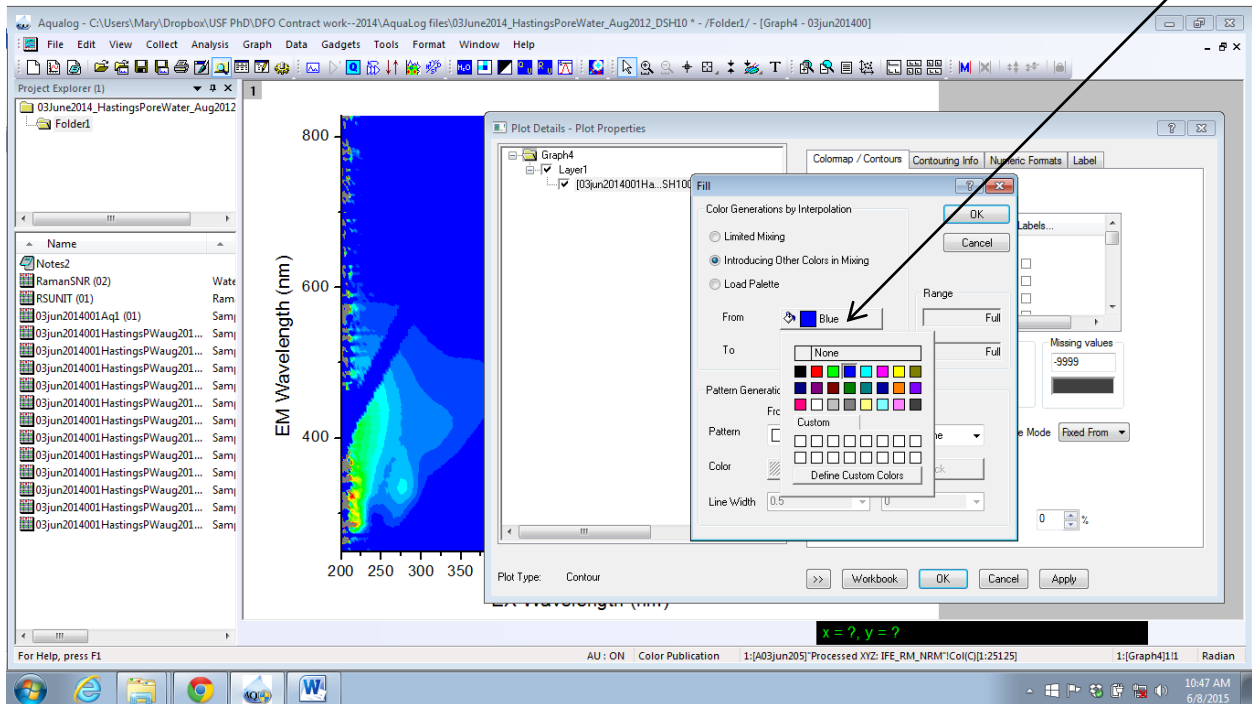
Click on the 'Color Map/Contours' tab, then click on 'Level'. The 'Set Levels' box appears:



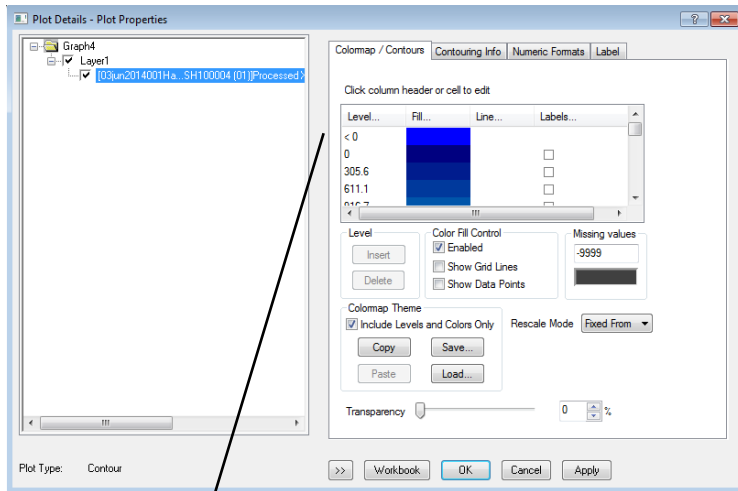
The 'From' field will probably contain a negative number; change it to 0. Then you'll need to manipulate the 'To' field to determine the true maximum. Begin by deleting the final 0, then choose 'OK', then 'Apply'. Move the 'Plot Details' box to the right so you can continue changing the figure in the 'To' field until the fluorescence peak appears in red, similar to the following figure.



I recommend changing EEM color configuration as follows: Change '# Major Levels' field to 36 and leave '# Minor Levels' at 0, click 'OK'. Then click on 'Fill' heading; 'Fill' box appears. Click on 'Blue' to bring up additional color choices, then click on 'Navy' square (first box in 2nd row). Click 'OK'.

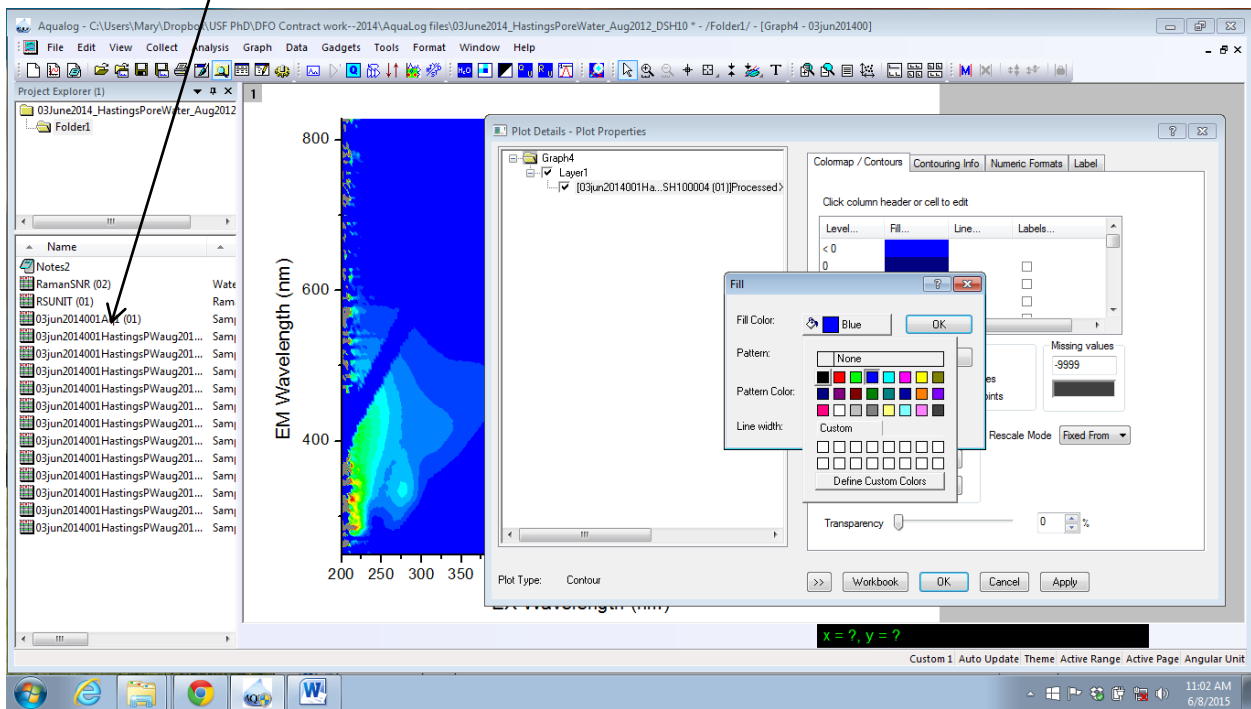


'Plot Details' now looks like this:

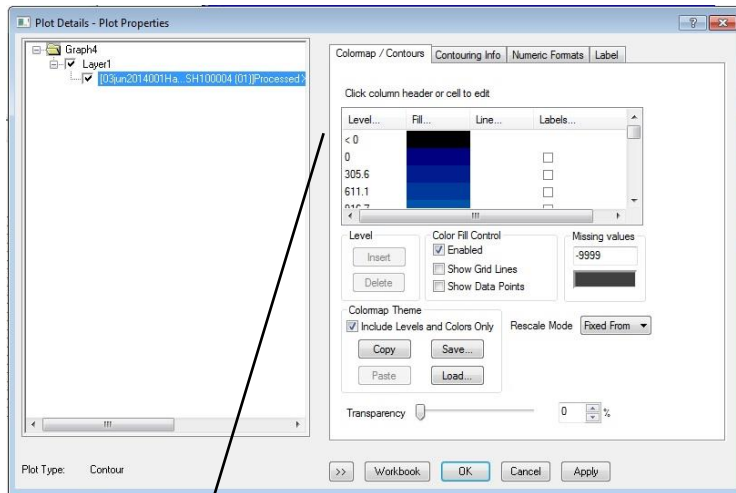


Click on blue bar next to '<0'.

In 'Fill' box, click on 'Blue', then select 'Black' square (1st box, 1st row). Click 'OK'.

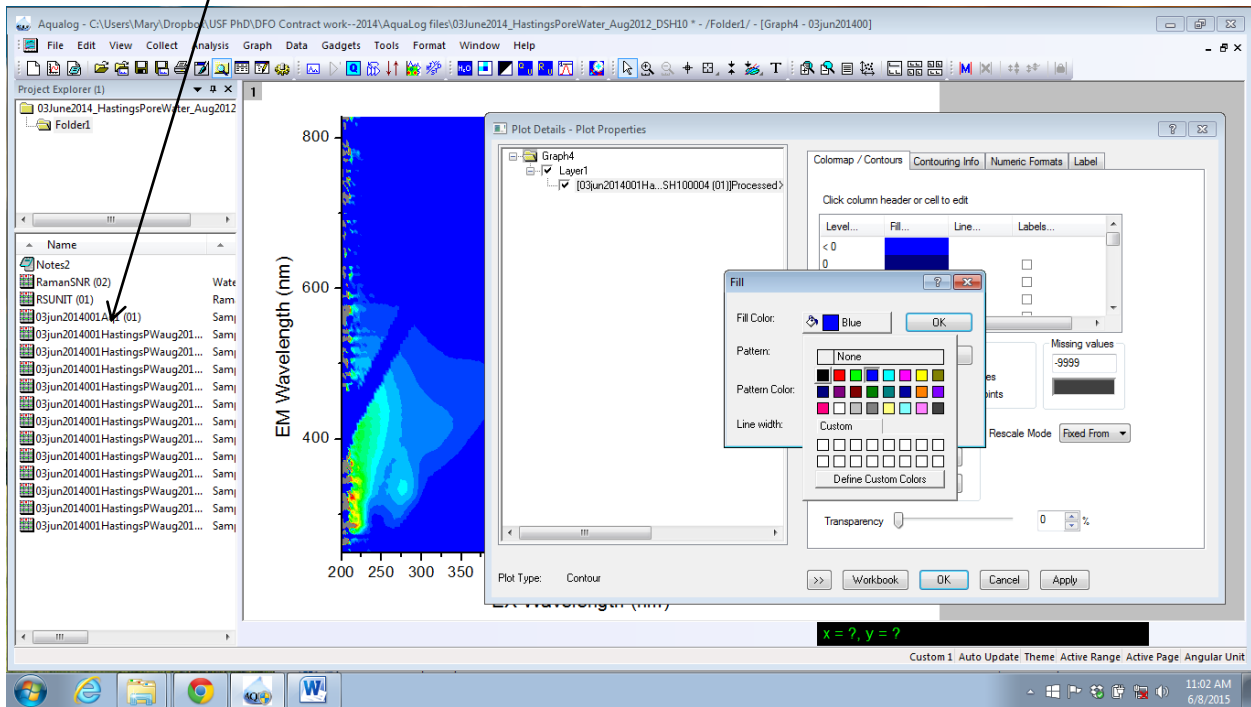


'Plot Details' now looks like this:

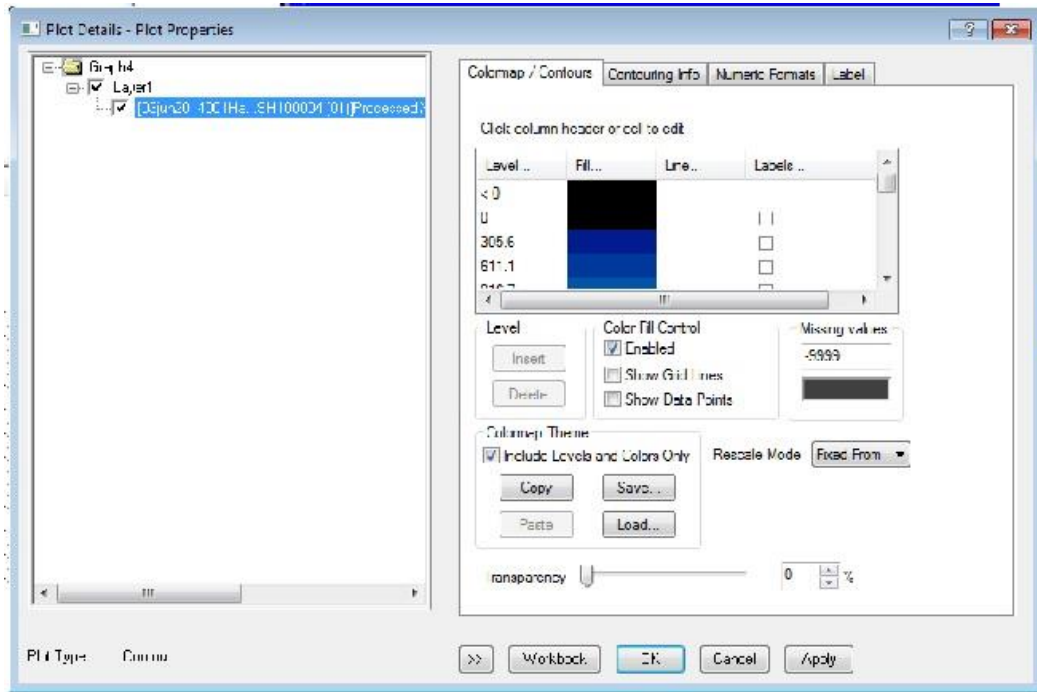


Click on blue bar next to '0'.

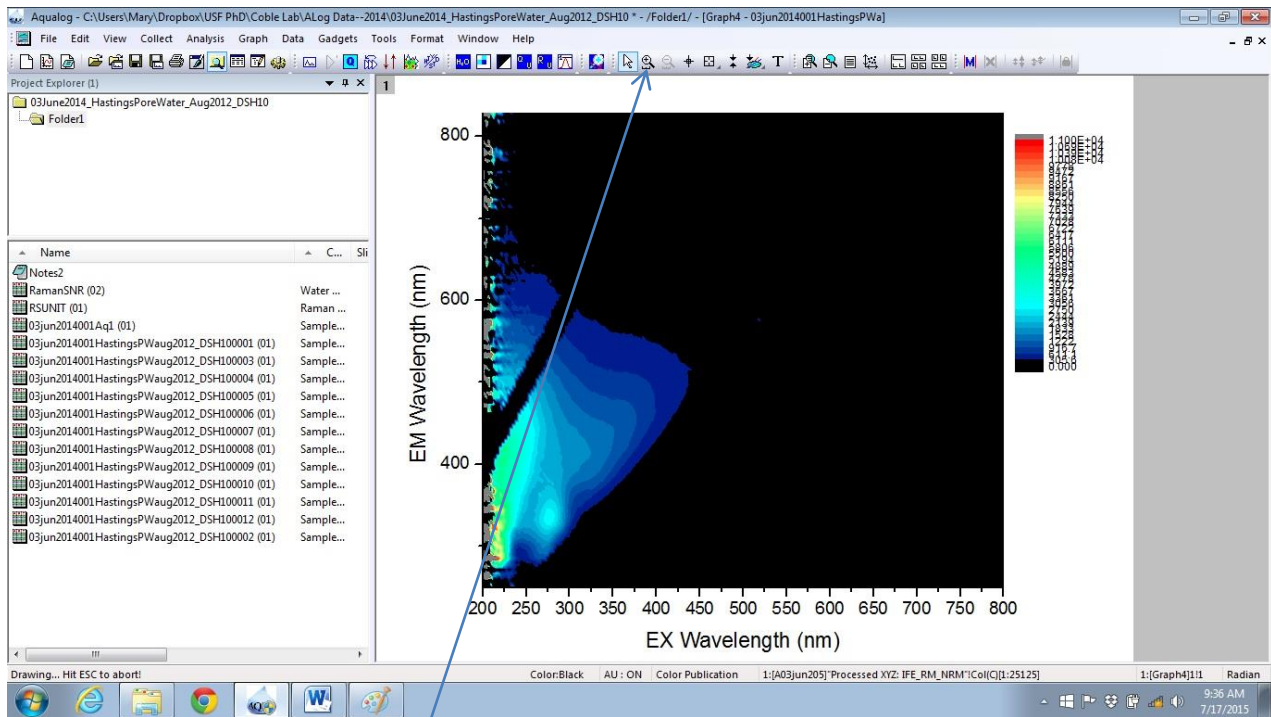
In 'Fill' box, click on 'Blue', then select 'Black' square (1st box, 1st row). Click 'OK'.





Plot Details' now looks like this:




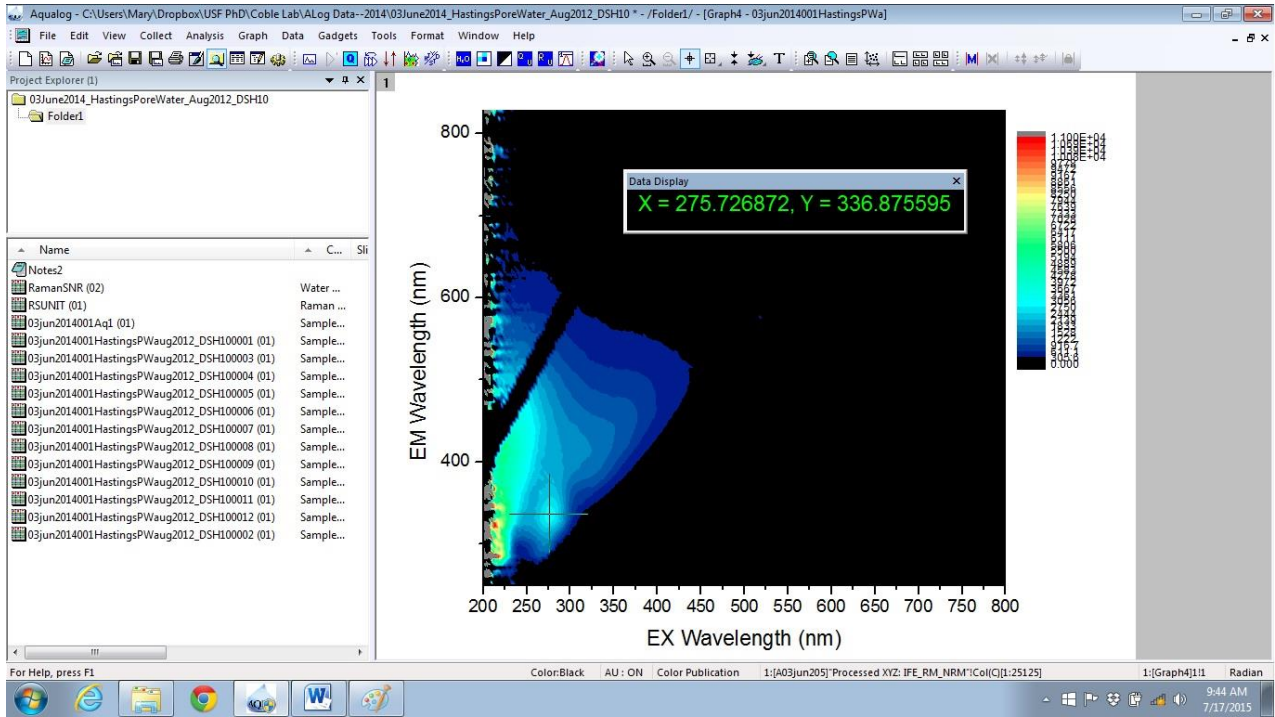
Click 'OK', 'OK' to get back to the main image processing window, which will now look like this:



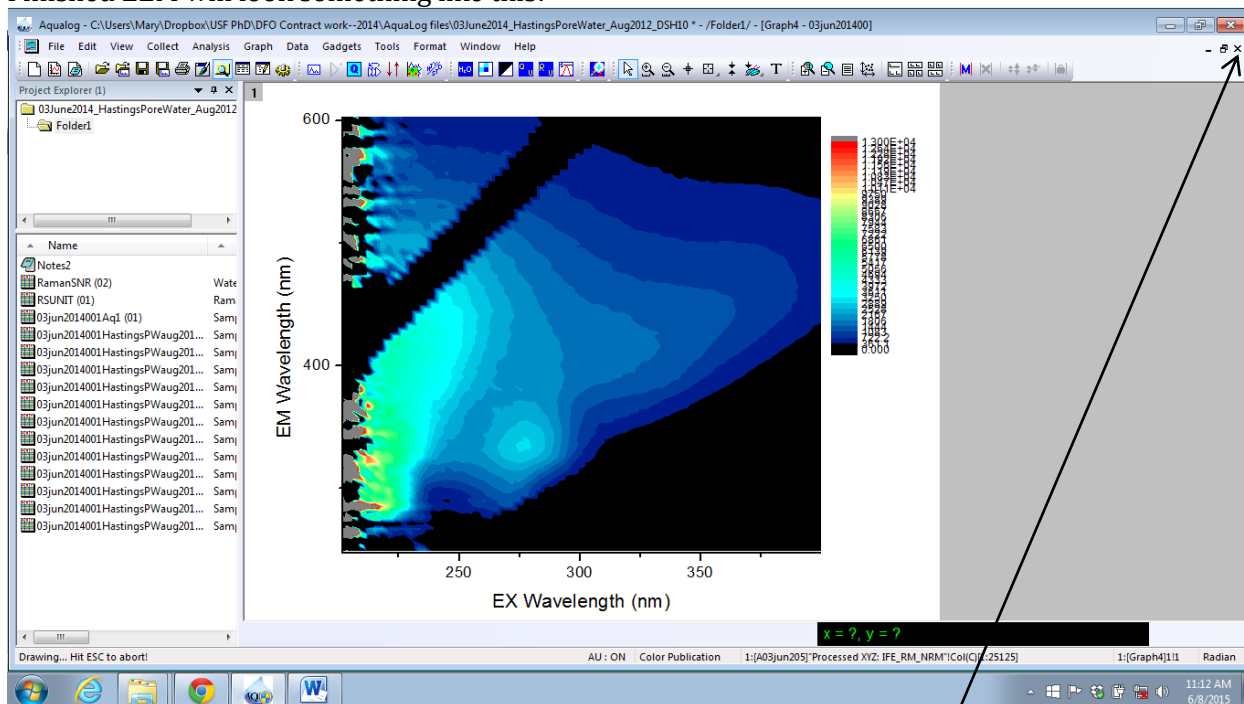
At this point, the zoom in  tool can be used to crop the contour plot for better resolution.

The zoom out  tool can then be used to zoom out again to the previous view. Repeat this process as many times as you'd like until you have the view you want to save.

While the image processing window is active, you can also click on the Screen Reader tool  and then anywhere in the active window to determine exact excitation/emission coordinates of any features of interest.



Finished EEM will look something like this:




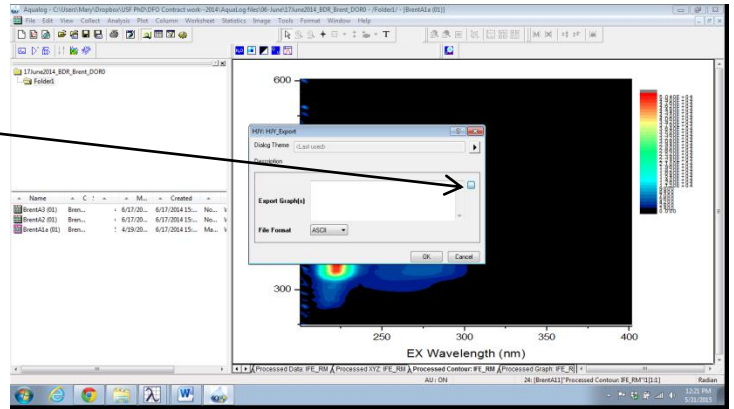
Note: Since the emission correction is quite high at low excitation wavelengths (to compensate for low lamp intensity in this region), it may be necessary to disregard apparent high-level fluorescence which is in fact “noise,” especially in samples with low fluorophore concentration.

When satisfied with processing, X out of the image processing window.

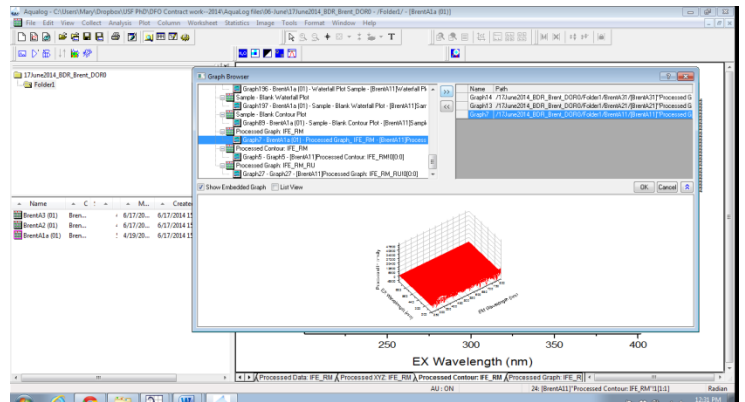
IMPORTANT: Once you close the image processing window, you CANNOT reopen and zoom back out to the full EEM contour plot. You can, however, select the Sample – Blank Waterfall Plot tab and then reapply the IFE and Rayleigh Masking Tools. This will re-create the original ‘Processed Contour:IFE_RM’ which you will then have to reprocess.

Save Project and Export .dat files after every 5-6 samples:
 From dropdown menu, select File → HJY Export.

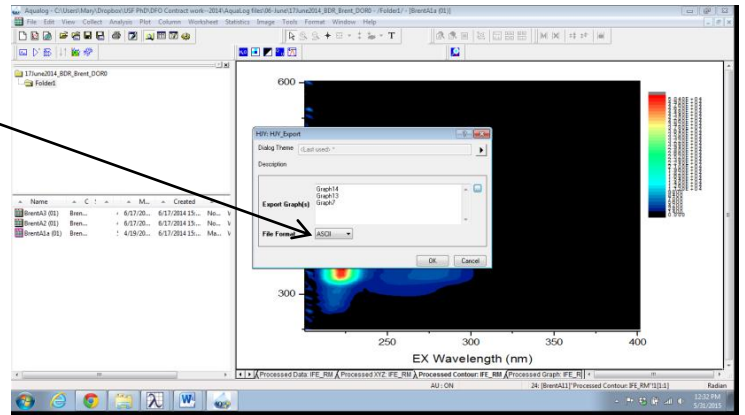
Click  to select files for export.



Highlight each 'Graph# - filename (01) - Processed Graph_IFE_RM', then click >> to copy file to the right.
 Repeat for each sample in this file.
 Click 'OK'.



Be sure File Format ASCII is selected.
 Click 'OK'.



Select file location for exporting. Click 'OK'.
 Close Script Window when export is complete.
 Close Project.


Exported .dat files can then be imported directly into Solo software and/or MATLAB for PARAFAC modelling.

To report fluorescence max/CDOM concentration:

For reporting in Raman Units (RU), double-click on the appropriate RSUNIT graph, either in the 'Test' project for the day or within the appropriate sample project. Click on the 'RSU_Adjust' tab. In the 'Integration Time' column, replace '1' in the first row with the integration time used for the sample of interest. Copy the resulting data which appears in the 'RSU_Adjust' column, 'Area' row. This factor will be used to put sample results in RU. You may choose to paste this data into an Excel spreadsheet to track RSU for each day and/or group of samples.

To convert sample raw intensity counts to RU, open the project file open, double-click the appropriate sample file, then click on the 'Processed Graph: IFE_RM' tab. From the menu bar choose 'Analysis → Aqualog Analysis Tools → Simple Math Menu.' Select 'Math Function: Divide' and 'Operand: Constant'. Copy Raman Unit factor from the RSUNIT file (or from the Excel file) and paste into the 'Constant' box. Be sure 'Keep Source Graphs' is checked, then click 'OK.' Processing will add 2 tabs to the project: 'Processed Graph: IFE_2' and 'Processed Data: IFE_2'; double-clicking each tab allows renaming (e.g., 'Processed Graph: IFE_RM_RU' and 'Processed Data: IFE_M_RU'). Data can then be exported as a .dat file or copied and pasted into Excel. Unfortunately, there's no way to generate a new Processed Contour with RU in the Aqualog software, however.

To export a processed EEM image:

Click on File → Export → As Image File. Choose appropriate image type from dropdown list (.jpg, .png, etc.) and click on  to the right of 'File Name(s)' dropdown box to choose a location and input file name. Click 'Save', then 'OK'. X to close unnecessary 'Script Window' which appears.

An Important Caveat

Fluorescence results are valid only when absorbance is ≤ 0.6 . If 0.1 sec integration time results in $> 65,535$ counts, absorbance may be too high. Check the sample absorbance on 'Abs Spectra Graphs' tab. If absorbance is > 0.6 , sample must be diluted and run again.

And a Note on Clean-up

Cuvettes should be cleaned with appropriate solvent(s) according to fluorophores present in the sample(s). For samples containing petroleum, cuvettes should be rinsed 3x with DCM, then 3x with methanol. For samples containing CDOM and/or proteins, rinsing 3x with methanol should be sufficient. Cuvettes should then be allowed to air dry and rinsed thoroughly before reuse as solvent residue may affect fluorescence.

APPENDIX D
EEM CONTOUR PLOTS

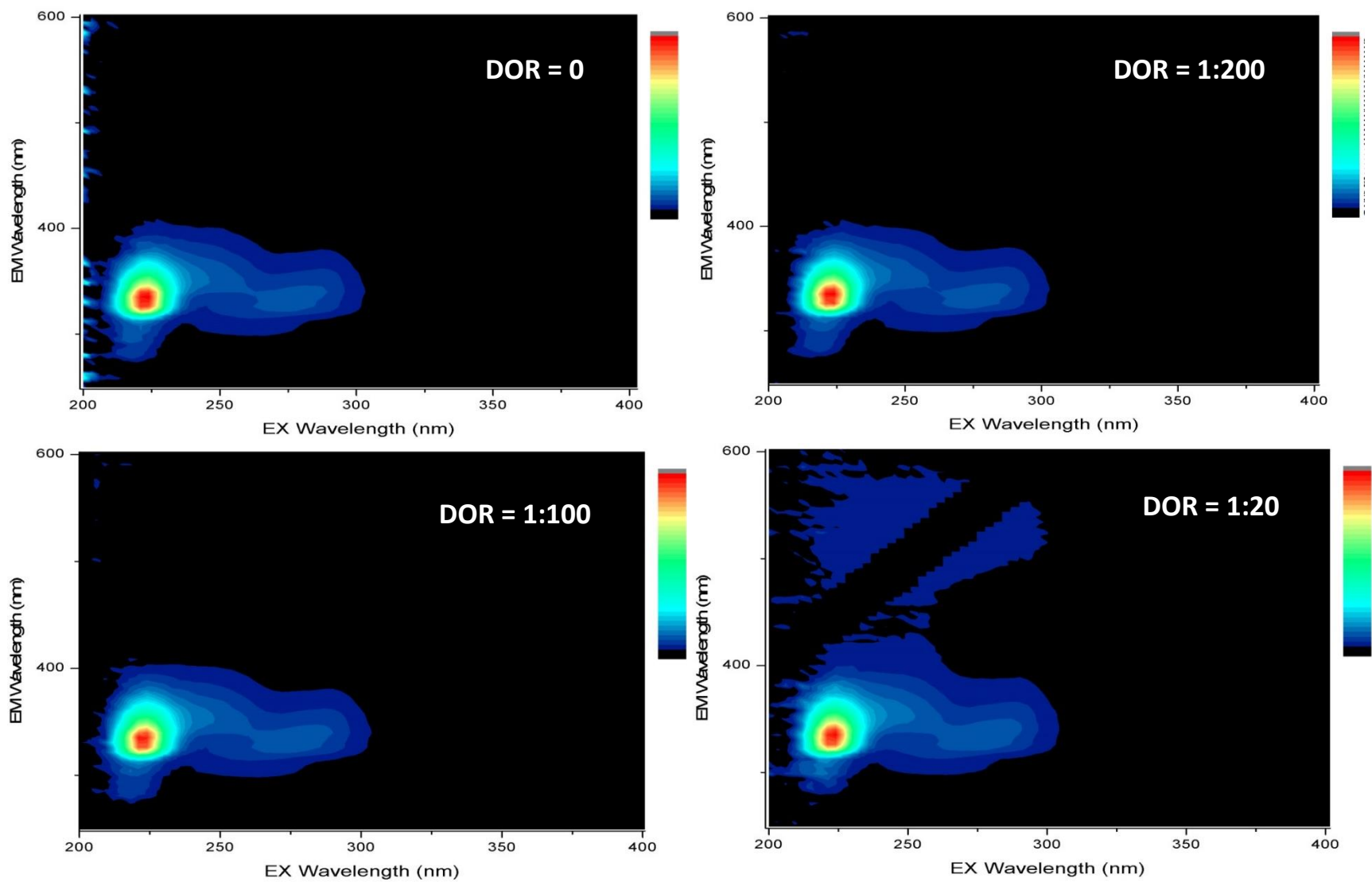


Figure D.1. Light Oil Category – IFO-40 oil with dispersant EEMs. Colored contours represent intensity, scaled to maximum fluorescence peak (red).

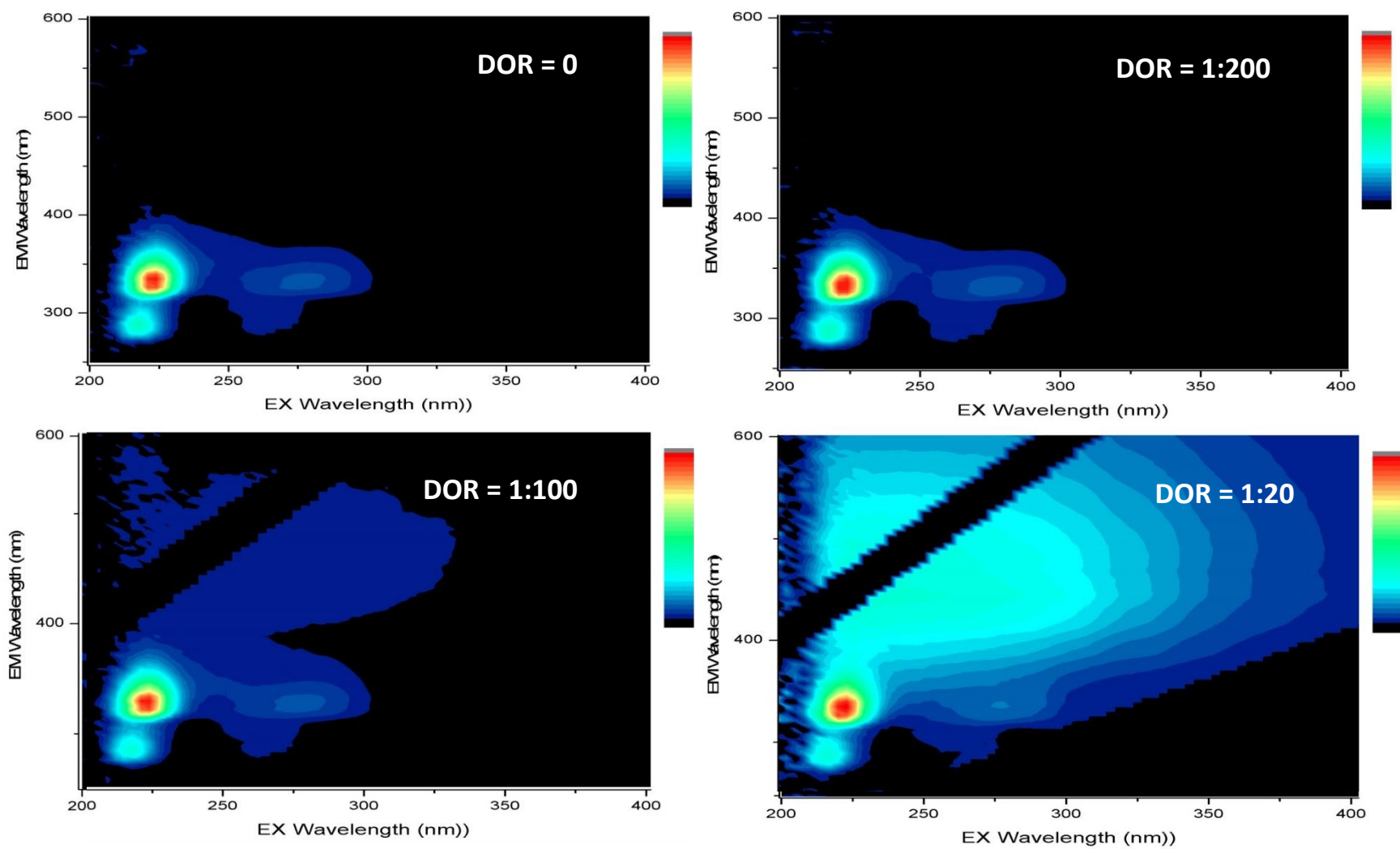


Figure D.2. Light Oil Category – Arabian Light crude oil with dispersant EEMs. Colored contours represent intensity, scaled to maximum fluorescence peak (red).

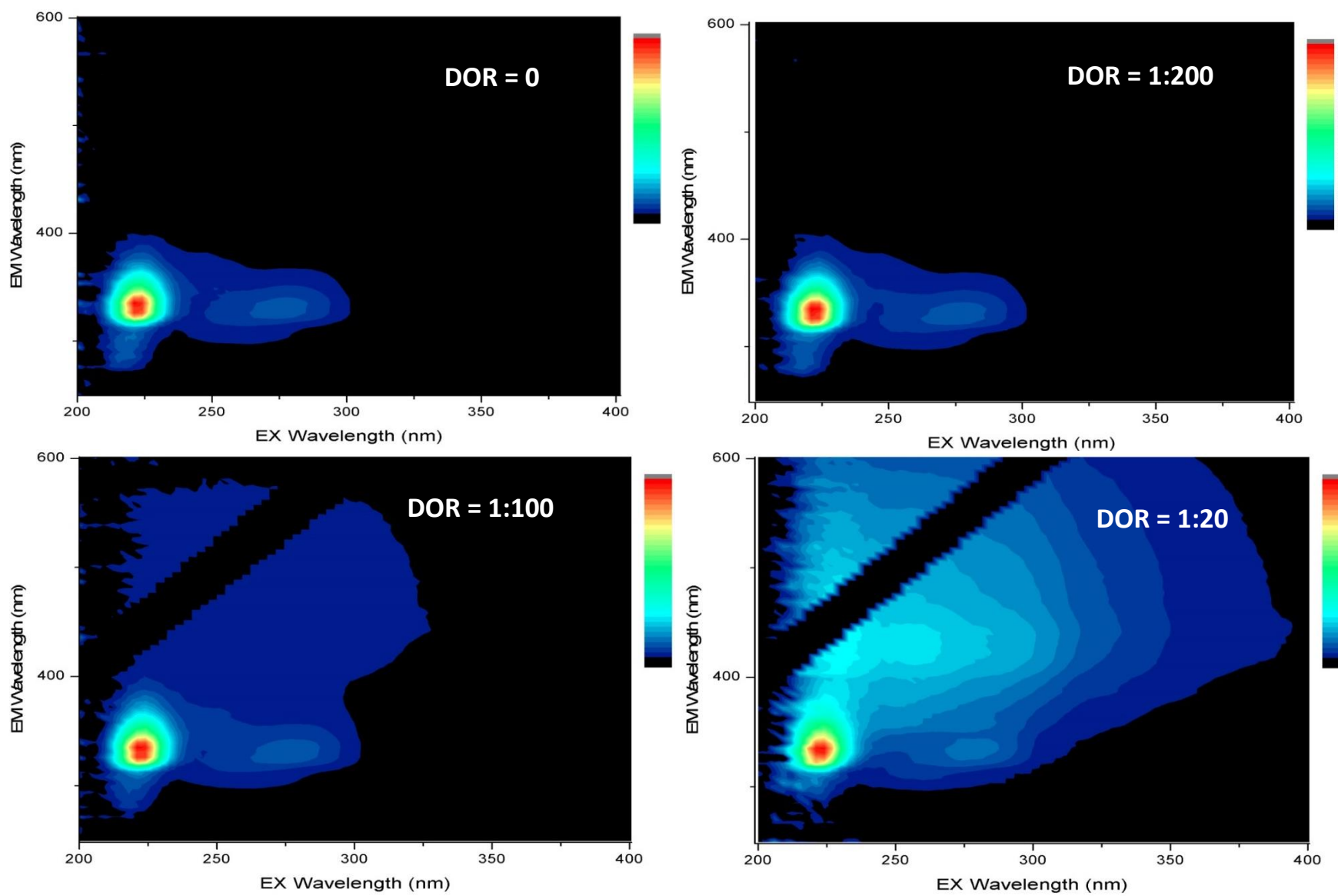


Figure D.3. Light Oil Category – Brent crude oil with dispersant EEMs. Colored contours represent intensity, scaled to maximum fluorescence peak (red).

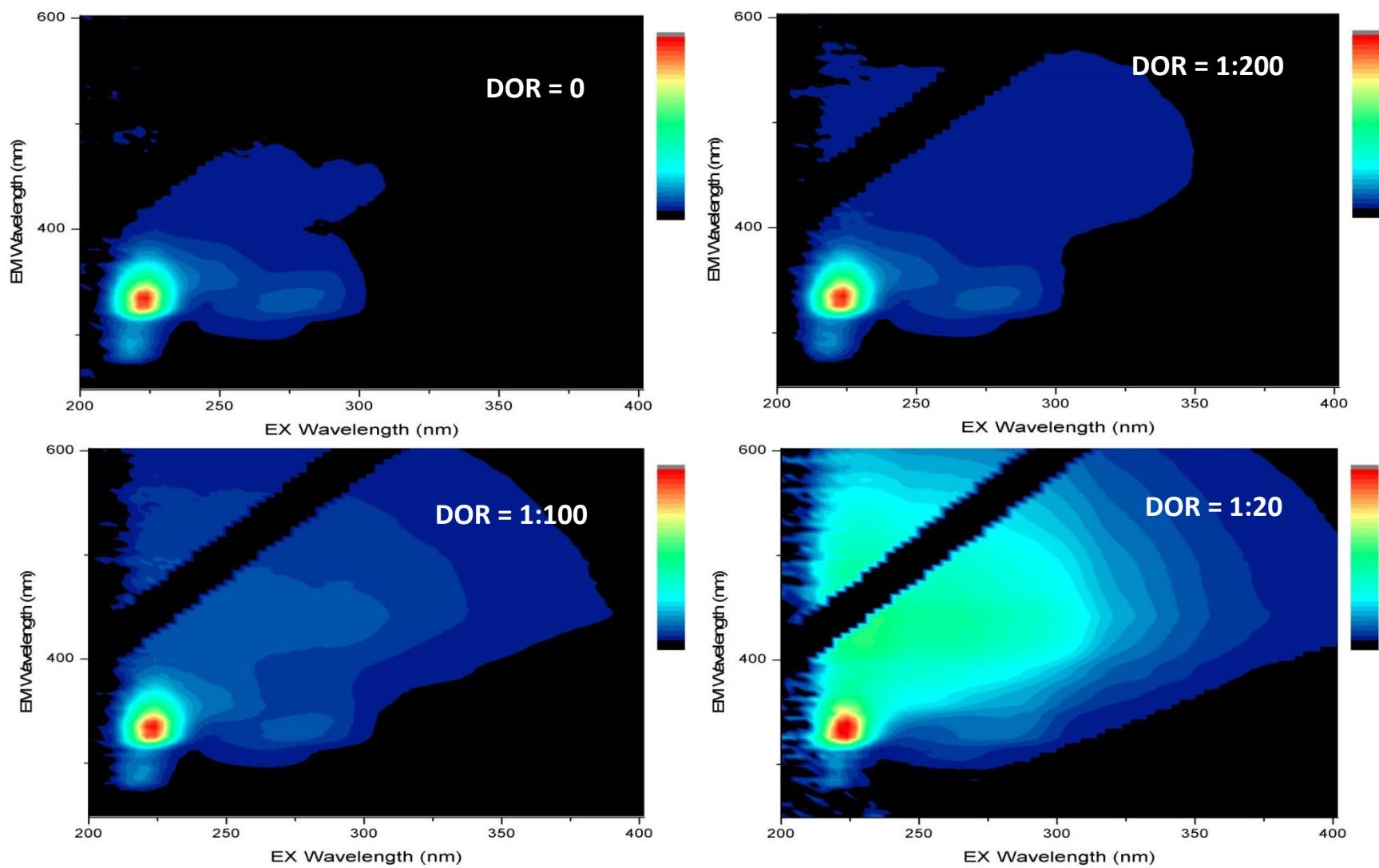


Figure D.4. Light Oil Category – Federated crude oil with dispersant EEMs. Colored contours represent intensity, scaled to maximum fluorescence peak (red).

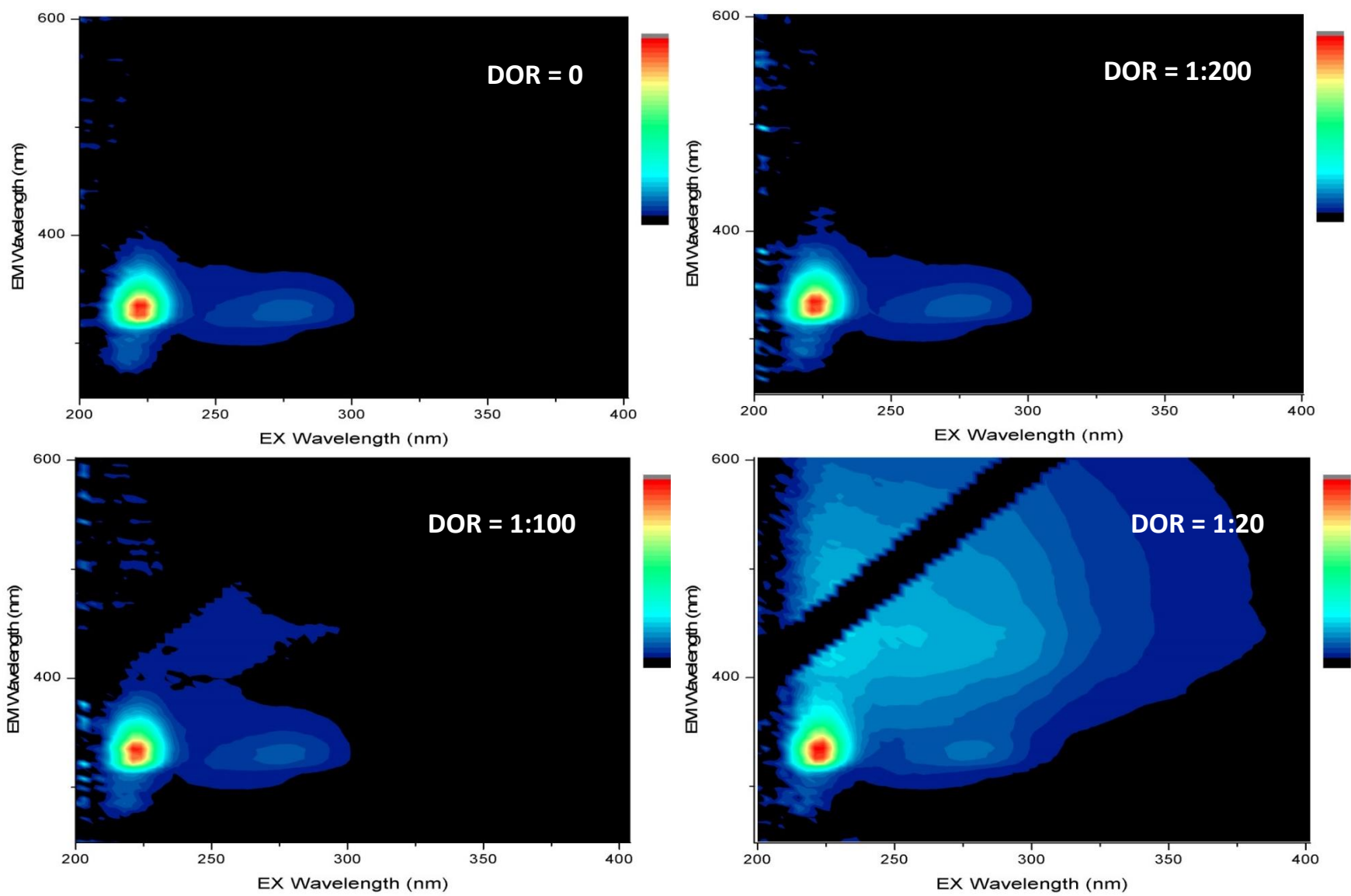


Figure D.5. Light Oil Category – Gullfaks crude oil with dispersant EEMs. Colored contours represent intensity, scaled to maximum fluorescence peak (red).

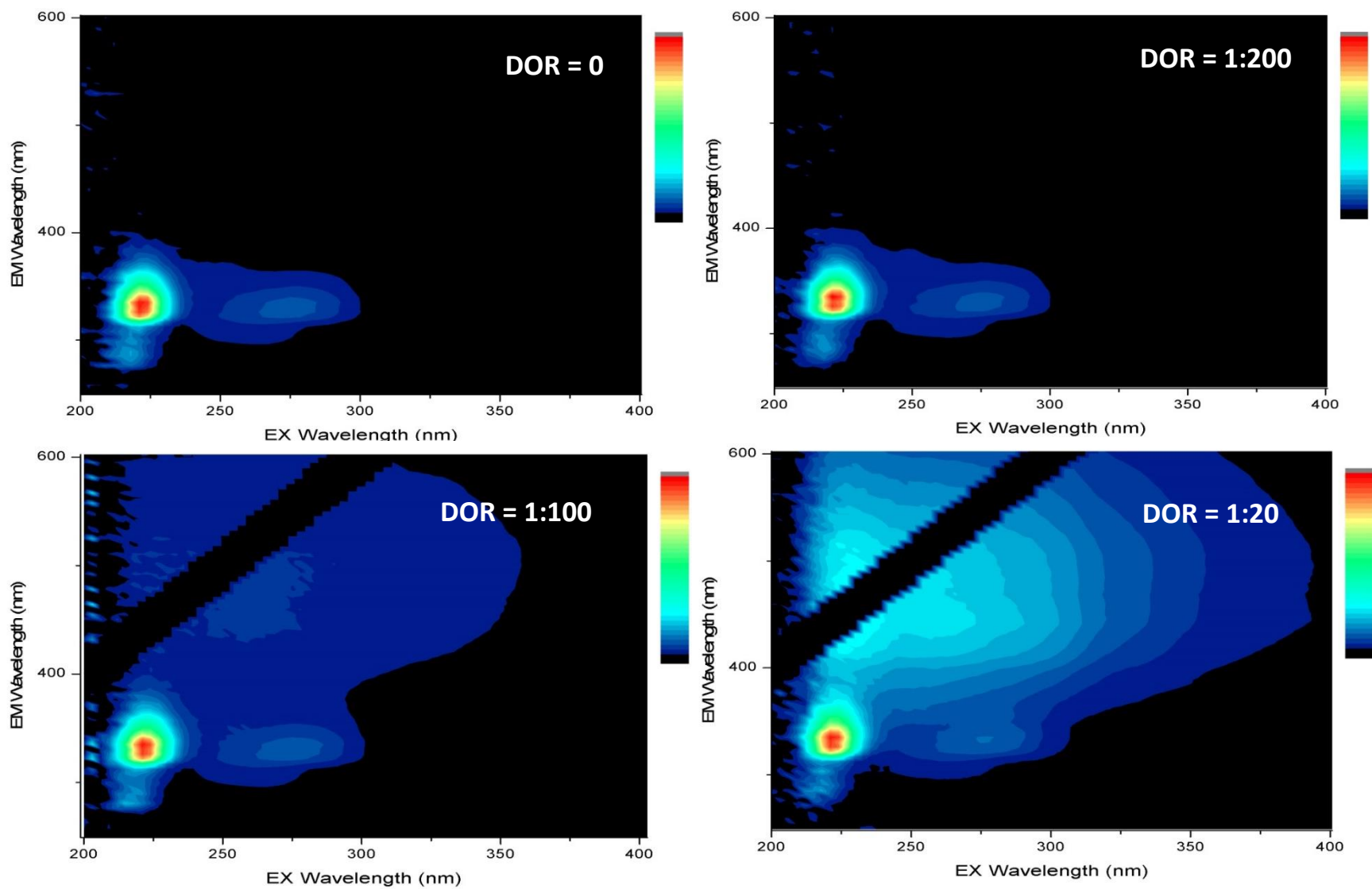


Figure D.6. Light Oil Category – Hibernia crude oil with dispersant EEMs. Colored contours represent intensity, scaled to maximum fluorescence peak (red).

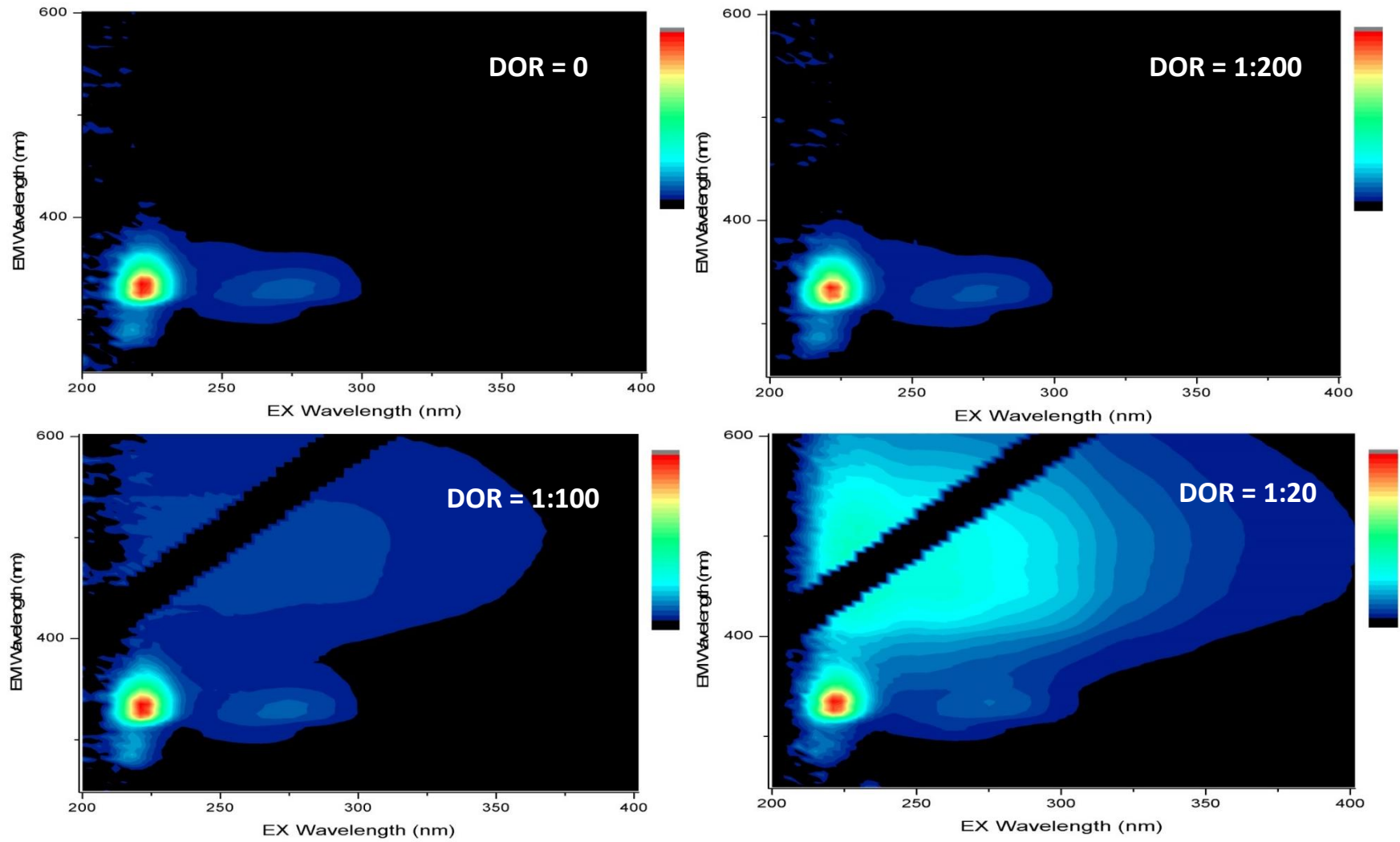


Figure D.7. Light Oil Category – MC252 (Discoverer Enterprise) crude oil with dispersant EEMs. Colored contours represent intensity, scaled to maximum fluorescence peak (red).

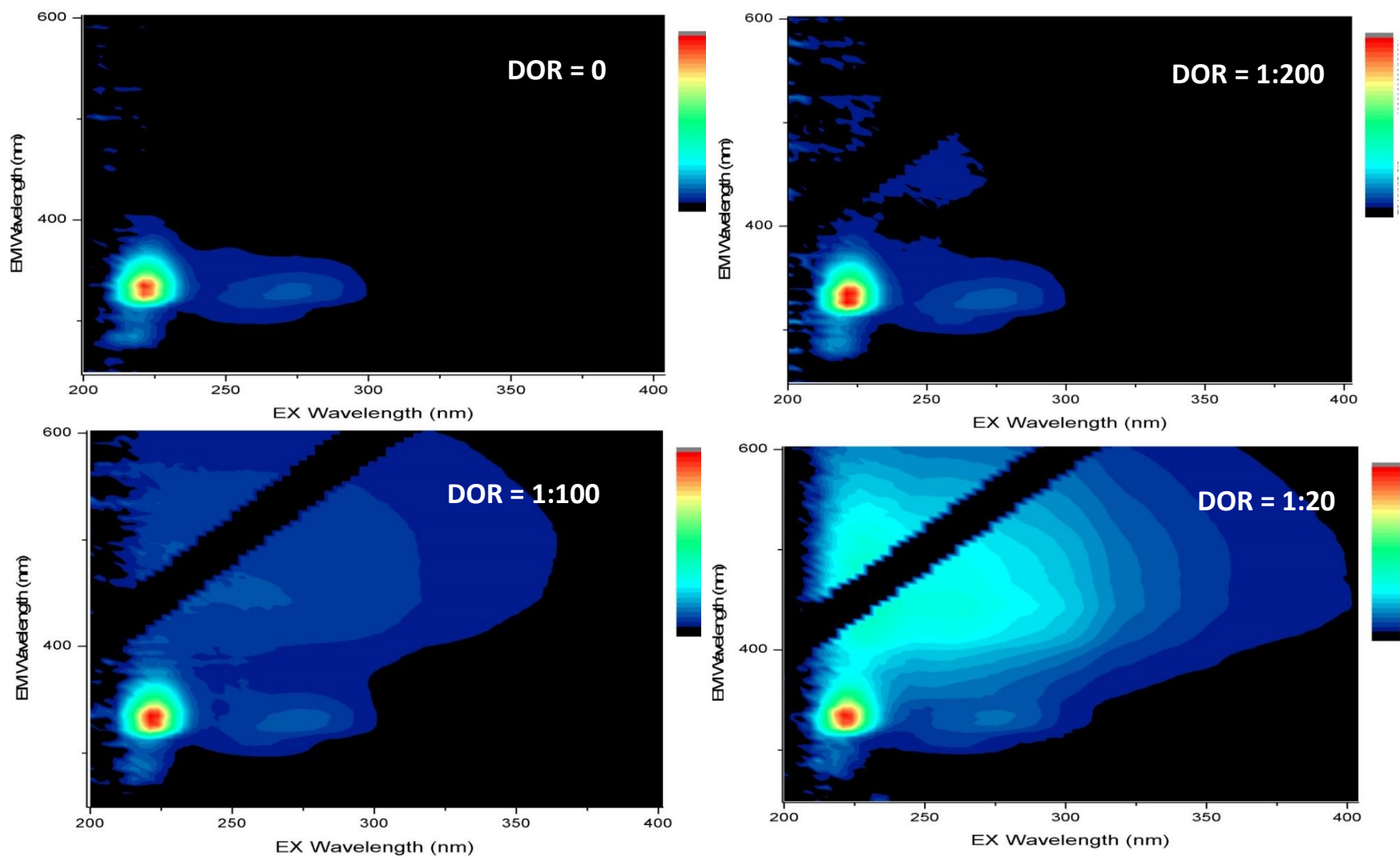


Figure D.8. Light Oil Category – MC252 (Generic) crude oil with dispersant EEMs. Colored contours represent intensity, scaled to maximum fluorescence peak (red).

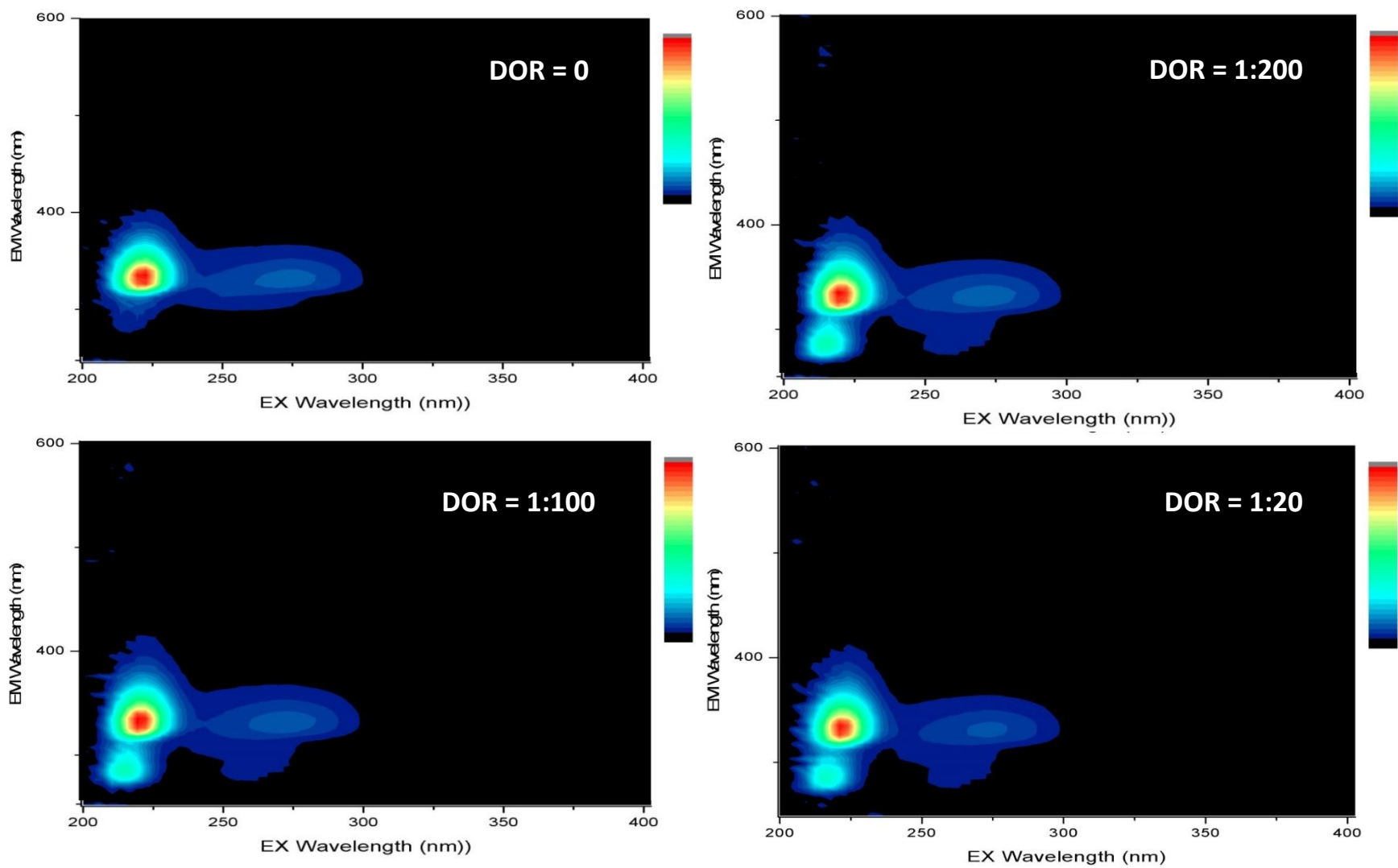


Figure D.9. Light Oil Category – Scotian Shelf Condensate crude oil with dispersant EEMs. Colored contours represent intensity, scaled to maximum fluorescence peak (red).

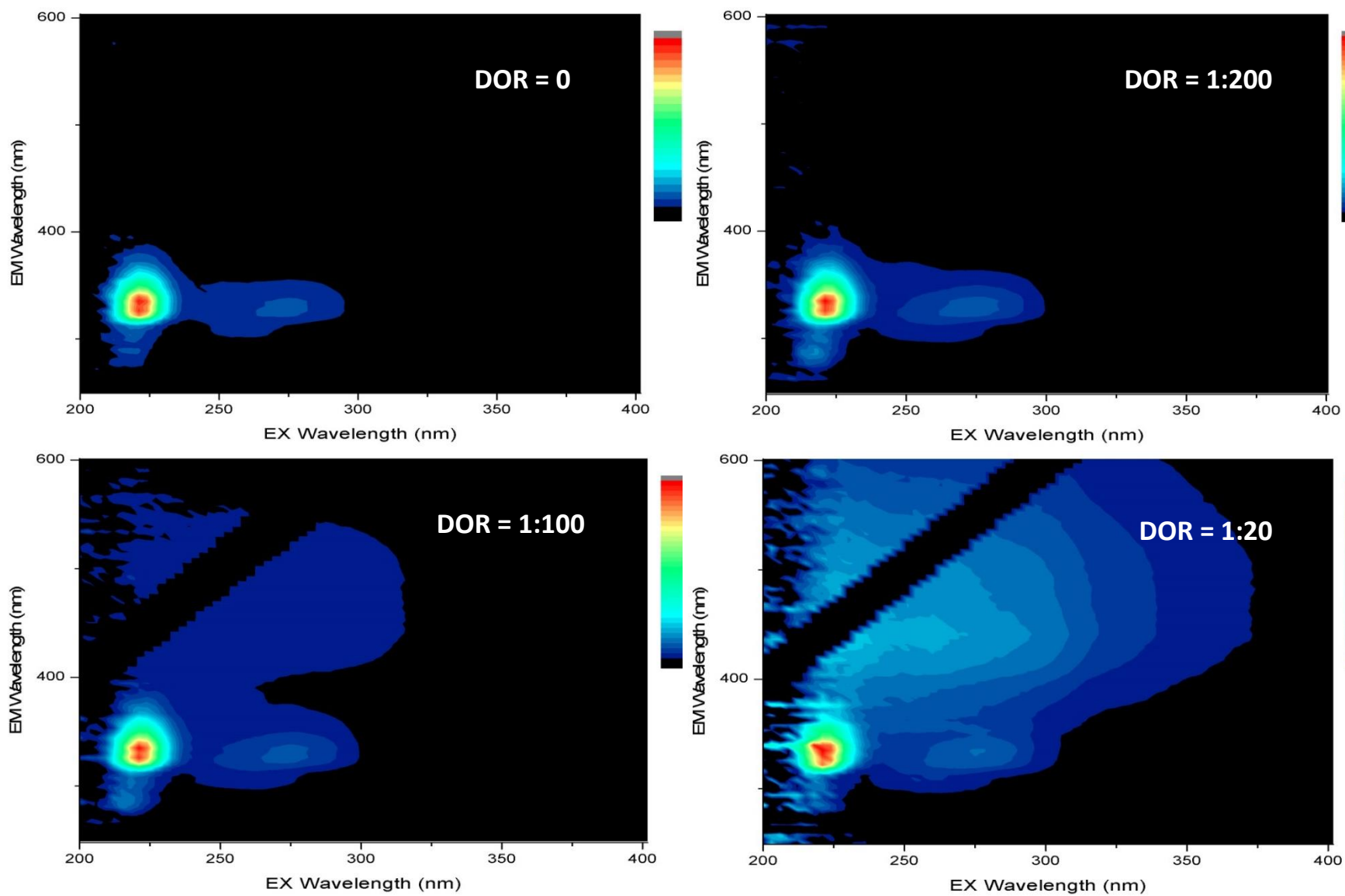


Figure D.10. Light Oil Category – Sea Rose crude oil with dispersant EEMs. Colored contours represent intensity, scaled to maximum fluorescence peak (red).

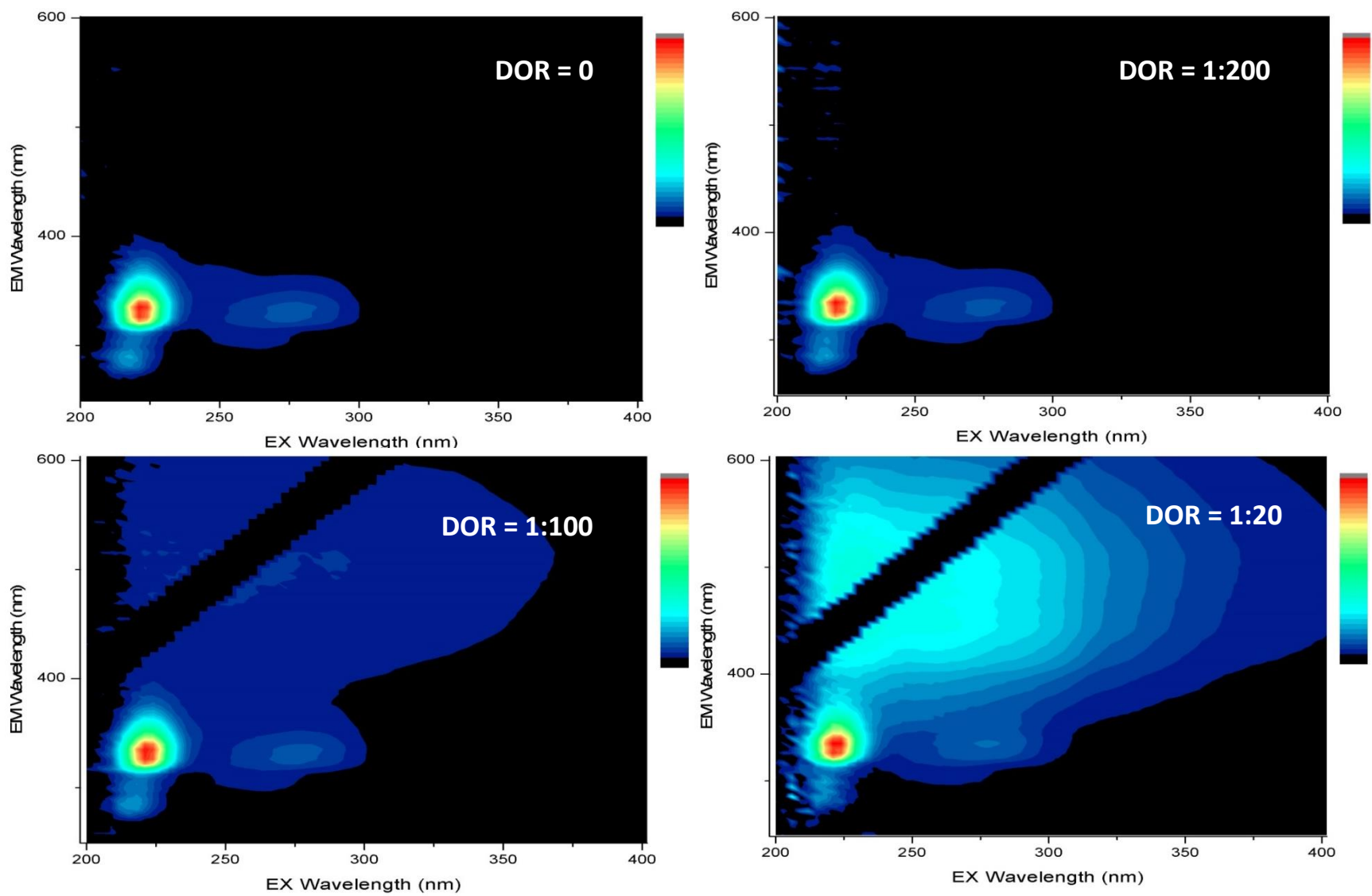


Figure D.11. Light Oil Category – Terra Nova crude oil with dispersant EEMs. Colored contours represent intensity, scaled to maximum fluorescent peak (red).

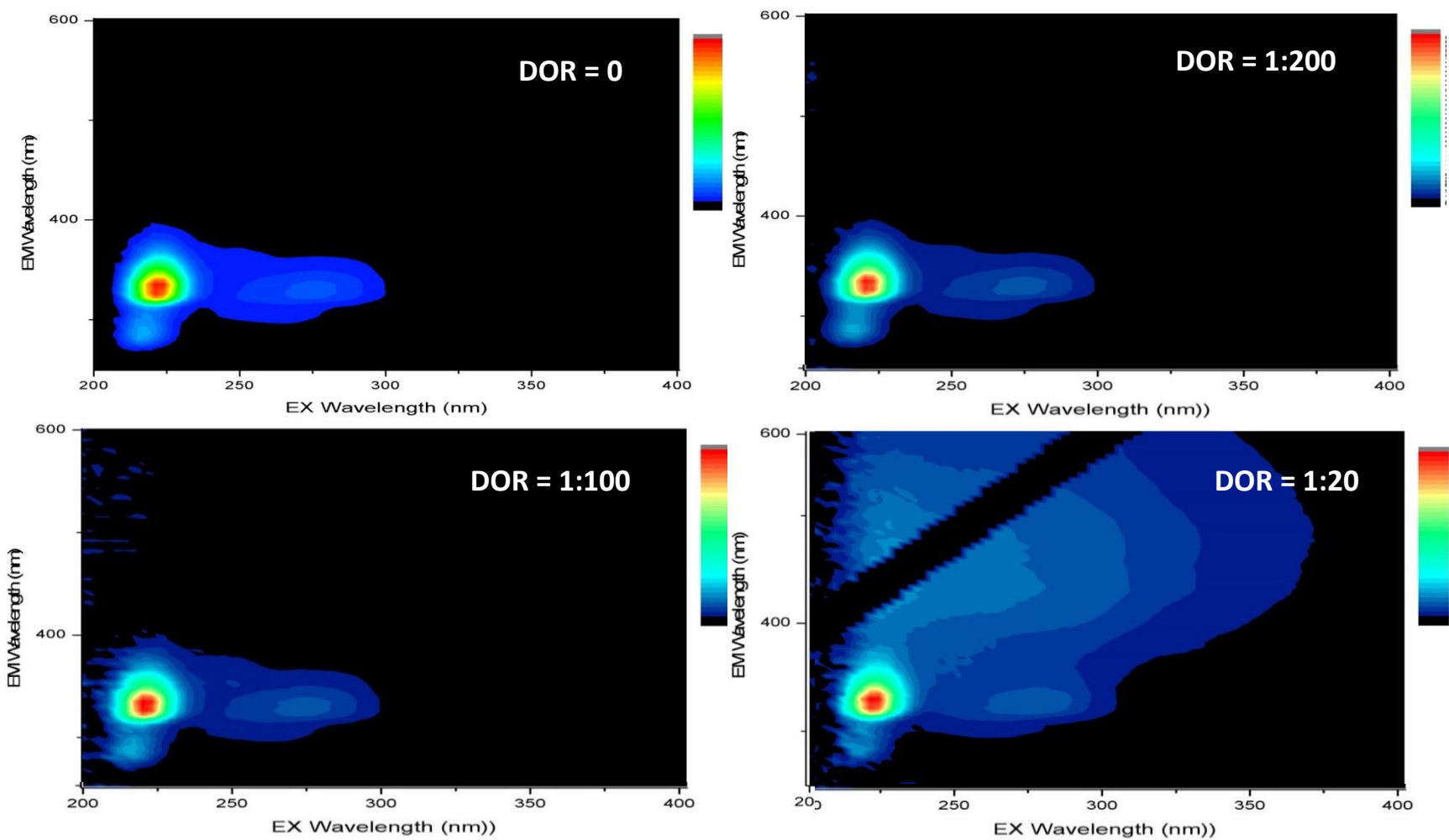


Figure D.12. Medium Oil Category – ANS (Alaskan North Slope) crude oil with dispersant EEMs. Colored contours represent intensity, scaled to maximum fluorescence peak (red).

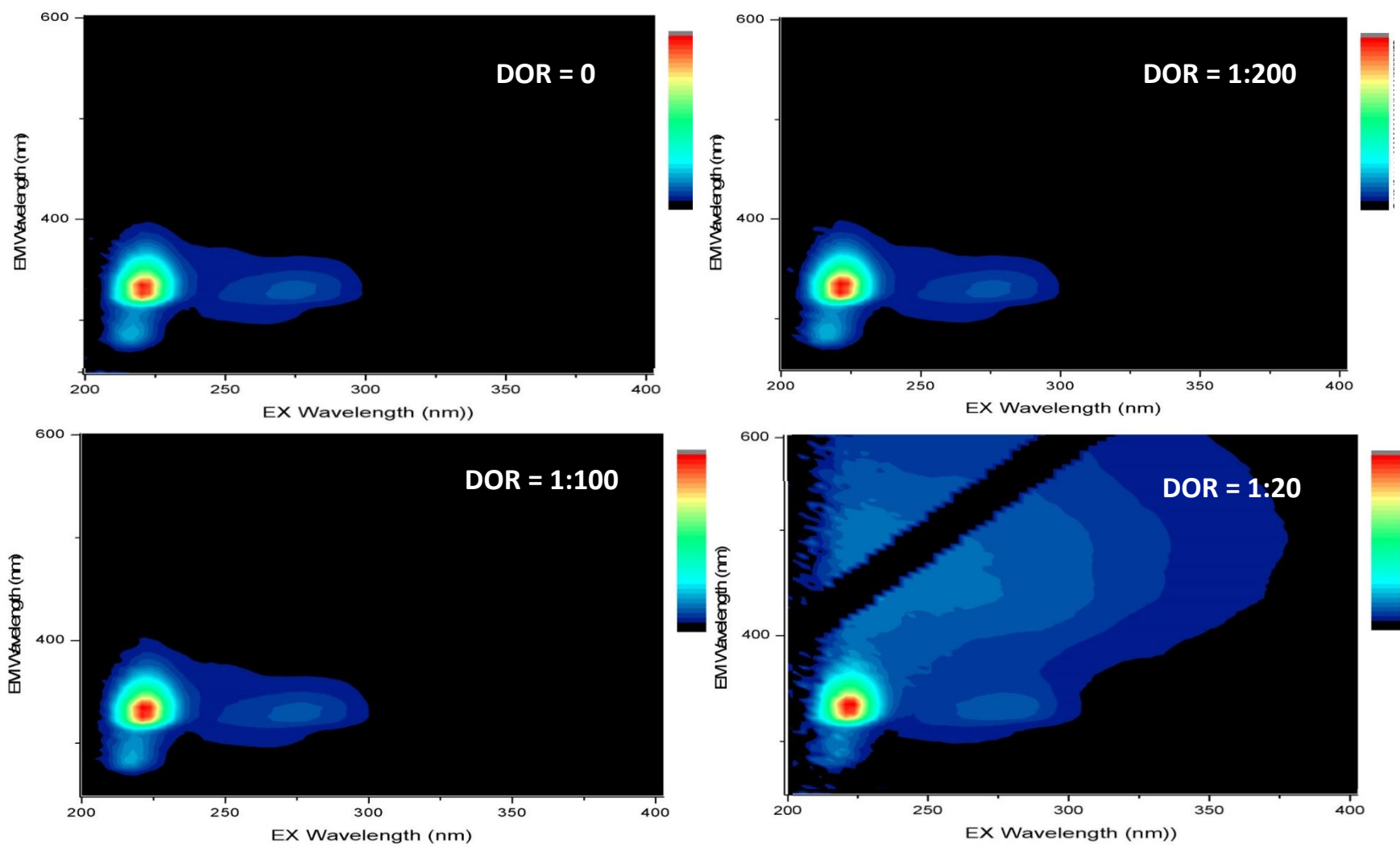


Figure D.13. Medium Oil Category - 10% Weathered ANS (Alaskan North Slope) crude oil with dispersant EEMs. Colored contours represent intensity, scaled to maximum fluorescence peak (red).

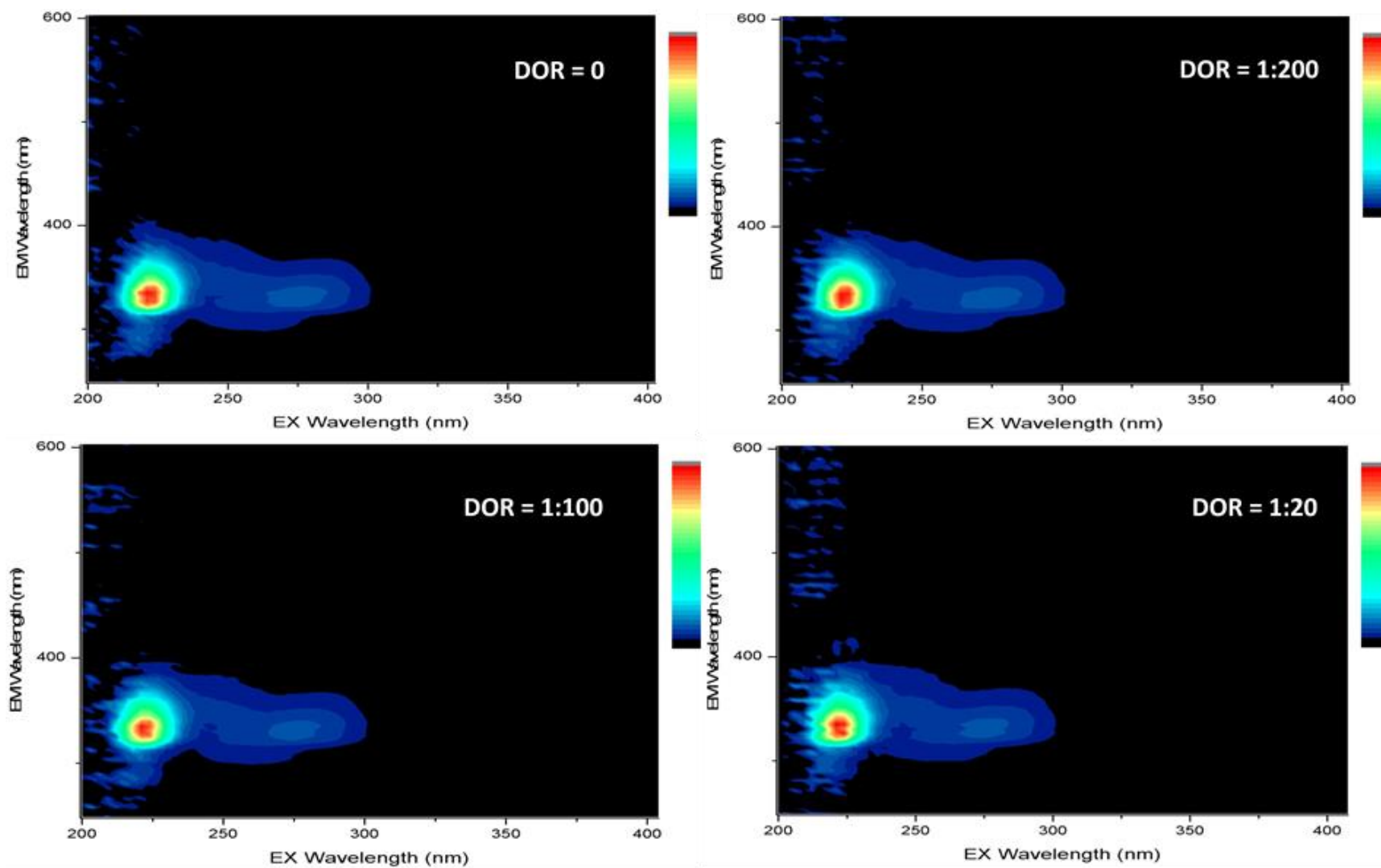


Figure D.14. Medium Oil Category – Heavy IFO-120 oil with dispersant EEMs. Colored contours represent intensity, scaled to maximum fluorescence peak (red).

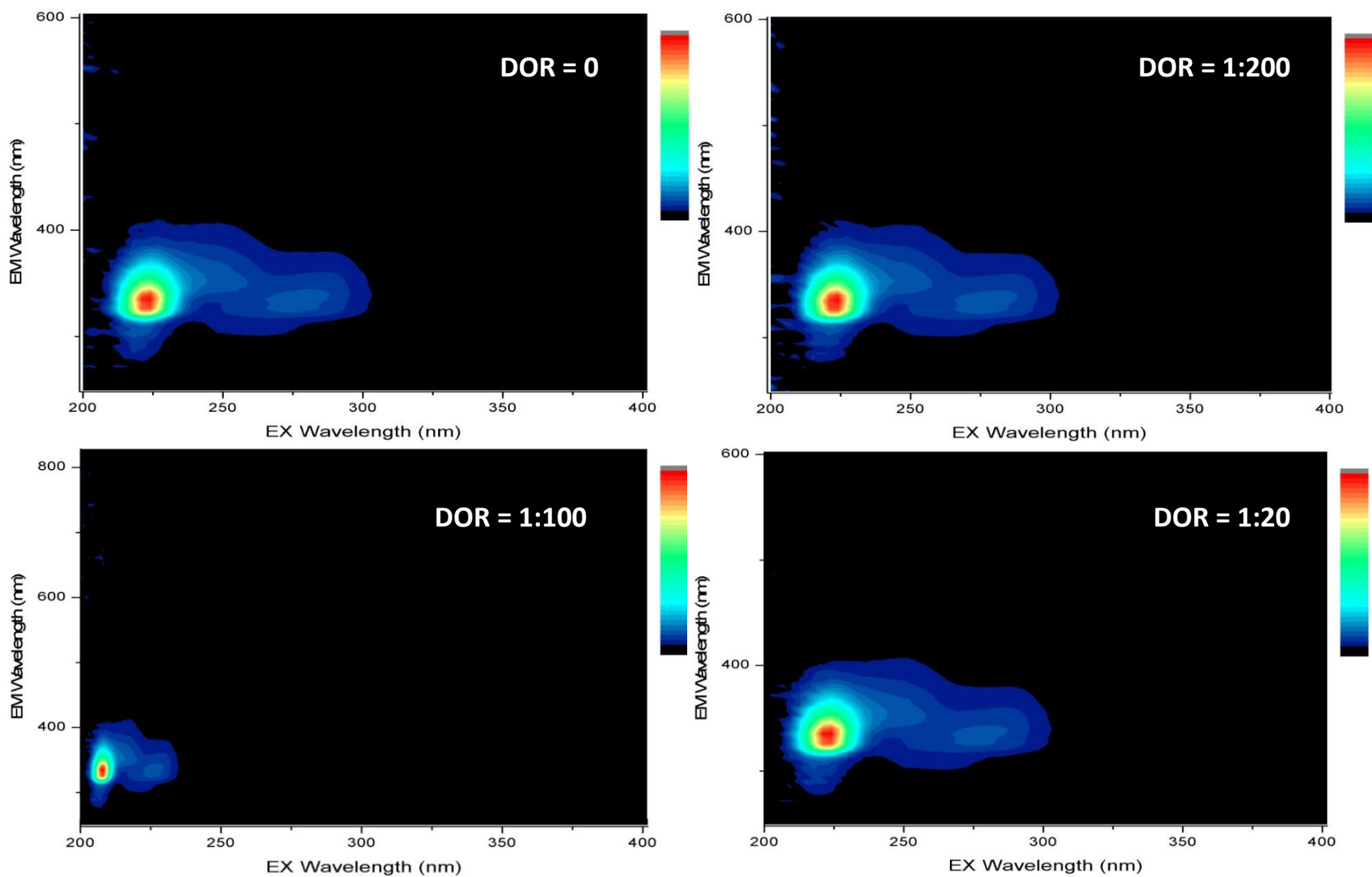


Figure D.15. Medium Oil Category - Heavy IFO-180 oil with dispersant EEMs. Colored contours represent intensity, scaled to maximum fluorescence peak (red).

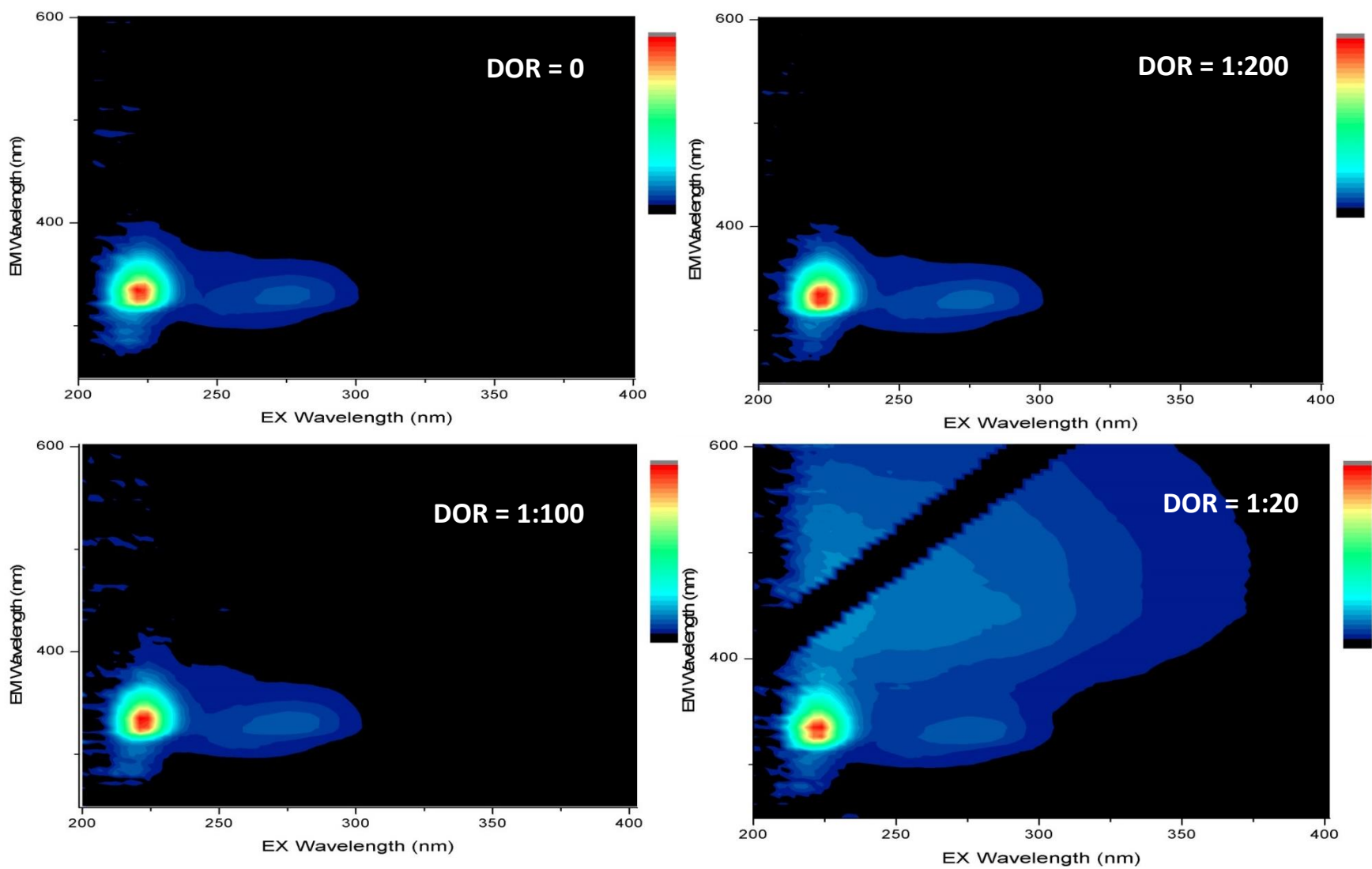


Figure D.16. Medium Oil Category – Heidrun crude oil with dispersant EEMs. Colored contours represent intensity, scaled to maximum fluorescence peak (red).

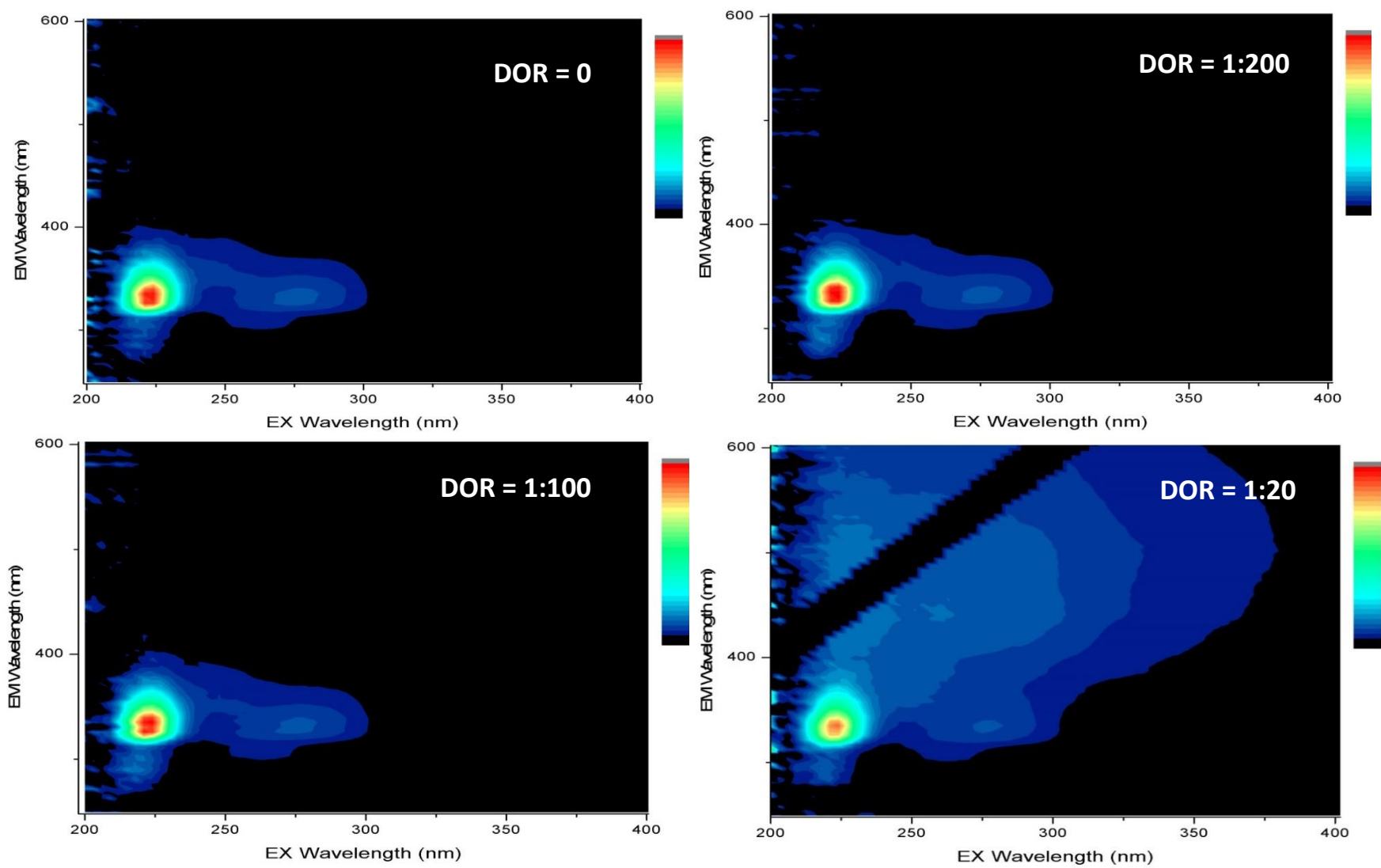


Figure D.17. Medium Oil Category – Lago crude oil with dispersant EEMs. Colored contours represent intensity, scaled to maximum fluorescence peak (red).

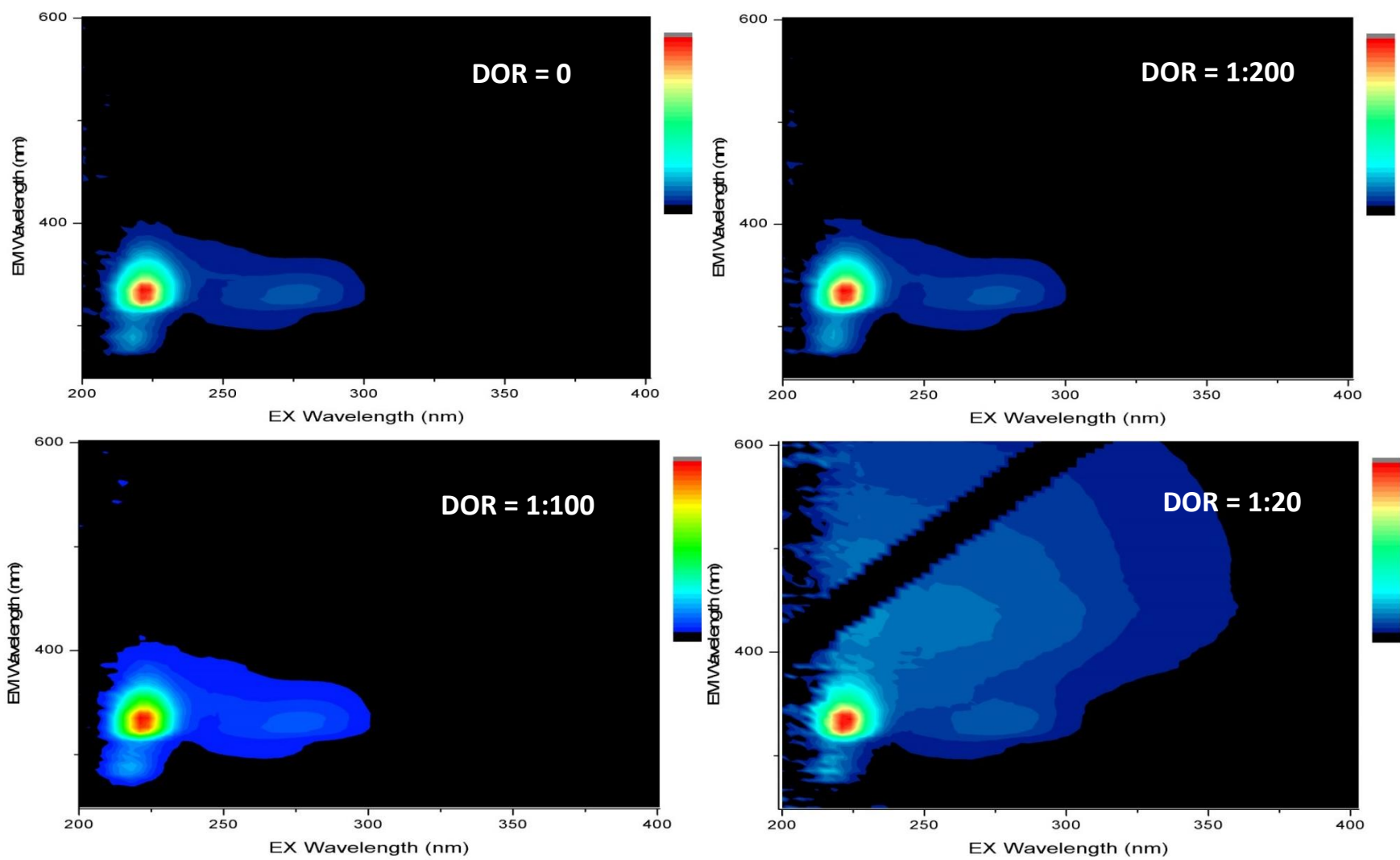


Figure D.18. Medium Oil Category – Mesa crude oil with dispersant EEMs. Colored contours represent intensity, scaled to maximum fluorescence peak (red).

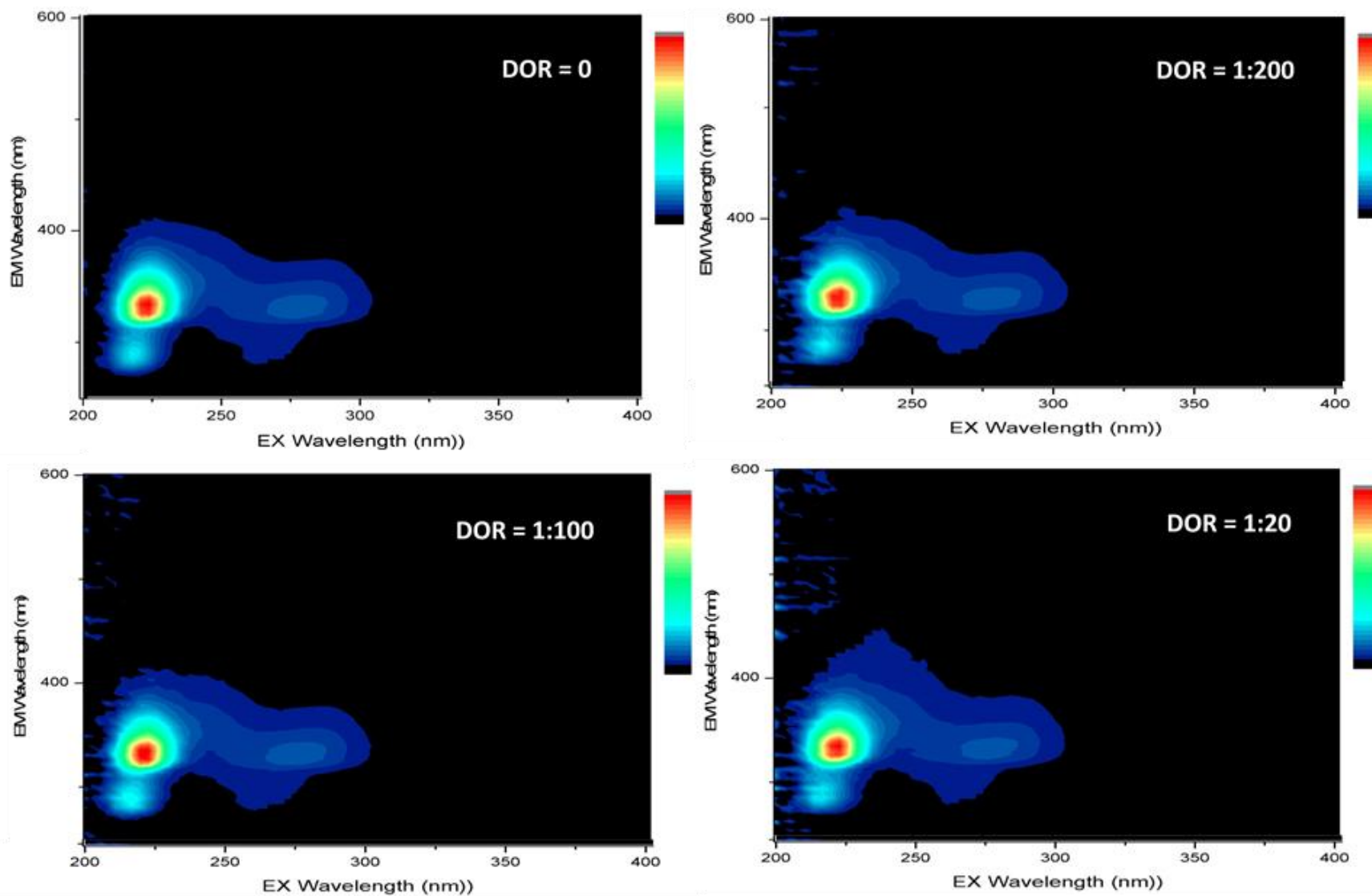


Figure D.19. Medium Oil Category – Santa Clara crude oil with dispersant EEMs. Colored contours represent intensity, scaled to maximum fluorescence peak (red).

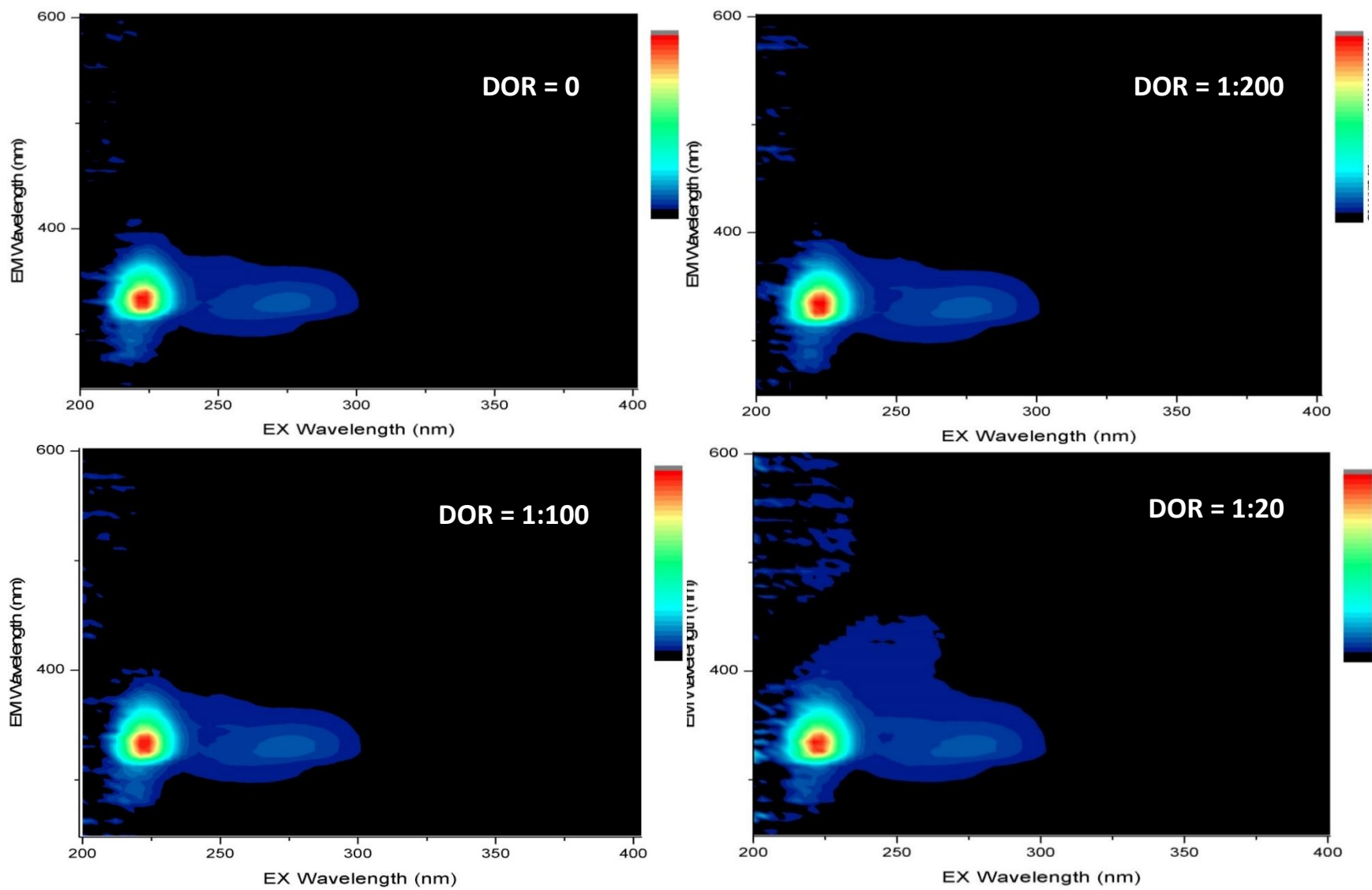


Figure D.20. Medium Oil Category – Vasconia crude oil with dispersant EEMs. Colored contours represent intensity, scaled to maximum fluorescence peak (red).

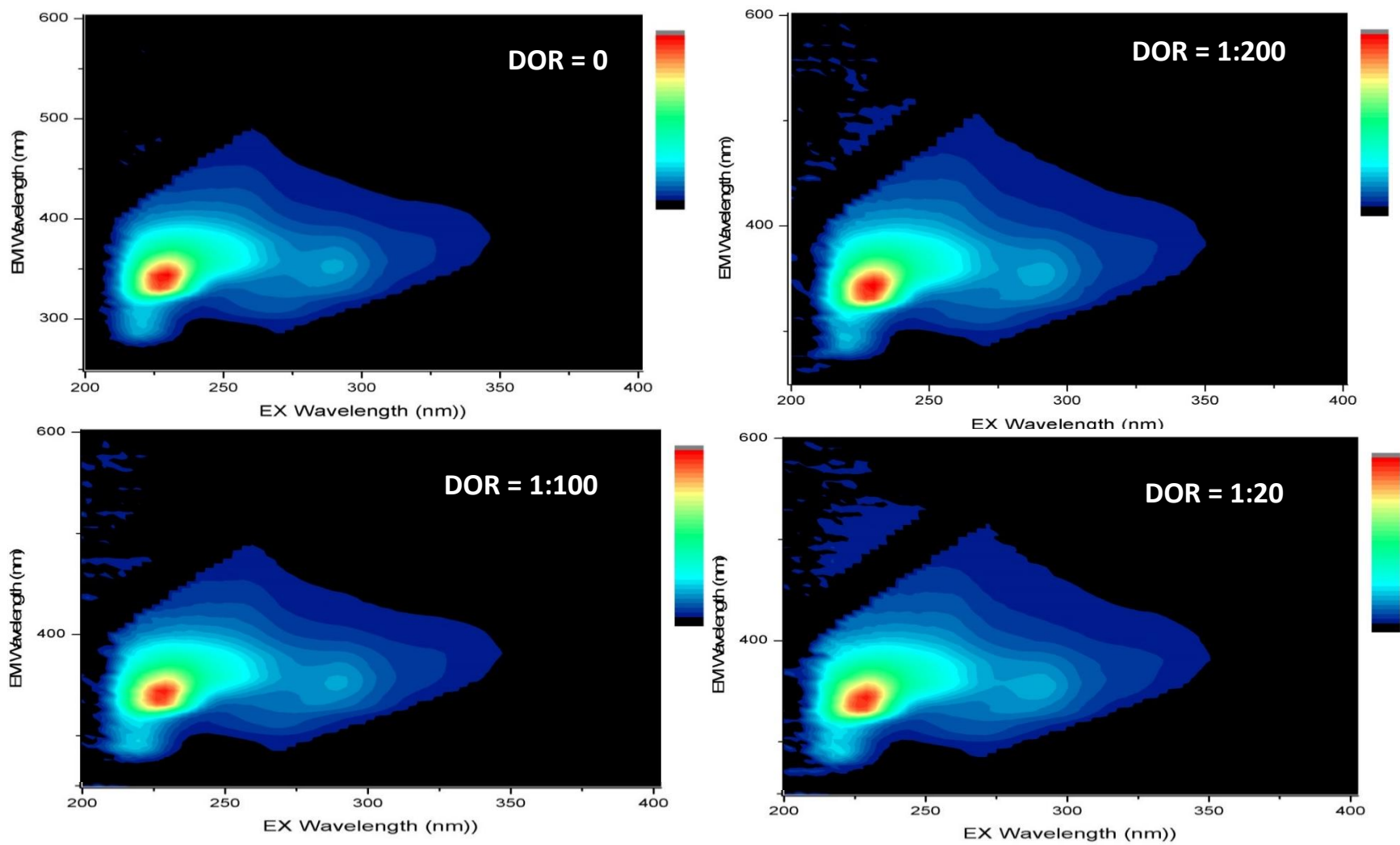


Figure D.21. Heavy Oil Category – Belridge crude oil with dispersant EEMs. Colored contours represent intensity, scaled to maximum fluorescence peak (red).

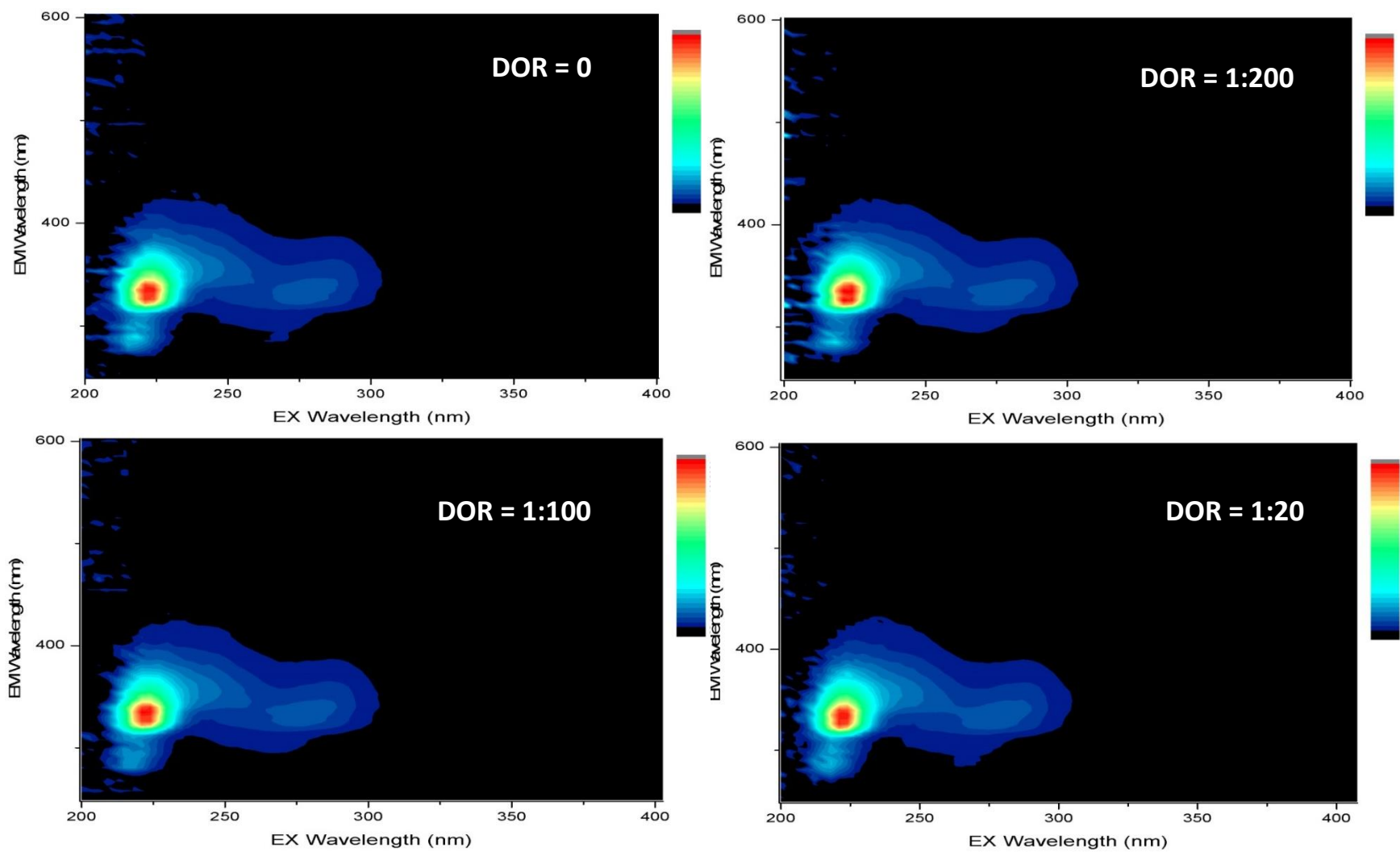


Figure D.22. Heavy Oil Category – Hondo crude oil with dispersant EEMs. Colored contours represent intensity, scaled to maximum fluorescence peak (red).

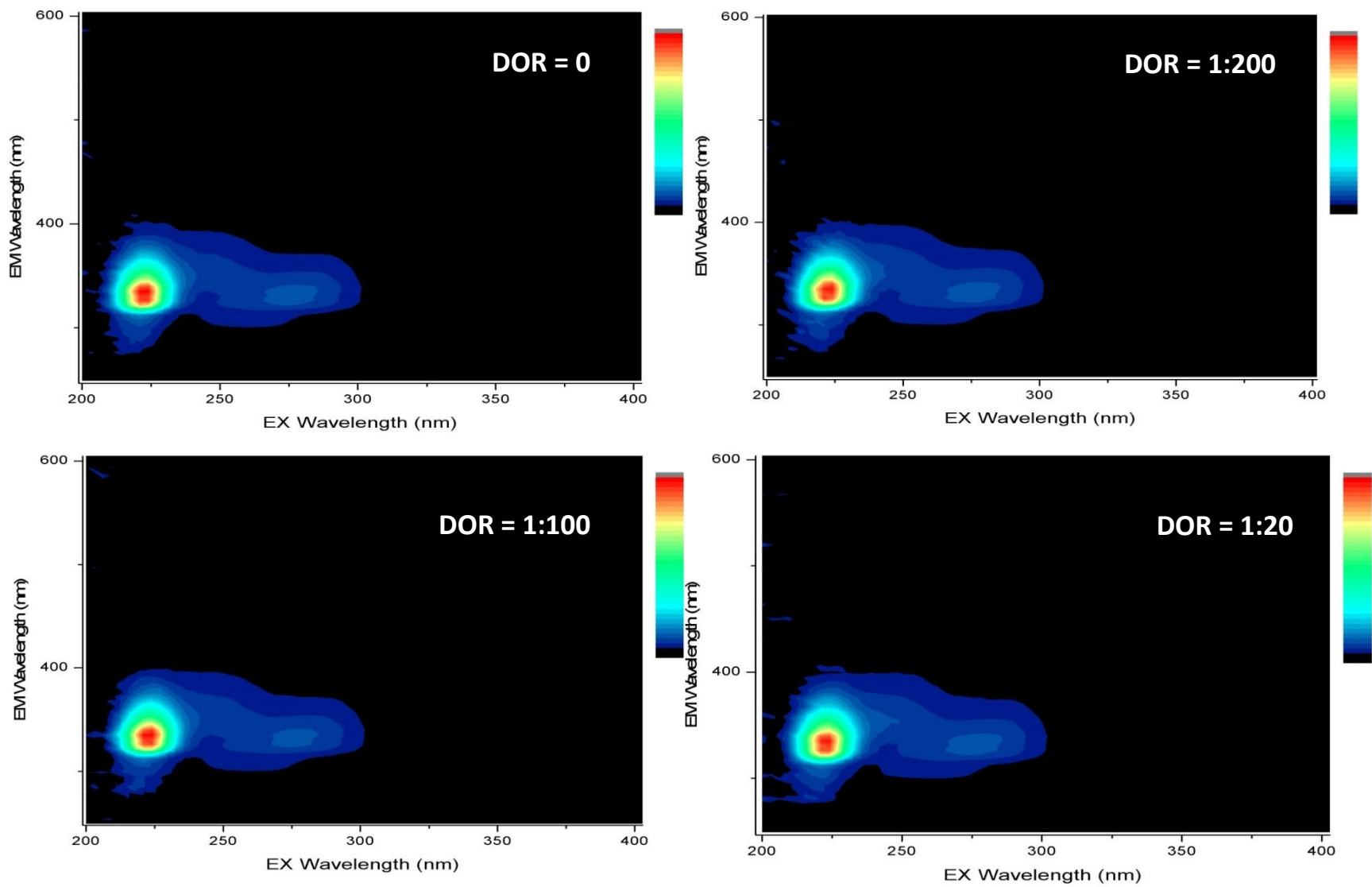


Figure D.23. Heavy Oil Category – IFO-300 crude oil with dispersant EEMs. Colored contours represent intensity, scaled to maximum fluorescence peak (red).

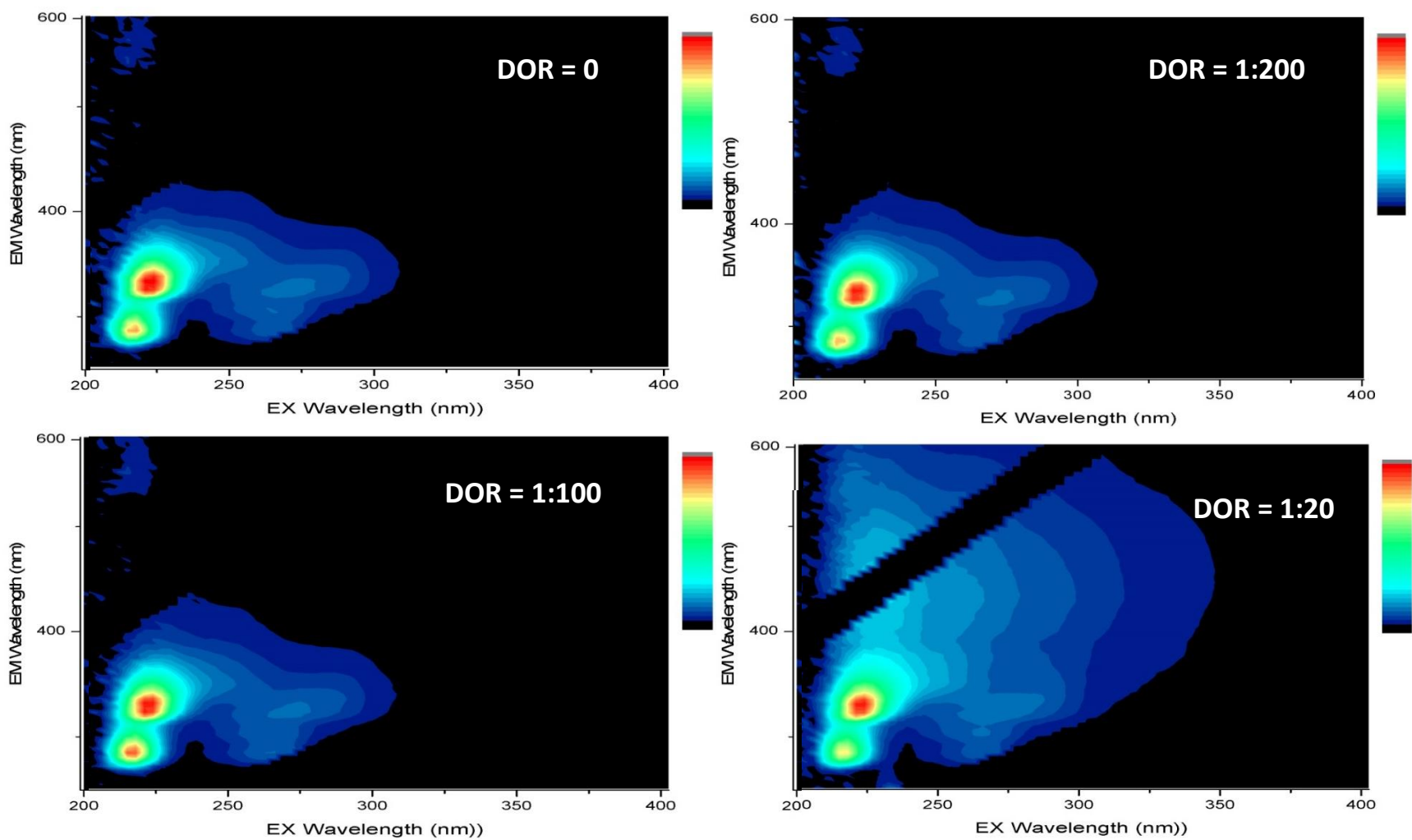


Figure D.24. Dilbit Oil Category – Access Western Blend oil with dispersant EEMs. Colored contours represent intensity, scaled to maximum fluorescence peak (red).

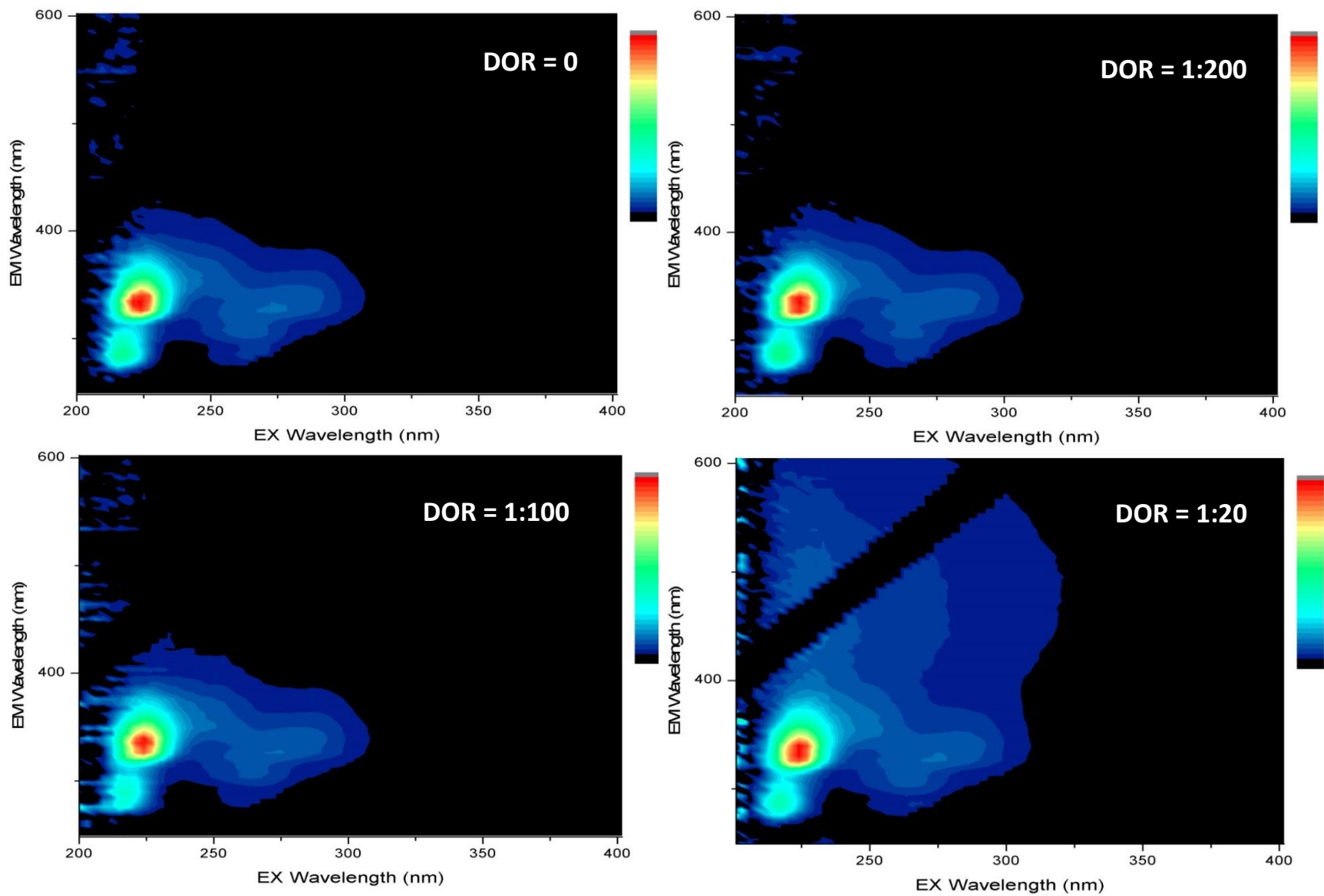


Figure D.25. Dilbit Oil Category – Cold Lake oil with dispersant EEMs. Colored contours represent intensity, scaled to maximum fluorescence peak (red).

APPENDIX E

FIELD SAMPLE DEPTH PROFILES AND EEMS

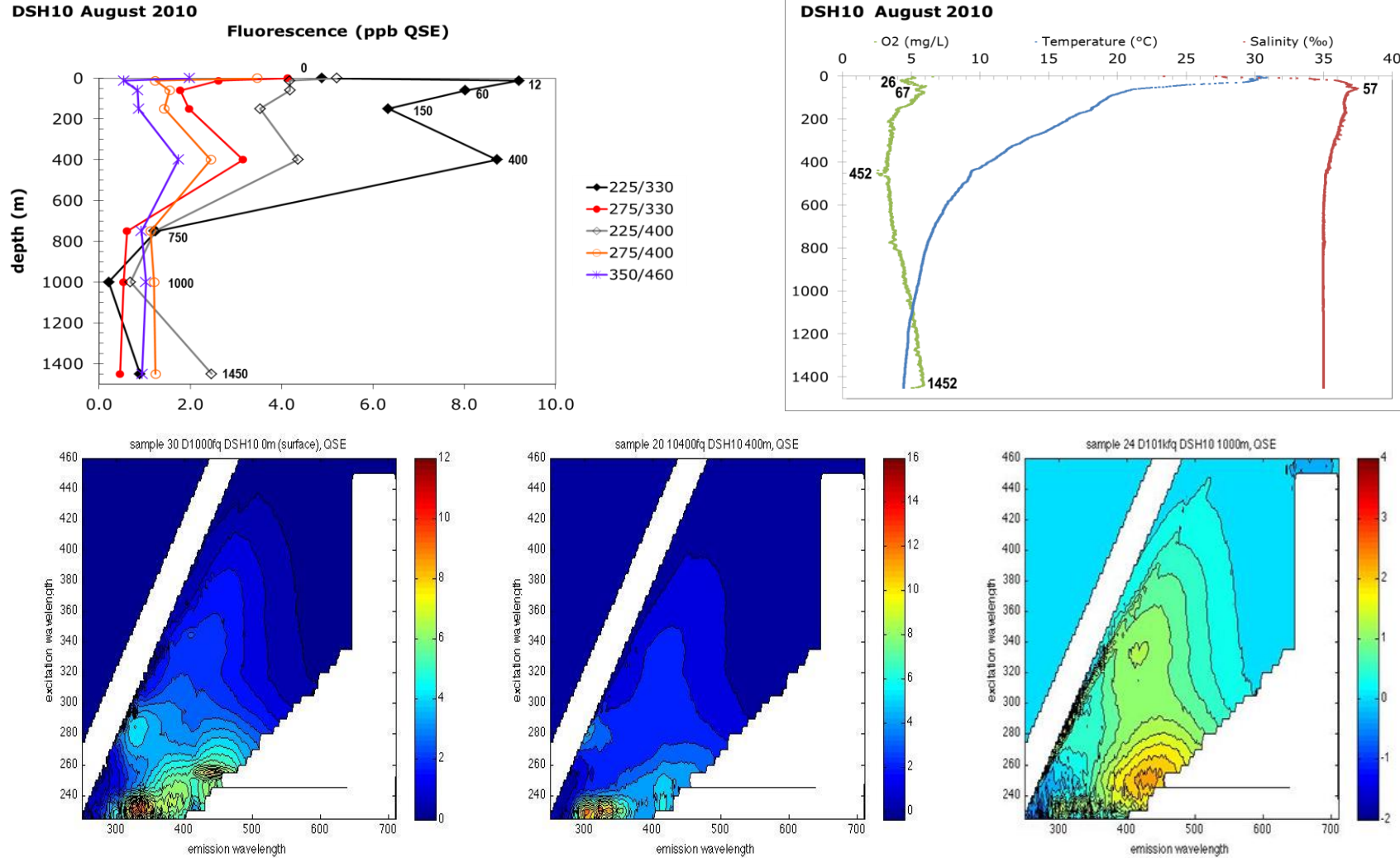


Figure E.1. Plot of fluorescence intensity at five selected excitation/emission pairs (top left) for all water samples collected aboard the R/V *Weatherbird II* at DSH10 on 10 August 2010 and depth profile of CTD data for dissolved oxygen and salinity (top right). EEMs of water samples collected at the surface, 400 m and 1,000 m (bottom, left to right).

DSH08 December 2010

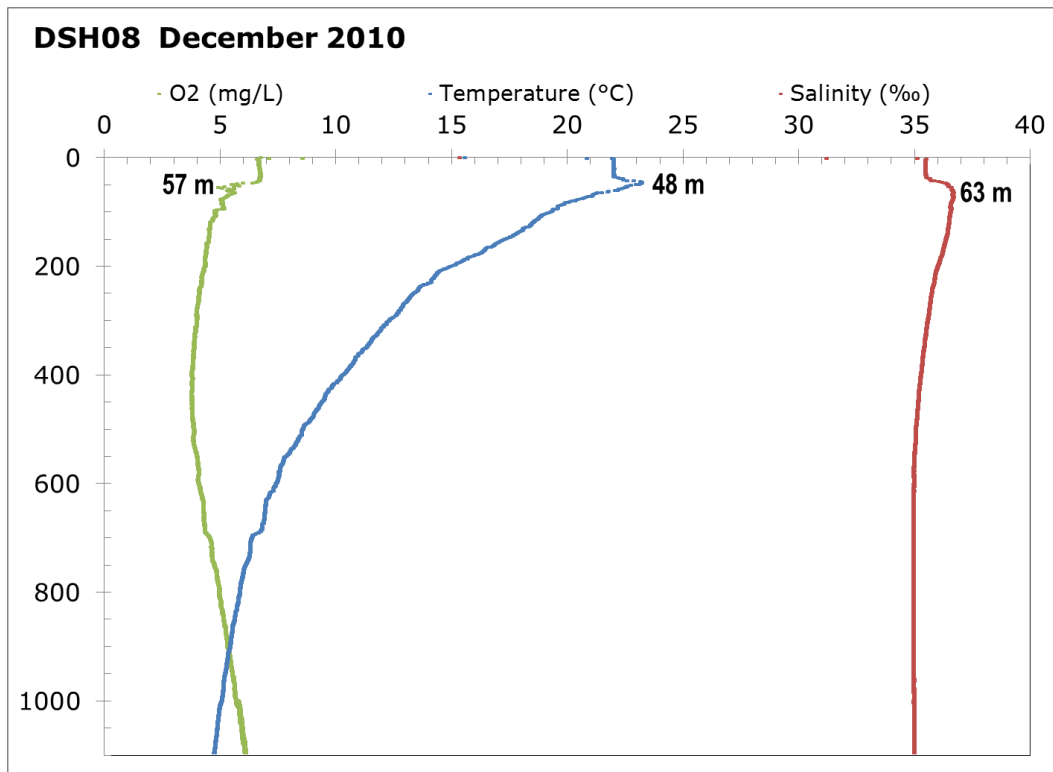
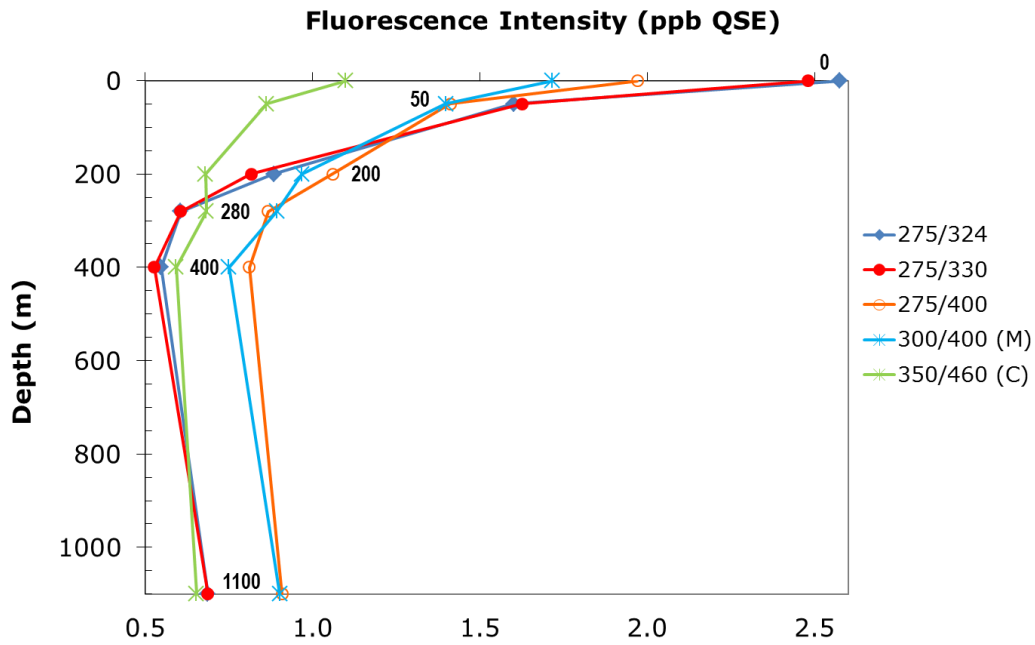


Figure E.2. Fluorescence intensity at selected Ex/Em wavelength pairs for all water samples at DSH08 in December 2010 (above) and depth profile for oxygen, temperature and salinity from CTD data (below). In the fluorescence depth profile, both Ex/Em 275 nm/324 nm and 275 nm/330 nm track the presence of oil, while Ex/Em 300 nm/400 nm (Peak M) and Ex/Em 350 nm/460 nm (Peak C) track FDOM.

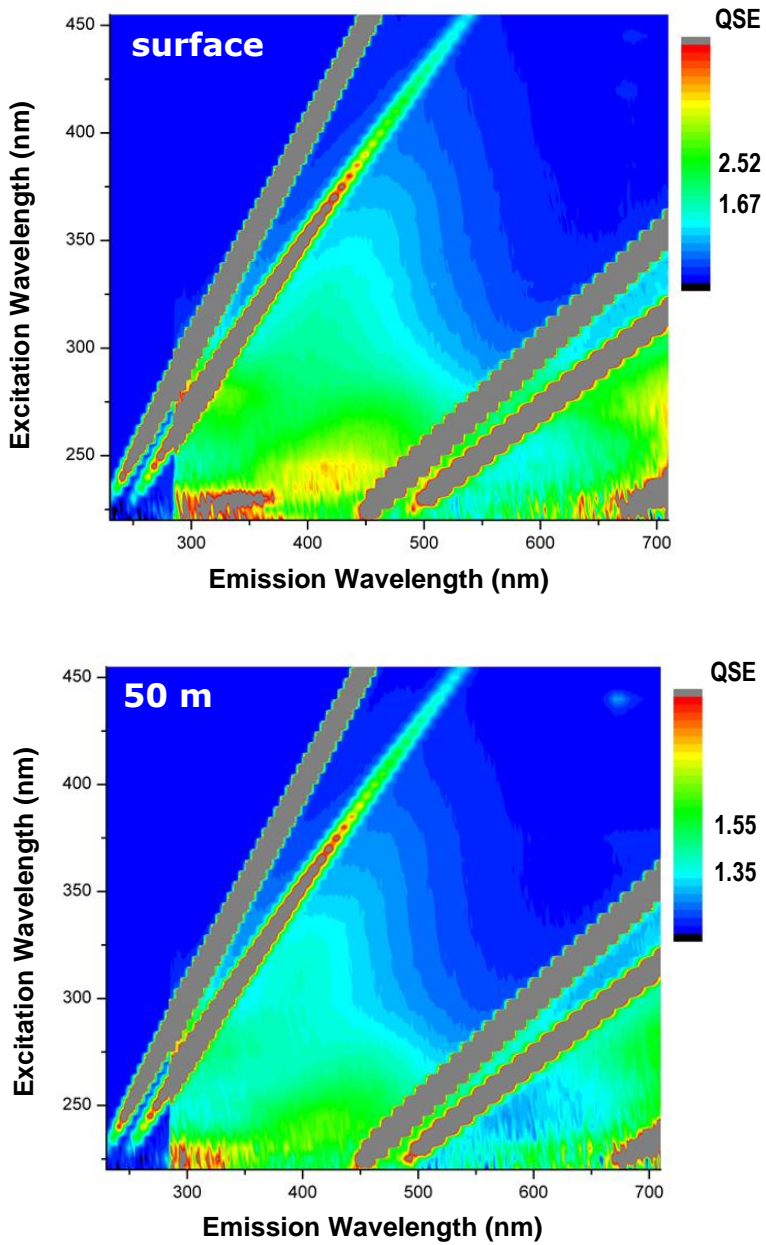


Figure E.3. EEMs of water samples with highest oil-type fluorescence signatures at DSH08 in December 2010: at the surface (above) and at 50 m (below). Maximum concentration in the oil-type fluorescence region (Ex/Em 275 nm/325 nm) is indicated, as well as CDOM fluorescence (300 nm/400 nm), on color bars.

DSH08 February 2011

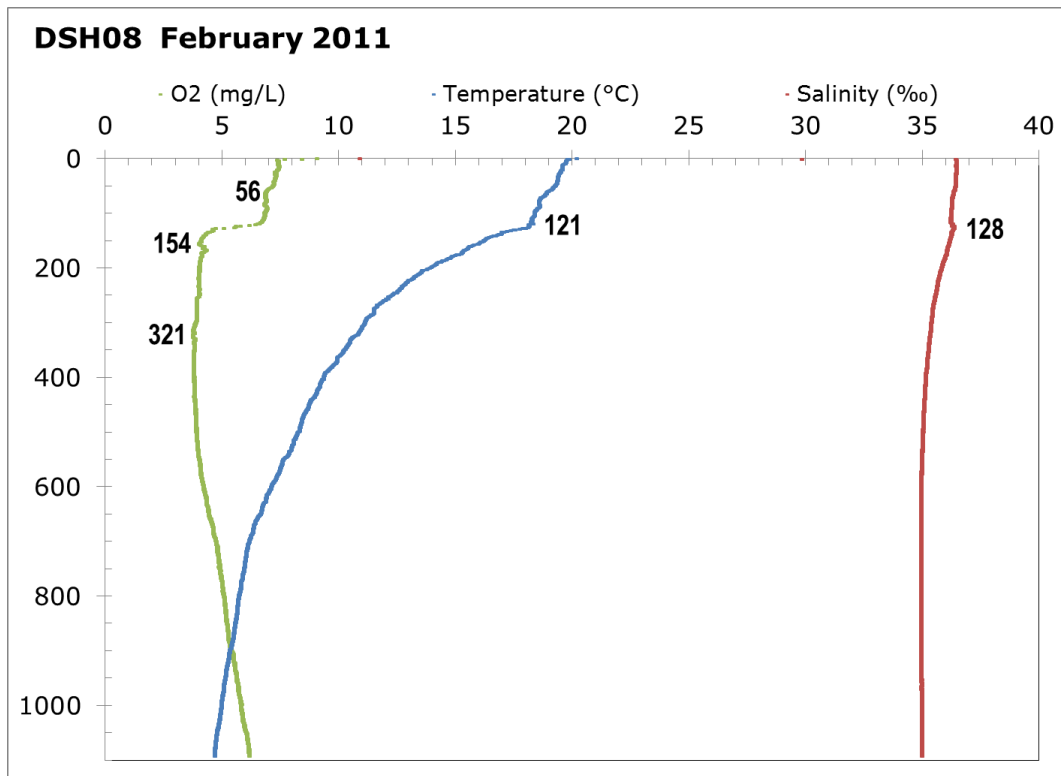
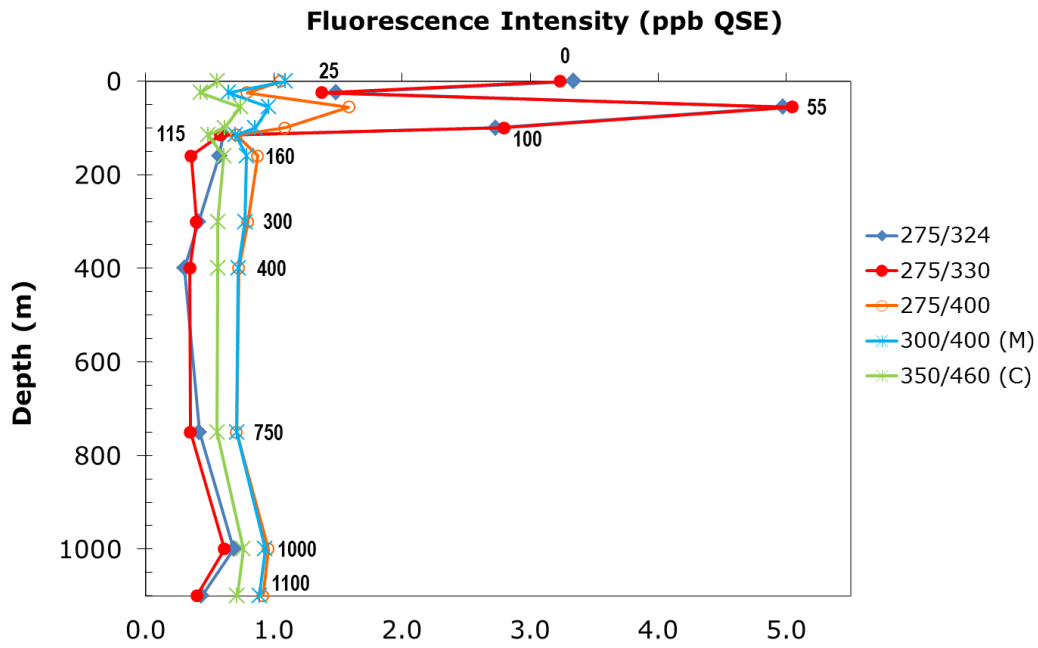


Figure E.4. Fluorescence intensity at selected wavelength pairs for all water samples at DSH08 in February 2011 (above) and oxygen, temperature and salinity (below) from CTD data. In the depth profile, both Ex/Em 275 nm/324 nm and 275 nm/330 nm track the presence of oil while Ex/Em 300 nm/400 nm (Peak M) and Ex/Em 350 nm/460 nm (Peak C) track FDOM.

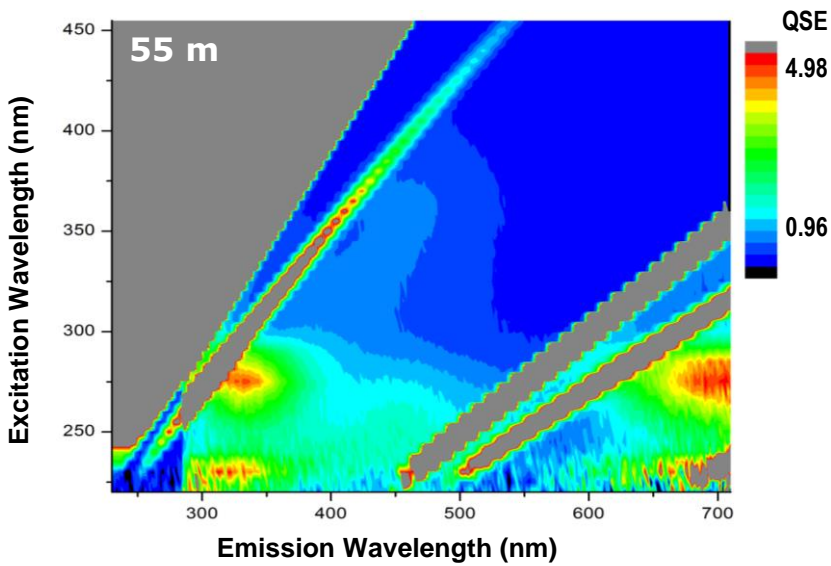
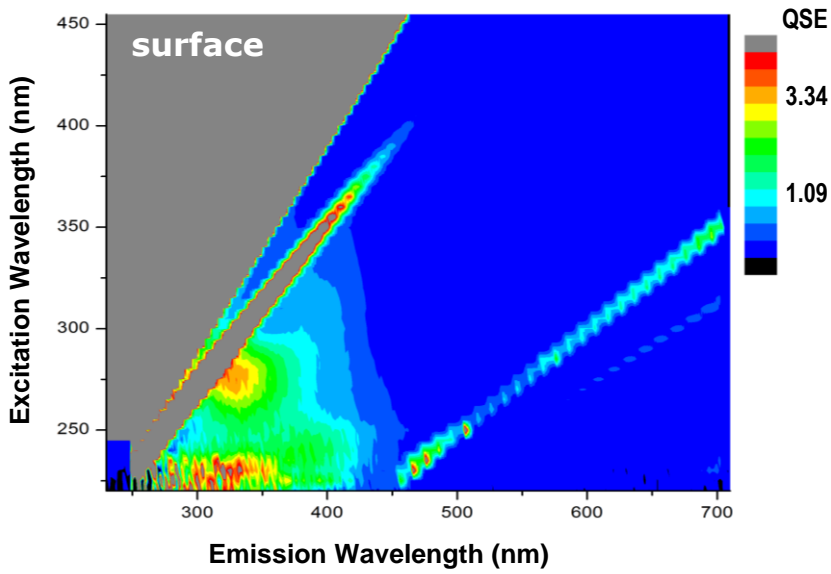


Figure E.5. EEMs of water samples at the surface (above) and at 55 m (below) at DSH08 in February 2011, both showing oil fluorescence signatures. Maximum concentration in the oil-type fluorescence region (Ex/Em 275 nm/325 nm) is indicated, as well as CDOM fluorescence (Ex/Em 300 nm/400 nm), on color bars.

DSH08 May 2011

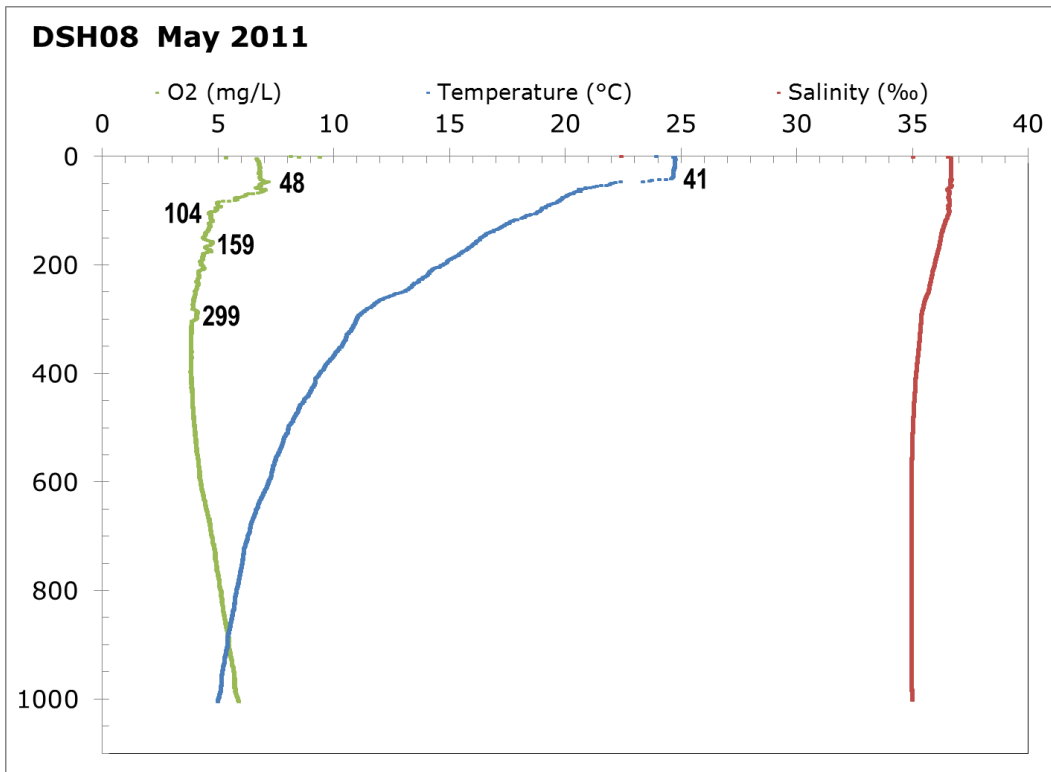
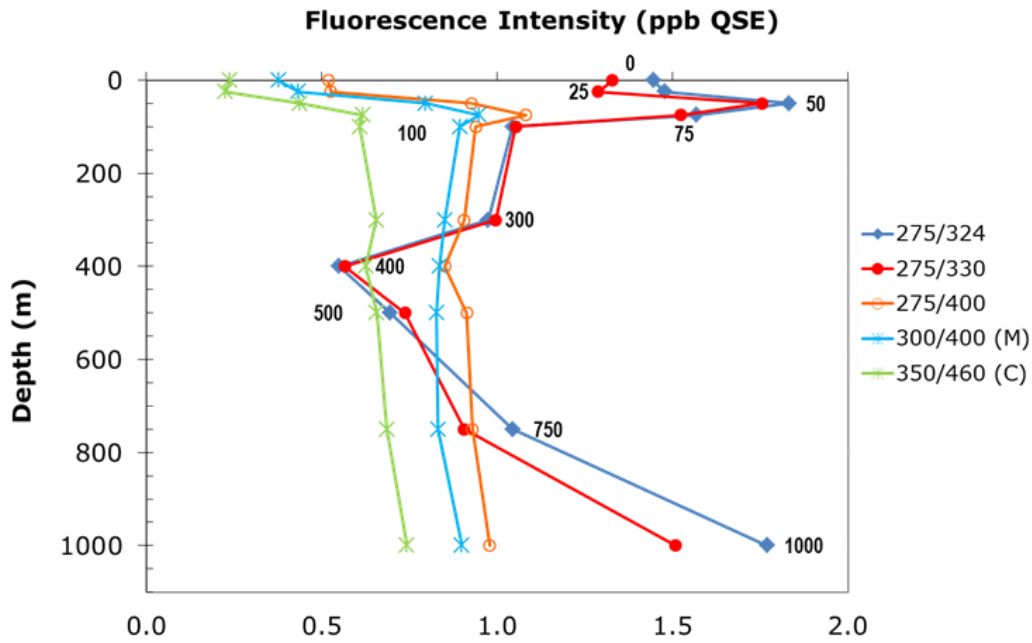


Figure E.6. Fluorescence intensity at selected wavelength pairs for all water samples at DSH08 in May 2011 (upper) and oxygen, temperature and salinity (lower) from CTD data. In the fluorescence depth profile, both Ex/Em 275 nm/324 nm and 275 nm/330 nm track the presence of oil, while Ex/Em 300 nm/400 nm (Peak M) and Ex/Em 350 nm/460 (Peak C) track FDOM.

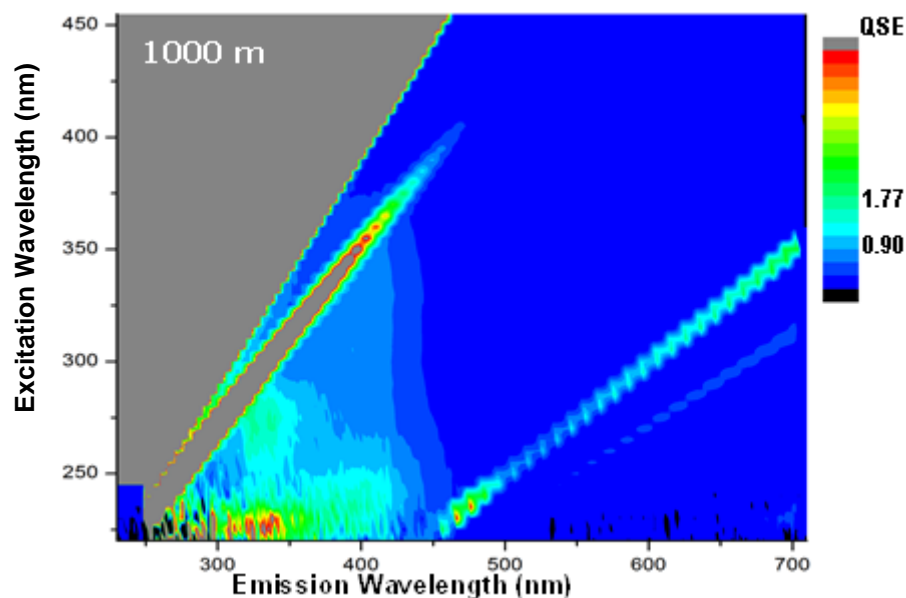
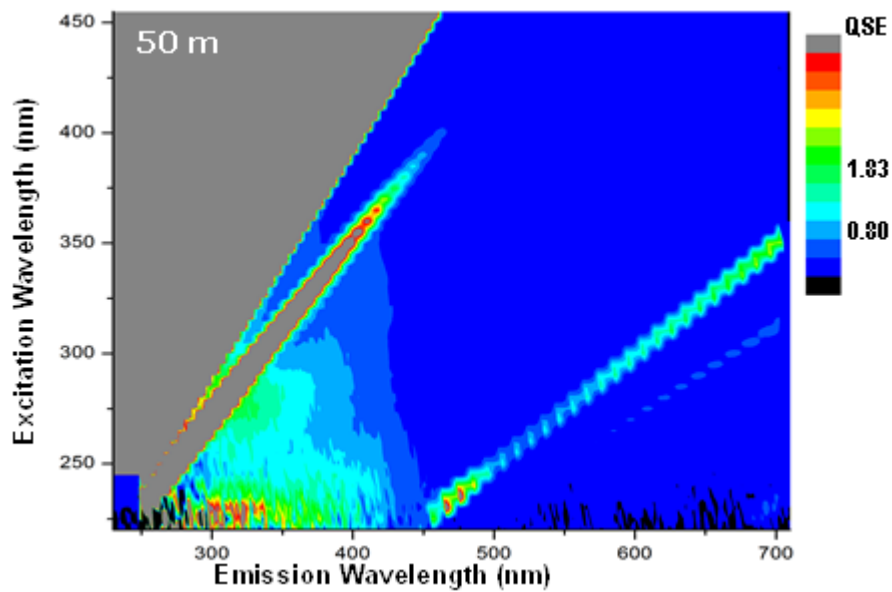


Figure E.7. EEMs of water samples at 50 m (top) and 1000 m (bottom) at DSH08 in May 2011 both show reduced oil signatures. Maximum concentration in the oil-type fluorescence region (Ex/Em 275 nm/325 nm) is indicated, as well as CDOM fluorescence (Ex/Em 300 nm/400 nm), on color bars.

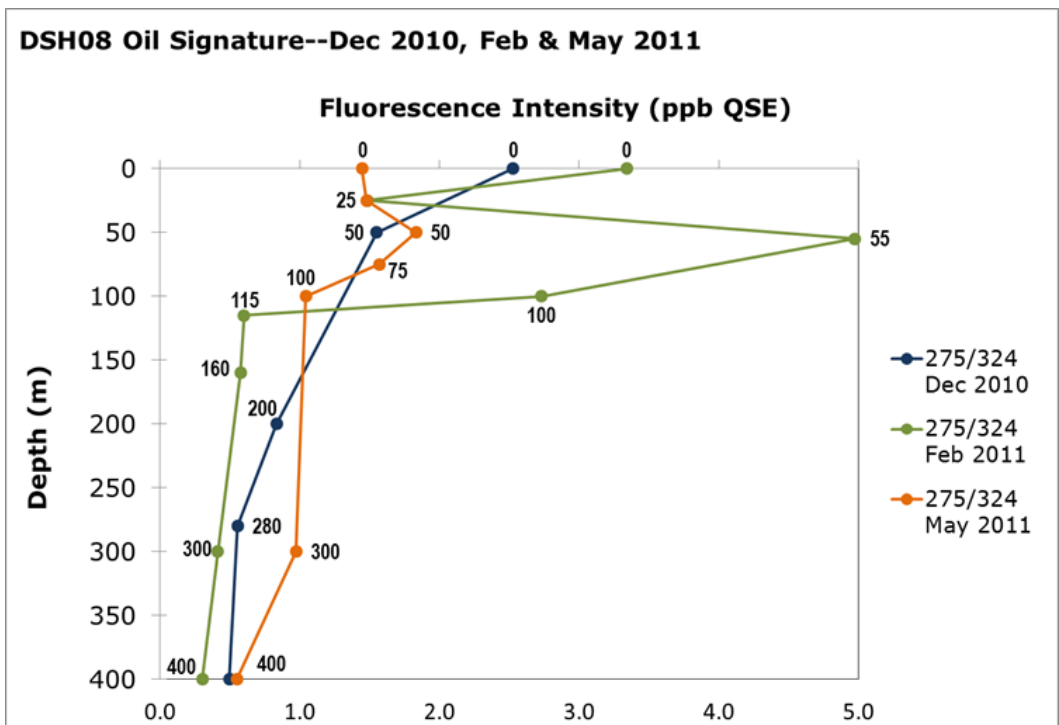
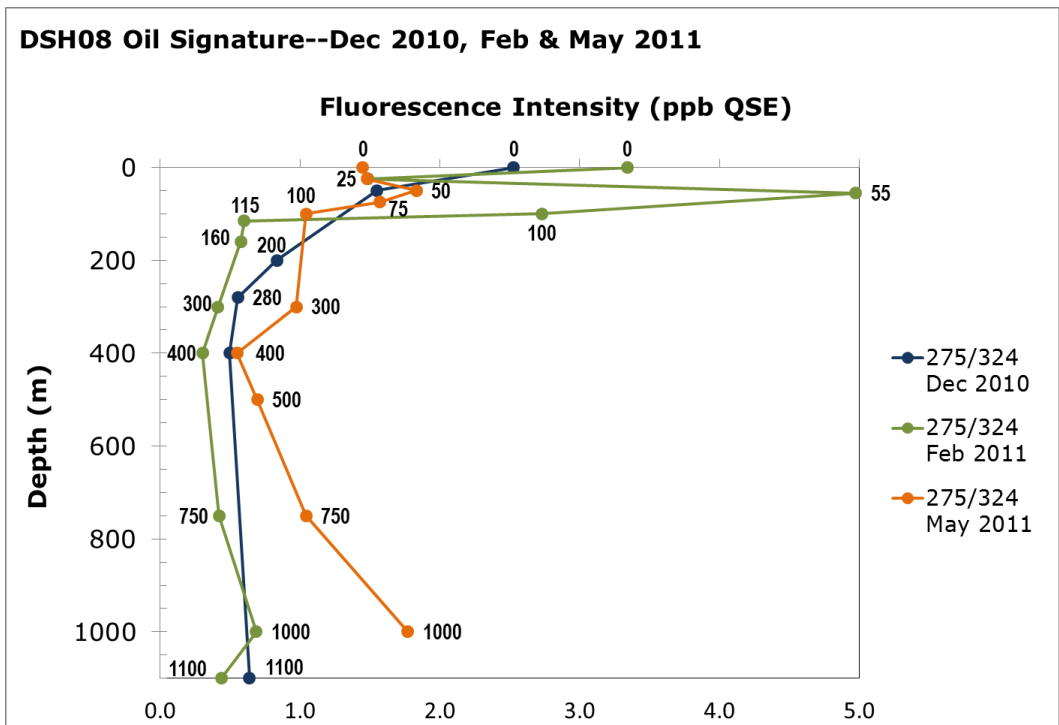


Figure E.8. Fluorescence intensity at Ex/Em 275 nm/324 nm, indicative of the presence of oil in the water column, at DSH08 in December 2010, February 2011, and May 2011 for all depths (above) and for depths only to 400 m (below) in order to visually separate samples collected at shallower depths.

DSH10 December 2010

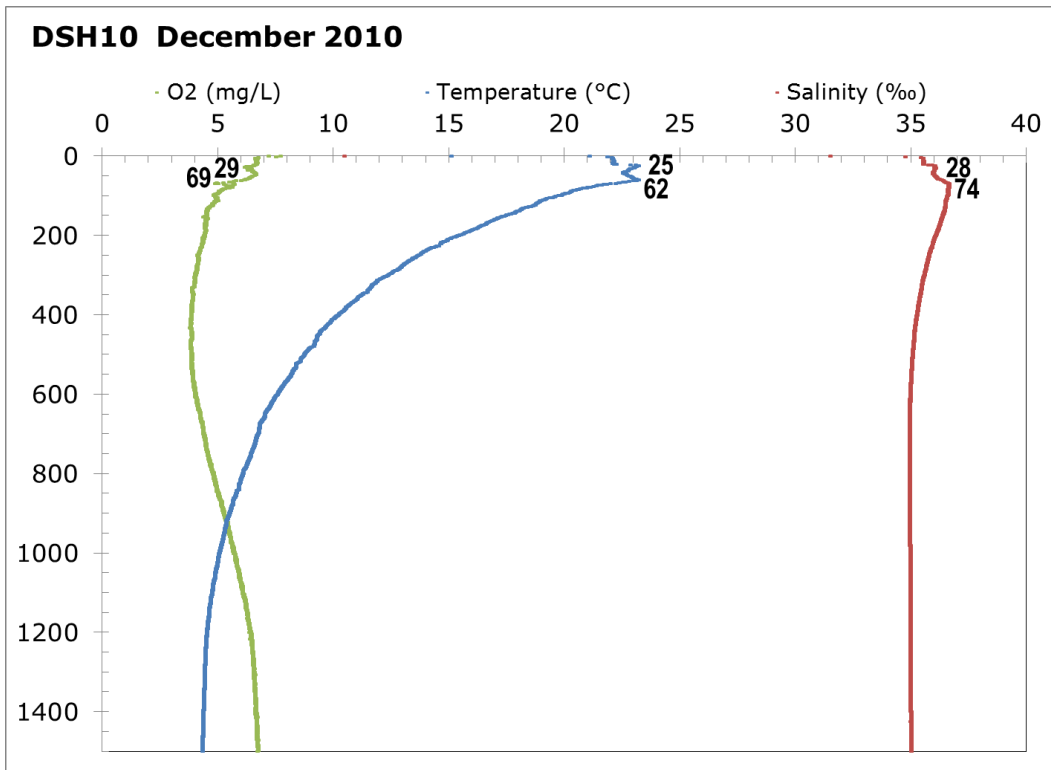
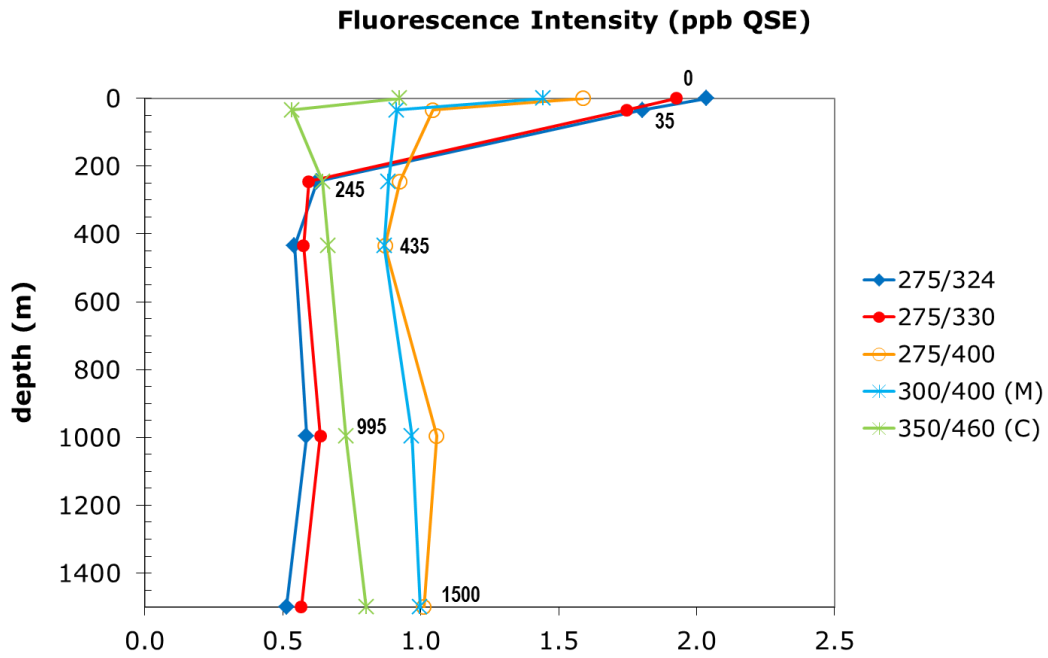


Figure E.9. Fluorescence intensity at selected wavelength pairs for all water samples at DSH10 in December 2010 (above) and oxygen, temperature and salinity (below) from CTD data. In the fluorescence depth profile, both Ex/Em 275 nm/324 nm and 275 nm/330 nm track the presence of oil while Ex/Em 300 nm/400 nm (Peak M) and Ex/Em 350 nm/460 (Peak C) track FDOM.

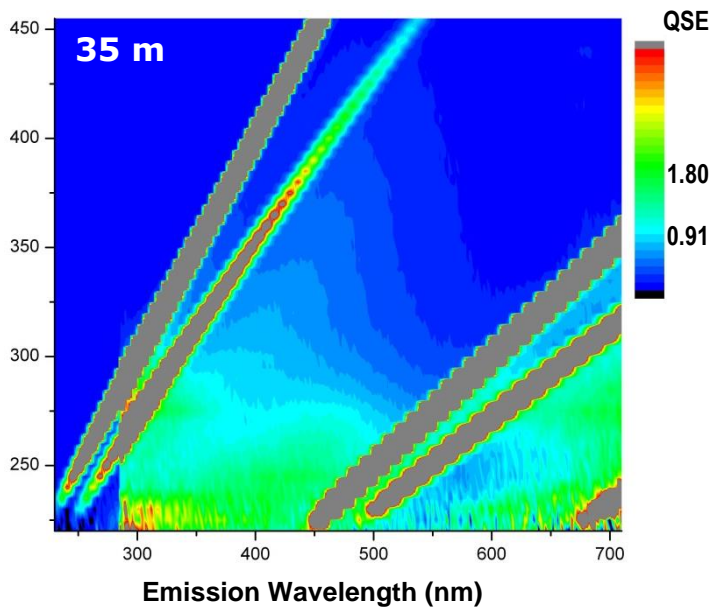
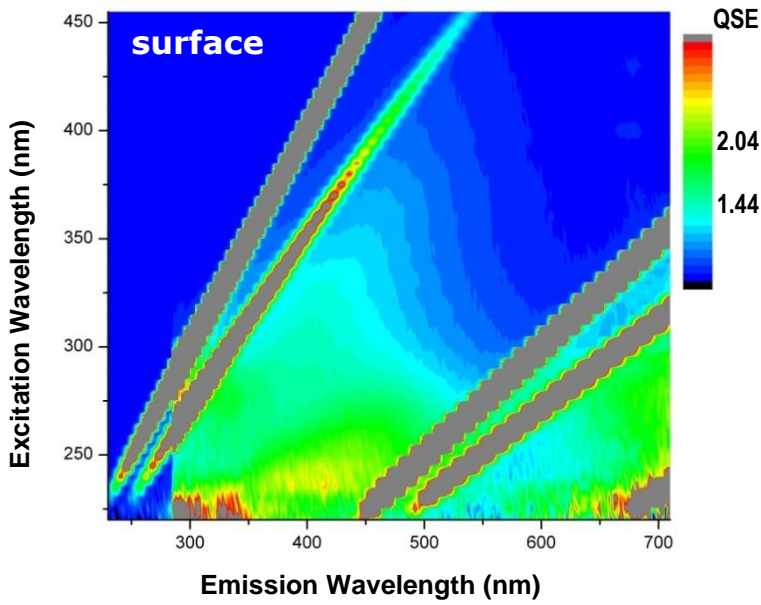


Figure E.10. EEMs of water samples at the surface (top) and 35 m (bottom) at DSH10 in December 2010. Maximum concentration in the oil-type fluorescence region (Ex/Em 275 nm/325 nm) is indicated, as well as CDOM fluorescence (Ex/Em 300 nm/400 nm), on color bars.

DSH10 February 2010

Fluorescence Intensity (ppb QSE)

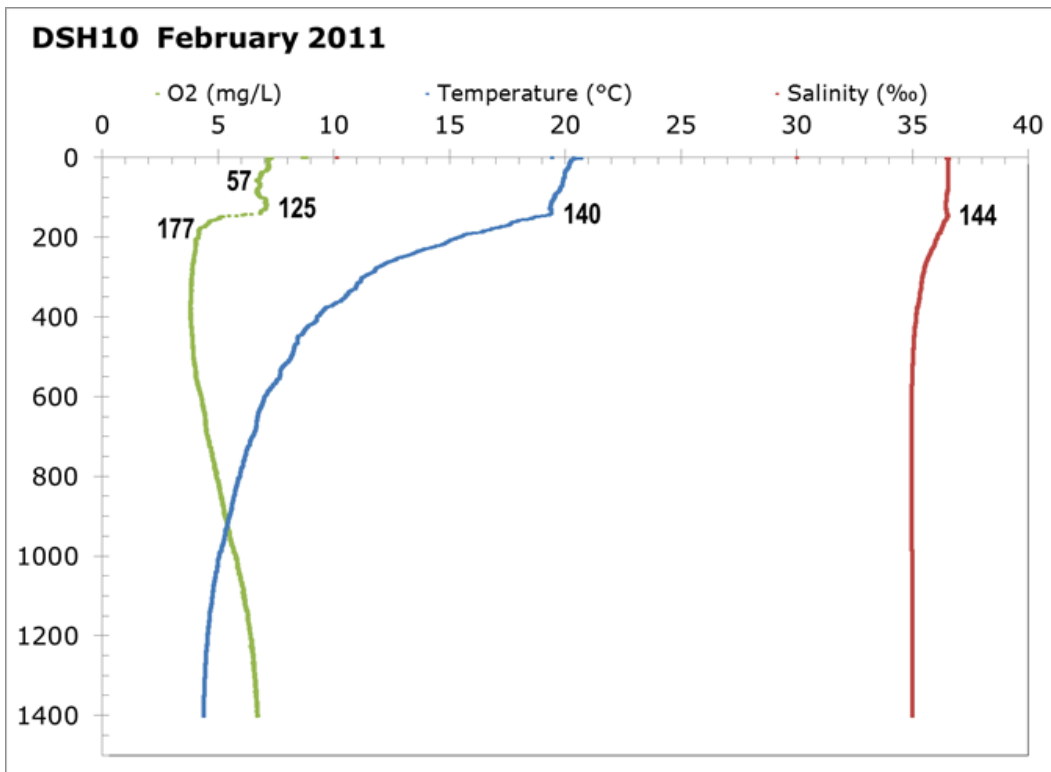
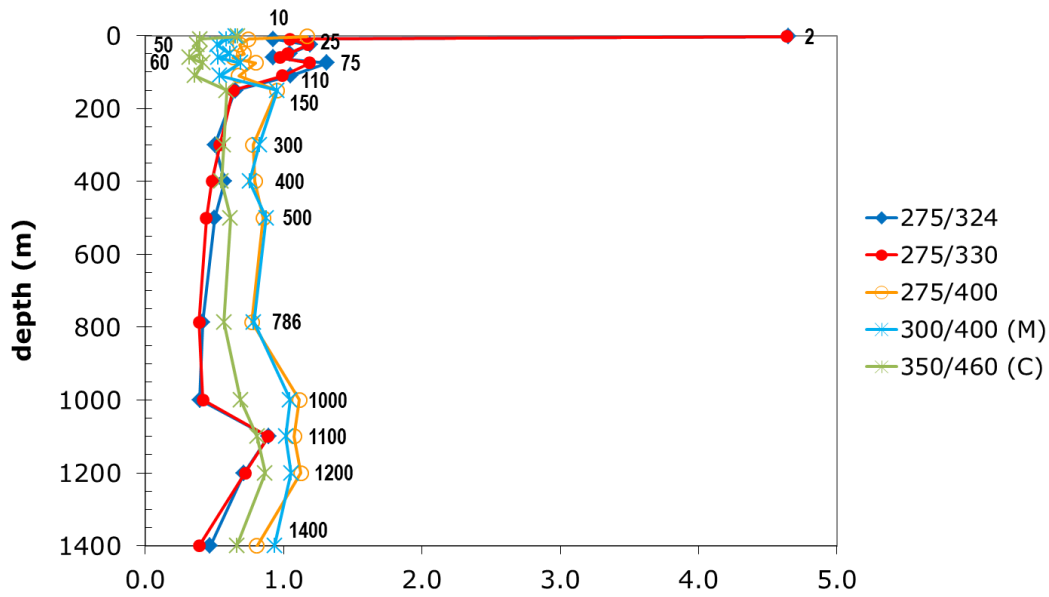


Figure E.11. Fluorescence intensity at selected wavelength pairs for all water samples at DSH10 in February 2011 (upper) and oxygen, temperature and salinity (lower) from CTD data. In the depth profile, both Ex/Em 275 nm/324 nm and 275/330 nm track the presence of oil while Ex/Em 300 nm/400 nm (Peak M) and Ex/Em 350 nm/460 (Peak C) track FDOM.

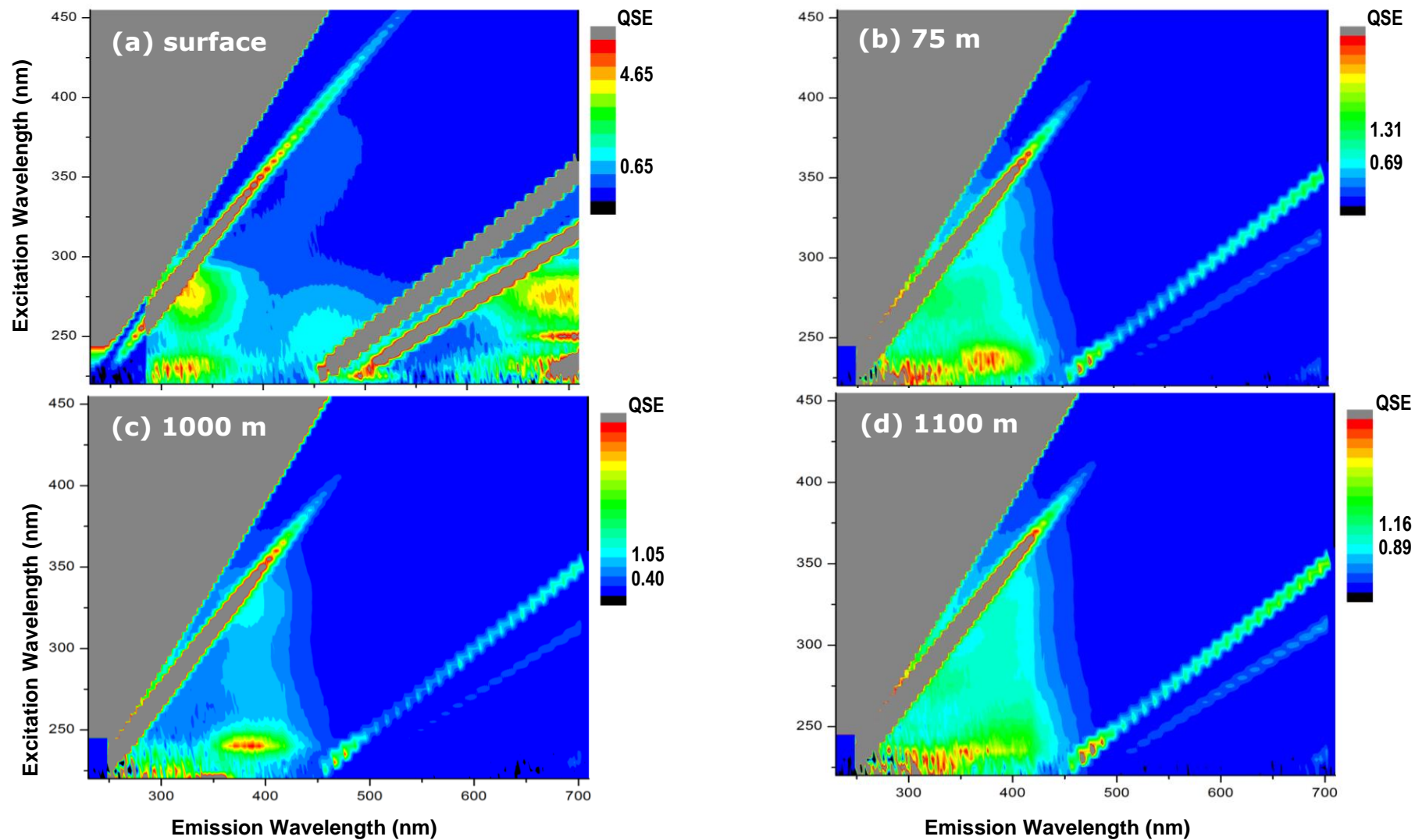
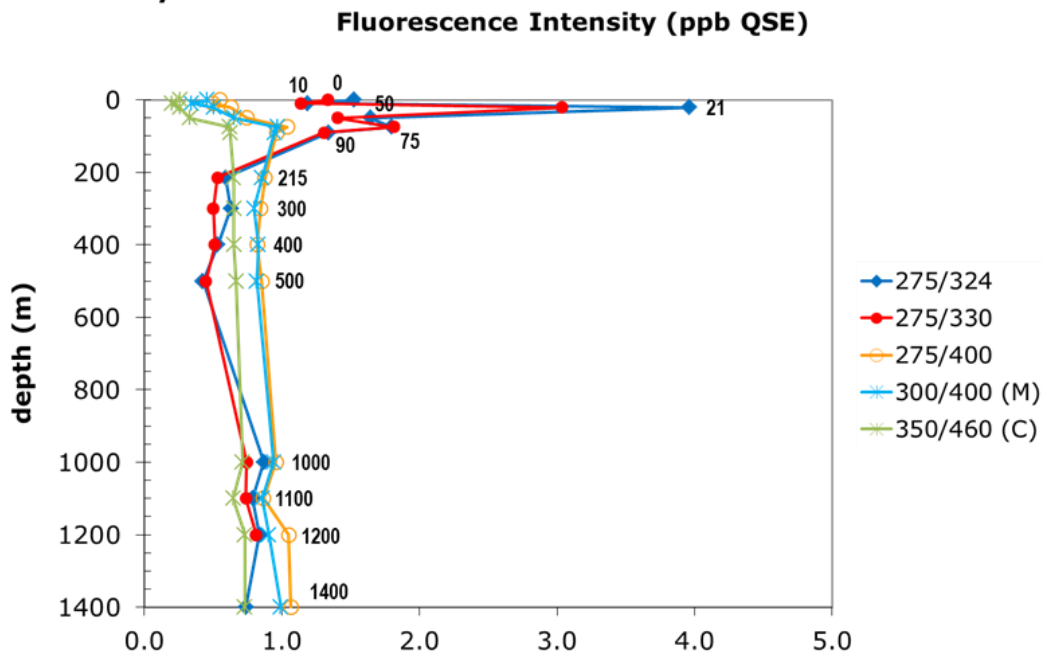


Figure E.12. EEMs of water samples (a) at the surface (b) 75 m (c) 1000 m and (d) 1200 m at DSH10 in February 2011. Maximum concentration in the oil-type fluorescence region (Ex/Em 275 nm/325 nm) is indicated, as well as CDOM fluorescence (Ex/Em 300 nm/400 nm), on color bars.

DSH10 May 2010



DSH10 May 2011

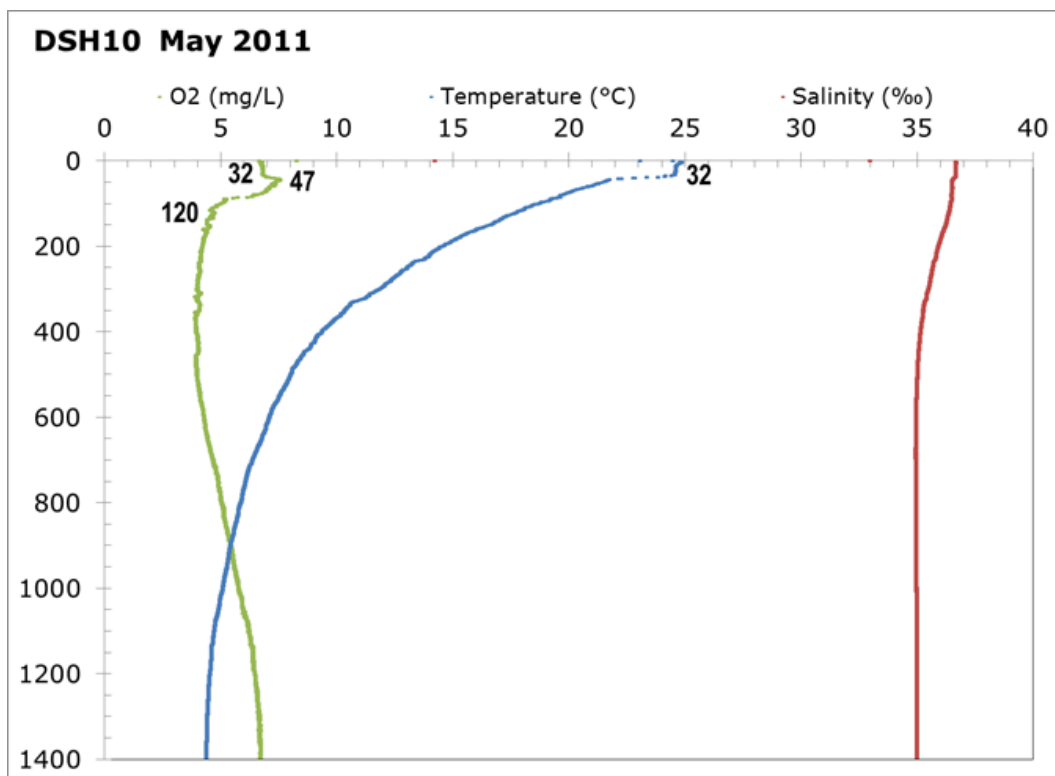


Figure E.13. Fluorescence intensity at selected wavelength pairs for all water samples at DSH10 in May 2011 (upper) and oxygen, temperature and salinity (lower) from CTD data. In the fluorescence depth profile, both Ex/Em 275 nm/324 nm and 275 nm/330 nm track the presence of oil while Ex/Em 300 nm/400 nm (Peak M) and Ex/Em 350 nm/460 (Peak C) track FDOM.

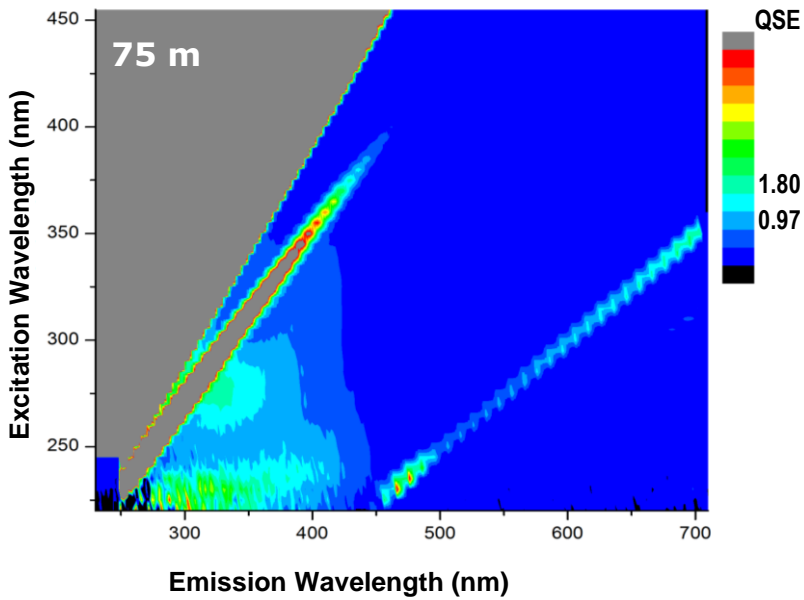
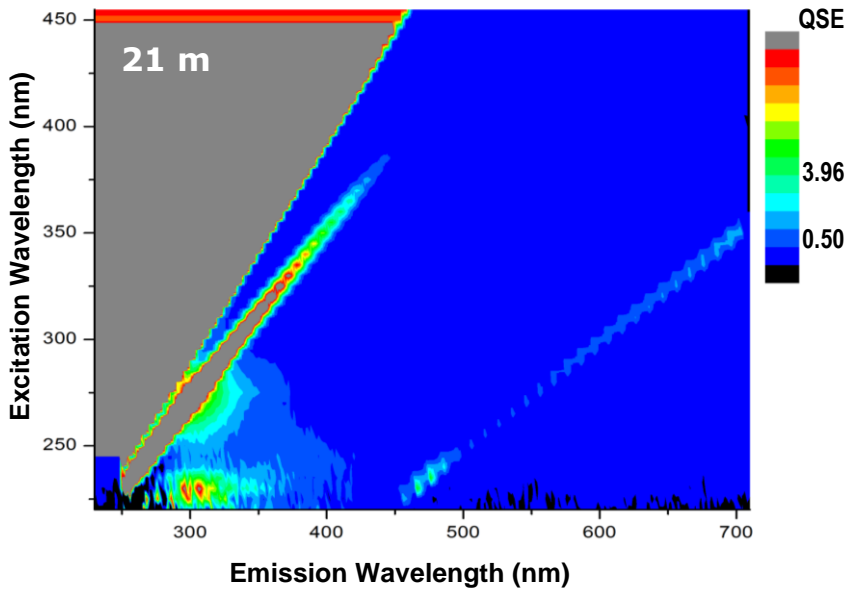


Figure E.14. EEMs of water sample at 21 m (top) and 75 m (bottom) at DSH10 in May 2011. Maximum concentration in the oil-type fluorescence region (Ex/Em 275 nm/325 nm) is indicated, as well as CDOM fluorescence (Ex/Em 300 nm/400 nm), on color bars.

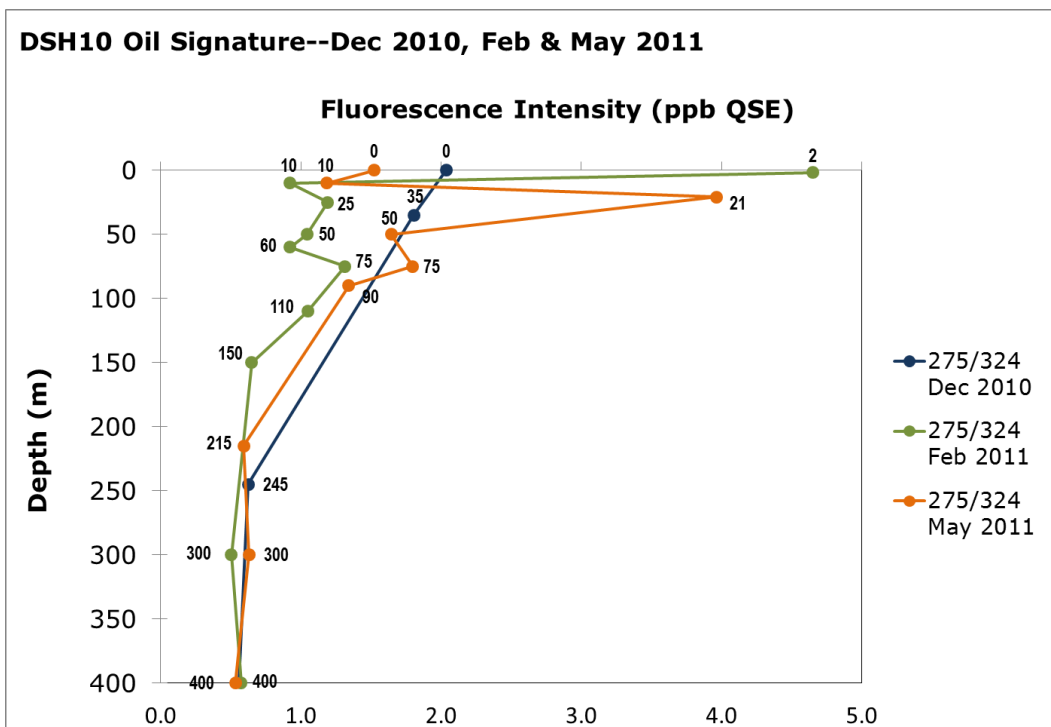
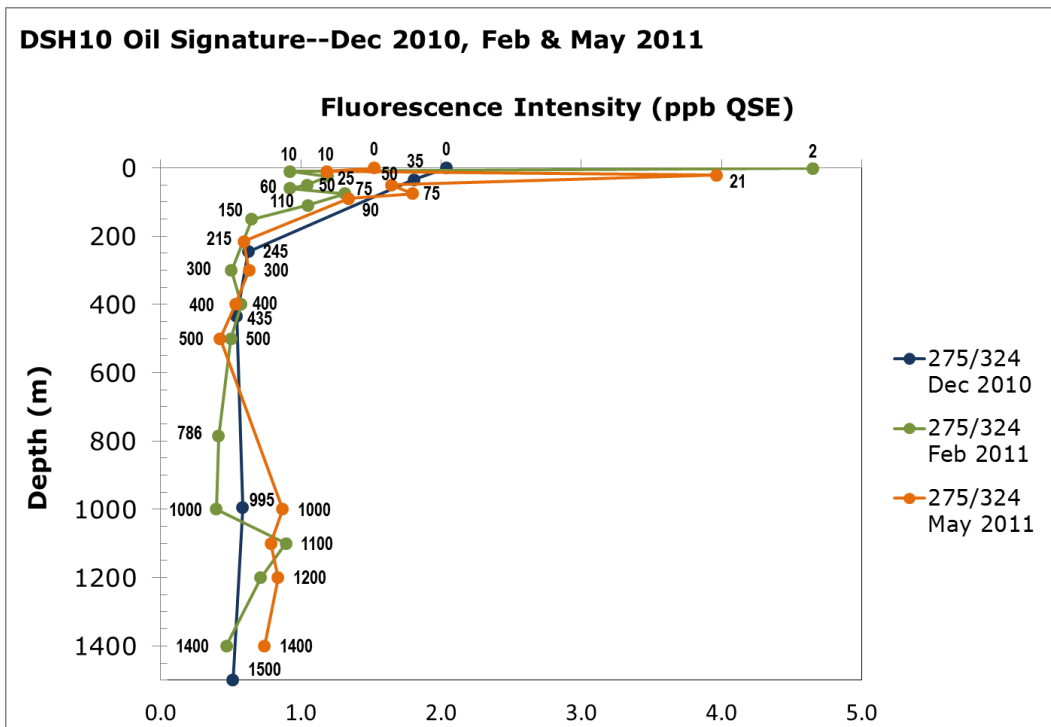


Figure E.15. Fluorescence intensity at Ex/Em 275 nm/324 nm, indicative of the presence of oil in the water column, in December 2010, February 2011, and May 2011 at DSH10 for all depths (upper) and for depths only to 400 m (lower) in order to visually separate samples collected at shallower depths.

PCB06 December 2010

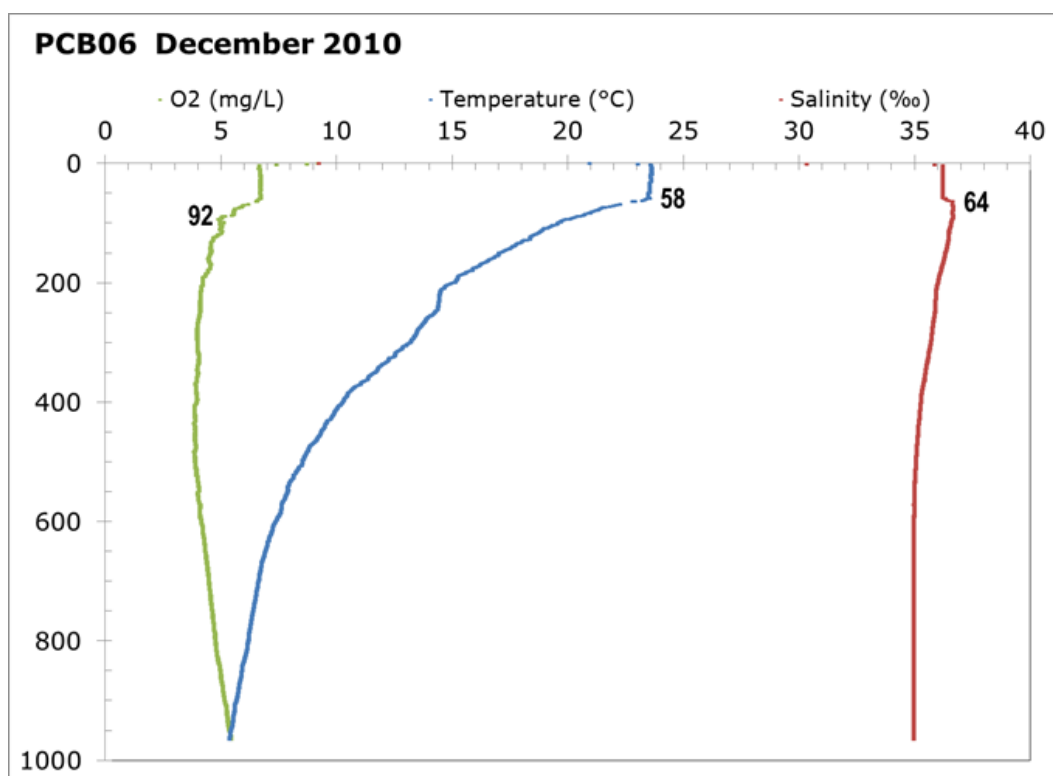
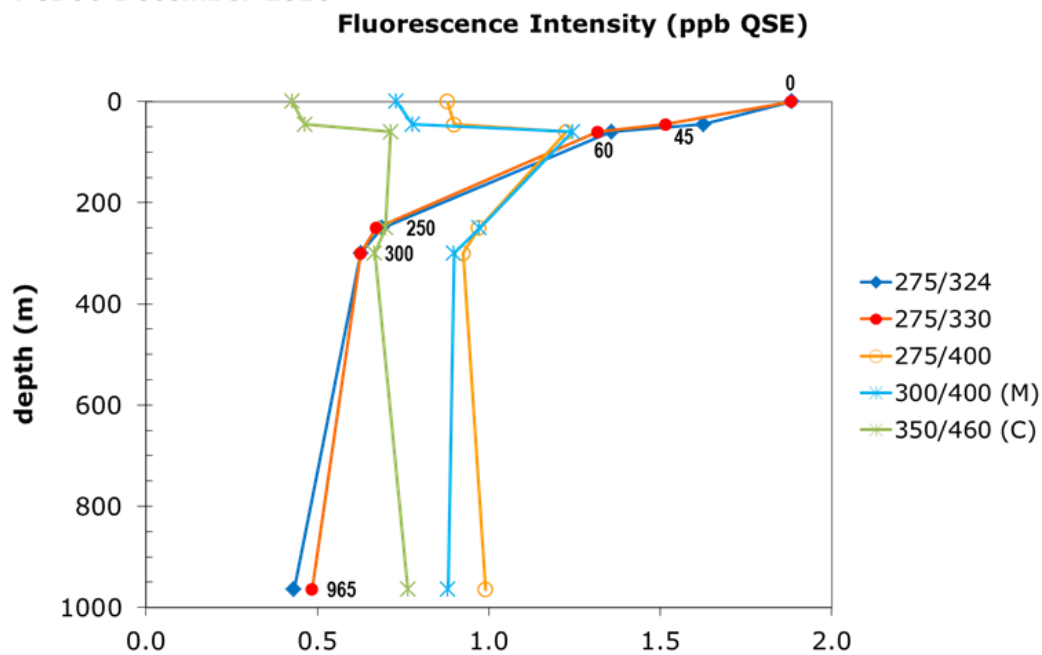


Figure E.16. Fluorescence intensity at selected wavelength pairs for all water samples at PCB06 in December 2010 (upper) and oxygen, temperature and salinity (lower) from CTD data. In the fluorescence depth profile, both Ex/Em 275 nm/324 nm and 275 nm/330 nm track the presence of oil while Ex/Em 300 nm/400 nm (Peak M) and Ex/Em 350 nm/460 (Peak C) track FDOM.

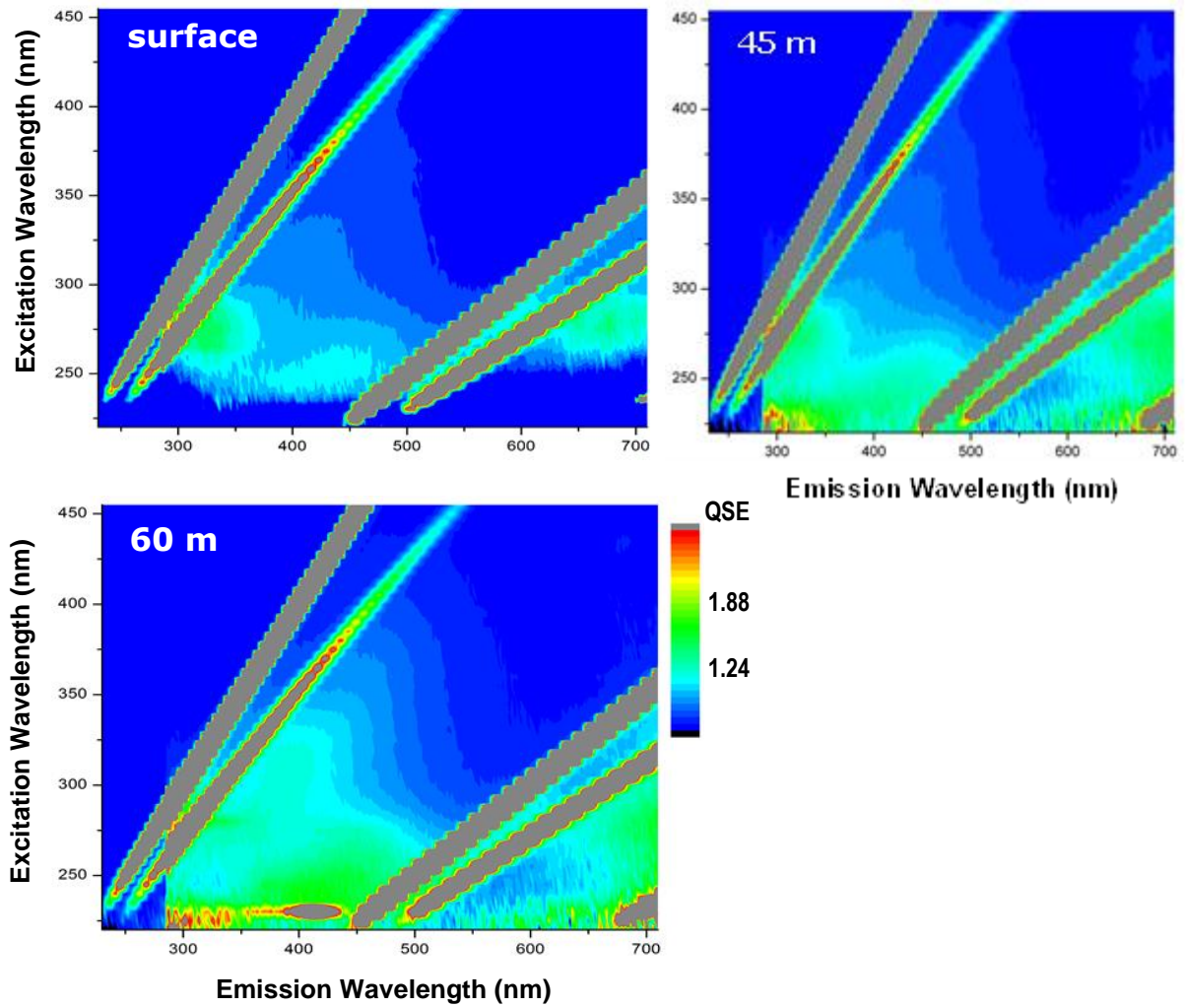


Figure E.17. EEMs of water samples at the surface (top left), 45 m (top right), and 60 m at PCB06 in December 2010. Concentration at the oil-type fluorescence region of Ex/Em 275 nm/325 nm and at the CDOM fluorescence region of Ex/Em 300 nm/400 nm is indicated on the color bar (scale is the same in all three EEMs)

PCB06 February 2010

Fluorescence Intensity (ppb QSE)

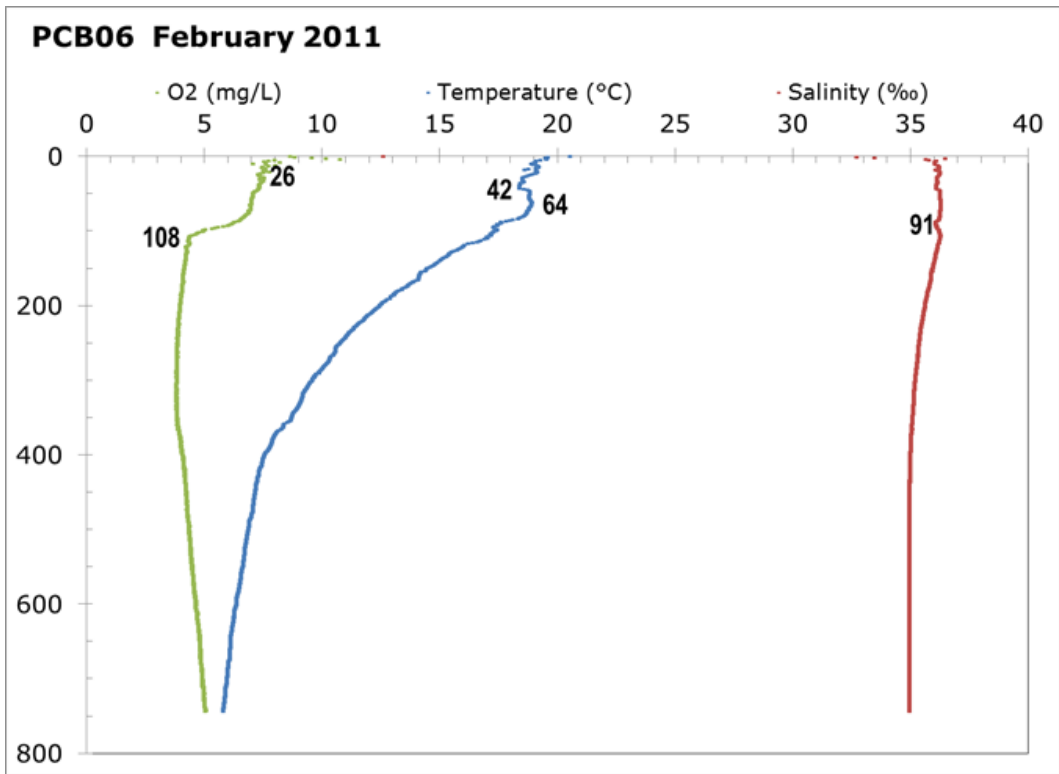
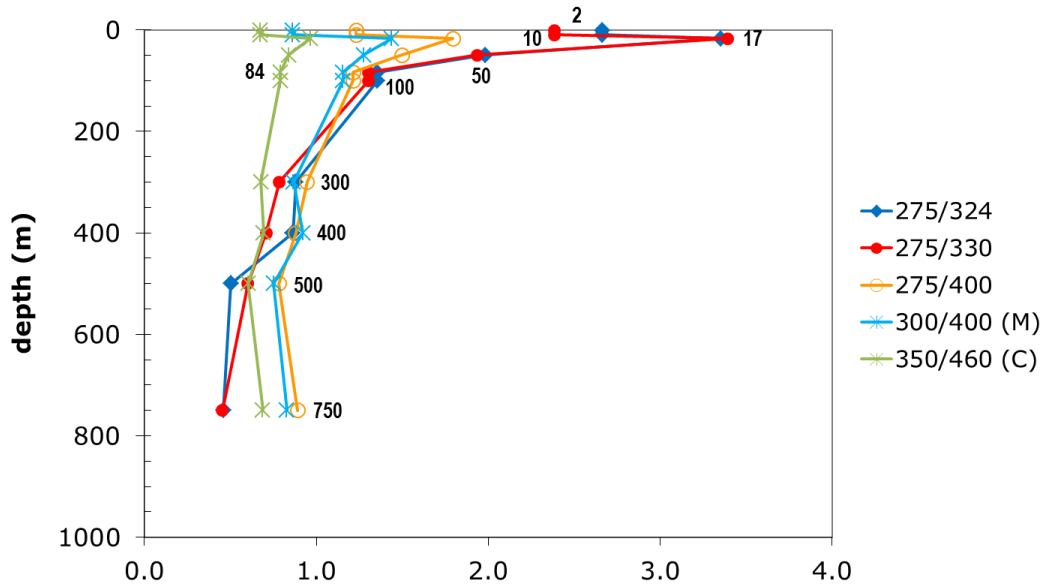


Figure E.18. Fluorescence intensity at selected wavelength pairs for all water samples at PCB06 in February 2011 (upper) and oxygen, temperature and salinity (lower) from CTD data. In the fluorescence depth profile, both Ex/Em 275 nm/324 nm and 275 nm/330 nm track the presence of oil while Ex/Em 300 nm/400 nm (Peak M) and Ex/Em 350 nm/460 (Peak C) track FDOM.

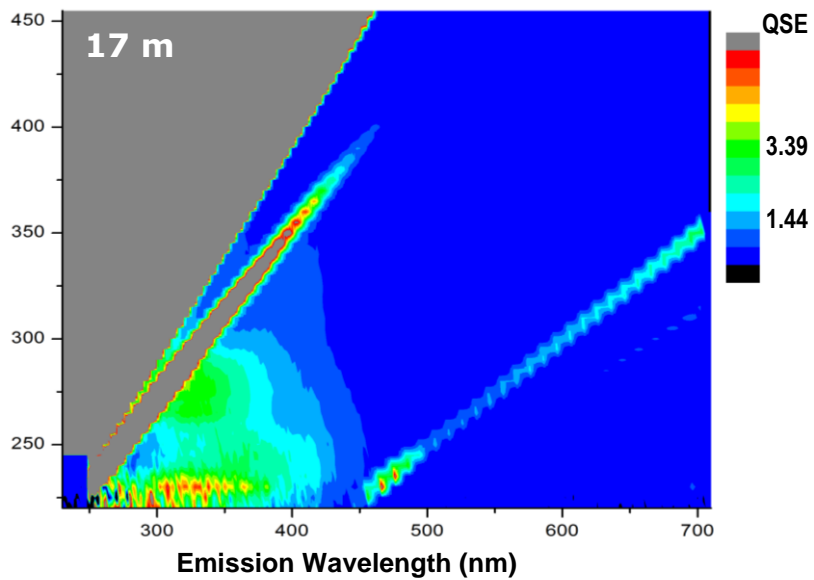
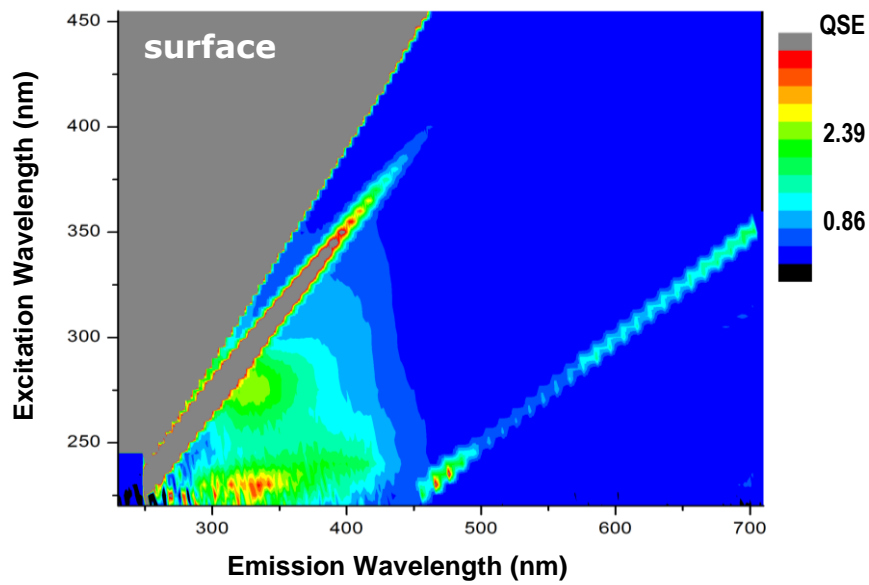


Figure E.19. EEMs of water samples at the surface (top) and 17 m (bottom) at PCB06 in February 2011. Maximum concentration in the oil-type fluorescence region (Ex/Em 275 nm/325 nm) is indicated, as well as CDOM fluorescence (Ex/Em 300 nm/400 nm), on color bars.

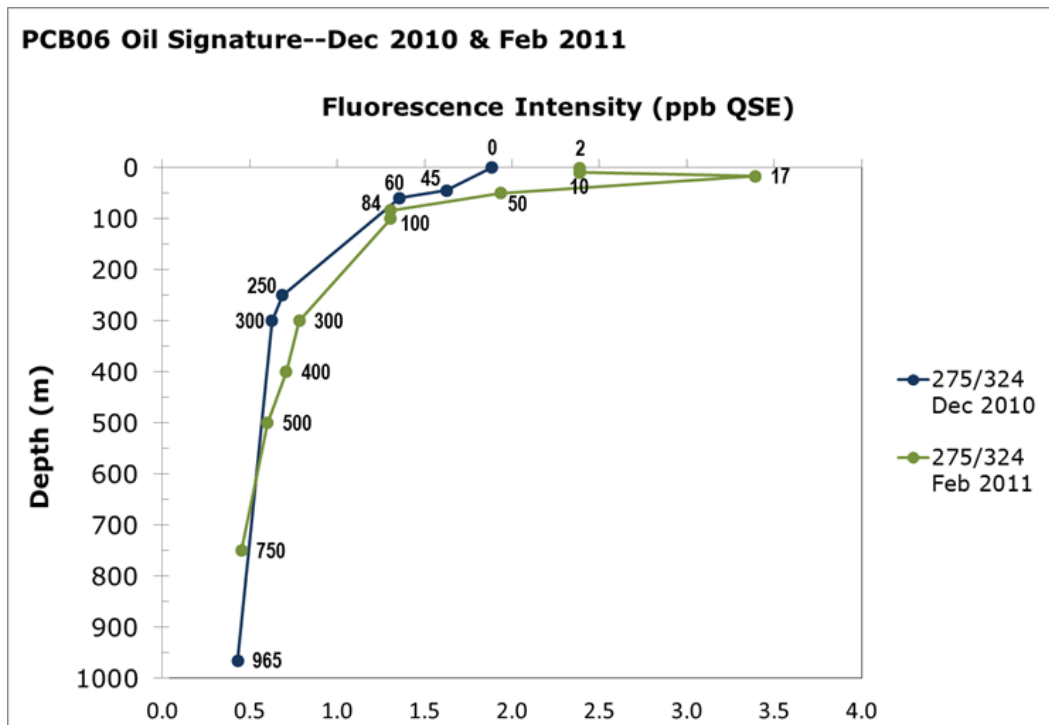


Figure E.20. Fluorescence intensity at Ex/Em 275 nm/324 nm, indicative of the presence of oil in the water column, in December 2010 and February 2011 at PCB06 for all depths.

APPENDIX F
REPRINT PERMISSIONS

Submersible Optical Sensors Exposed to Chemically Dispersed Crude Oil: Wave Tank Simulations for Improved Oil Spill Monitoring

Author: Robyn N. Conmy, Paula G. Coble, James Farr, et al

Publication: Environmental Science & Technology

Publisher: American Chemical Society

Date: Feb 1, 2014

Copyright © 2014, American Chemical Society



PERMISSION/LICENSE IS GRANTED FOR YOUR ORDER AT NO CHARGE

This type of permission/license, instead of the standard Terms & Conditions, is sent to you because no fee is being charged for your order. Please note the following:

- Permission is granted for your request in both print and electronic formats, and translations.
- If figures and/or tables were requested, they may be adapted or used in part.
- Please print this page for your records and send a copy of it to your publisher/graduate school.
- Appropriate credit for the requested material should be given as follows: "Reprinted (adapted) with permission from (COMPLETE REFERENCE CITATION). Copyright (YEAR) American Chemical Society." Insert appropriate information in place of the capitalized words.
- One-time permission is granted only for the use specified in your request. No additional uses are granted (such as derivative works or other editions). For any other uses, please submit a new request.

BACK

CLOSE WINDOW



Oceanographic conditions in the Gulf of Mexico in July 2010, during the Deepwater Horizon oil spill

Author: R.H. Smith, E.M. Johns, G.J. Goni, J. Trinanes, R. Lumpkin, A.M. Wood, C.R. Kelble, S.R. Cummings, J.T. Lamkin, S. Privoznik

Publication: Continental Shelf Research

Publisher: Elsevier

Date: 1 April 2014

Published by Elsevier Ltd.

Order Completed

Thank you for your order.

This Agreement between Dr. Mary Abercrombie ("You") and Elsevier ("Elsevier") consists of your license details and the terms and conditions provided by Elsevier and Copyright Clearance Center.

License Number 4702031301351

[Printable Details](#)

License date Nov 04, 2019

Licensed Content

Licensed Content Publisher Elsevier
Licensed Content Publication Continental Shelf Research
Licensed Content Title Oceanographic conditions in the Gulf of Mexico in July 2010, during the Deepwater Horizon oil spill
Licensed Content Author R.H. Smith, E.M. Johns, G.J. Goni, J. Trinanes, R. Lumpkin, A.M. Wood, C.R. Kelble, S.R. Cummings, J.T. Lamkin, S. Privoznik
Licensed Content Date Apr 1, 2014
Licensed Content Volume 77
Licensed Content Issue n/a
Licensed Content Pages 14
Journal Type S&T

About Your Work

Title Use of Spectrofluorometry for Detection of Petroleum Hydrocarbons in the Marine Environment
Institution name University of South Florida
Expected presentation date Dec 2019

Order Details

Type of Use reuse in a thesis/dissertation
Portion figures/tables/illustrations
Number of figures/tables/illustrations 1
Format both print and electronic
Are you the author of this Elsevier article? No
Will you be translating? No

Additional Data

Portions Figure 7 on pg. 127